NASA Contractor Report 3722

Long Life Feasibility Study for the Shuttle Infrared Telescope Facility

CONTRACT NAS2-11155
JUNE 1985

NASA

NASA Contractor Report 3722

Long Life Feasibility Study for the Shuttle Infrared Telescope Facility

Lockheed Missiles and Space Company, Inc.
Palo Alto Research Laboratory
Palo Alto, California

Prepared for
Ames Research Center
under Contract NAS2-11155

National Aeronautics
and Space Administration

Scientific and Technical Information Branch

1985

FOREWORD

This report was prepared by Lockheed Missiles & Space Company, Inc., for NASA (Ames Research Center). Numerous useful discussions were held between NASA and LMSC personnel which has contributed significantly to the content of this report. LMSC is a confident of the conclusions presented here, but it must be noted that the long-life mission configuration described was constrained by NASA to provide maximum comparability with previous studies, and not necessarily to pursue an optimized systems approach to long mission lifetime issues for SIRTF.

Within LMSC, the cryogen studies which constitute the bulk of this report were done for the SIRTF program office by the Thermal Sciences Group lead by M McCargo. L. Naes, as cryo task leader, was chiefly responsible for their excellent contributions. The secondary actuator studies were supported by the advanced controls group under R. Stewart, with Dr. K. Lorell and Dr. J. Auburn making the key contributions in that area.

CONTENTS

ILLUSTRATIONS

TABLES

Section 1
INTRODUCTION AND SUMMARY

This study addresses the feasibility of extending the cryogen lifetime of the Shuttle Infrared Telescope Facility (SIRTF). The current design concept uses supercritical helium gas to provide cooling below 10 K for 7 days and below 20 K for an additional 7 days. Unless significant improvement can be made, evolution of this major research facility to free flyer or space station missions will be impossible, and SIRTF will remain a (frequently) reusable shuttle payload. LMSC feels the very large external tank for 6 month lifetimes in the DOS free-flyer is unrealistic.

Lockheed looked at several approaches to extending SIRTF lifetimes to 6 months (for a space station mission) and to 2 years (for a free flyer). Because of the limited scope of this study, a number of key parameters were taken as given, including several key mission parameters chosen to retain comparability with the Phase A baseline. The major purpose of this study was to identify the key issues for a long mission SIRTF program, and to determine the design impact on the SORTIE mission to retain the option of future growth. The key results are:

- Solid hydrogen can meet the thermal requirements and provide substantial lifetimes; a 6-month design is comparable in mass to the baseline system, and a 2-year design is less than 500 kg larger
- Cryogen tanks should be internal to the telescope vacuum shell to minimize parasitic heat loads.
- The superfluid helium required for instrument cooling is well shielded from external heat loads by the solid cryostat. Its size is then determined dominantly from science instrument heat loads.
- Mission design is a key to long lifetimes; large sun exclusion angles can reduce the aperture heat load more than an order of magnitude from the baseline system; 90 deg sun avoidance is recommended for 2-year missions, which would then be similar in size to the 6-month system

described here. Even with this constraint, careful orbit design and observing will have 4 to 6 sr available at any time, and full sky access every 6 months.

- o Conduction cooling by direct thermal links from internal cryotanks most efficiently uses the heat of sublimation of solid cryogens, and also minimizes the effects of thermal transients; it can also provide these advantages for liquid or superfluid helium systems.
- o Earthshine does not contribute significantly to the aperture heat load, so that an aperture shade design limit of 60 deg should be used even if the sun avoidance angle is larger. A symmetric shade would be appropriate in this case to avoid complex roll operations while observing.
- o Advanced technologies in cryogen tank support and insulation are available which will reduce parasitic heat loads more than an order of magnitude, and should be incorporated in any SIRTF concept.
- o Internal heat dissipation of 1.0 W (science instruments), 0.2 W (secondary actuator), and 1.0 W (FGS total load) dominate the system design and any reductions will increase mission lifetime directly, especially if parasitic loads are reduced.

1.1 STUDY CONSTRAINTS

Nine items were identified as constraints on this study. Lockheed did not investigate any implications of these constraints or any alternatives. These items were:

(1) Use the phase A concept description from the NASA internal study ("red book") as the telescope baseline

(2) Optics shall be kept below 10 K for at least 30 days, and shall not exceed 20 K at mission end

(3) Instrument heat loads from the Phase A baseline shall be used*

(4) Purge gas is not required

(5) Cryogen refurbishment on orbit is not required

*NASA Ames provided some modifications to be the Phase A heat loads.

(6) Sun avoidance angle may be increased to 60 deg
(7) Design mission profile will be provided by NASA (described below)
(8) Image motion compensation shall be assumed
(9) Both a vacuum cover and a dust cover shall be included

1.2 MISSION PROFILE

The SIRTF long life mission was defined by NASA as a circular orbit at 400-km altitude with an inclination of 46.5 deg. For an earth avoidance angle of 60 deg, this inclination is the minimum allowable for full sky coverage in missions as short as 6 months. The remaining parameters are given in Table 1-1.

Two reference orbits were provided which include observations from 5- to 20-min long of 13 objects. These are not specific astronomical sources, but were selected by NASA to be representative of SIRTF mission heating profiles. The observations are given in Table 1-2. For the 6- and 24-month missions in this study, the total heat loads were derived from a mixture of these two orbits, with one out of five orbits represented by orbit 1 and four of five by orbit 2.

The time profile of internal heat generation is also critical to the cryogen system lifetime. NASA directed that the secondary mirror actuators be assumed to generate 200 mW continuously, and provided a detailed profile of MIC instrument heat loads described in Section 4. The FGS generated 1.0 W, with 10 percent of that absorbed at the 10 K station in the MIC.

Figures 1-1 and 1-2 specifically show the time histories of sun and earth avoidance angles for Orbits 1 and 2, respectively. Orbit 1 has about half of its time with some sun illumination on the inner surface of the symmetric sunshade, including 40 of the 90 min near the 60-deg design angle, so that the sunshade is fully illuminated during this period. The earth illumination is within the sunshade for all but the few minutes observing object number 2. Orbit 2 is much more benign in its contribution to aperture heat load. Only

Table 1-1 SIRTF REFERENCE MISSION I

Altitude: 400 km
Inclination: 46.5 deg
Solar angle of orbit plane: -23 deg
Data: 22 June 1989
Solar Position: R. A.: 6 h
Dec.: 23.5 deg
Earth avoidance angle: 60 deg
Orbit 1 occurs 20 percent
Orbit 2 occurs 80 percent
Slew between observations: 3 min

Table 1-2 SIRTF REFERENCE MISSION II

Orbit 1				Orbit 2			
No.	R.A. (h)	Dec (deg)	Duration (min)	No.	R.A. (h)	Dec. (deg)	Duration (min)
1	14	62	6	9	18	-46	19
2	17	50	6	10	0	0	20
3	18	-29	7	11	22.5	75	8
4	20	8	6	12	13.5	75	8
5	23	40	6	13	12.5	12	20
6	1	40	15				
7	6	83	5				
8	11	40	15		(3-min slewing between objects)		

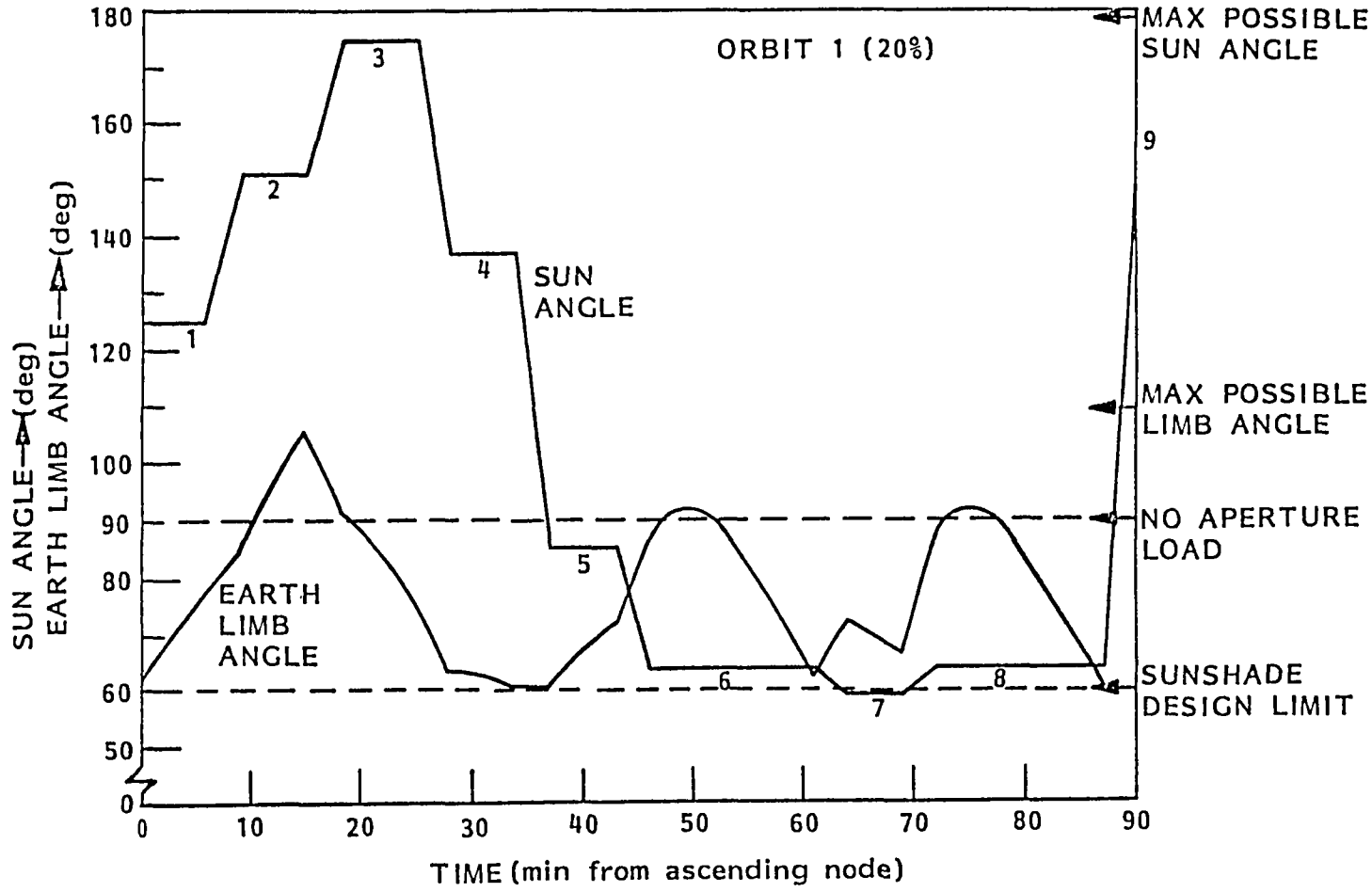

Fig. 1-1 SIRTF Long-Life Reference Mission - Orbit 1

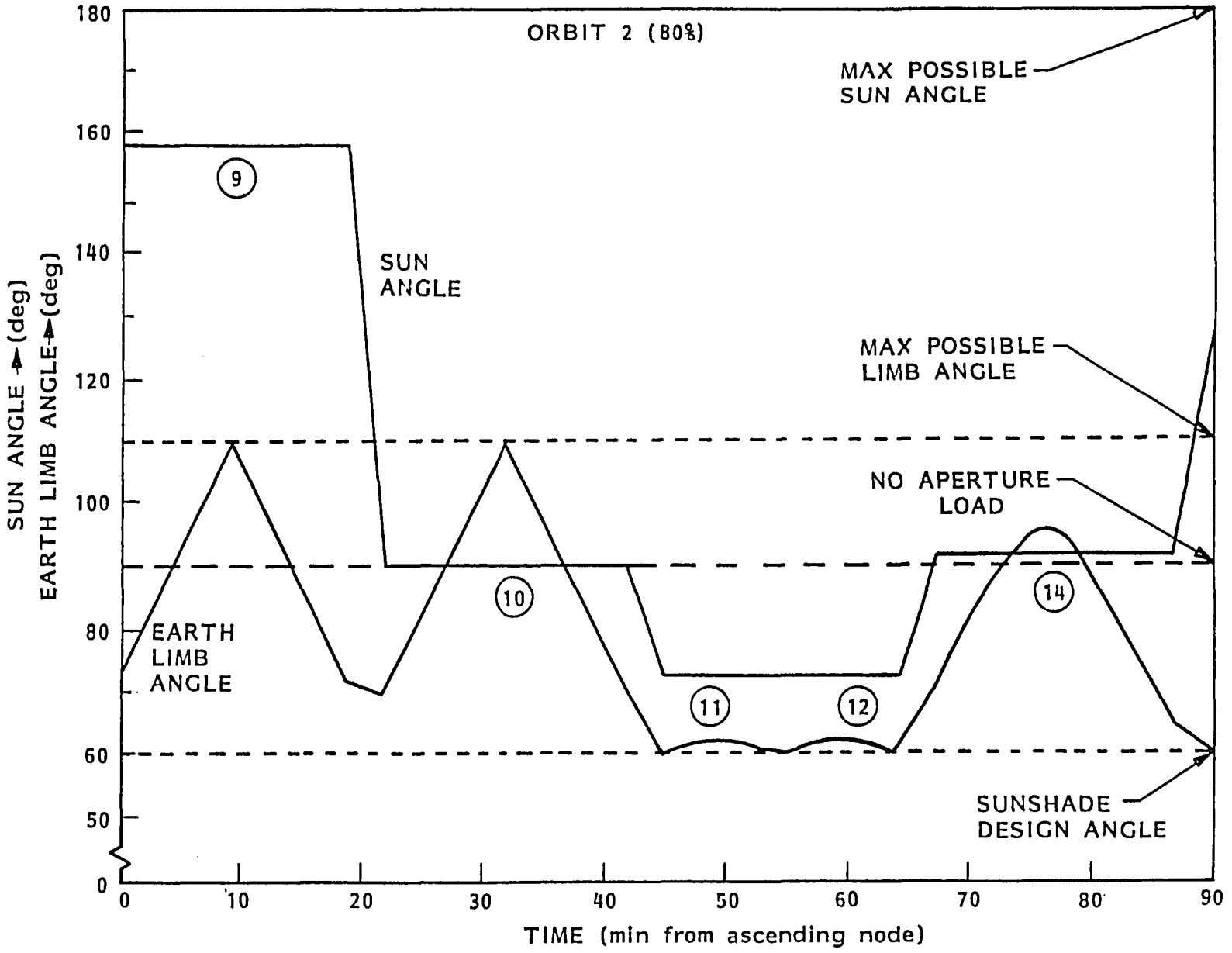

Fig. 1-2 SIRTF Long-Life Reference Mission - Orbit 2

25 min of slewing and observation of objects 11 and 12 contribute any solar illumination, and much more of the orbit avoids earth illumination than in Orbit 1.

It should be noted that Figs. 1-1 and 1-2 do not follow immediately from the observing table. Since as much as 30 min observing a single object are available without violating earth limit constraints (60-deg avoidance), a time shift of up to 15 min for Orbit 1 or 10 min for Orbit 2 could be made. This would cause noticeable differences in the earth limb angles, without changing the sun avoidance time history. However, in both orbits, the sequence of observations constrained this time slip to less than 2 min because of earth limb violations which would occur in the sequence of observations.

No assessment was made of the real pointing history during the slew intervals. These were simply taken as straight lines connecting the end points (sun and earth angles) of one observation with the beginning of another. It is even possible that in making the sun angle slew linear, the earth angle could violate the design criteria. This question was ignored and we simply assumed that the slew would occur in a way which did not violate any requirement. The slew acquisition, and settling times of the baseline IPS gimbal system may take much more than the 3 min assumed here.

The mission profile for SIRTF will affect a number of other areas in addition to cryogen heat load, including zodiacal light, stray light, and bright objects. All these will be as significant in the total system design and should be considered as carefully as the heat load issue. Furthermore, no verification was made by either Lockheed or NASA that the thirteen objects of the Long-Life Study Reference Mission are fully representative of the ultimate SIRTF requirements. We strongly recommend the development of a comprehensive Design Reference Mission (DRM) for future design studies of SIRTF. By comparison, Space Telescope established a DRM including over 500 stars before its Phase B study, and addressed both the selection and sequencing of these possible observations. In SIRTF's case, a 50 to 100 percent increase in cryogen lifetime may be achieved over the 6-month baseline presented here

simply by shifting observations over the 6- to 12-month lifetime to avoid any sun-induced aperture heat load. (Twelve month lifetime would be achieved with this design by keeping the sun angle larger than 90 deg.)

1.3 TWO-YEAR MISSION DESIGNS

This study was to address three aspects of long-life missions. One, can a cryogen system be designed to provide 2-year free-flyer lifetimes within the given constraints? Two, can a 6-month system be designed, and how is that different from the 24-month system? Three, what impact would the design characteristics of these systems have on the approach taken in the Phase A Sortie mission? By NASA direction, most of the attention of this study was on the design approach for a 6-month lifetime.

Figure 1-3 shows the Phase A baseline system, consisting of an 85-cm aperture cassegrain telescope, a 45-deg exclusion angle sunshade and forebaffle, and an external tank supercritical helium gas cryogen system. Within the temperature requirements given, solid hydrogen using internal tanks and conductive cooling was found to be the most effective cryogen approach. Figure 1-4 shows the preliminary design configuration of a solid hydrogen system with a 60-deg exclusion angle sunshade for a 2-year lifetime, including 50 percent margin (36-month design lifetime). The toroidal tank is three times larger than any existing flight-qualified solid cooler, but does not represent any identifiable technical risk other than size. This figure is drawn in the same scale as Fig. 1-3, showing a length reduction of over 1 m in sunshade, forebaffle, and electronics, with a diameter increase of less than 40 cm at the aperture shade. Note that the envelope diameter at the Phase A external tank location is actually reduced by 60 cm. A jettisonable vacuum cover has been assumed for this configuration, which would be acceptable for a free-flyer. The large vacuum shell required to contain the cryogen tank allowed the sunshade radiator to be moved from the lateral surface (Phase A approach) to the forward aperture plane. This eliminated external sun loads on the aperture shade, and improved the radiator sun pointing geometry. These

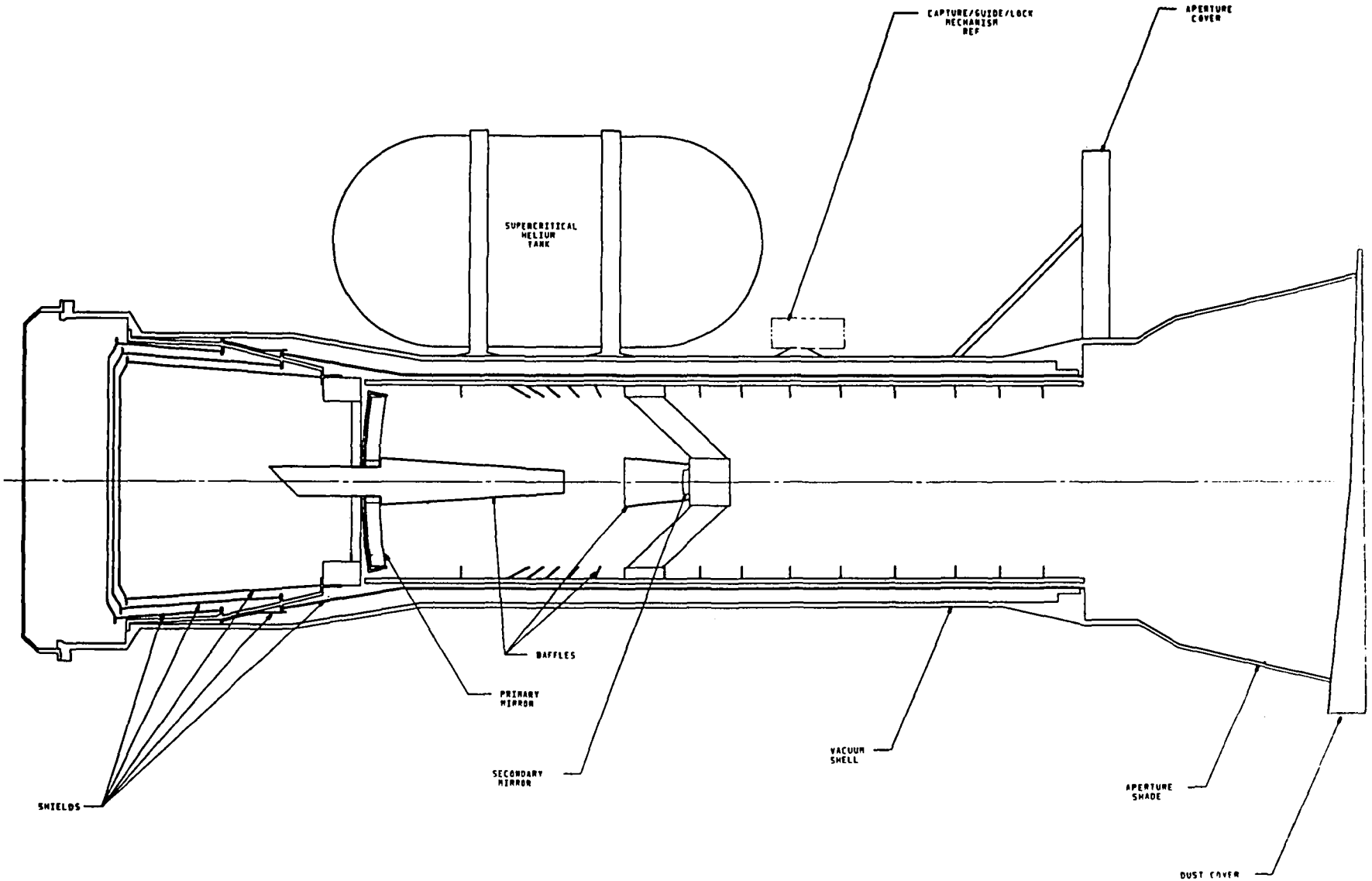

Fig. 1-3 SIRTF Phase A Baseline

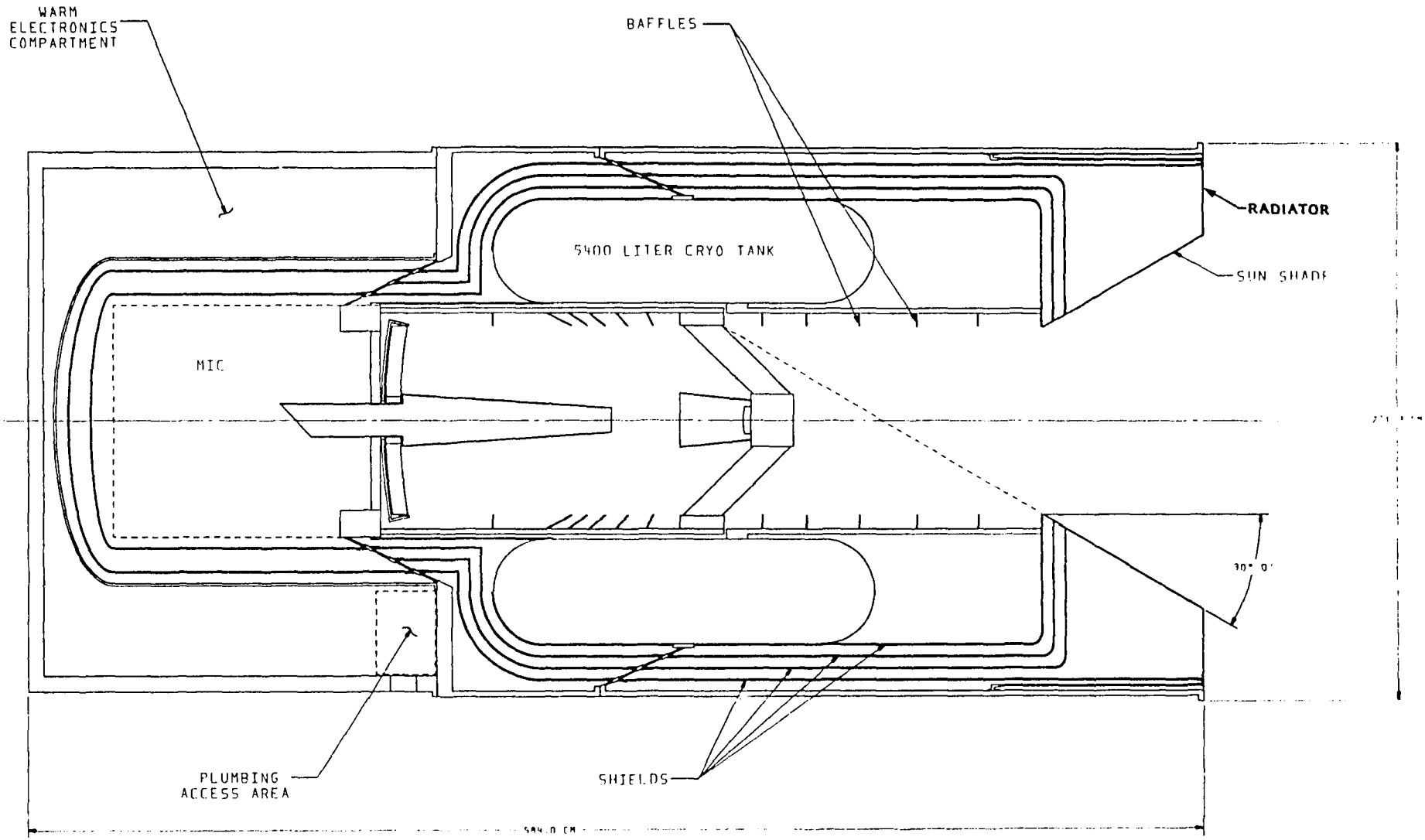

Fig. 1-4 SIRTF Long-Life Study Baseline (24 month)

two characteristics reduced the sunshade temperature from the 230 K average of the Phase A design to 185 K for the Long-Life Reference Mission which substantially reduced the aperture heat load.

Two other aspects of the 2-year system envelope were briefly investigated. Figure 1-5 shows the configuration of the previous figure with the Phase A optics system replaced by an advanced technology cassegrain system using an f/1.2 primary mirror. This reduces overall telescope length by 86 cm, with the cryo tank (as before optimally shaped for the 2-year lifetime) now filling the available vacuum space. Finally, Fig. 1-6 presents a 1.25-m aperture variation of the advanced optics technology configuration. Because of the volumetric efficiency of the toroidal tank, the overall diameter only increases by 17 cm; the length remains below the design of Fig. 1-4 by 13 cm.

1.4 SIX-MONTH MISSION BASELINE DESIGN

The 6-month design approach was taken as a derivative of the 2-year configuration. A preliminary design trade was made between an improved helium system (Phase A derivative) and a solid hydrogen system, and significant mass and volume advantages still favor hydrogen for even this shortened mission. Figure 1-7 shows the volume requirements for various cryogens. A fully optimized helium system could be no more than a factor of 2 better than shown here, and the conclusion would not change. Figure 1-8 shows the configuration for this 6-month design, and further detailed discussions of this may be found in Sections 6 through 9 of this report. Included in this figure are the vacuum cover and pointing gimbal which might be used on a sortie mission, or on a spacelab-adapted platform for a space-station mission.

No detailed investigation was made of the vacuum cover design issues related to sortie or platform operations, although the hot-capping problem of the 1975 Hughes Aircraft Company design study would exist with this concept. Since this study focused on less constrained operations on a space station or a free flyer, hot capping was not considered critical. Careful consideration of this should be made for the sortie mission uses of a SIRTF designed for free-flyer operation, but that was beyond the scope of the current study.

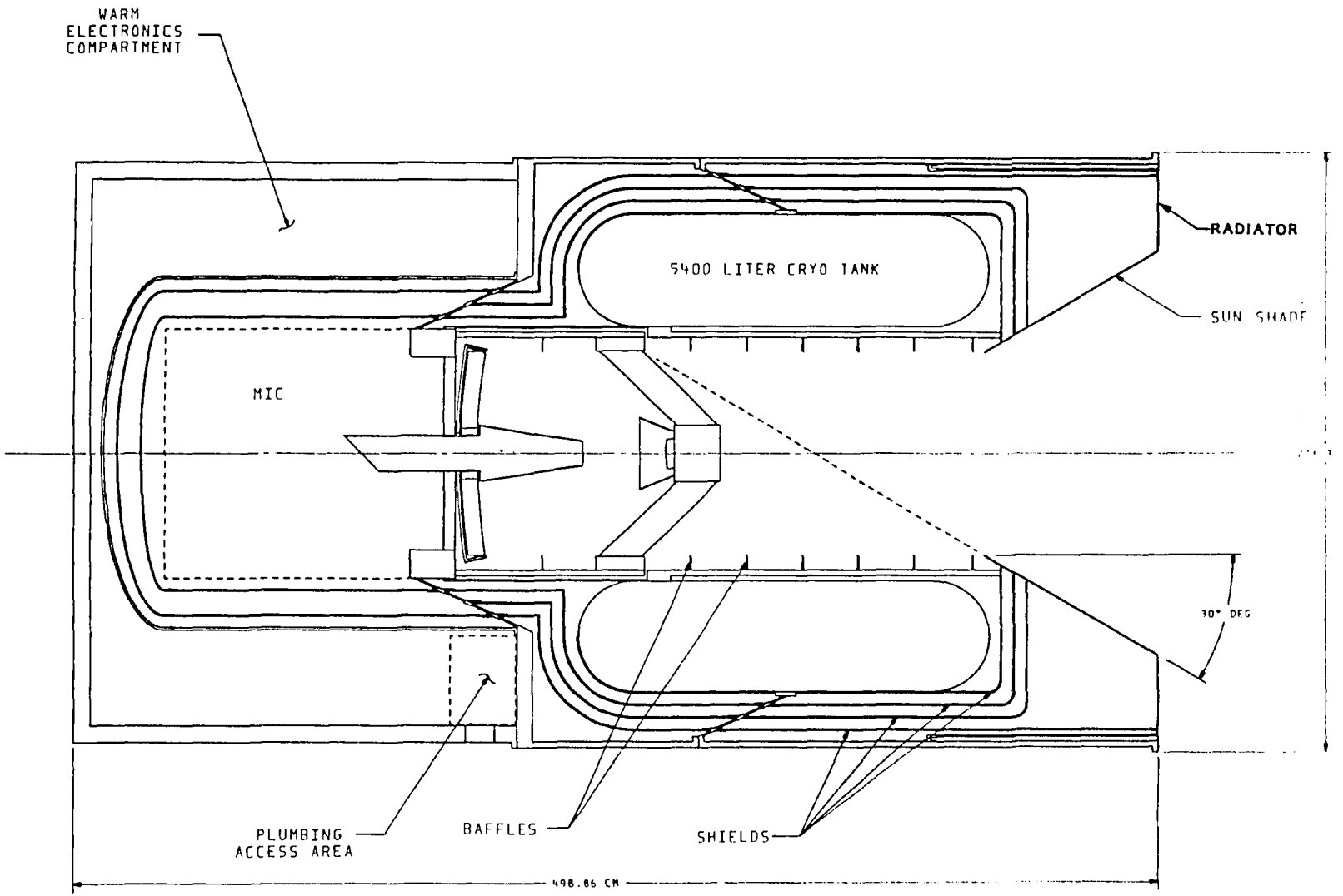

Fig. 1-5 SIRTF Long-Life System Advanced Optics Technology

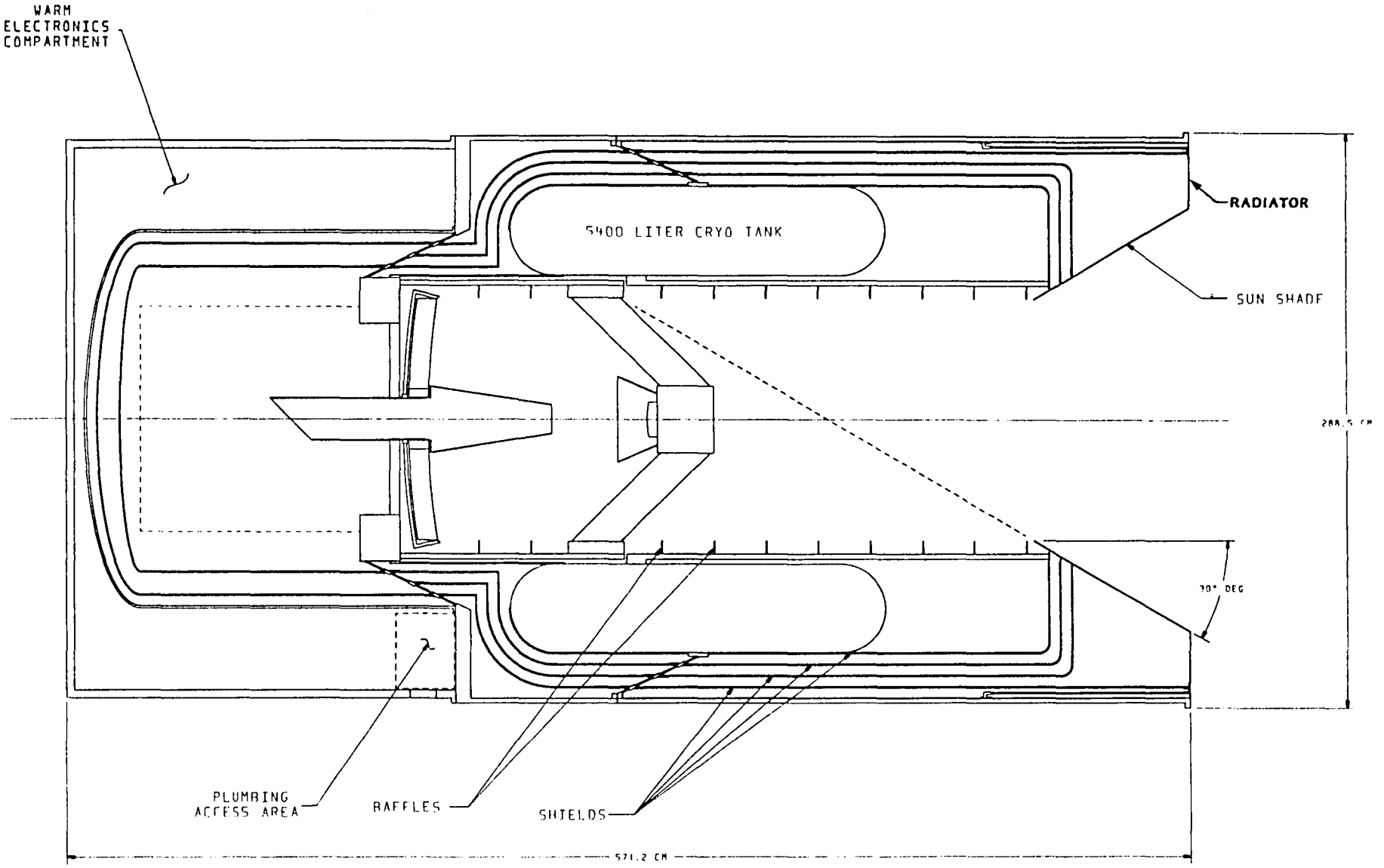

Fig. 1-6 SIRTF Long-Life System 1.25-m Alternative

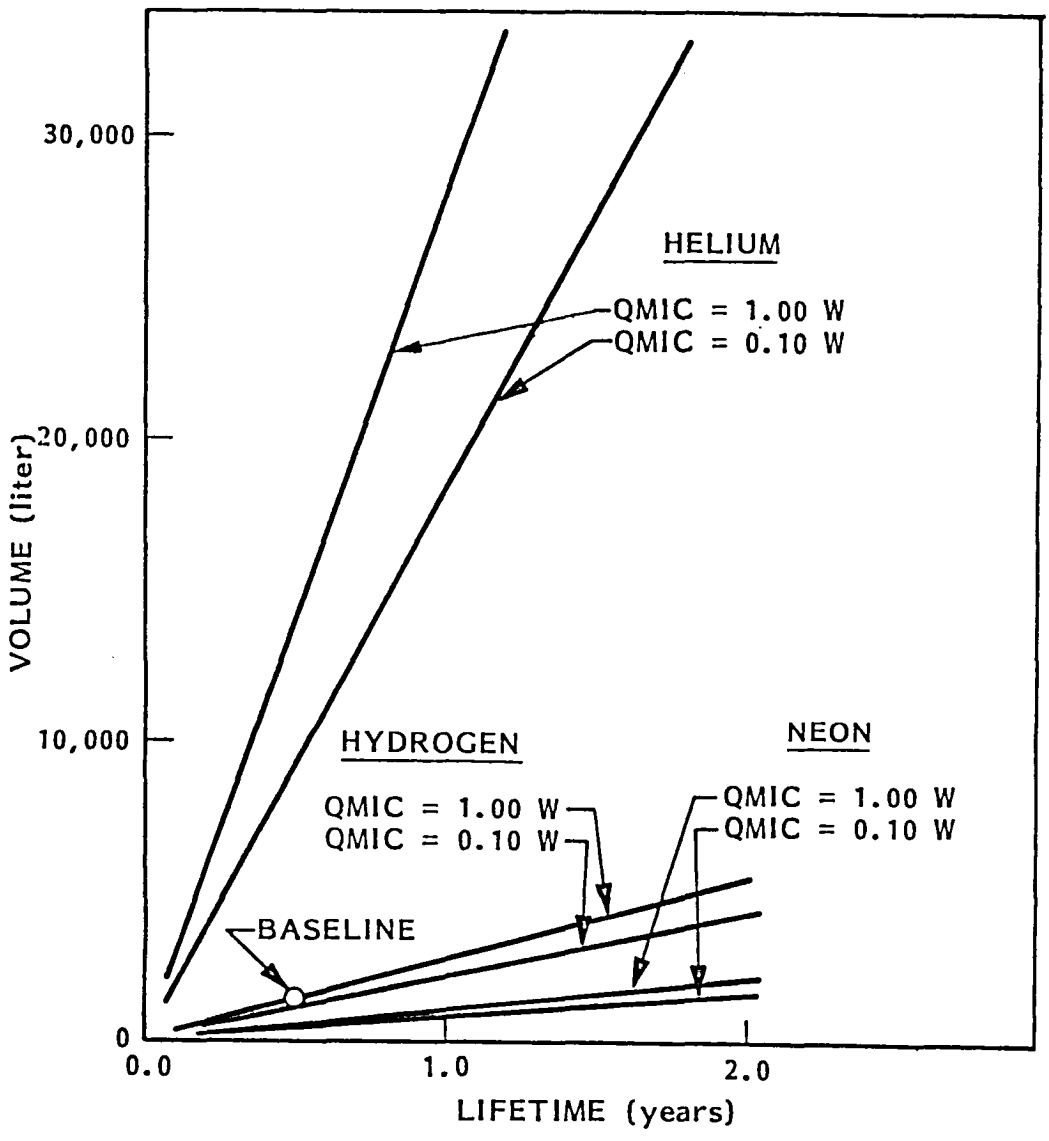

Fig. 1-7 Required Cryogen Tank Volume Versus Lifetime

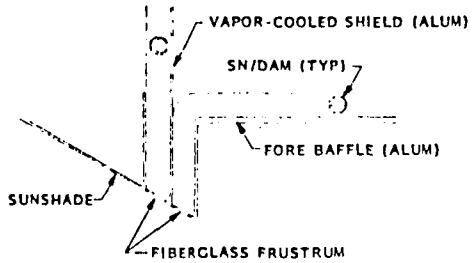

DETAIL A, MLI BLANKET TERMINATION

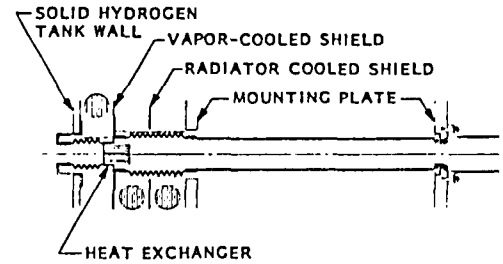

DETAIL B, ORBITAL VENT LINE

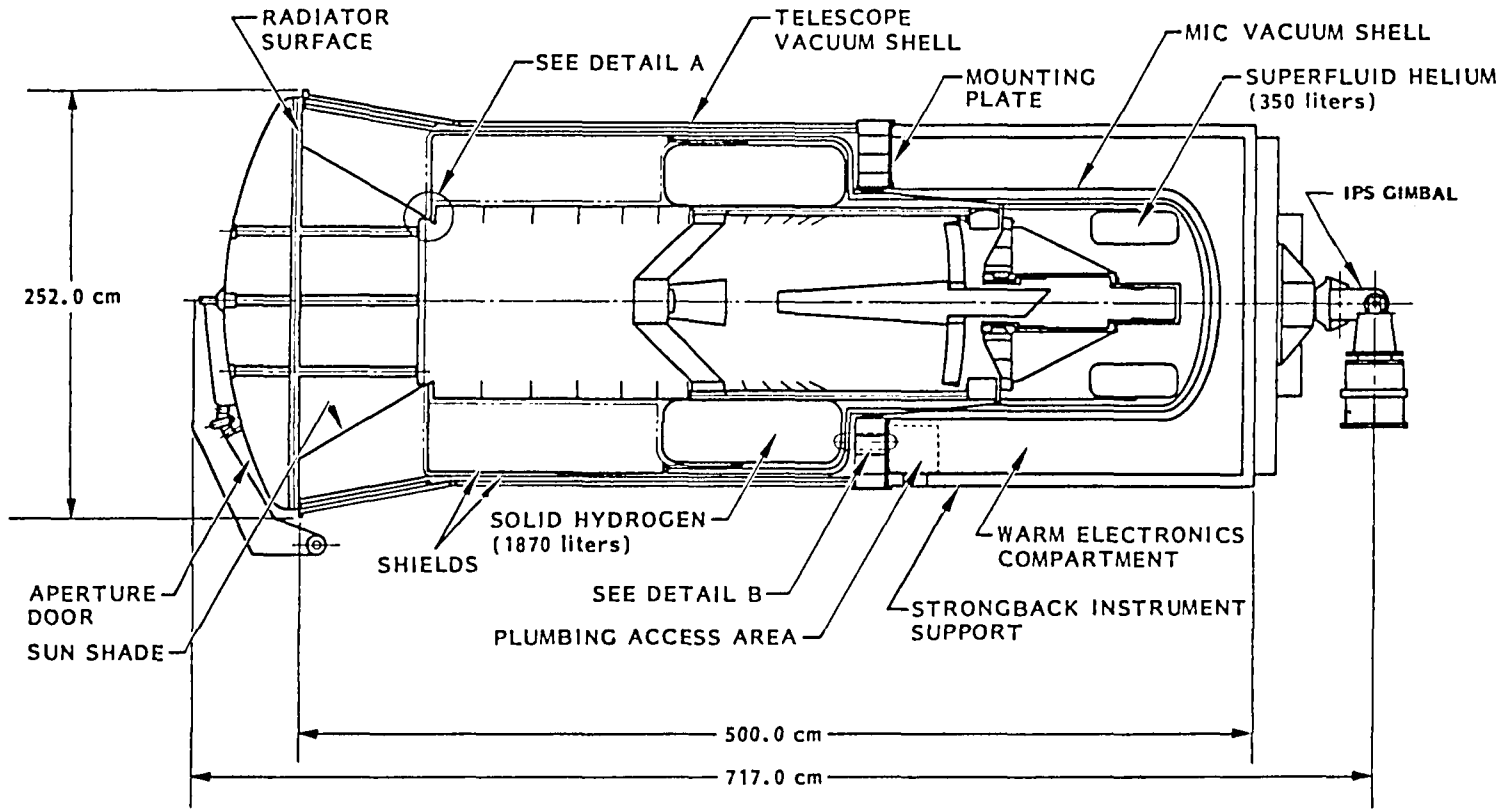

Fig. 1-8 SIRTF Baseline Configuration (6-Month)

This 6-month design was taken as the baseline approach for the Long-Life Mission Study, and was investigated as presented in the remainder of this report. Two significant technical issues were identified which are important to successful implementation of this design, and were investigated in additional detail. First, the solid hydrogen must be used with a low back pressure vent to keep the telescope within the 10 K requirement. Second, the secondary mirror, with its actuator heat load and high thermal impedence through the spider arms, was the critical element in meeting the temperature requirement.

The vent line was designed to meet the back pressure requirements, while providing sufficient vapor cooling to the vapor-cooled shield internal to the vacuum shell. The connection to the VCS is made with a heat exchanger in the vent line at a single point on the VCS. Preliminary calculations verified the cooling of the VCS, but full three-dimensional analysis should be done in the future. This approach is being used in a similar 1,000-liter solid hydrogen flight cooler, and will be tested with an engineering model in 1983-1984. The bulk solid hydrogen then has an equilibrium temperature below 7.9 K and remains virtually unchanged for the duration of the mission.

The secondary mirror is cooled by careful selection of the conduction paths, and is shown to remain below 9.2 K in the given configuration. Further reduction of this could be achieved by using pure copper cooling straps internal to the spider arms. Use of the superfluid vent gas from the MIC was considered which did reduce the secondary mirror temperature to below 9.0 K. However, the large variation in helium flow rate caused by the time history of MIC instrument heat loads resulted in dT/dt gradients beyond NASA-specified requirements. These excursions are to lower temperatures that are desirable, with the secondary falling as low as 8.5 K, but thermal gradient induced noise eliminated this consideration. The primary mirror temperature varies between 9.0 and 9.2 K in all cases because of the changing MIC instrument heat loads as the six instruments are switched. Active control of the superfluid flow (with heaters) could provide a constant flow that would hold the optics at the lower temperatures, but may use significant amounts of cryogen.

1.5 SORTIE MISSION DESIGN IMPACT

The Long-Life Mission configuration cannot be achieved by small adaptations of the Phase A baseline. Instead, the sortie mission design must incorporate key design characteristics of the long-life mission configuration so that use or adaptation is possible for later long-life missions. Some details of the long-life design, such as the solid hydrogen vent line discussed in this report can be deleted from the sortie system, and incorporated later by modification. A few design characteristics, however, must be included from the beginning in a sortie mission which is similar to the reference mission of this study. These include internal tanks, conduction cooling directly from the cryotank (rather than long vapor plumbing lines), a forward radiator for the sunshade, and shielding of the sunshade outer surface from solar illumination. No consideration was made for a sortie mission sun angle of 45 deg rather than the 60-deg figure of this study. However, a sunshade extension could accommodate that change.

One approach to sortie adaptation is to change the cryogen choice. Using normal boiling point liquid helium at 4.2 K in the 6-month system hydrogen tank will provide a 26 day lifetime assuming the same mission model, and ignoring thermal loads caused by the shuttle. The lower temperature of the cryogen would give a noticeably lower operating temperature in the baffles and optics (4.8 to 5.5 K). The hydrogen vent heat exchanger would be much less efficient, but the substantially higher vent rate would probably compensate. Alternatively, the sortie system could include longer vent lines wraping the VCS which would then be replaced for the longer mission. An absolute pressure valve to maintain pressure in the tank would be needed at the warm end.

Another possibility would be the use of supercritical gas in the tank, which would then be designed to contain the higher pressure at some weight penalty. Again, different vent gas routings could be used for sortie and for longer missions.

Both of these approaches avoid the shuttle system safety requirements which could apply to a hydrogen cooler on sortie missions. (Free flyer delivery

safety will be addressed by UARS for 1989 flight.) However, the easiest approach to the sortie mission would be to use the 6-month system as designed, with solid hydrogen cooling. This would allow the sortie mission to serve as a full demonstration of the long-life operations. The tank might be only partially loaded (less than 20 percent) to minimize weight, or the excess cryogen of a full tank could be used for sortie missions with much more severe sun pointing than the reference mission. The sun avoidance design angle probably should not be violated in such a mission, however; significant problems could occur if the sun directly illuminated the black forebaffles. An add-on sunshield extension could be used to permit viewing closer to the sun than the 60-deg design exclusion angle.

If some rebuilding or modification of SIRTF were acceptable in adapting the sortie optimized SIRTF to a long-life mission, then there are only a few key issues which must be faced in the initial design.

First, the cryotanks should be internal to the vacuum shell. This is needed in any long life mission to minimize parasitic heat loads, and is required for solid cryogens where conduction cooling is used. Sufficient volume internal to the vacuum shell should be provided for the future tanks and heat shields if those items are not designed for dual purpose.

Second, shielding the sunshade from external surface solar heating should be provided, either by extension of the vacuum shell as used in this study or by a separate heat shield. The vacuum shell of Fig. 1-8 could be terminated at the end of the forebaffle, and a Phase A sunshade used for a sortie mission; the vacuum shell and entire sunshade would be modified or replaced for the longer mission.

Third, direct thermal conduction to the cryotanks (rather than vapor cooling lines) should be used for both sortie and longer missions even with helium. This approach would provide maximum damping of temperature transients, avoiding possible thermal noise induced by chopping and IMC. The vent gas of helium, if used in the sortie mission, could be used to cool intermediate heat

shields. This plumbing would be changed in adapting to longer missions when solid hydrogen is used in the cryotanks.

1.6 LIFETIME EXTENSION OF THE SIX MONTH BASELINE

Modification of the Long Life Baseline 6-month design to 1-year and longer missions is in some ways easier than the sortie modifications discussed above. Longer missions can be operated at larger sun-avoidance angles than used in this study, reducing the cryogen heat load by one-third and increasing the lifetime, with no hardware changes at all. 1-year missions are possible with this simple change.

Two design changes could be incorporated in the baseline which would improve lifetime without increasing the tank size or weights. First, advanced technology thermal isolation such as PODS, could be used in place of the fiberglass cones taken from previous work and used in this study. Second, the MLI blankets could be constructed with the current SOA graded spacer concepts. Together these would reduce the parasitic heat loads by nearly 1 W. Both of these choices could be made in the initial system design with only minor cost impact, or could be changed later at higher cost.

Another lifetime-gaining approach would be to reduce the internal heat generation. The 0.2 W from the secondary actuator could be reduced by lower chopping duty cycle or frequency, such as the 60 to 70 percent, 5 to 10 Hz used on GIRL, and its operation could be restricted to less than full time as was assumed here. Heat loads less than 20-mW could be achieved at this critical optical element.

The fine guidance sensor could be removed from the cold chamber saving a total of 1.0 W heat load. However, this would require a completely different approach to pointing control, and probably should be done in initial design rather than by any modification. Also, the 1.0-W science instrument heat load may be lowered for long-lifetime, high reliability missions. Lockheed did not, however, consider how this would affect science instrument concepts,

or even if this is possible. Variations in these MIC loads should be minimized, which would allow the use of SfHe vapor for optics cooling.

If the parasitic heat loads are reduced as described, the aperture heat load becomes almost 50 percent of the cryogen burden; this is all absorbed in the forebaffle region. A secondary cryogen directly coupled to the forebaffle and optimized for this cooling could provide at least a 50 percent lifetime increase. Combined with the other changes, a SIRTF Long-Life Mission may achieve 18 to 24 months without using the very large tanks of the preliminary 2-year mission designs.

For these long lifetimes, the superfluid instrument cryogen will be large if the baseline heat loads are used. However, LMSC feels lower power could be achieved in high reliability instruments designed for long-life missions. If so, the superfluid tank could be similar to the 350 liters of this study. For IRAS-like instrument heat loads, even less superfluid would be needed for long SIRTF missions.

1.7 SECONDARY ACTUATOR INVESTIGATION

In addition to the cryogen lifetime issues discussed above, a part of this study focused on the design of a secondary actuator which could meet the 200 mW heat load requirement and also provide the dynamic performance required for IMC and chopping. Section 10 describes this investigation, where Lockheed's electrodynamic actuator concepts were applied to SIRTF. Section 11 reports the results of early IR&D experiments designed to validate the analytical work. Under some reasonable assumptions, heat loads as low as 60 mW are estimated for an actuator which meets SIRTF's requirements for 1-axis chopping. More pessimistic assumptions could increase this estimate to 300 mW, but this would have little impact on the long-life baseline results. The analyses of Section 10, and the Lockheed-funded measurements of Section 11, are significant in that they confirm that electrodynamic actuators can meet all the SIRTF actuator requirements.

Section 2
CRYOGENIC STUDY CONSTRAINTS

The object of this study is to assess the feasibility of extending the lifetime of the baseline SIRTF concept from the current 15 days to at least 6 months - with extension to 2 years also considered. To achieve the longer lifetime, changes in both the mission constraints and cryogen system design were explored to effect a lower net cryogen heat load while maintaining an efficient utilization of the available cryogen. Study constraints imposed on LMSC as effecting the cryogenic system design include the following:

- The telescope configuration is given by the SIRTF Phase A Concept Description.
- The optics temperature for extended missions are to be less than 10 K for the first 30 days and shall not exceed 20 K at the end of the mission.
- The instrument heat loads will be as given for the Phase A baseline.
- Aperture purging by the venting vapors will not be required.
- Cryogen subsystem refurbishment on orbit is not required.
- Both a vacuum-sealed aperture cover and a vented dust cover will be required.
- The sun avoidance angle may be increased from 45 to 60 deg, with effects on even larger sun-avoidance angles to be considered. To evaluate system performance, NASA/ARC will provide the mission profile giving altitude, inclination, and look-angles.

From this study, LMSC has concluded that extending SIRTF's lifetime to between 6 to 24 months is not practical within reasonable mass and volume constraints by simply increasing either the size or number of the current SIRTF external SCHe tanks. Tank volumes as large as 15,000 liter and cryogen (plus tankage) mass as high as 2,600 kg would be required to provide 6 months of cooling.

The large heat of sublimation of solid cryogens was found to be a more effective coolant, with solid hydrogen meeting the low temperature requirements. Detailed analyses have shown that temperatures of both the primary and secondary mirrors can be maintained below 10 K and that their temporal temperature gradients are less than one-tenth the maximum allowed excursion of 3.6 K/h. The required tank size for a 6-month mission is 1,870 liters, with less than a 400-kg tankage plus cryogen mass.

This report documents the selection of solid hydrogen as the baseline cryogen system for the long-life SIRTF mission. The baseline configuration is described, followed by a detailed description of the baseline performance and sensitivity to changes in the operating parameters.

Section 3
APERTURE SHADE CONFIGURATION STUDY

For the 15-day sortie SIRTF configuration to meet the baseline science objective, a mission profile was developed by NASA/ARC which required pointing SIRTF to within 45 deg of the sun. To accommodate this pointing requirement without imposing overwhelming thermal loads to the SIRTF cryogenic subsystem, a sunshade is required to eliminate direct or reflected solar illumination on the cooled forebaffle. Optical design considerations also require a zero geometrical view factor from the sunshade inner surface to both the secondary mirror and spider assembly so that no scattering sources are generated within the telescope FOV. These coupled requirements determine the minimum forebaffle plus sunshade length and the entrance diameter as a function of the sunshade envelope cone half-angle. These relationships are shown in Fig. 3-1.

The minimum length of the forebaffle and sunshade is 365 cm at a cone half-angle of 26 deg, with the sunshade diameter at 260 cm. The strong dependence of the diameter with cone half-angle shows that a 40-cm reduction in diameter to 220 cm can be achieved with only a 10 cm increase in length to 375 cm at the minimum possible cone half-angle of 22.5 deg. For cone half-angles of less than 22.5 deg, source vectors at the limiting pointing angles will be reflected directly into the cold forebaffle so these angles are not allowed.

The Phase A baseline sunshade design and performance characteristics for the sortie SIRTF mission are described in the Perkin-Elmer final technical report for the Phase A study, ER-409. In that report it was shown that the aperture heat loads dominate the cryogen requirements for the current SIRTF sortie mission. For both a sortie and long life mission it is desirable to reduce the magnitude of the aperture heat load to reduce the cryogen mass requirements. Two candidate approaches to achieve this goal are to employ a

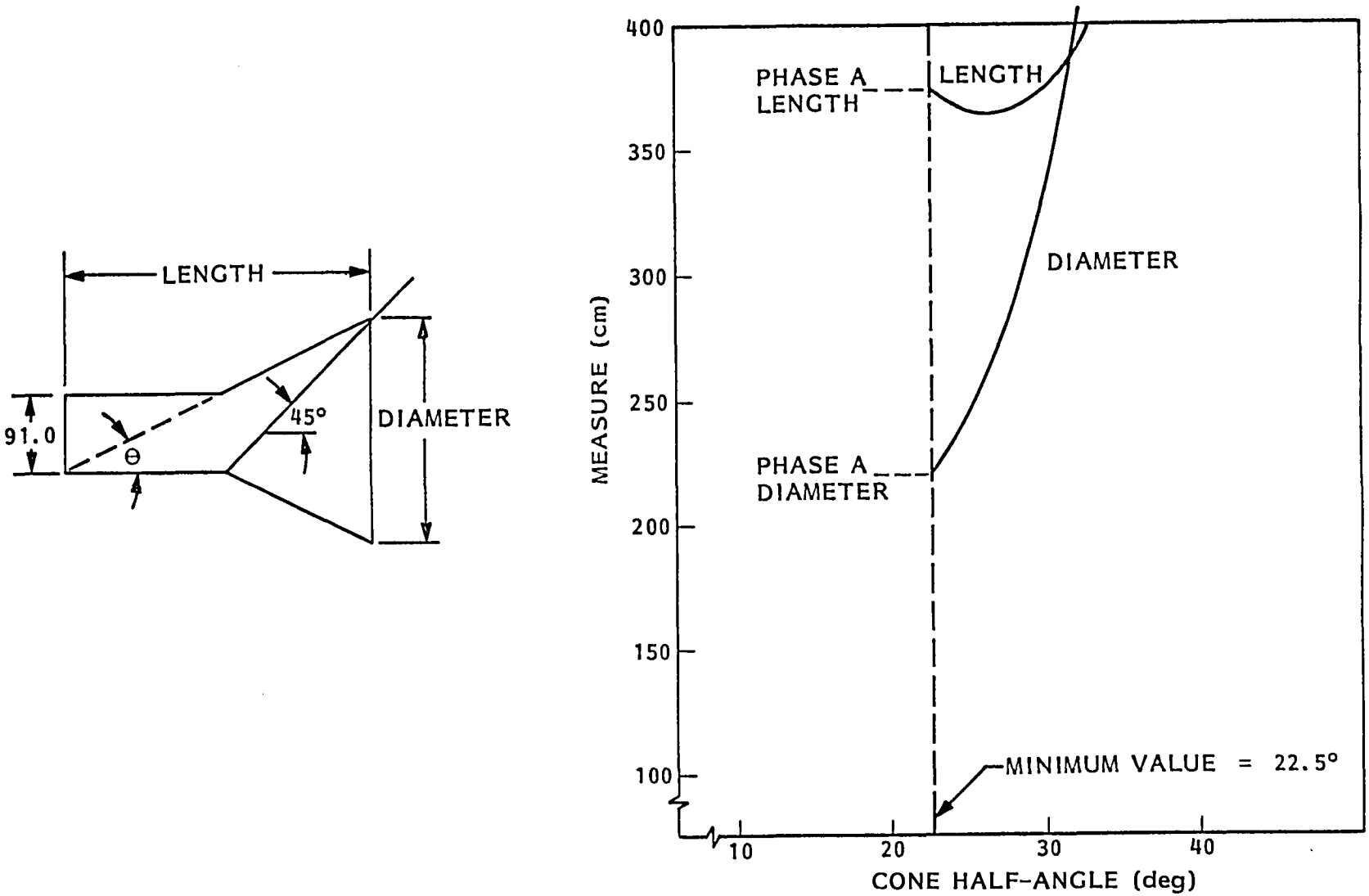

Fig. 3-1 Sunshade and Forebaffle Length and Diameter Requirements (45-deg Avoidance Angle)

more efficient sunshade design and/or to place more stringent requirements on the allowable sun and earth limb pointing angles.

The most direct approach toward reducing the aperture heat load is to increase the pointing angle limits from the Phase A baseline value of 45 deg to some larger value. Because of the longer mission time, complete sky coverage and all science objectives can be met during a 6-month mission with a relaxation in the pointing requirements to 60 deg from the earth limb. Further, a significant reduction in the aperture heat load from the sortie baseline can be expected by specifically designing the sunshade to reject illumination only up to the 60-deg pointing requirement. An additional reduction in the aperture heat load can be achieved by maintaining a 90-deg sun avoidance angle, if missions as long as 2 years are contemplated. For 2 year missions sky coverage can be obtained for at least 8 months in any part ot the sky.

The minimum required forebaffle plus sunshade length and entrance aperture diameter for the sunshade designed for a 60-deg avoidance angle is shown in Fig. 3-2 as a function of the sunshade envelope cone half-angle. Here, the minimum cone half-angle is seen to be reduced to 15 deg for the 60-deg avoidance angle, at which point source vectors at the limiting pointing angle will be reflected into the cold forebaffle. The 91.0-cm forebaffle diameter derived from the Phase A baseline study is assumed throughout this analysis.

At the 15-deg minimum cone half-angle, the minimum allowable sunshade aperture diameter of 124 cm is achieved at the expense of a forebaffle plus sunshade length of 402 cm, which is just 27 cm longer than the Phase A sortie design. A sizable reduction in length can be affected at the expense of a larger sunshade aperture diameter by increasing the cone half-angle. At the Phase A diameter of 220 cm, achieved by using a 36.4-deg cone half-angle, the length may be reduced by nearly 200 cm to 215 cm. The selection of cone half-angle within the physical limits of the shuttle bay will be made on the basis of minimum aperture load as discussed below.

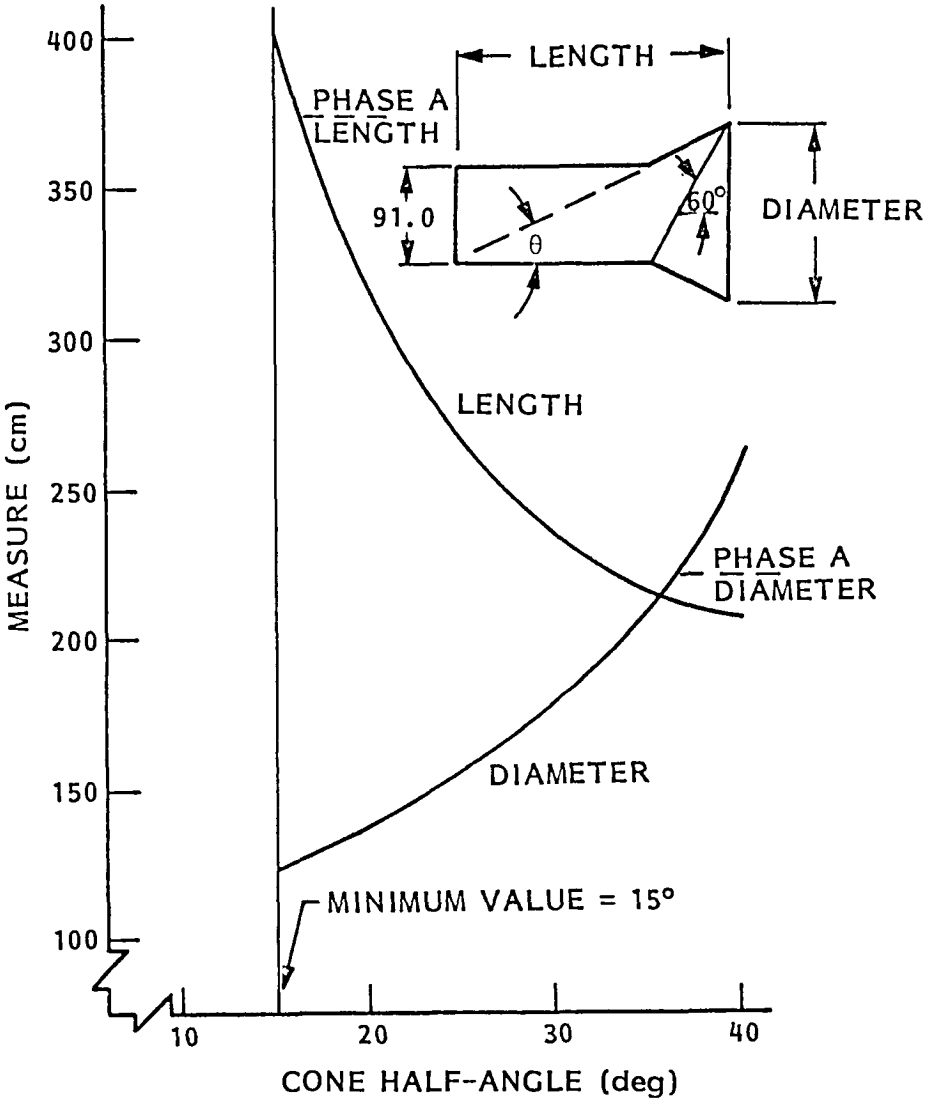

Fig. 3-2 Sunshade and Forebaffle Length and Diameter Requirements (60-deg Avoidance Angle)

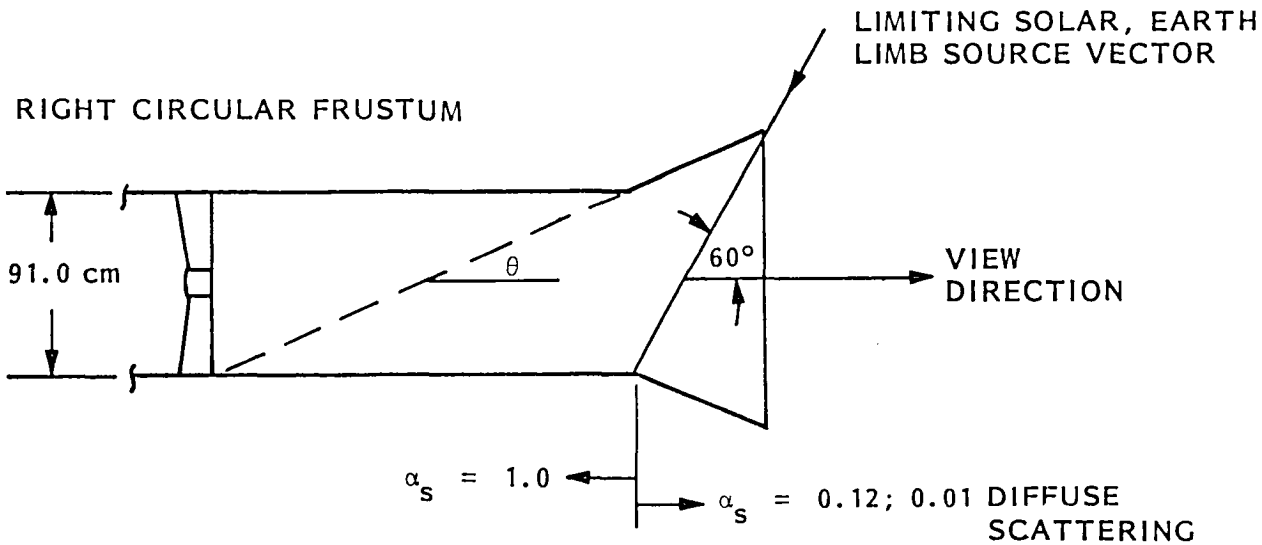

Fig. 3-3 Right Circular Frustum Sunshade and Forebaffle Configuration

Three different sunshade configurations were analyzed as candidates for a SIRTF long-life mission sunshade.

The right circular frustum, shown in Fig. 3-3, is the simplest and least complex of all the sunshade options studied. The sunshade inner surface is taken to be polished aluminum, having optical properties of α_s/ϵ = 0.12/0.05 with a 1.0 percent diffuse scattering coefficient - the same optical properties as for the Phase A sunshade inner surface. Later sections, especially section 9, will discuss the sensitivity of the cryogen system design to these assumptions. These values were used to provide maximum comparability with previous analyses and do not represent LMSC's judgement. Inside the forebaffle, the surfaces are taken to be black* with α_s/ϵ = 1.0/1.0. The length of the forebaffle is set by the requirement that the geometrical view factor of the sunshade to both the secondary mirror and spider assembly is zero. This requirement is satisfied by placing the spider

---

* Although such a material remains elusive for the far IR, these properties are justified for conservative heat load calculations.

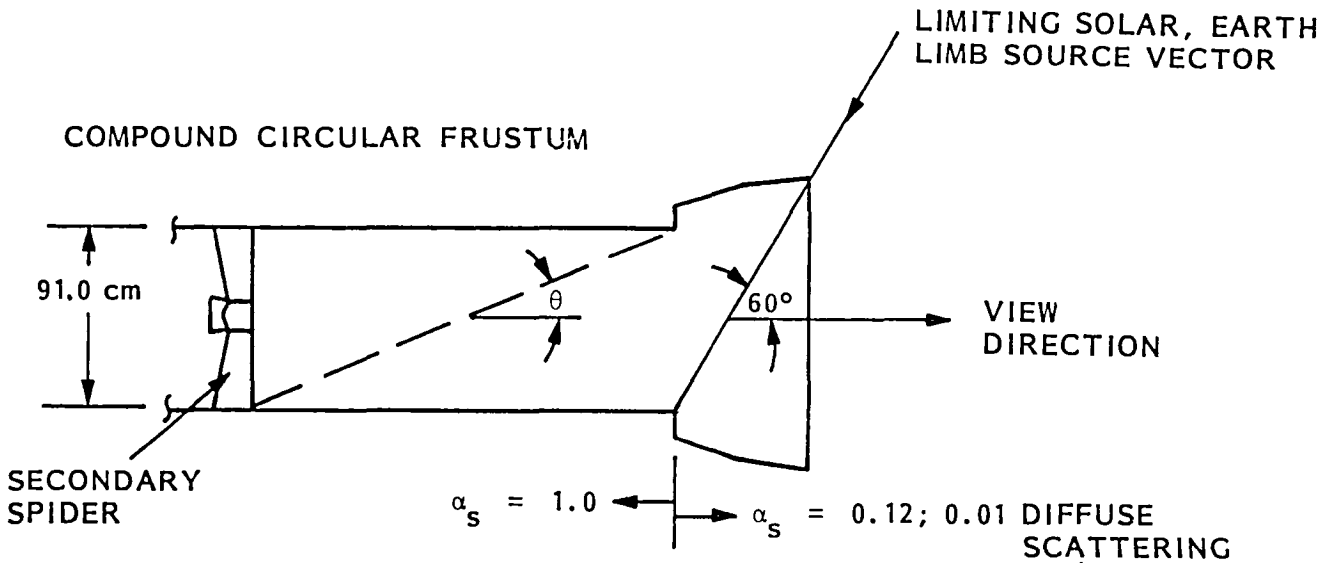

Fig. 3-4 Compound Circular Frustum Sunshade and Forebaffle Configuration

termination at the forebaffle beyond the forebaffle intersection with the extended sunshade surface as shown by the dotted line in Fig. 3-3.

The optical properties and geometry requirement for the compound circular frustum, shown in Fig. 3-4, are identical to those for the right circular frustum. This configuration was used in a previous study to reduce the sunshade diameter by about 20 cm. This sunshade is constructed of two right circular frustums of different cone half-angles. The inner frustum has a cone half-angle of 15 deg to ensure that rays at the 60-deg limiting pointing angle are reflected parallel to the aperture plane before again striking the inner frustum surface to begin the ray's exit from the sunshade cavity. The half angle of the outer frustum is less than the 15-deg half-angle of the inner frustum and, once specified, determines the location of the intersection between the inner and outer frustum (by ensuring that no reflected ray from the outer frustum enters the aperture) as well as the location of the intersection between the inner frustum with the aperture plane. For this

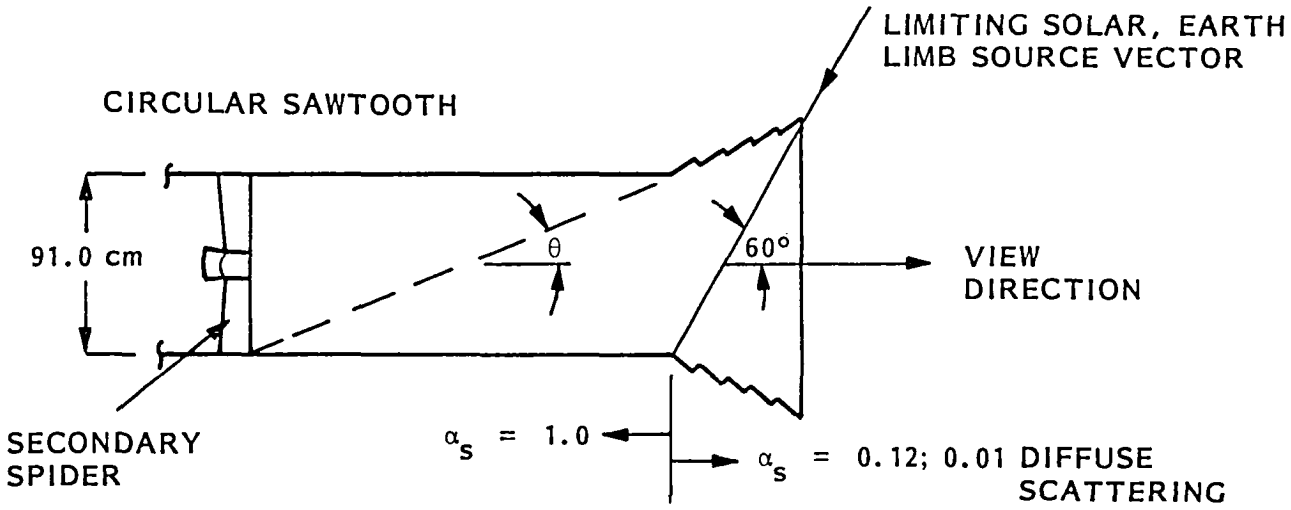

Fig. 3-5 Circular Sawtooth Sunshade and Forebaffle Configuration

analysis the cone half-angle of the outer frustum was taken to be 7.5 deg, again to match the configuration of previous studies.

The third sunshade concept studied is the sawtooth configuration as shown in Fig. 3-5. Once again, the optical properties and geometry requirements are as given for the right circular frustum. The sunshade consists of a number of cavities which are formed by a surface at a blaze angle greater than the cone half-angle and a second surface perpendicular to the blaze surface, extending out to the envelope defined by the sunshade cone half-angle. The point of termination at the envelope edge defines the location for the start of the adjacent cavity. In this study, the blaze angle of the cavity was taken to be twice the envelope cone half-angle. The sawtooth configuration allows using a large surface reflection angle so that limiting angle sun rays are rejected in a single bounce, while retaining the sunshade envelope near the minimum cone half angle (which would require at least 2 bounces for sun ray rejection).

The performance of all three candidate sunshade configurations has been determined by finding the scattered solar heat load into the cold forebaffle as a function of the incident solar angle and cone half-angle. Scattering effects are limited to the 1 percent surface diffusivity. Sunshade section interfaces were treated at ideal.

Heat loads for a right circular frustum sunshade are shown in Fig. 3-6. In this figure an interesting performance characteristic is clearly demonstrated. Specifically, the number of surface reflections occurring inside the sunshade aperture has a considerably larger effect on the net aperture heat load than does the aperture diameter (i.e. the incident heat load to the sunshade). Pointing to within 60 deg of the sun with a right circular frustum sunshade having a cone half-angle of 15 deg results in the aperture heat rate of 2.95 W, an improvement over that possible with the Phase A sunshade design configuration. Increasing the cone half-angle to 30 deg increases the energy incident to the sunshade by approximately a factor of two (diameter increases from 127 to 179 cm), yet the scattered aperture heat load is seen to decrease by nearly a factor of three to 1.03 W. The differential would be even larger for scattering coefficients greater than 1 percent.

The observed reduction in heat load is due to two complimentary features of the design. First, the sunshade having a 15-deg cone half-angle forces the incoming rays to make at least two bounces off the inner surface before the energy is reflected out the aperture. In general, more than two bounces will be necessary for those rays that do not pass through the sunshade centerline. As the cone half-angle is increased, the number of bounces required to reject the incident energy is reduced to the point where many rays will require only a single reflection (at $\theta \geq 30$ deg) to exit the sunshade cavity. The second effect is in the fact that as the cone half-angle becomes larger, the effective solid angle subtended by the aperture at points along the sunshade becomes smaller, and the forebaffle significantly shorter.

The performance of the compound frustum sunshade as shown in Fig. 3-7 is worse than the right circular frustum for all cone half-angles. Although sizable

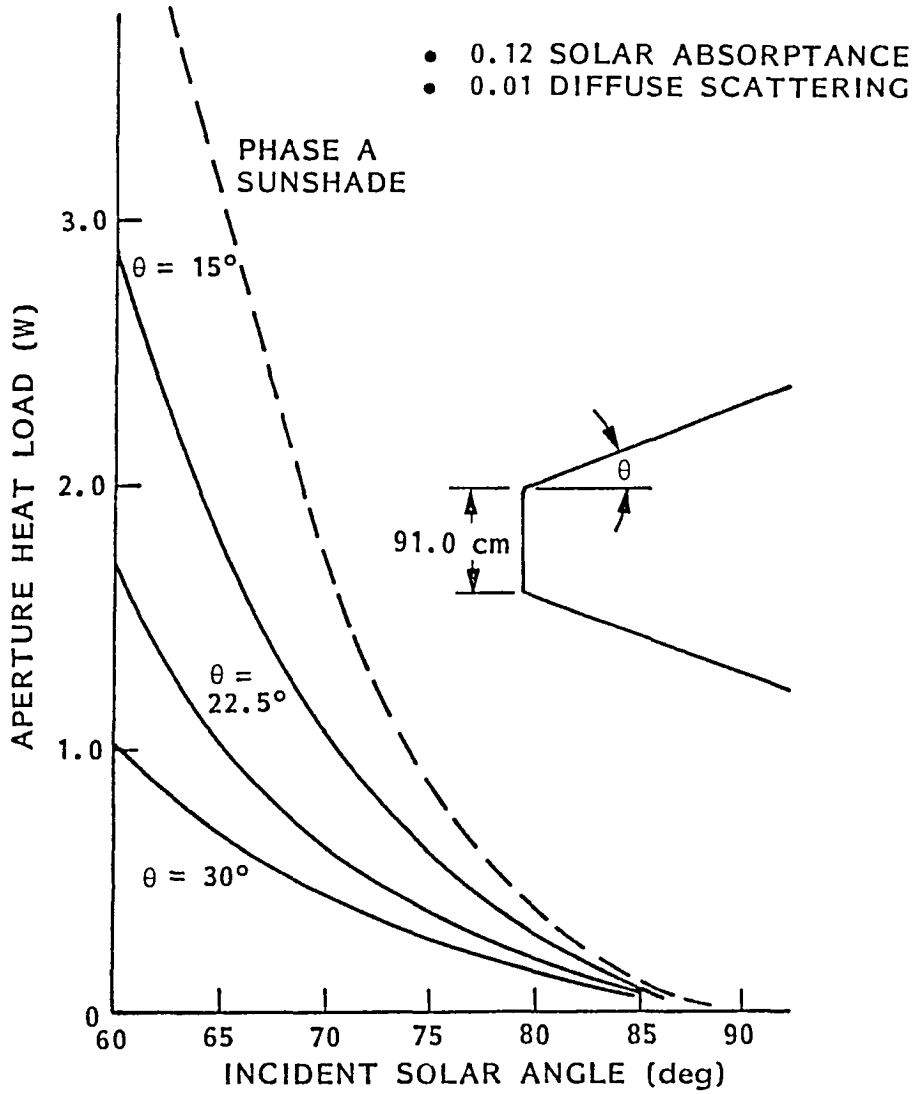

Fig. 3-6 Scattered Solar Aperture Heat Load for Right Frustum Sunshade

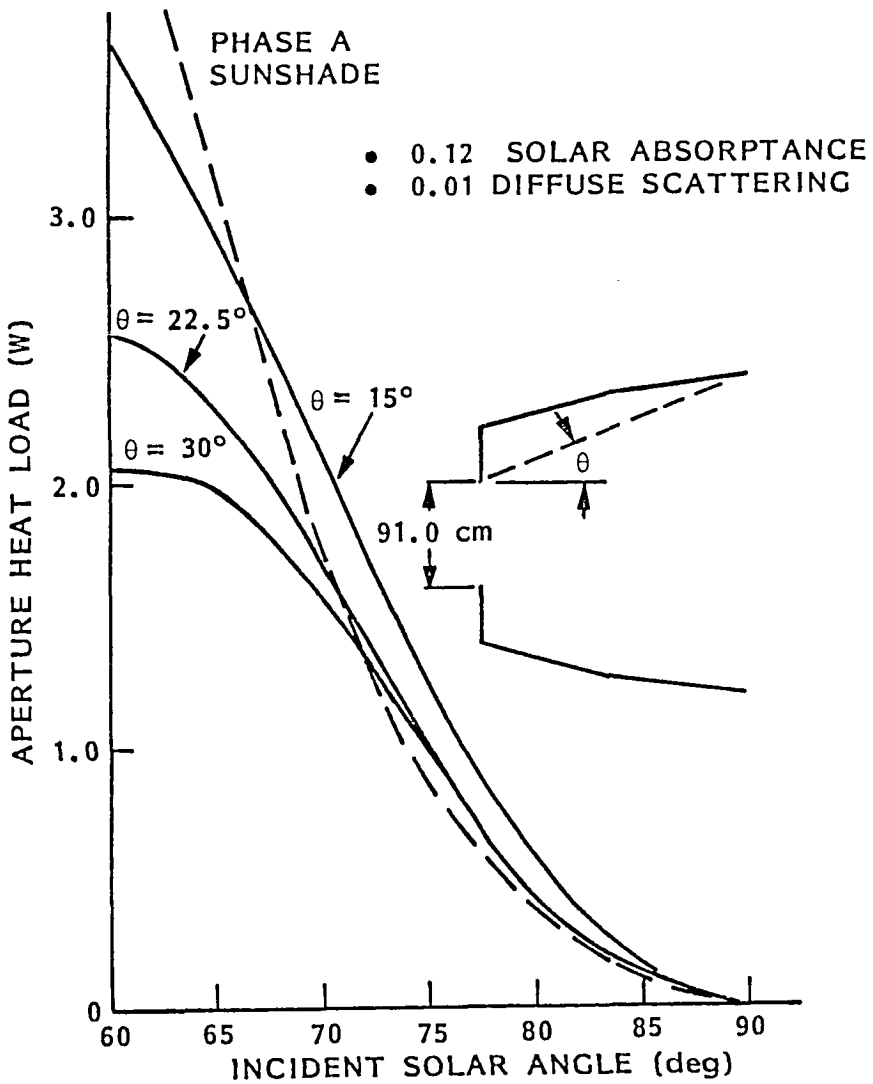

Fig. 3-7 Scattered Solar Aperture Heat Load for Compound Frustum Sunshade

reductions in the aperture heat load are realized by increasing the cone half-angle when pointing to within 60 deg of the sun, the relative change for pointing angles greater than 70 deg is small. Further, the performance is similar to that of the Phase A sunshade - designed for pointing to within 45 deg from the sun. In the Phase A design, the purpose of using the compound frustrum was to reduce the sunshade aperture diameter by approximately 20 cm. LMSC feels that this was probably a poor trade in light of the superior thermal performance of the simpler right frustrum sunshade. While this is clear from the data presented for 60 deg design angle, LMSC feels it would also be true for a 45 deg design angle.

The performance of the sawtooth sunshade is shown in Fig. 3-8. For cone half-angles of 15 and 22.5 deg, the scattered solar aperture heat load is lower than that derived for either the compound frustum or the right circular frustum at the limiting pointing angle of 60 deg. For pointing angles greater than 70 deg, the performance is similar to the right circular frustum.

In comparing the three candidate sunshade configurations for thermal performance, technical design risk, manufacturability, and cost, LMSC feels that the proper selection should be the right circular frustum with a cone half-angle of 30 deg. This configuration represents a straightforward design approach which can easily be adopted into the current SIRTF configuration, and would have a length of 240 cm and an aperture diameter of 179 cm. The small improvement of the sawtooth approach is not sufficient to justify the risks that should be assigned to edge effects (which were ignored).

Besides the scattered aperture heat load, a thermal load will be imposed on the aperture by the infrared self-emission of the sunshade inner surface. The thermal load for both the Phase A baseline and selected long-life mission sunshade is shown in Fig. 3-9 as a function of the sunshade radiating temperature ($\varepsilon = 0.05$). These heat rates are shown as first-order approximations in that only contributions from initial source vectors are considered. Secondary, tertiary, and higher-order terms were not included in this level of the study.

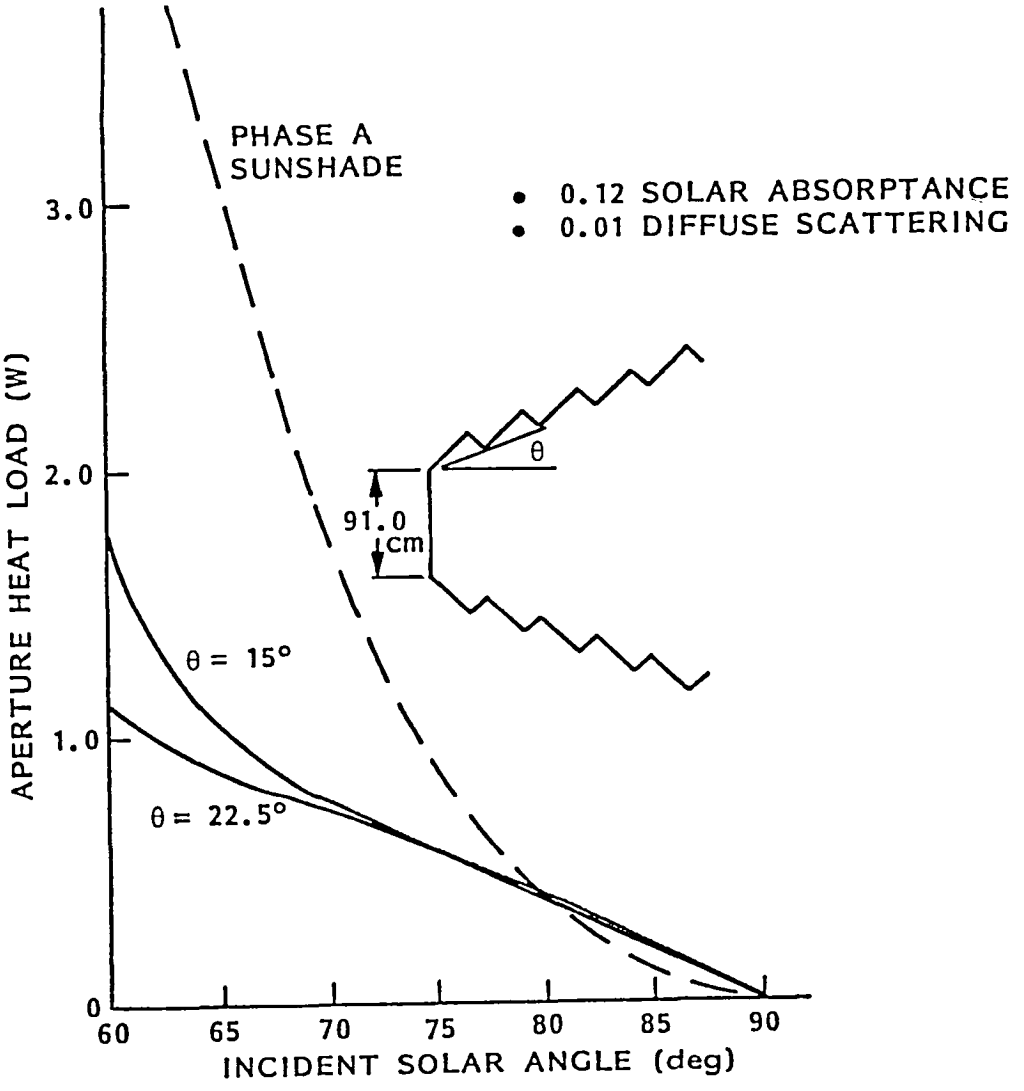

Fig. 3-8 Scattered Solar Aperture Heat Load for Sawtooth Sunshade

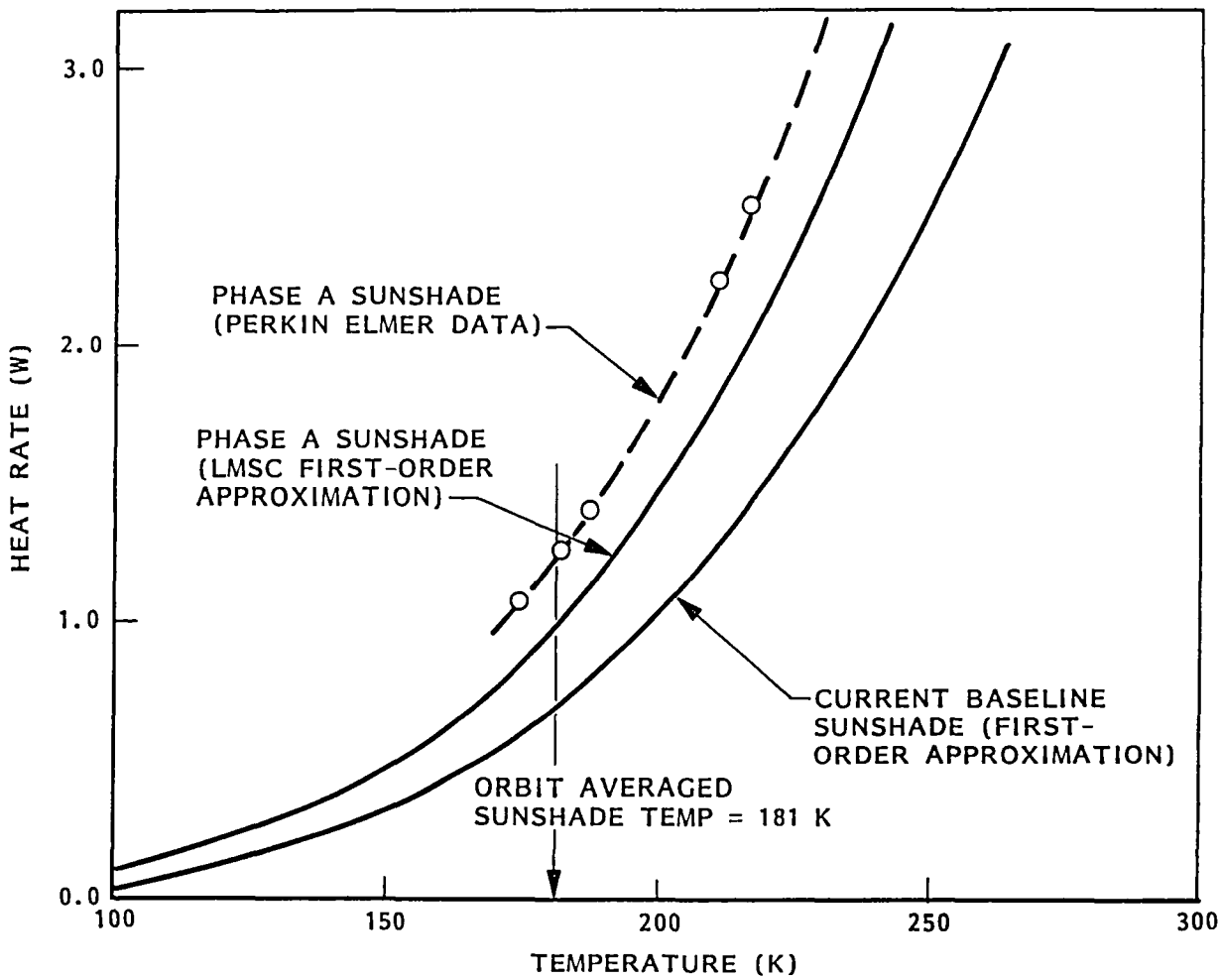

Fig. 3-9 Radiated Aperture Heat Load Versus Sunshade Temperature (ε = 0.05)

Section 4
MISSION PROFILE/INSTRUMENT HEAT RATES

4.1 APERTURE HEAT LOAD

For the SIRTF long-life mission, NASA/ARC developed a reference mission pointing profile to be used in the calculation of the nominal aperture heat load. This mission pointing profile consists of two reference orbits with orbit 1 occurring 20 percent of the time and orbit 2 occurring 80 percent of the time. Details of the objects used as reference sources and observation times spent on each source have been described in Section 1.

In Fig. 4-1, the pointing angles for orbit 1 of the long-life reference mission (20 percent duty cycle) are shown. Source viewing for times less than 37 min into the orbit imposes no aperture heat load from scattered solar heat because the sun lies behind the entrance aperture, indicated by sun angles greater than 90 deg. At 37 min, slewing to source 5 initiates a scattered solar heat load as the telescope axis is pointed to within 85 deg of the sun.

Observation of source 5 proceeds for 6 min, at which time the telescope is slewed for 3 min to point at source 6. Observing source 6 requires pointing to within 64 deg of the sun, as does source 8 for 15 min. Sandwiched between sources 6 and 8, a 3-min slewing both to and from source 7 is executed, which points the telescope to the limiting 60-deg solar avoidance angle. Observation of source 7 continues for 5 min.

During observation of the several sources in orbit 1, the earth limb is positioned from the limiting 60-deg avoidance angle (for short periods of time) to beyond 90 deg where no aperture heat load from scattered albedo or earthshine will be realized.

The orbit 2 long-life reference mission (80 percent duty cycle) pointing angles are shown in Fig. 4-2. For this orbit a significantly lower scattered solar heat load is imposed on the aperture than for the orbit 1 reference

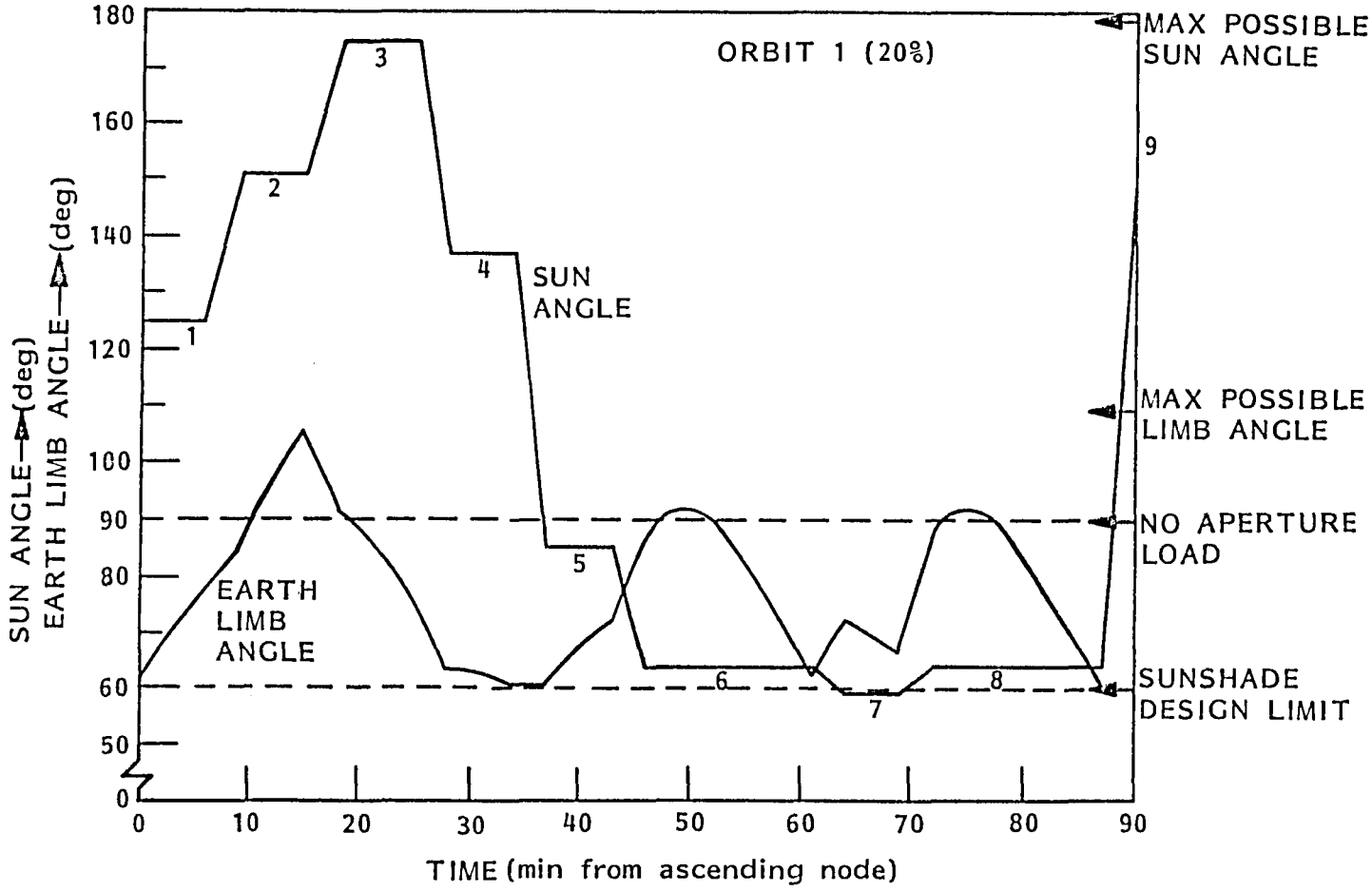

Fig. 4-1 SIRTF Long-Life Reference Mission - Orbit 1

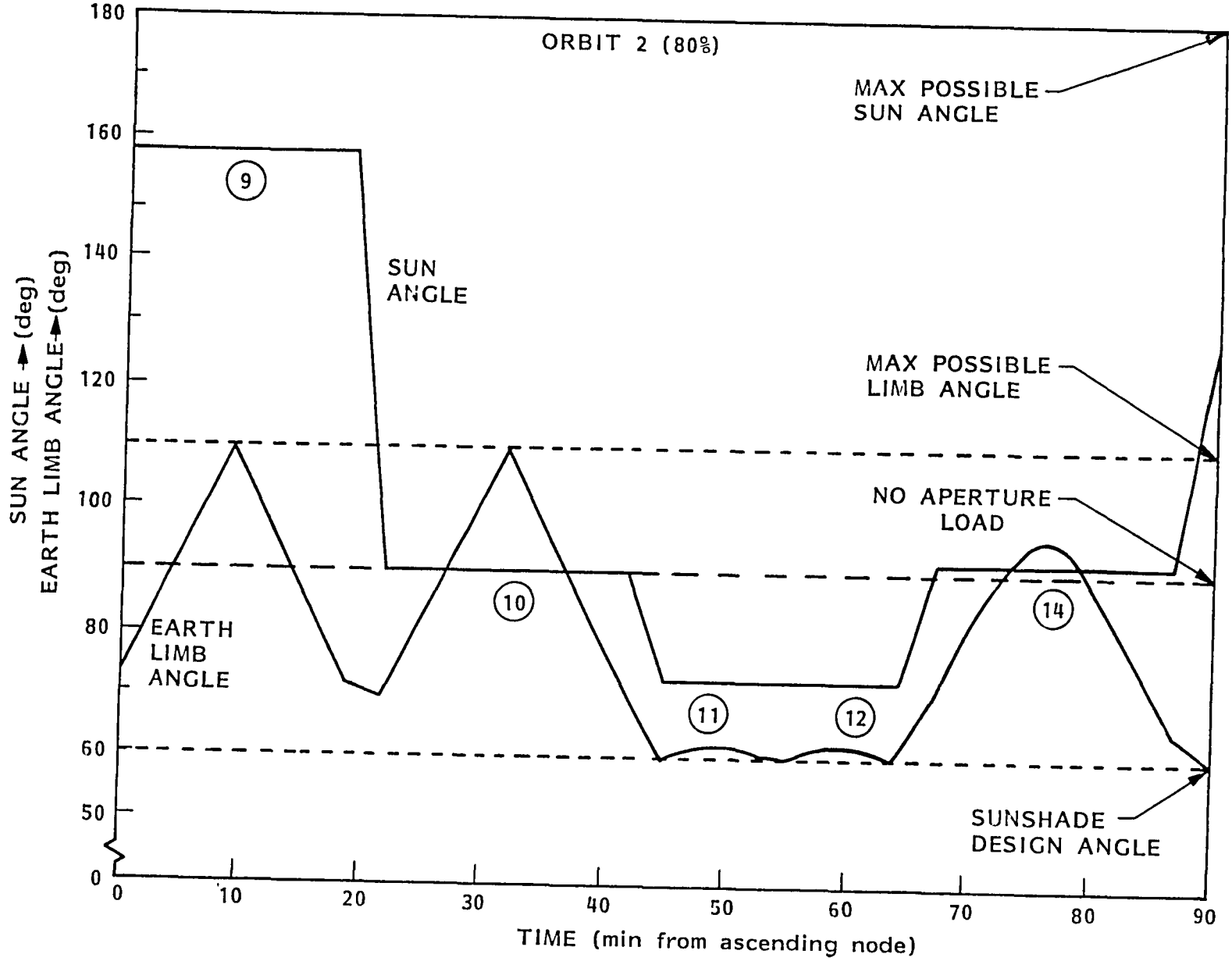

Fig. 4-2 SIRTF Long-Life Reference Mission - Orbit 2

mission. No solar load is imposed until 42 min into the orbit, at which time the telescope begins a 3-min slew from source 10 to 11. This maneuver brings the telescope to within 73 deg of the sun, which is maintained for the entire 19.5-min period required for the consecutive observation of both sources 11 and 12. Subsequent to the viewing of source 12, the telescope begins a 3-min slew to avoidance angles larger than 90 deg for the remainder of the orbit. Although only moderate sun avoidance angles are encountered during this orbit, extended (19.5 min) viewing at the limiting 60-deg avoidance angle to the earth limb is encountered during the viewing of sources 11 and 12.

Coupling the sunshade performance characteristics as given in Fig. 3-6 with the time dependent pointing requirements of the reference mission results in the aperture scattered solar heat load profile given in Fig. 4-3. For orbit 1, a peak heat load of 1.03 W is realized at the limiting avoidance angle of 60 deg, with an orbit averaged value of 0.381 W. The orbit 2 heat loads are considerabely lower, having a peak value of 0.36 W and averaging 0.088 W over the entire orbit. Weighting the contribution of each orbit heat load by its duty cycle yields an effective time-averaged aperture heat load of 0.147 W from scattered solar.

Aperture heat rates were also determined for scattered earthshine and albedo (assuming 100 percent albedo as a worst case). As shown in Fig. 4-4, the time averaged albedo and earthshine scattered aperture heat rates are 0.011 W and 0.006 W, respectively. These time averaged values differ only slightly from the orbit averaged values for the two reference orbits and together represents only 10 percent of the total scattered environmental heat load (solar + albedo + earthshine) into the aperture. Indeed, the total scattered environmental heat load of 0.164 W represents only 17 percent of the total 0.96-W aperture heat load, with the 0.80-W IR sunshade self-emission being the dominant term.

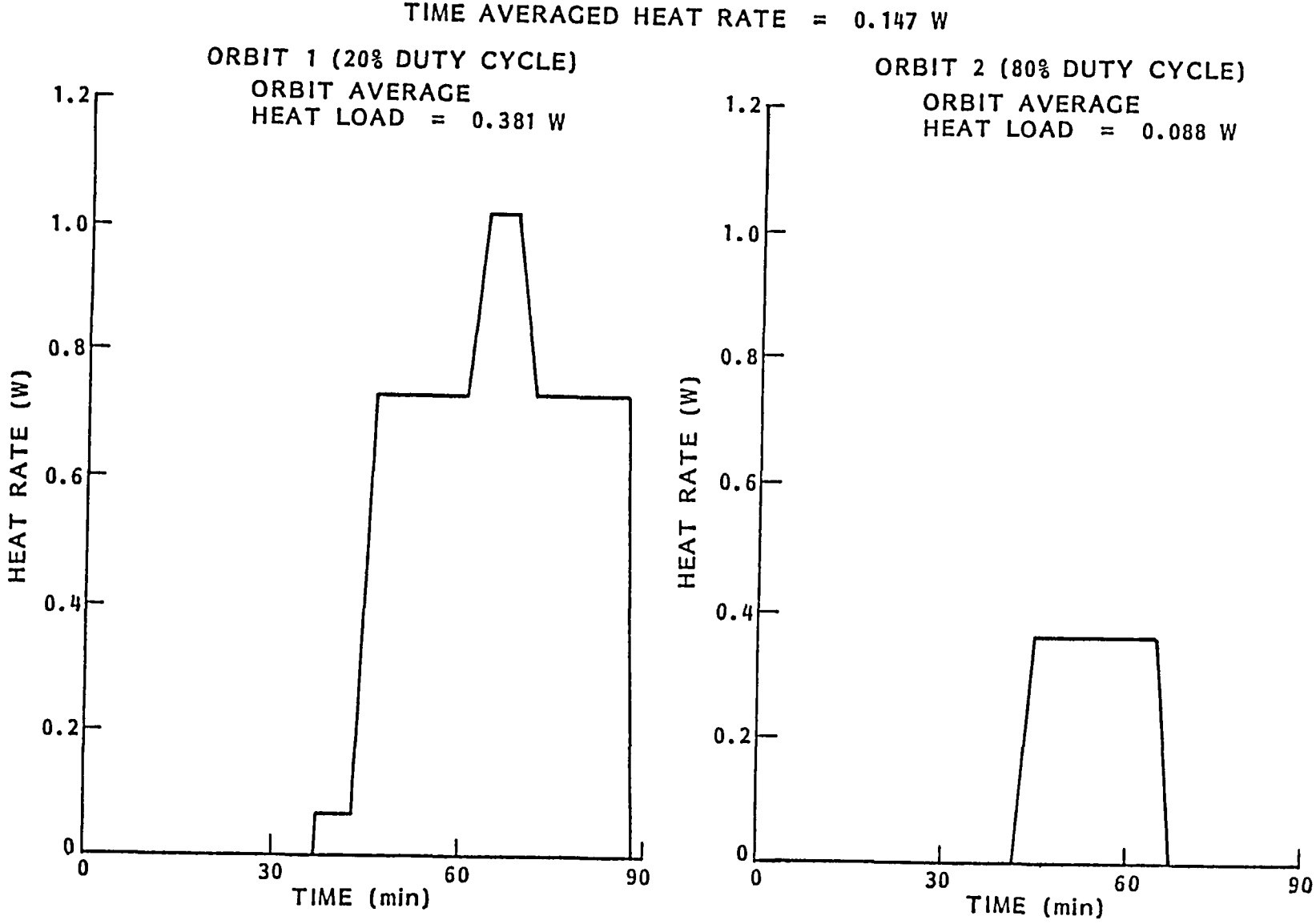

Fig. 4-3 Aperture Heat Load Profile from Scattered Solar (α_s/ϵ = 0.12/0.05, 1 percent Diffuse Scattering Coefficient)

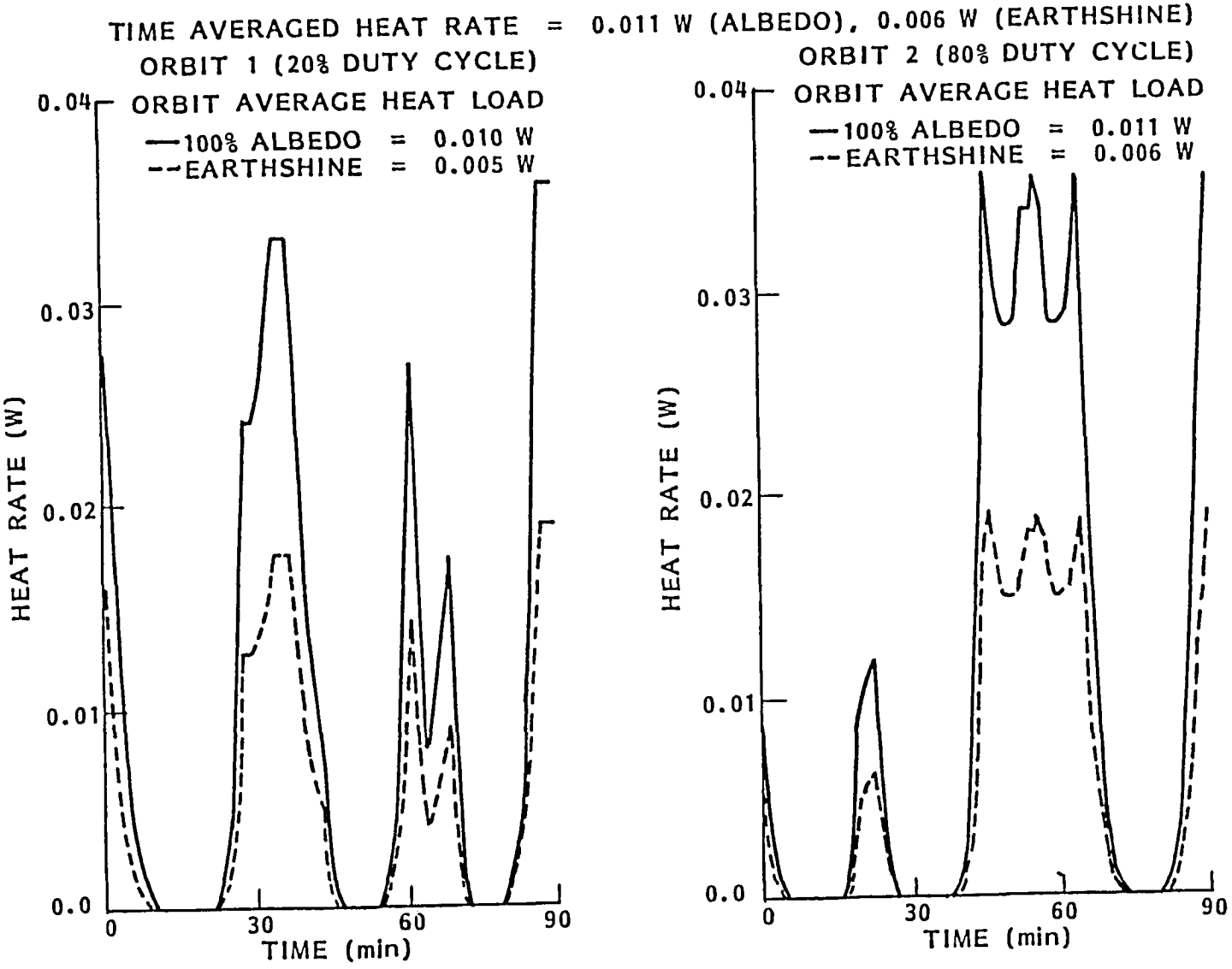

Fig. 4-4 Aperture Heat Load Profile from Scattered Albedo and Earthshine (α_s/ε = 0.12/0.05, 1 percent Diffuse Scattering Coefficient)

4.2 INSTRUMENT HEAT LOAD

Generated power profiles in the MIC were taken from the Phase A baseline, except where additional margin in the design was desired by NASA/ARC.

In the 10 K temperature zone, ER-408 (Design Optimization Study Report, 1979) established a typical timeline in which six instruments are sequenced through a 10-min warmup leading into a 20-min observation period, which is then followed by a 10-min post-calibration.* At any one time, only one instrument is operating, with one other instrument in warmup, and another instrument in a calibration. The power profile for the six MIC instruments is as shown in Fig. 4-5. During the operation phase, the instrument dissipates 0.50 W. Dissipated power reduces to 0.30 W during the warmup and calibration periods, and to finally 0.10 W during quiescent periods. As suggested in ER-408, instruments 4 and 6 (Faint Object Spectrograph and Composite Fourier Transform Spectrometer) are primarily low-temperature instruments which do not dissipate power into the 10 K temperature zone. For these instruments, only a quiescent dissipation of 0.10 W is assessed throughout the entire timeline in the 10 K temperature zone.

The total power dissipated into the 10 K temperature zone as a function of time is shown in Fig. 4-6. Throughout the 120-min period required of observation, the dissipated power varies from 0.80 to 1.20 W, with a time averaged value of 1.0 W. For comparison, the power profile developed for the instruments as given in Table 1-7 in ER-408 is also shown in Fig. 4-6.

Two other temperature zones exist in the MIC which require cooling by the superfluid helium system. The first is a 6 K temperature zone which is vapor cooled by the SFHe boiloff; the second is a < 2 K temperature zone which will be cooled by conductive coupling to the superfluid helium dewar. The generated heat load profile in both temperature zones is shown in Fig. 4-7.

---

* The defined reference mission did not necessarily correlate source observations with instrument operations.

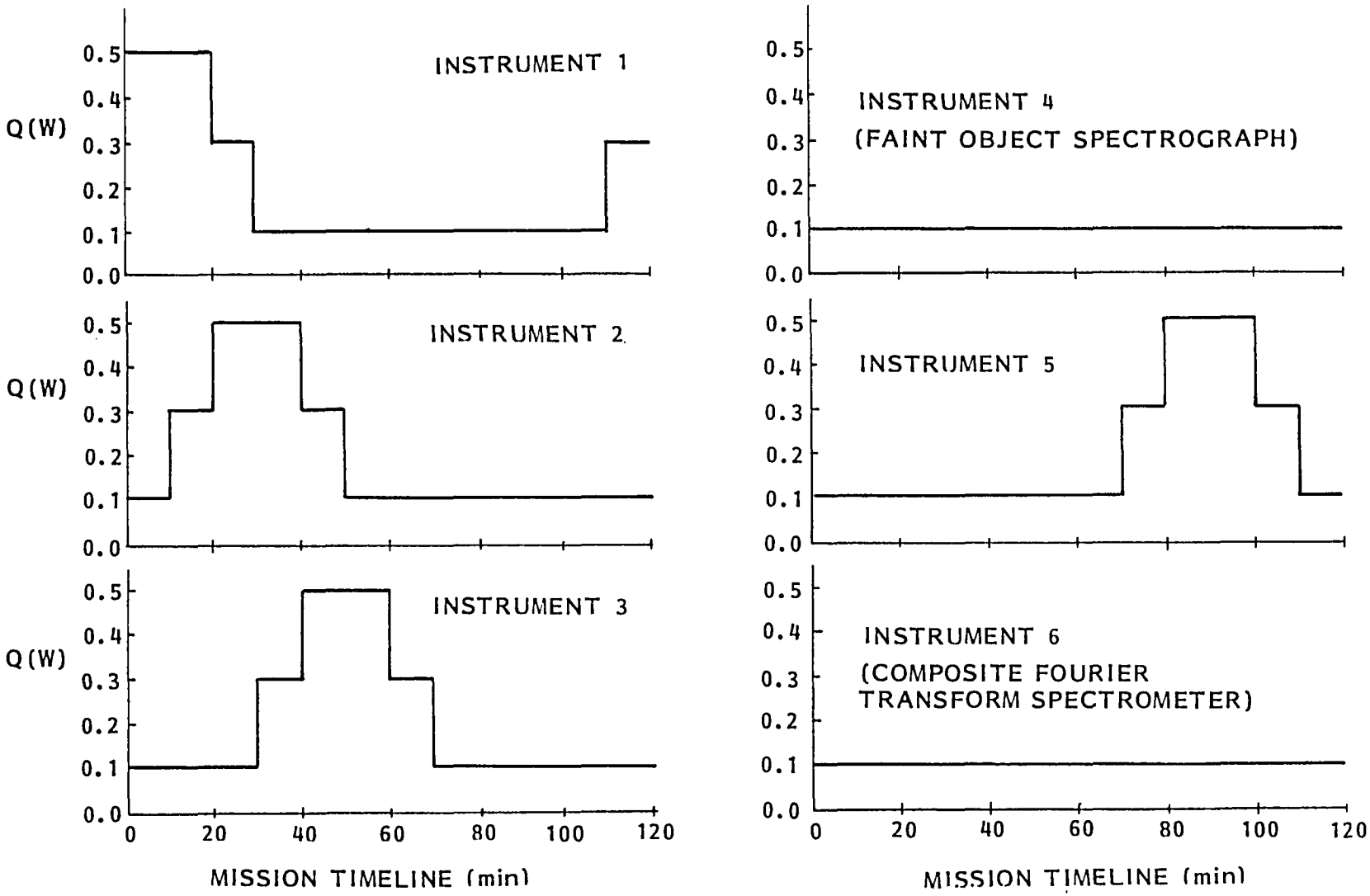

Fig. 4-5 MIC Instrument Heat Load Profile - 10 K Zone

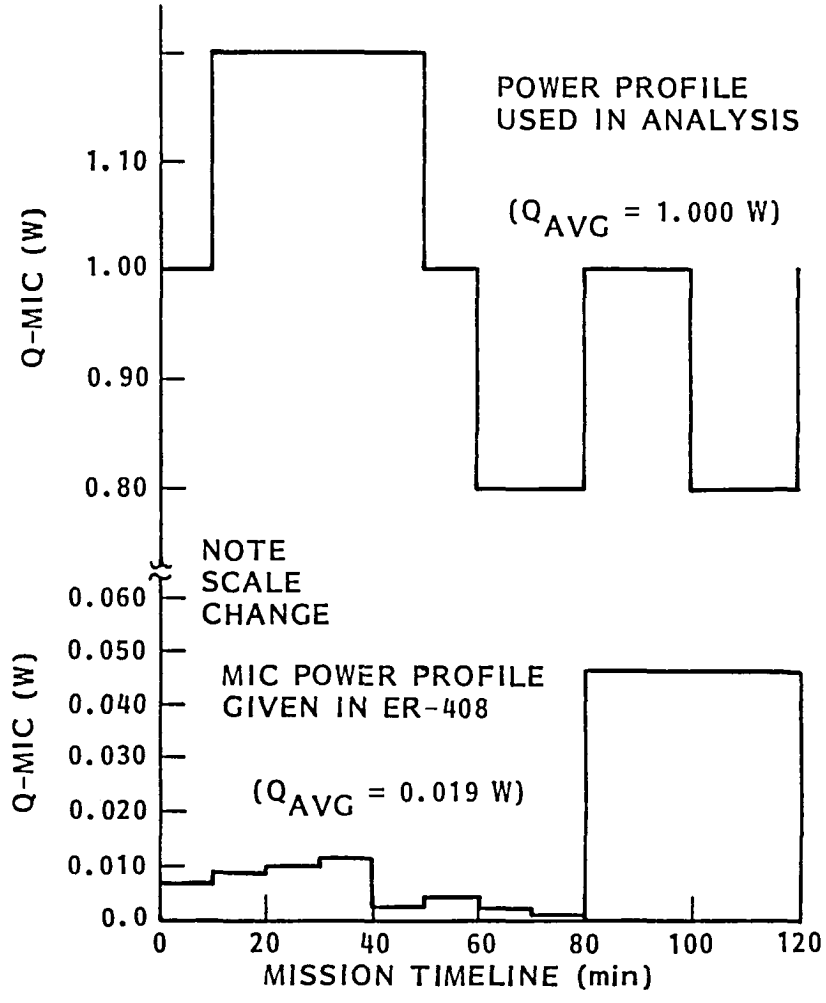

Fig. 4-6 Total MIC Instrument Heat Load Profile - 10 K Zone

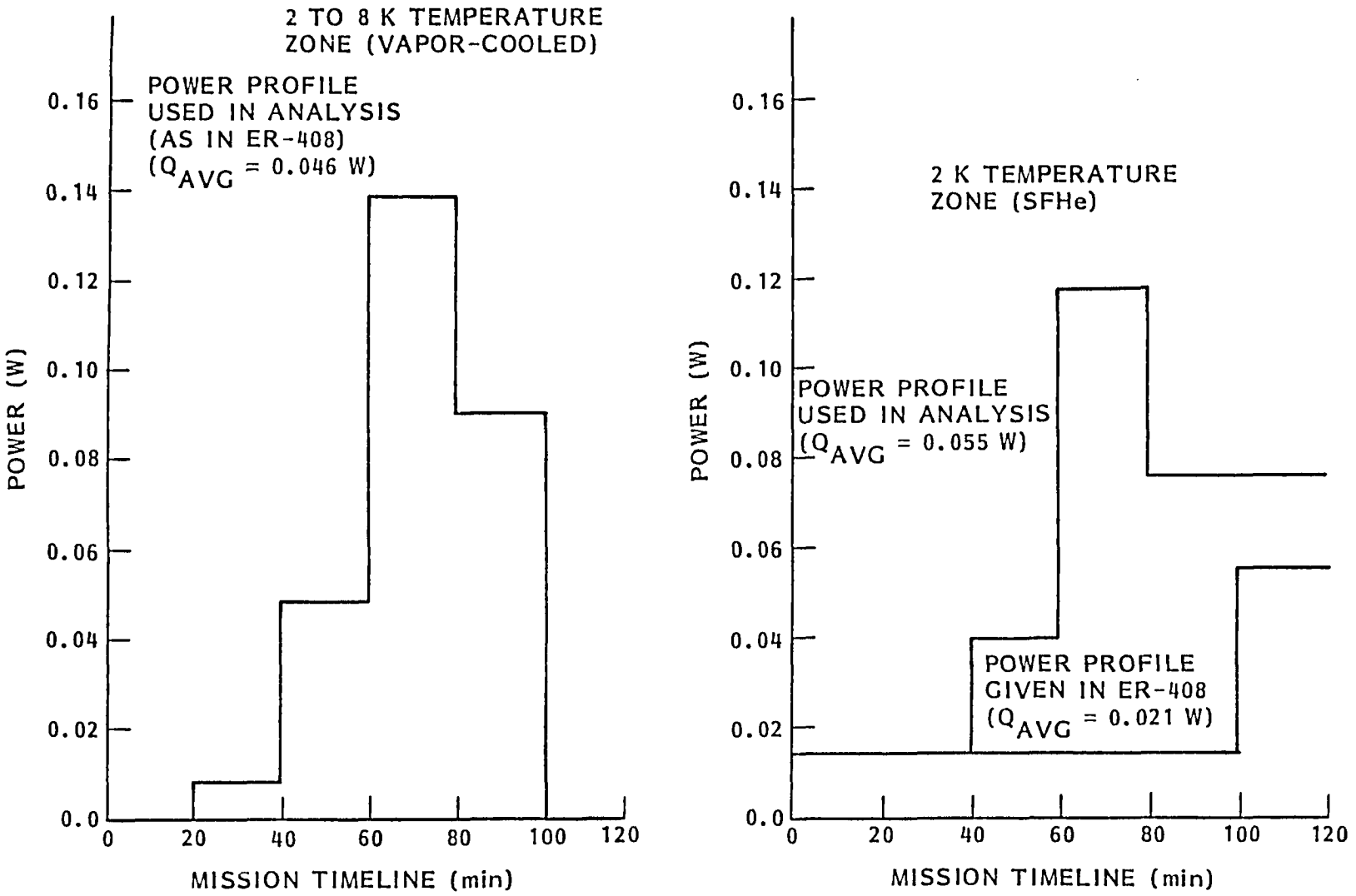

Fig. 4-7 MIC Instrument Heat Load Profile (6 K and 2 K Temperature Zone)

The profile in the 6 K temperature zone is taken directly from ER-408 without modification, giving a time averaged heat load of 0.046 W. NASA/ARC wished to increase the duty cycle from 16 to 50 percent in the 2 K temperature zone for the long life study to provide more design margin. It was determined from the analysis, however, that even for the higher duty cycle, there were periods where additional vapor cooling was needed to provide the required cooling at the 6 K temperature zone. The resulting power profile imposes a time averaged heat load of 0.055 W. Further refinement and tradeoffs will be needed in defining the flight instrument cooling requirements. The 6°K station was provided as an "opportunity cooling" station, but here its cooling needs are seen to drive the design.

The final power source to be identified within the MIC is that generated by the fine guidance sensor. Here LMSC used results derived from the Phase A study, namely, that by carefully balancing a series of thermal links, the heat leak to the 10 K temperature zone could be maintained at 0.10 W while rejecting 0.90 W at an inner vapor-cooled shield. No review of such a design was made in this study.

A summary of the baseline instrument heat rate either absorbed or dissipated at the 10°K temperature zone is given in Table 4-1. An average of 2.27 W results from the time averaged contributions described above.

Table 4-1 BASELINE INSTRUMENT HEAT RATE (10°K TEMPERATURE ZONE)

Item	Heat Rate (W)
MIC	1.00
FGS	0.10
Actuators (Secondary)	0.20
Sunshade Radiated	0.80
Sunshade Scattered Solar	0.15
Sunshade Scattered Albedo + Earthshine	0.02
	Sum = 2.27 W

Section 5
TRADE STUDIES

LMSC has developed a very general one dimensional finite difference computer program (CRYOP) to use in performing preliminary design of cryogen coolers. Inputs to the program include:

- Type of cryogen(s)
- Boundary temperatures (cryogens, radiator-cooled shield, and ambient)
- Type of MLI (DAM/Tissuglas or DAM/Silk Net), layer density, and degradation factor from flat plate performance
- Type of support system - systems available for study include monocoque fiberglass tube bundles (of from one to four tubes) or the LMSC-developed PODS* system
- Axial and transverse static structural loads for sizing the support system for both stress and buckling
- Number of plumbing lines to each cryogen
- Number of vapor-cooled shields between temperature zones
- Instrument heat loads
- Geometry constraints on the tank size, support tubes, and vacuum shell
- Required lifetime

When executed, CRYOP will optimize the design for a minimum-weight cryogen system. Included in the optimization process are:

- The relative location of all vapor-cooled shields within the insulation blanket
- The required thickness of the MLI blanket
- The optimum length and diameter relationships for the cryogen tank
- Preliminary sizing of the support tubes

---

* "Feasibility Study for Long Lifetime Helium Dewar," by R. T. Parmley, NASA-CR166254, Dec 1981.

After the optimization process, CRYOP will then provide as output a listing of the following:

- All input parameters
- Complete description of the optimized geometry, including the vapor-cooled shield location(s), MLI blanket thickness, and cryogen tank dimensions
- Detailed cooler and instrument heat load breakdown by function
- Preliminary weights estimate

CRYOP was used to determine the preliminary size and mass requirements for the long-life SIRTF configuration. A detailed trade matrix was performed for a NBP liquid helium, solid hydrogen, and solid neon system in which the number of vapor-cooled shields was varied from 1 to 3 and where the instrument-generated heat rates from the aperture, MIC (10 K temperature zone), and FGS were varied from 0.50 to 3.00 W (2.27 W being the nominal value for a 1.0 W MIC heat load). Both the state-of-the-art (SOTA) monocoque fiberglass folded tube support system and advanced SOTA PODS configuration were studied for design lifetimes of 6 and 24 months. Warm boundary temperature for the CRYOP trades is taken to be 185 K, which will be provided by a space radiator and radiator cooled shield as described in Section 6. The ambient shell temperature remains at 300°K as for the Phase A baseline, although passive thermal control coatings can be used to reduce this temperature to between 200 to 250°K once in orbit. Because the high vapor cooling realized in the helium systems nearly eliminates the telescope and instrument parasitic heat rates, the helium trade reduced to one in which the instrument heat load was the only true parameter effecting the cryogen mass flow rate. Such was not the case for the hydrogen and neon systems.

In Figs. 5-1 and 5-2, the required cryogen volume and mass (including tankage mass) are as shown functions of lifetime. The configuration for which these curves were derived is one where only a single vapor-cooled shield is used, coupled at the midpoint of a folded monocoque fiberglass support tube assembly. Alternate design configurations will be discussed below. The system which exhibits the minimum volume is the neon system which, for a

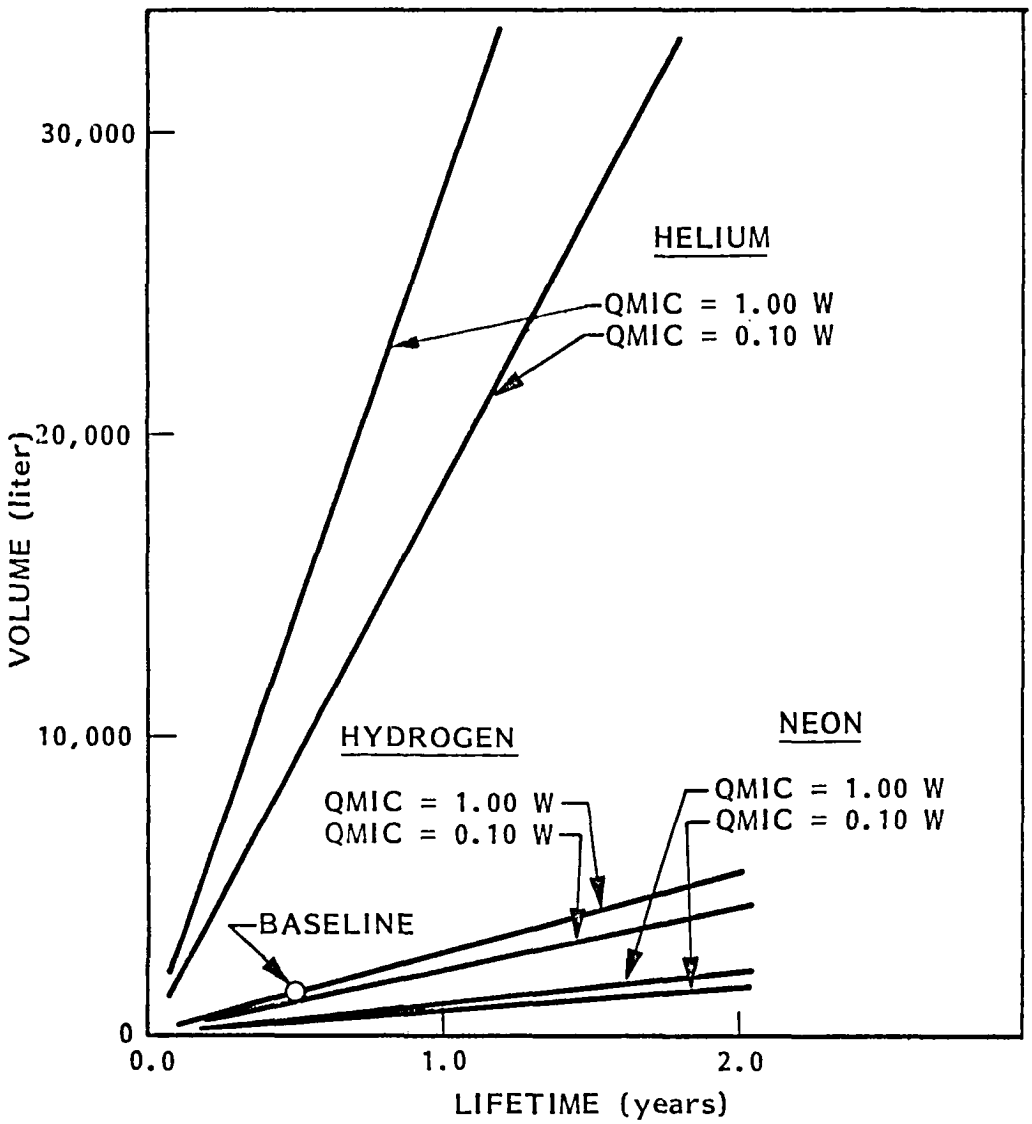

Fig. 5-1 Required Cryogen Tank Volume Versus Lifetime

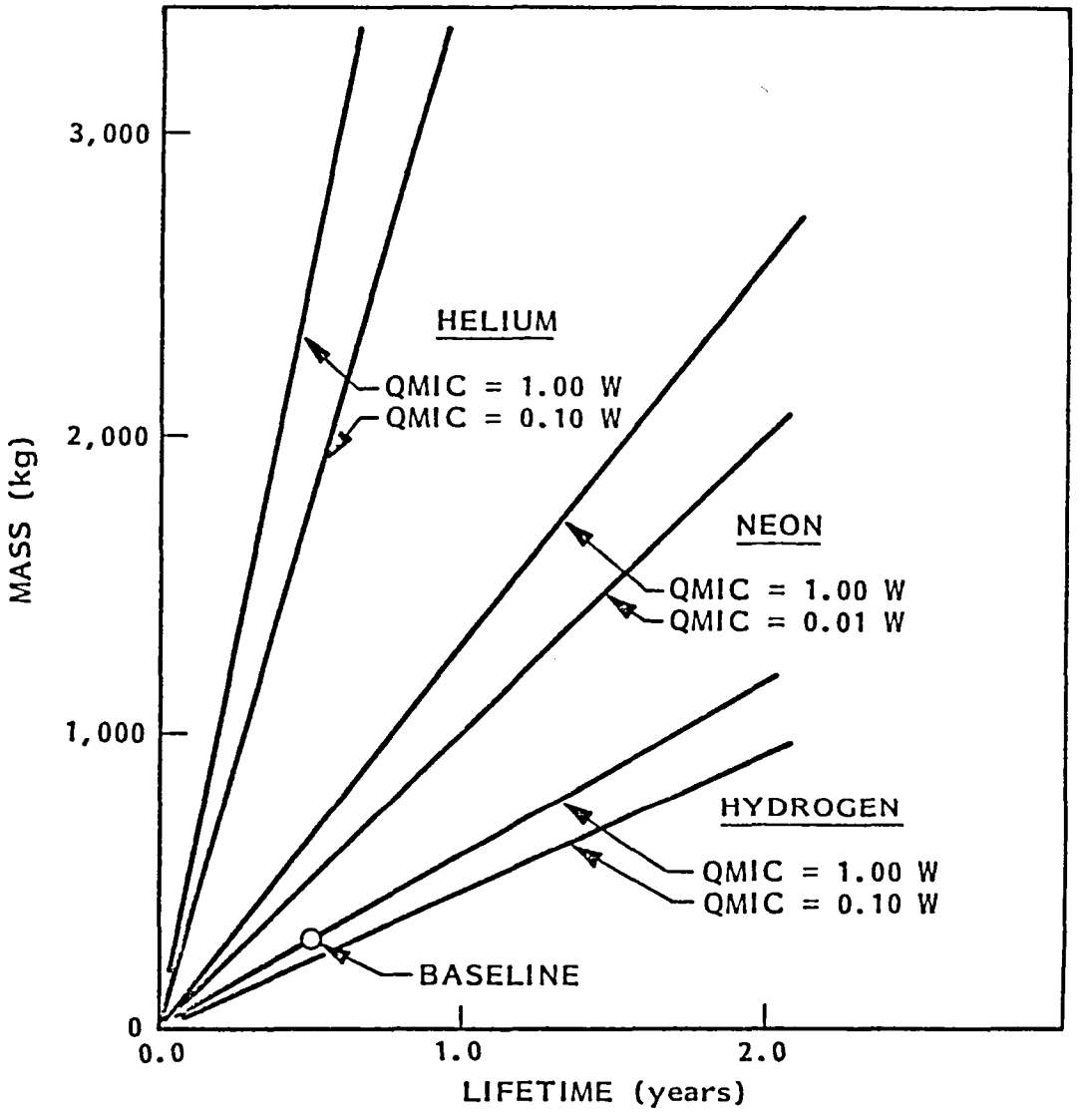

Fig. 5-2 Cryogen (Including Tankage) Mass Versus Lifetime

6-month lifetime at a 1.0-W MIC load, requires 600 liters of cryogen. The volume requirement for the corresponding hydrogen system is higher at 1560 liters, while yet being the lightest of all three systems.

Neon was carried in the trades to see if substantial gains in mass and to a lesser extent volume could be achieved with a warmer (15 K) neon system over hydrogen (8 K). If such gains did exist, there would be some incentive to consider a hybrid hydrogen/neon system in which hydrogen would provide cooling for only the first 30 days, when cooling to less than 10 K is required. For the remaining lifetime of the mission, the subcooled neon would first warm to its 15 K operating temperature after depletion of the solid hydrogen and maintain the optics temperature to less than the required 20 K. As can be seen however, no mass driver exists in favor of neon or a hydrogen/neon hybrid system.

The hydrogen system is seen to be a superior selection on both a mass and volume basis than the helium system; being better than 8.5 times lower in mass (2560 kg versus 300 kg) and 8.7 times smaller in volume (13,600 liter versus 1560 liter). Lifetime extensions of helium to 2 years is clearly unreasonable, with refillable or replaceable cryogen tanks being the only viable approach. Some improvement in the helium system is possible by a more efficient utilization of the vent gas. CRYOP uses the sensible heat to exclusively cool the facility vapor-cooled shields for reducing the dewar parasitics. A more optimal design however would be to use the sensible heat of the vent gas to remove a portion of the 10°K heat load. At best, the effect of a more optimal flow network would be to reduce the mass and volume requirements of the helium system by a factor of 2. Though a sizeable improvement, the hydrogen remains the preferred system from the aspect of size and volume. Only substantial changes in system concept which would reduce the total heat loads as given in Table 4-1 would change this tradeoff.

This analysis did not show any noticeable differences between Sf He, NBP He or ScHe. Earlier studies for SIRTF sortie missions also found little difference in overall performance for types of helium.*

The solid hydrogen system ensures a very stable temperature platform which will remain below 10 K throughout the entire mission. Orbital experience on CO_2, NH_3, and CH_4 solid cryogens have shown that both short-term (orbital) stability to within ± 0.10 K under varying thermal loads and long-term (beginning-life to end-of-life) stability to within 1.0 K can easily be maintained. This latter temporal gradient reflects the change in thermal resistance between the cryogen and instrument as the solid cryogen sublimes away from the instrument interface during its lieftime. Further, the maintenance of this temperature stability is inherent in the simple and highly reliable cryogen flow management system. No flow control valves or other active cold mechanisms of unproven flight quality and reliability are required for either the cryogen management or temperature control.

The only features that detracts from the selection of hydrogen lies in the safety aspect of using a flammable material over the inert helium, giving rise to attendant complications during ground handling and test and the small design temperature margins to maintain 10 K operation.

Through a sequence of technology contracts with NASA/GSFC, LMSC has demonstrated the procedures and safety requirements for filling, operating, and off-loading a solid hydrogen cooler. Results of these studies are feeding directly into the advanced design definition phase of an instrument (CLAES) which is scheduled to fly aboard the Upper Atmospheric Research Satellite (UARS) in 1988. CLAES will be cooled by a 944-liter solid hydrogen cooler, requiring only SOTA technology (as will SIRTF). The testing and safety

---

* Although the trade studies assumed NBP liquid helium, they are still quite accurate in comparing to SCHe. For SCHe at 50 psia, the volume requirement increases from 13,600 liters to 14,200 liters, assuming that the 10 K temperature is maintained only for 30 days, relaxing to 20 K thereafter.

procedures currently being developed for CLAES will also be directly applicable to SIRTF. For example, it has been shown that the cooler plumbing can be designed to accommodate either solid hydrogen or liquid helium during laboratory operations. CLAES has adopted the philosophy that the majority of all ground testing with the instrument can be performed with liquid helium. Solid hydrogen need only be used during the heat rate and acoustic qualification tests. This philosophy can also be applied to SIRTF as all internal plumbing is compatible with operation with either helium of hydrogen.

LMSC also acknowledges that the temperature margin available with solid hydrogen is a critical systems issue. For that reason, the study summarized in Section 8 was performed. There it can be found that the optics can be maintained to less than 10°K for at least the first 30 days in the mission.

In light of all the above considerations, LMSC has selected solid hydrogen as the baseline cryogen for the long-life SIRTF mission.

The effect that other geometries have on the mass and volume requirements are shown in Figs. 5-3 and 5-4. In Fig. 5-3 the cryogen system mass required for a 6-month design life is shown as a function of the number of vapor-cooled shields for both the SOTA and advanced SOTA (PODS) support system concept. In both cases the two vapor-cooled shield systems offered the lowest system mass - but not by a sufficient margin (~ 100 lb) to justify the additional system complexity. A more dramatic change of 490 lb results by using the PODS support mechanism in lieu of the folded tube concept. As seen by the change in cryogen mass of ~ 60 lb at the baseline heat rates, this reduction is not driven by the lower rates and smaller tank size. Rather, the change is due to the different mass of the support mechanism itself.

Because of the lower system mass and impressive thermal performance, PODS is the preferred support configuration for the long-life SIRTF configuration. It was not incorporated into the current baseline, however, because LMSC felt it

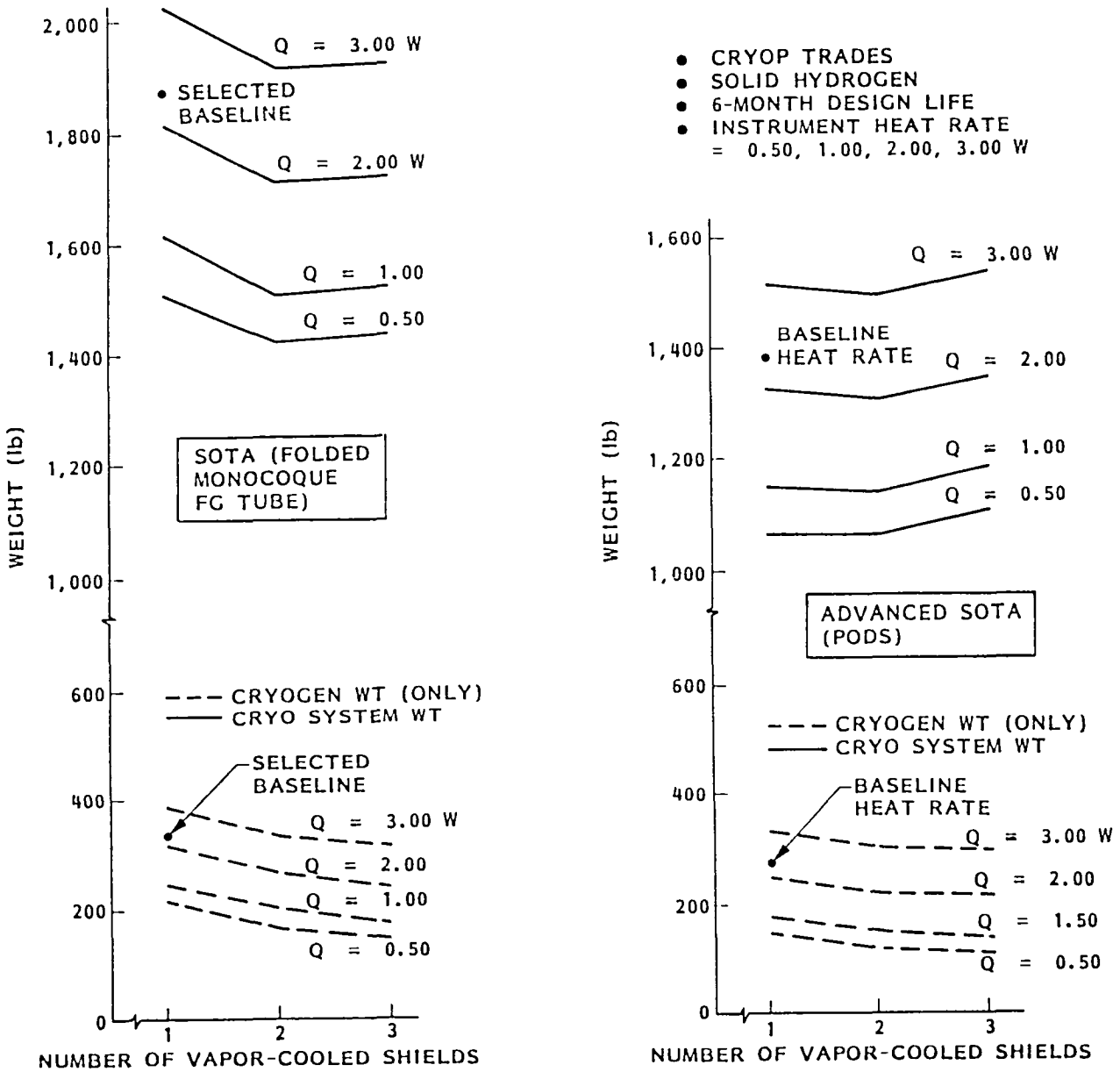

Fig. 5-3 Cryogen System Weight Versus Number of Vapor-Cooled Shields

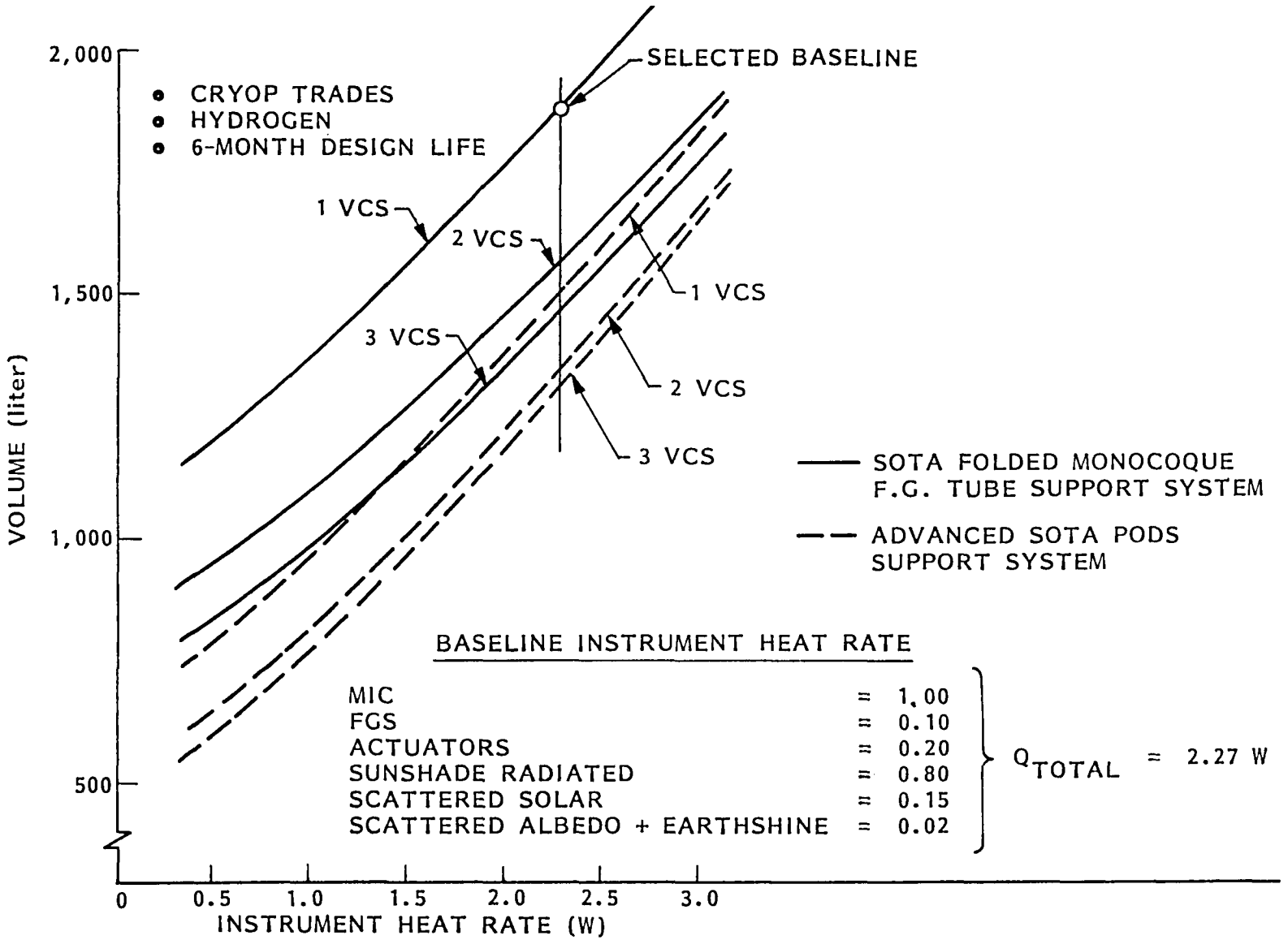

Fig. 5-4 Cryogen Volume Requirement Versus Absorbed and Generated Heat Rate at the 10 K Temperature Zone

was important in this feasibility study to incorporate only demonstrated and conservative technology into the baseline design.

In Fig. 5-4 the tank volume required for the 6-month design is shown as a function of the instrument generated heat rate at the 10 K temperature zone. The volumes as shown were taken directly from the CRYOP trade studies, which include a 20 percent contingency factor for uncertainty in heat rates and a 10 percent ullage. At the baseline instrument heat rates of 2.27 W (1.0 W in the MIC), the required volume for a 6-month mission is 1870 liters (the 20 percent contingency factor is the difference between this figure and the 1560 liters given in Fig. 5-1 for the same operating conditions). Although the mass requirement changed by 5 percent when two vapor-cooled shields are used, a larger 16 percent decrease in the volume requirements is realized. No significant reduction in volume is achieved by adding a third vapor-cooled shield.

The tank configuration identified as best for the long-life SIRTF mission is a toroid contained within the telescope vacuum space, positioned over the telescope barrel between the telescope secondary mirror and MIC optical bench. The trade process which led to this tank configuration is summarized in Fig. 5-5. External tanks such as that configured in the Phase A 15- and 30-day baselines are not practical for a subliming solid cooler. The remote location of the cooler makes direct conduction coupling to the dewar impractical and, because the solid hydrogen operates near 8 K, a very low temperature driver exists to effectively use the sensible heat of vapor cooling. The primary advantage gained by using solid hydrogen lies in the efficient use of the high heat of sublimation, which is wasted by the external tank approach.

Even for the SCHe systems, the concept of adding tanks in modular fashion to increase lifetime soon approaches a point of diminished returns. As an example, Table 3-9 in ER-408 shows that the cryogen flowrate realized during the standby mode is 0.030 g/s. If this flowrate represents the minimum boil-off from the dewar due to its system parasitics, then the maximum cryogen

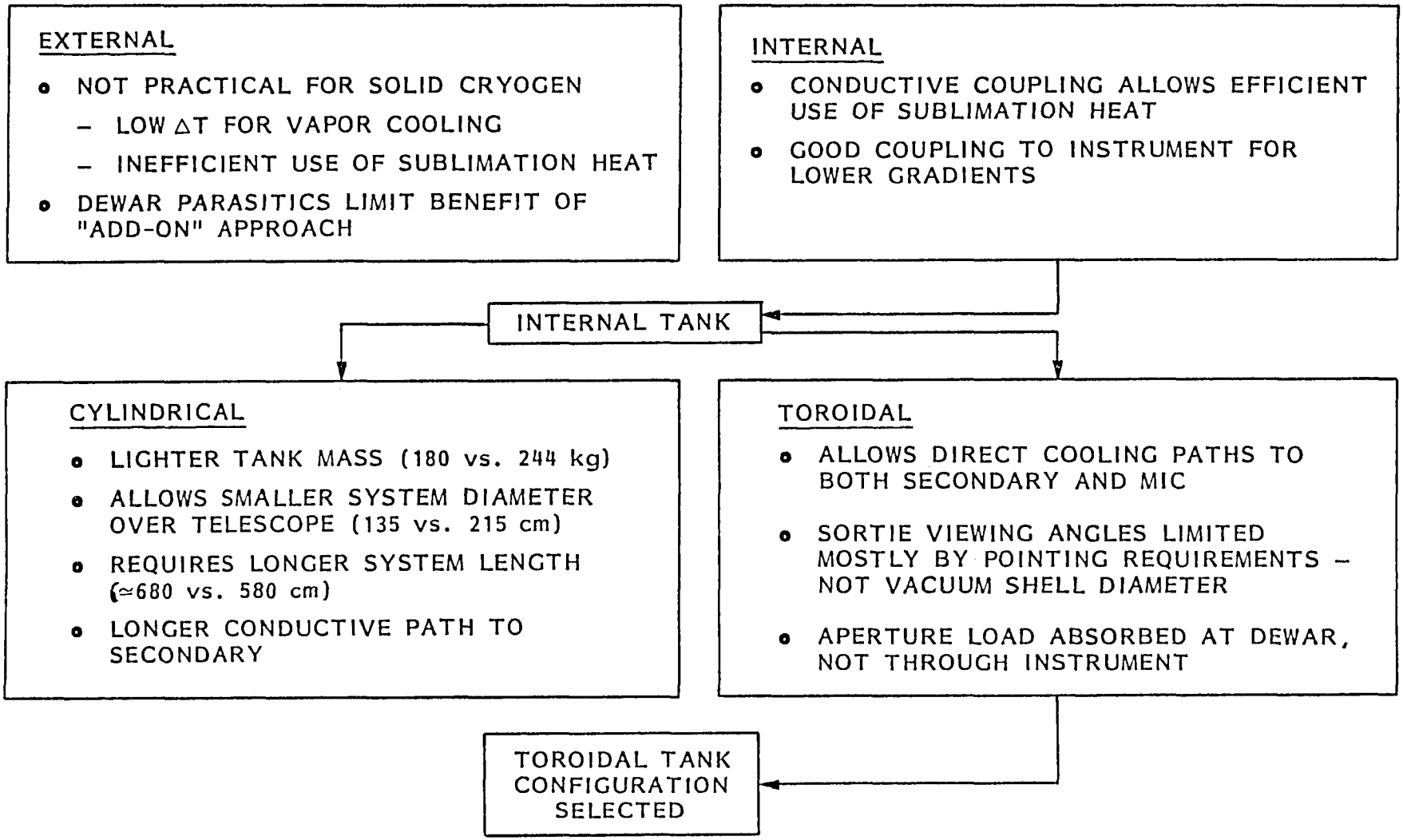

Fig. 5-5 SIRTF Long-Life Mission Tank Configuration Trade Matrix

lifetime obtained from the dewar is 2.5 months for two 1300 liter tanks. Increasing the number of tanks by some factor N increases the available flowrate to the instrument by the same factor N, but the lifetime provided by the cryogen system remains invariant at 2.5 months. Helium storage in a single large spherical tank with advanced technology thermal isolation could improve this lifeline tank noticeably but the high volume required for the SIRTF heat loads still makes helium impractical.

For the SIRTF long-life mission, an internal tank is preferred because a more direct conductive coupling can be achieved (which translates directly to lower system temperature gradients), and because a more efficient utilization of the heat of sublimation can be accomplished. With an internal tank, either a cylindrical or toroidal tank geometry can be employed by SIRTF.

A cylindrical tank has definite advantages over a toroidal tank in mass (180 versus 244 kg) and diameter (135 versus 215 cm). The cylindrical tank produces longer system length by about 100 to a value of ~ 680 cm because the tank must be located behind the MIC. However, length is not a major system constraint for either the SIRTF sortie or long-life mission. The primary reason for not employing a cylindrical tank lies in the fact that cooling of the secondary mirror is considerably more difficult with a cylindrical tank. The toroidal tank allows cooling to be accomplished directly at the base of the spider assembly, which was found to be necessary to ensure that the secondary mirror temperatures could be maintained to below 10 K (see Section 7.1). A second benefit of wrapping the cooler about the telescope barrel occurs by allowing the varying aperture heat load to be absorbed at the cooler, without having to be transported through the telescope structure to a rear mounted cryogen tank. This feature of the design greatly dampens the temporal temperature gradients experienced by the primary and secondary mirrors.

The toroidal tank will impose a larger system diameter than will a cylindrical tank mounted aft of the instrument. In Figs. 5-6 and 5-7 the deployed SIRTF telescope is shown at the limits of excursion in both azimuth and elevation

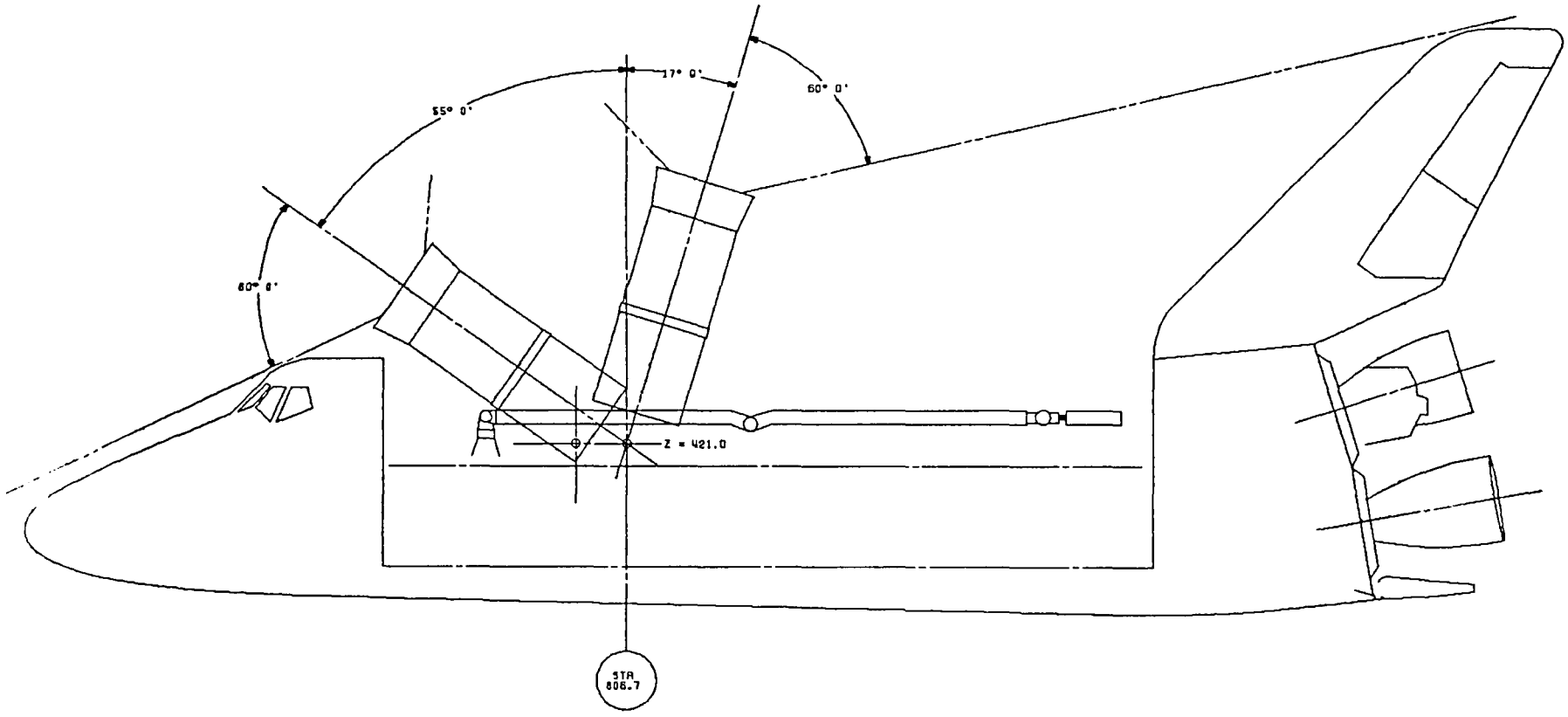

Fig. 5-6 SIRTF Viewing Angles - Elevation

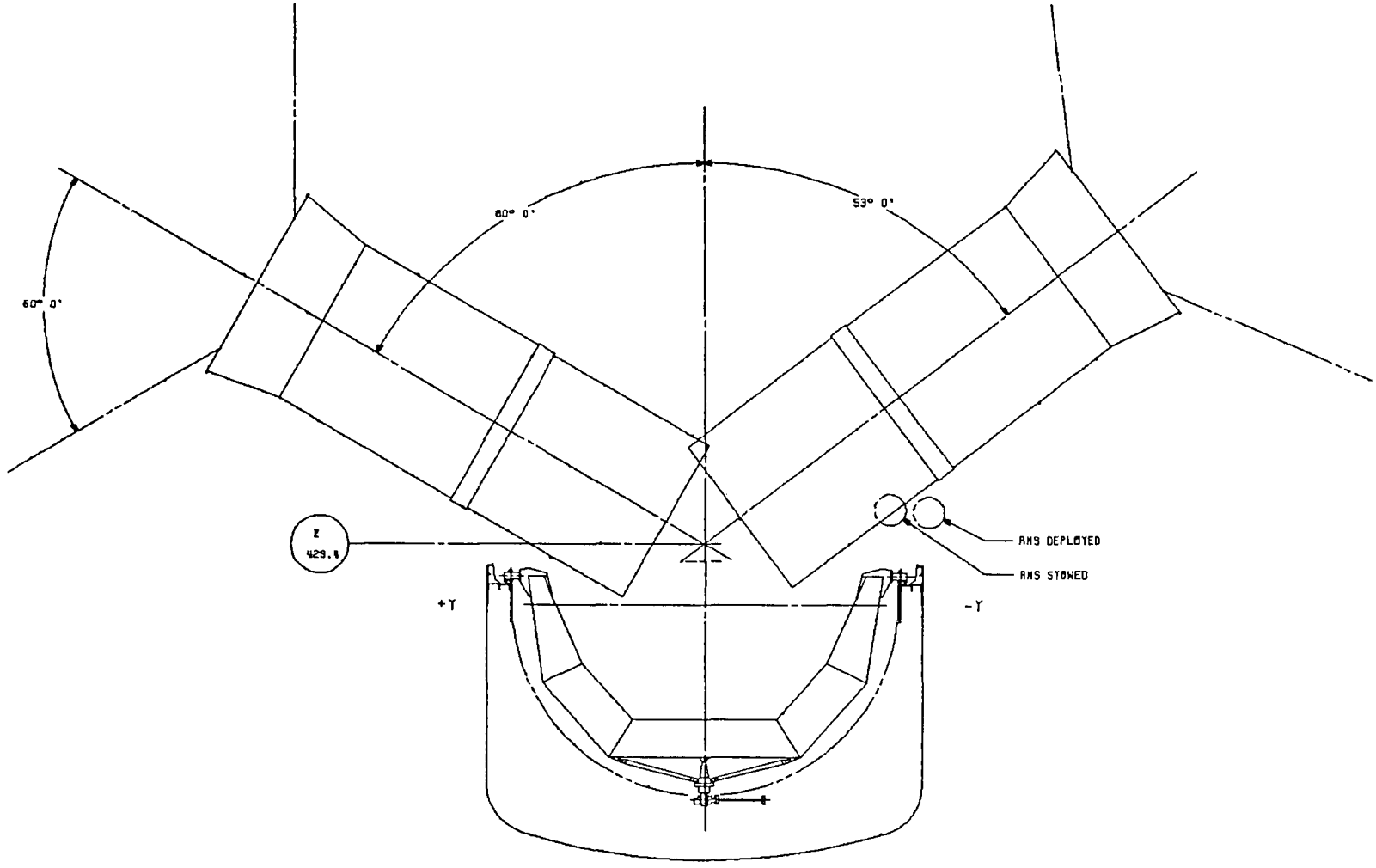

Fig. 5-7 SIRTF Viewing Angles - Azimuth

direction for this larger diameter. As can be seen, elevation angles are limited not by structural interferences caused by the vacuum shell diameter but rather from the instrument pointing constraint that no structure lie within 60 deg from the telescope axis dictates the elevation limits. If the telescope is allowed to view to less than 60 deg from the telescope axis, then the aperture has a direct view factor to warm structure, resulting in large thermal loads to the fore-baffle. A total view angle of 72 deg is allowed, which compares to the Phase A allowable of 90 deg. Interestingly, the reduced range results from the shorter telescope length achieved by relocating the warm electronics and shortening the sunshade/fire baffle for the 60 deg design criteria. In azimuth, the same ± 60 deg of travel is allowed as for the Phase A baseline, provided the remote manipulating structure (RMS) is deployed. That should not be a problem though, since the RMS will probably not fly aboard a SIRTF-dedicated shuttle launch.

Section 6
BASELINE CONFIGURATION

A layout of the long-life SIRTF baseline configuration is shown in Fig. 6-1. The facility is contained within a cylindrical volume 252 cm in diameter by 717 cm long, of which 580 cm measures from the entrance aperture to the aft surface gimbal interface plate. By comparison, the long-life design is only 26 cm larger in diameter at the entrance aperture than the Phase A, 15-day baseline configuration (226 cm), while being shorter by 173 cm.

In the development of the long-life SIRTF configuration, certain features of the Phase A design were taken to be fixed by contractual requirement. These include the telescope optical system geometry (mirror 85-cm diameter, f/24 system, f/2.3 primary), the MIC optical bench and beam switch configuration, telescope metering structure and mirror mounting technique, and the fine guidance sensor configuration. Outside of these constraints the design was free to evolve as best suited to maximize the long-life performance.

The long-life SIRTF design provides three separate cooling platforms for use by both the instrument and telescope facility: superfluid helium, solid hydrogen, and a space radiator system. In addition, vapor cooling from both the SFHe and SH_2 is used for cooling at two separate temperature zones.

The SFHe is contained in a 350-liter toroidal tank which is mounted within the MIC assembly by a single fiberglass support tube. Instrument cooling at 2 K is achieved through flexible copper straps which conductively couple the instrument to the dewar. The SFHe boil-off is routed from the dewar to a 6°K heat station. From this point, the flow is directed to a vapor-cooled shield which surrounds the entire 10 K temperature zone, including the solid hydrogen tank, telescope forebaffle, and MIC housing.

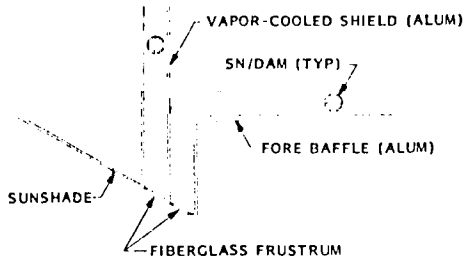

DETAIL A, MLI BLANKET TERMINATION

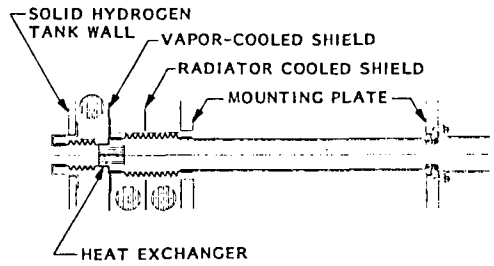

DETAIL B, ORBITAL VENT LINE

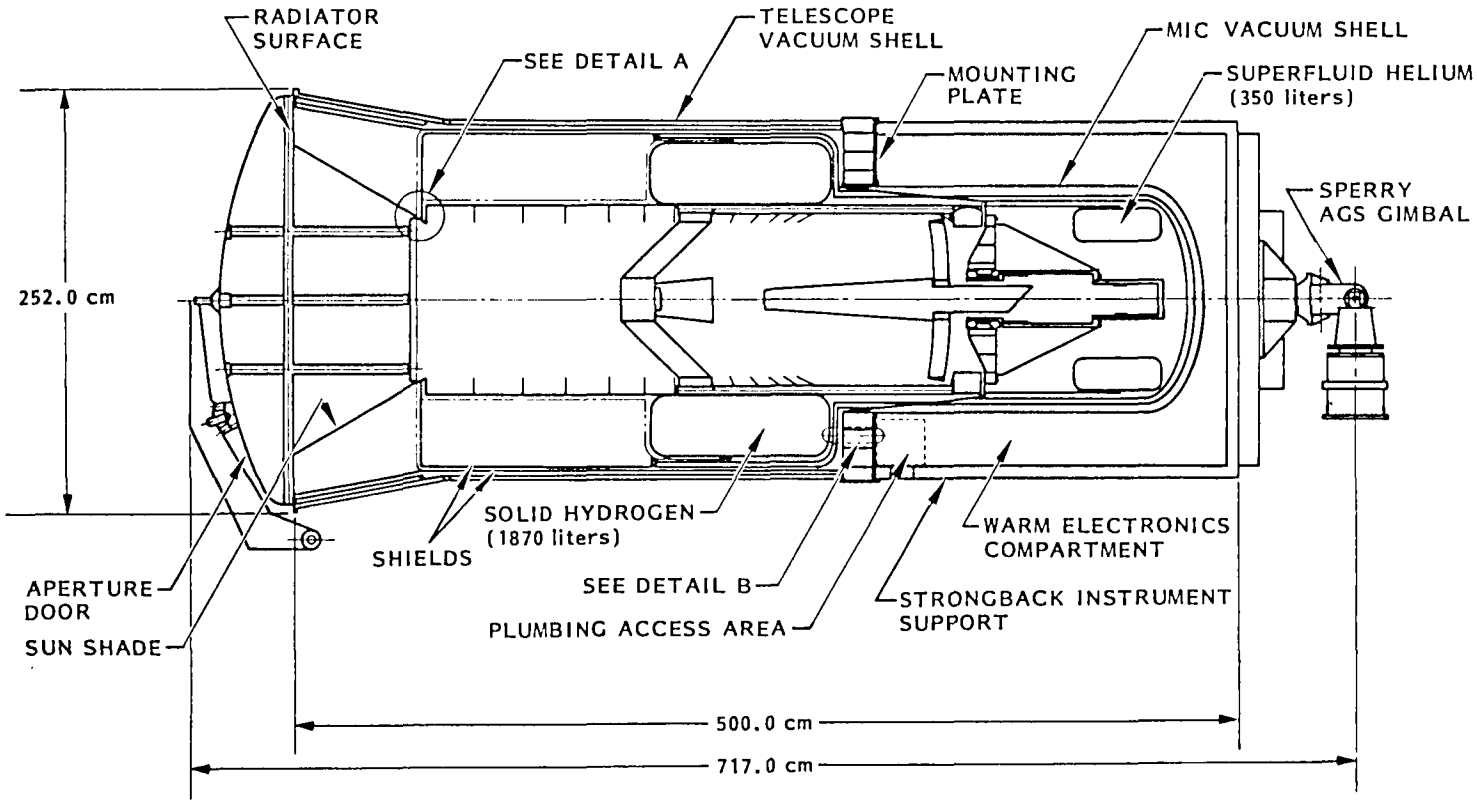

Fig. 6-1 SIRTF Baseline Configuration

The solid hydrogen is contained within an 1870-liter toroidal tank. Internal to the tank is a 1.7 percent dense aluminum foam heat exchanger which is used to reduce the internal temperature gradients as the hydrogen sublimes away from the tank walls. The hydrogen tank is located over the optics metering structure, extending just into the region beyond the secondary spider assembly towards the optical forebaffle. The tank outer diameter and length were taken directly from the CRYOP trade studies for the minimum mass configuration.

Instrument cooling is provided through a 101-cm diameter by 0.127-cm thick copper tube which extends from a flexible braid/shrink fit assembly near the dewar aft inner wall to the primary mirror mounting ring within the MIC assembly. Cooling of the secondary mirror is augmented by a flexible coupling between the base of the spider arm assembly and the dewar wall. In this same area of the dewar the forebaffle is epoxy bonded to the dewar to allow the varying environmental heat load to be absorbed directly by the cryogen and not through the optical structure.

Vented hydrogen vapors are routed through a short section of plumbing to a compact heat exchanger which is coupled to the vapor-cooled shield described above. No further hydrogen vapor cooling is utilized downstream of the heat exchanger.

Support of the tank relative to the main mounting plate is provided through a folded monocoque fiberglass tube assembly containing two tubes. At the fold point the vapor-cooled shield is supported.

The sunshade was made internal to the vacuum shell to eliminate solar heating of its external surface, with the vacuum cover then moved to the forward surface to provide complete sealing for contamination and dust control. For a free flyer the vacuum cover would be discarded on orbit. Return from orbit would occur after cryogen depletion, so that contamination and condensation would be less significant, and a replacement cover could be brought with the recovery mission. For a sortie or space station mission the cover would hinge as shown to a payload bay or pallet structure. Only in the sortie mission

would this cause difficulties in heat load, and then only when the telescope is being stowed for return. The quick-closing concept for transient contamination problems in a shuttle mission could be provided by a lightweight barn door cover, probably in two pieces, for sortie missions. However, this is not needed for space station or free flyer missions and was not specifically addressed in this study.

Alternatively, a gate valve could be used behind the sunshade as in the Phase A concept. This would require a separate sunshade dust cover, neither of which are needed for the long missions, and both of which add significantly to the telescope moment-of-inertia (a problem for pointing and attitude control subsystems).

The sunshade will absorb a portion of the incident energy to its surface. In Fig. 6-2 the absorbed sunshade solar heat loads for the two reference mission orbits are shown, with an orbit averaged heat load of 70.5 W determined for orbit 1 and 21.8 W for orbit 2. The time averaged sunshade solar heat load is 31.6 W. Albedo and earthshine contribute another 3.1 W averaged heat load to drive the total time averaged sunshade heat load to 34.7 W. This load is too large to be accommodated reasonably by even an efficient cryogen such as solid ammonia, and because of the low emissivity of the sunshade surface it does not efficiently reject this heat load itself by reradiation.

To remove the absorbed sunshade heat load a passive radiator will be used, which is the same approach taken by the Phase A SIRTF design. Unlike the Phase A radiator concept, however, where the outer surface of the sunshade is used as the radiator surface, the long-life SIRTF configuration places the radiator at the forward edge of the sunshade, lying in the plane of the entrance aperture. Although this design forces the envelope diameter to increase slightly, lower radiator temperatures can be achieved because of the favorable pointing geometry in which the sun and earth limb avoidance to angles greater than 60 deg are maintained.

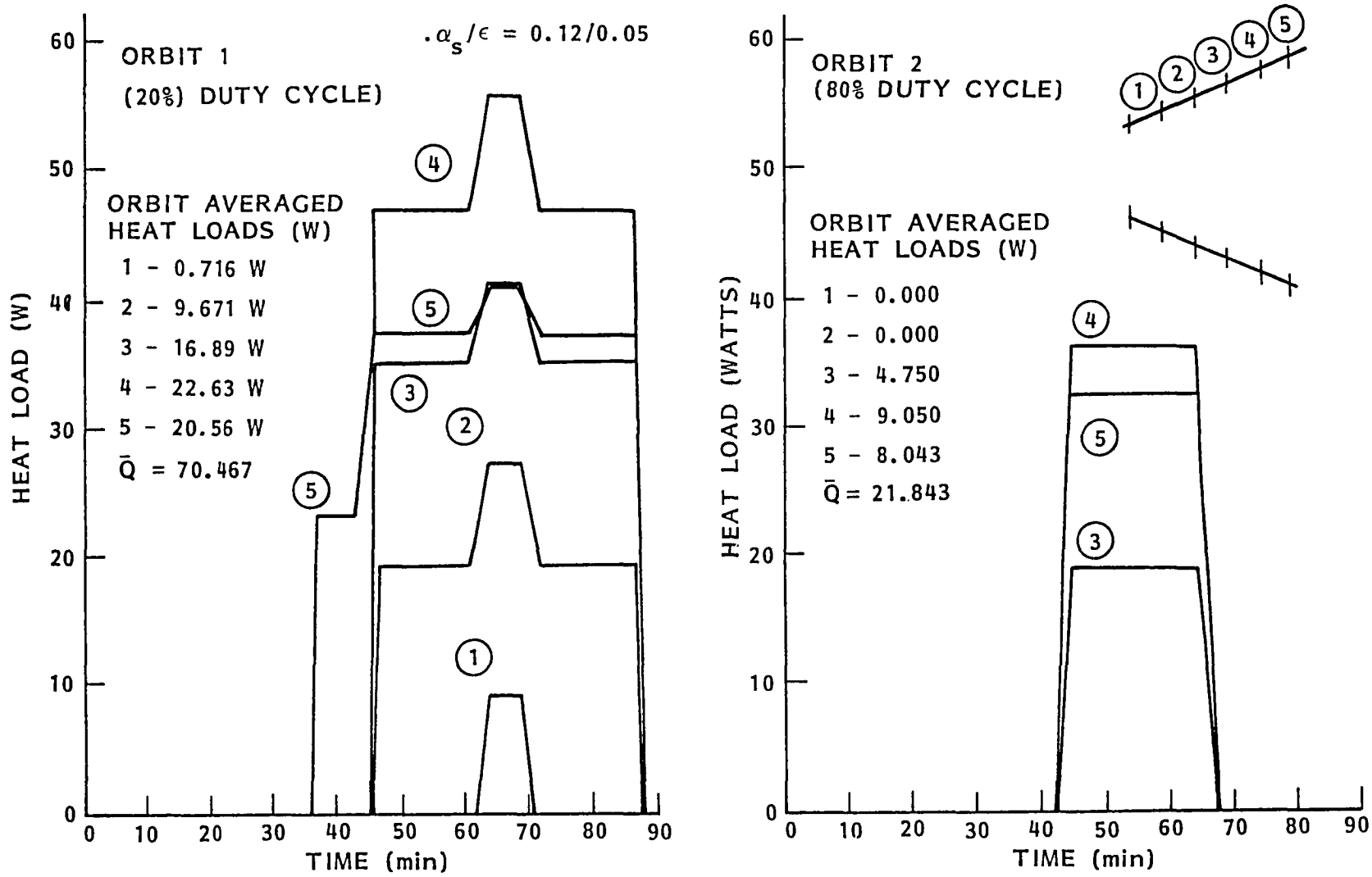

Fig. 6-2 Sunshade Absorbed Solar Heat Load (α_s/ϵ = 0.12/0.05)

For the reference mission the incident solar, albedo, and earthshine heat loads are shown in Figs. 6-3 and 6-4. Using an optical solar reflector with end-of-life (EOL) optical properties of α_s/ε = 0.16/0.86, the averaged net absorbed radiator heat load will be 43.0 W (267.4 W average insolation x 0.16 absorption = 42.76 W), with a total averaged radiation heat load of 77.5 W when the sunshade average heat load is included. The baseline radiator was sized to provide 91.2-W cooling (a 15 percent margin) at a temperature of 185 K, assuming an 80 percent radiator efficiency. An area of 1.92×10^4 cm^2 (240-cm OD by 182-cm ID) results. The OD would be 8-cm smaller without the 15 percent margin.

From the back of the radiator, a shield extends over the cooler and instrument to reduce the parasitic heat loads into the vapor-cooled shield and solid hydrogen dewar. Between all major temperature zones, thermal isolation is provided through a MLI blanket insulation system of silk-net/double aluminized mylar (SN/DAM). CRYOP determined that the minimum system mass was derived for a blanket thickness of 5.1 cm between the radiator-cooled shield and 10 K temperature zone with the vapor-cooled shield placed at the mid-point of the blanket. This optimum thickness was maintained throughout the system, except in the area of the solid hydrogen tank. Here, the gap was increased to 7.6 cm in order to more easily accommodate the dewar support tube assembly. Thickness of the blanket over the radiator-cooled shield was taken to be 1.3 cm. CRYOP does not calculate blanket edge effects; additional studies will be required to assess this.

For ground tests and operations prior to launch, an aperture door is required to maintain vacuum integrity, while at the same time imposing only a modest thermal load on the cryogen system. The selected door configuration shown in Fig. 6-1 is a warm oblate spheroid which presses against the telescope vacuum shell through an O-ring vacuum seal. Support of the door when open is through an arm which is hinged through a swing mechanism contained on a separate pallet from the one supporting the SIRTF gimbal system. Once closed and sealed, the arm is required to retract slightly to the point where launch loads are not transmitted through the arm to the telescope and cover door.

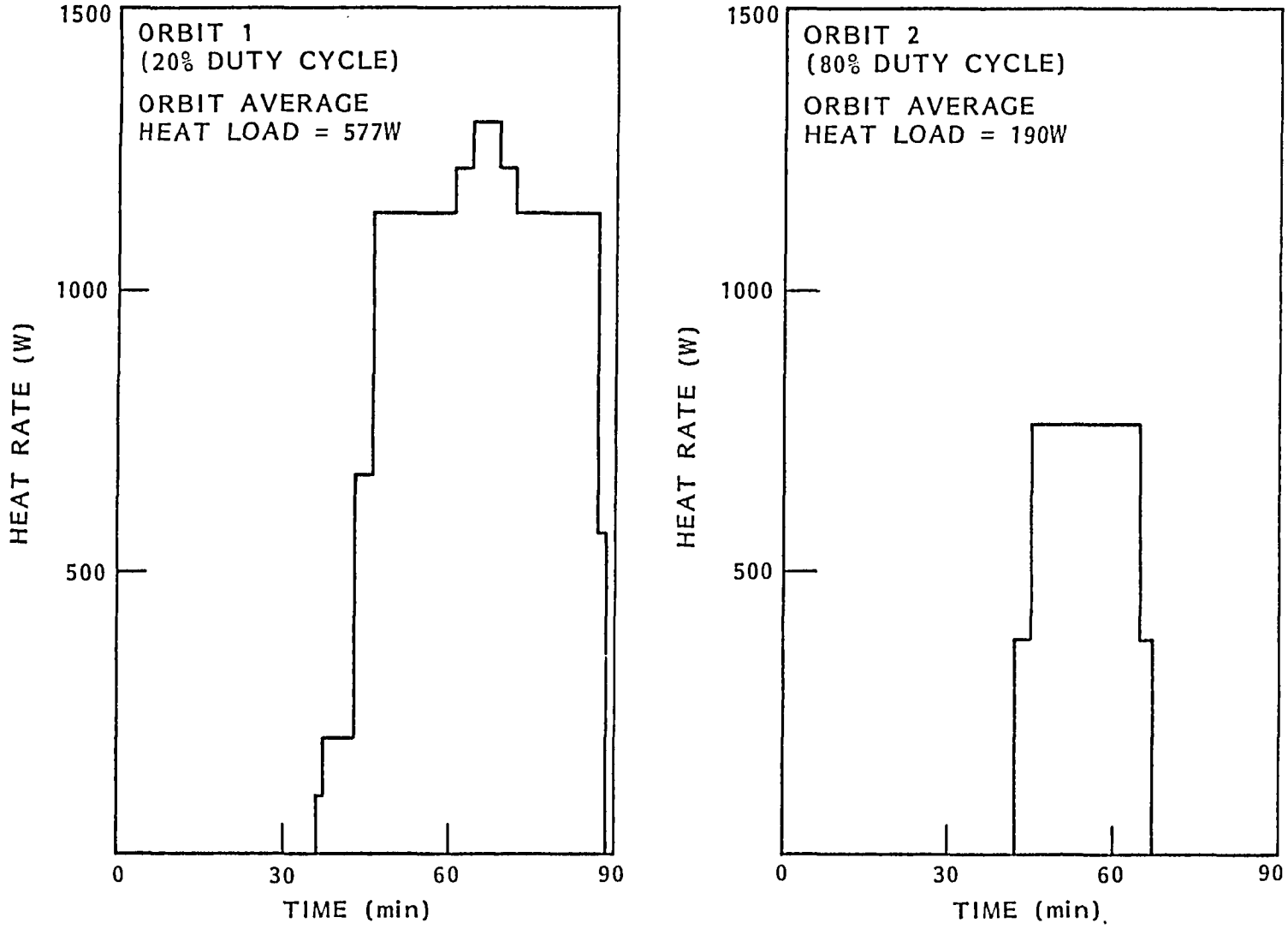

Fig. 6-3 Incident Solar Radiation to Radiator Surface
(α_S/ε = 0.16/0.86; Area = 1.92 x 10^4 cm^2)

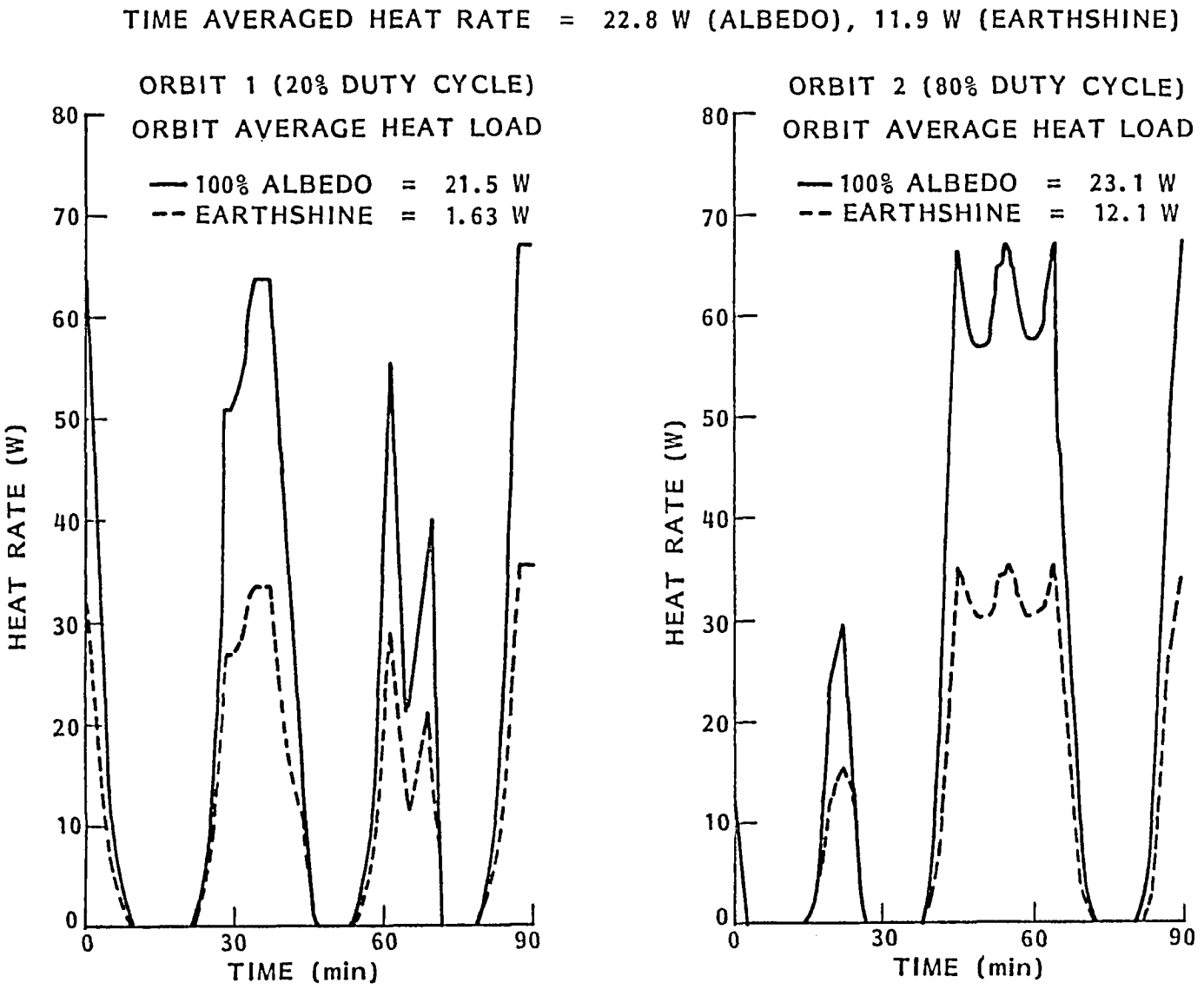

Fig. 6-4 Incident Albedo and Earthshine to Radiator Surface
(α_S/ϵ = 0.16/0.86; Area = 1.92 x 10^4 cm^2)

Thermal isolation of the aperture door to both the 10 K fore-baffle and radiator surface is maintained by two 1.3-cm thick SN/DAM insulation blankets. These blankets are supported off a thin aluminum shield which is held in place off the warm aperture door through several thin walled fiberglass tubes struts. The low thermal mass of this system avoids the use of an aperture cover cryogen system, but that would also be feasible for long life missions.

The MIC optical bench is supported by a fiberglass frustrum of a case which terminates on the main mounting plate. This mounting plate is a 20.3-cm thick annulus, egg-crated for lightness, through which all SIRTF-generated structural loads are directed. A "strong back" load transfer structure, which could be either a honey-combed cylinder or tubular truss, supports the main mounting plate to the Sperry AGS gimbal course pointing system. For a free flyer this structure would be removed and the mounting circle at the main plate used to attach a toridal spacecraft structure, keeping the S/C near the telescope center of mass.

Within the envelope defined by the strong back and SIRTF vacuum shell, an area is provided for access to the cooler plumbing lines (for ground servicing) and for location of the instrument warm electronic boxes. Placing the warm electronic boxes outside the vacuum space eliminates a major contamination risk to the cold optics, which LMSC feels is necessary for SIRTF. The Phase A design drawings show the electronics ambiguously within the vacuum shell.

From a user's standpoint, easy access to the instruments in the MIC is mandatory. The strongback configuration of the baseline provides the needed access and refurbishability. The vacuum shell over the MIC assembly can be removed without disturbing the insulation space over the cooler and without having to disconnect plumbing or electrical connections. The extensions of the radiator-cooled and vapor-cooled shields as well as a 10 K temperature zone boundary shield terminates at the MIC optical bench support tube in a male shrink fit connection. When warm, these connections open, allowing the shields with their insulation blankets to be removed. Access to the SFHe

dewar is now available, with limited access to the MIC instruments also possible. After disconnecting the SFHe plumbing lines in the MIC cavity, the SFHe dewar and support tube may be removed to give complete and unobstructed access to the MIC instruments.

To characterize the performance of the long-life SIRTF system described above, a detailed thermal math model of the long-life SIRTF configuration was generated. The model contains 157 nodes, connected in a network containing 400 conduction resistors and 25 radiation conductors. Both steady-state and transient analyses were performed with the model using temperature-dependent material properties in all cases. The structure of the model was selected so as to allow visibility into:

- Radial and axial temperature gradients within the MIC optical bench and fine guidance housing
- Temperature gradients within both the primary and secondary mirrors
- Temperature gradients through both the vapor-cooled and radiator-cooled shields
- Temperature gradients within the secondary mirror housing and spider assembly
- Temperature gradients within the sunshade and radiator
- Temperature gradients within the solid hydrogen dewar for the case when the hydrogen has sublimed away from the dewar wall after 1 month of orbital operation
- Temperature gradients between the dewar and instrument, including joint resistances generated by either epoxy bond joints or contact conductances

The model has an additional feature which allows the equilibrium solid hydrogen temperature to be calculated as a function of the mass flowrate in the steady-state cases. For transient cases, the varying heat load resulted in warming and cooling of the hydrogen in addition to maintaining the equilibrium sublimation flowrate.

The derived SIRTF long-life baseline steady-state heat rates are summarized in Table 6-1. A total heat load of 3.319 W to the solid hydrogen is calculated, of which only 1.013 W (or 30 percent of the total) is due to the instrument and cooler parasitic heat loads. The heat rate to the superfluid helium dewar is found to be 0.059 W.

For the baseline tank volumes of 1870 liters (SH_2) and 350 liters (SFHe), Table 6-2 shows that an ample lifetime contingency for two different fill options exists to ensure that the 6-month baseline mission can be met. In the first option, the dewar is only filled to a 95 percent liquid fill. The hydrogen is subcooled to a solid by liquid helium cooling coils which are routed internal to the hydrogen tank. During the solidifying process, the hydrogen density increases, resulting in a 22 percent tank ullage at its equilibrium operating temperature. For this fill option, the calculated hydrogen lifetime is 6.6 months, giving a 10 percent lifetime contingency to achieve the 6-month required lifetime. The calculated lifetime can be increased by approximately 40 percent by the second fill option, in which the dewar is topped-off to a 5 percent ullage after the liquid fill and solidifying process. The top-off is accomplished by metering the boil-off vapors from a laboratory liquid hydrogen tank into the SH_2 dewar while maintaining the solid in a subcooled state by the liquid helium coolant. Both fill techniques have been employed successfully on a laboratory solid hydrogen dewar and have been used in conjunction with other cryogens on flight cryostats (TEAL RUBY, LIMS, and LRIR).

The SFHe dewar is assumed to be filled and topped-off to a 15 percent ullage. The calculated lifetime equals the design lifetime, with the lifetime contingency available by the fact that the averaged generated instrument heat rate was taken to be 2.4 times the nominal value. The affect of this reduction on VCS performance has not been assessed. A porus plug would provide cryogen containment as in the Phase A design concept.

Operation in the sortie mode can be achieved by either off-loading the cryogen tanks with hydrogen (under filling) or filling the tank with helium. Because

Table 6-1 SIRTF BASELINE HEAT RATE

ITEM	HEAT RATE (W)
SOLID HYDROGEN	
INSTRUMENT	
MIC	1.000
FGS	0.100
ACTUATORS	0.200
APERTURE	
-SCATTERED SOLAR	0.147
-SCATTERED ALB. + EARTH	0.021
-SUNSHADE IR.	0.838
FG SUPPORT	0.351
MLI	0.072
LOST TO SFHe	-0.004
SUBTOTAL =	2.725 W
COOLER	
FG SUPPORT	0.338
MLI	0.252
PLUMBING	0.004
SUBTOTAL =	0.594 W
TOTAL HEAT LOAD TO HYDROGEN =	3.319 W
SUPERFLUID HELIUM	
INSTRUMENT DISSIPATION	0.055
COOLER SUPPORT	0.004
TOTAL HEAT LOAD TO SFHe =	0.059 W

Table 6-2 SIRTF BASELINE SYSTEM LIFETIME OPTIONS

HYDROGEN (1870 LITER)

FILL OPTION	DESIGN LIFETIME	CALCULATED LIFETIME
95% LIQUID FILL, WITHOUT TOP-OFF AFTER SUBCOOLING	6 MONTH	6.6 MONTH
LIQUID FILL, WITH TOP-OFF TO 5% ULLAGE WHILE SUBCOOLED	6 MONTH	8.4 MONTH

SFHe (350 LITER)

	DESIGN LIFETIME	CALCULATED LIFETIME
SFHe, 15% ULLAGE	6 MONTH	6 MONTHS

SORTIE OPTION (1870 LITER)

	DESIGN LIFETIME	CALCULATED LIFETIME
FILL WITH NBP HELIUM, 5% ULLAGE	–	26 DAYS

of the high helium flow rates, the dewar heat rate drops to 2.42 W - only 0.15 W above the sum of the absorbed and generated baseline heat rates - when helium is used instead of hydrogen. At this heat rate, a calculated lifetime of 26 days is available for the sortie mission. Normal helium would be retained in zero g by capillary action of the fine structure aluminum foam, or an external pressure valve would be needed to contain ScHe, as discussed in Section 8.

A mass summary of the SIRTF long-life configuration is given in Table 6-3. A total mass of 3100 kg is estimated, which includes 788 kg associated with the MIC, MIC instrument, electronics, and optical system taken from the previous study. A total of 1010 kg is charged to the cryogen system, including the sunshade radiator and all interior thermal isolation components. The remaining 1307-kg mass is charged to the facility external hardware. The Phase A total mass was 2947 kg.

Table 6-3 SIRTF BASELINE MASS SUMMARY (1 OF 2)

ITEM	MASS (kg)
CRYOGENIC SYSTEMS	
SFHe (350 LITER, 15% ULLAGE)	43
TOROIDAL SFHe TANK	63
ALUMINUM FOAM	16
FG SUPPORT TUBE	6
	SUBTOTAL = 128 kg
SOLID HYDROGEN (1870 LITER, 5% ULLAGE)	160
TOROIDAL H_2 TANK	158
ALUMINUM FOAM	86
FG SUPPORT TUBES	39
	SUBTOTAL = 443 kg
COPPER MIC COUPLER	33
MULTILAYER INSULATION BLANKETS	41
VAPOR-COOLED SHIELD	38
RADIATOR-COOLED SHIELD	104
SUNSHADE	12
RADIATOR	8
MIC FG SUPPORT TUBE	11
RADIATOR FG SUPPORT TUBE	23
	SUBTOTAL = 270 kg

Table 6-3 SIRTF BASELINE MASS SUMMARY (2 OF 2)

ITEM	MASS (kg)
FACILITY HARDWARE	
OPTICAL BENCH	190
MIC VACUUM SHELL	155
FORWARD VACUUM SHELL	95
APERTURE DOOR	410
INSTRUMENT/GIMBAL INTERFACE	240
	SUBTOTAL = 1090 kg
SIRTF INSTRUMENT	
INSTRUMENT (FROM PE ESTIMATES)	SUBTOTAL = 788 kg

SIRTF MASS SUMMARY, BY FUNCTION	
CRYOGENIC SYSTEMS	841
FACILITY EXTERNAL HARDWARE	1090
20% CONTINGENCY	386
MIC, INSTRUMENTS, OPTICS	788
TOTAL SIRTF SYSTEM MASS	= 3,105 kg

Section 7
BASELINE ANALYSES

In the development of the long-life SIRTF configuration, several analyses relating to specific aspects of the design were performed. In some instances, such as the orbital vent line and secondary mirror temperature analysis, their results were fundamental to the feasibility of using hydrogen for SIRTF. The results of these studies are described in the following paragraphs.

7.1 SECONDARY MIRROR TEMPERATURE ANALYSIS

The baseline design approach for the solid hydrogen system is to provide the necessary instrument cooling by conduction coupling to the solid hydrogen dewar. Initial screening of expected pressure drops within the orbital vent line showed that, while lower temperatures are possible, achieving a cryogen temperature much less than 8 K would be difficult, leaving only a 2 K margin for system gradients.

The secondary mirror presents the most severe cooling challenge because of its isolated location in the center of the optical beam suspended by the spider assembly. Actuator mechanisms, required for fine positioning of the mirror dissipates a continuous 0.20 W at the secondary mirror, and the coupling in the secondary housing, spider, and metering structure must be designed to efficiently remove this heat load while maintaining the mirror to below 10 K.

To specifically address this problem, a 29-node thermal mathematical model of the secondary structure was developed. The model geometry, with node locations, is shown in Fig. 7-1. The design configuration used, as with all optical aspects of this study, was taken from the previous study, with material and assembly methods chosen as described below to meet the needs of the long life approach.

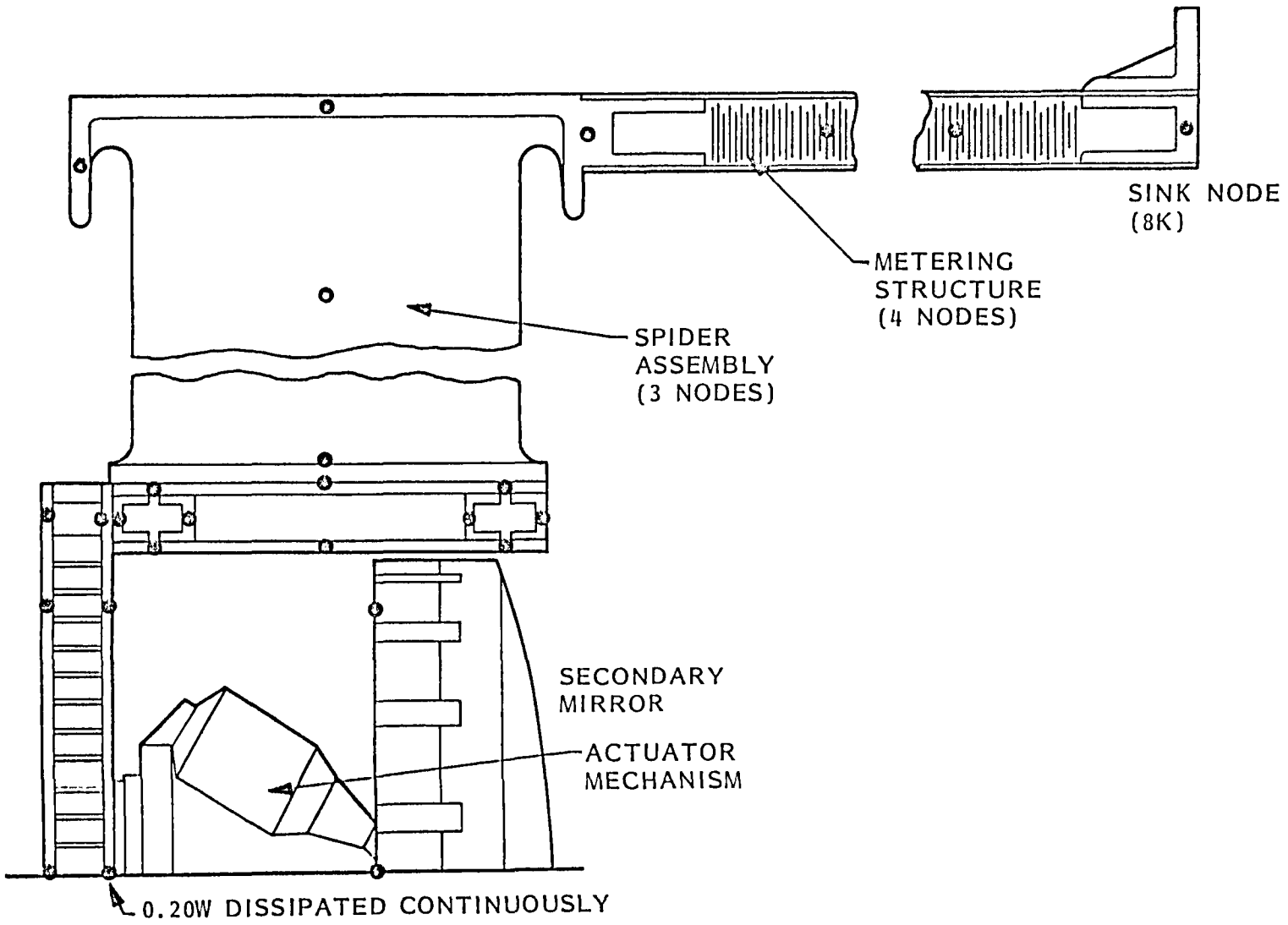

Fig. 7-1 Secondary Mirror Temperature Model Geometry

The actuator power is continuously dissipated into the back surface of the secondary housing, with 0.20 W taken as the nominal value. From this point of generation, the heat is distributed both radially and axially through the facing sheets and core of a 1.0-in.-thick aluminum honeycomb housing back surface. At the edge of the housing, the heat is directed to the spider assembly through the housing side wall, which is a double-walled cylinder (for rigidity) held together by four annular U-channels. The spider assembly consists of four arms, each having an $L/A_2 = 1.89\ cm^{-1}$, which terminates into an annular ring that is epoxy bonded to the metering structure. This metering structure is a 200-cm-long cylinder of 1.0-inch-thick aluminum honeycomb with end fixed at slightly over 8°K.

Because gradients are critical in this system, all joints within each module are epoxy bonded with a thickness of 0.005 in. assumed in all resistance calculations. For critical bonded joints, experimental confirmation of the conductance values will be needed on test samples. The boundary resistances (kapitza) if significant will be included in the overall joint resistance measurement. LMSC has had extensive experience in epoxy bonding of cryogenic systems to control bonding thickness and prevent delamination. Temperature dependent material properties were also used in the 6061-T6 aluminum structure.

The results of this study shown in Fig. 7-2 gives the secondary mirror temperature as a function of the actuator heat load. At the nominal actuator heat load of 0.20 W, the mirror temperature reaches 10.38 K - warmer than allowed. Examination of the data shows that a 1.4 K gradient occurs along the metering structure up to the spider base, clearly the largest single system gradient. A better performance was found by connecting the base of the spider arms directly to the solid hydrogen cooler by a number of flexible copper braids. For the second curve shown in Fig. 7-2, 50 braids, each 2.0 in. long and containing 496 strands of 0.005-in.-diameter wire (0.5 in. wide flat braid) will cool the secondary mirror to 9.26 K at the baseline actuator heat load. Indeed, for this configuration, the heat load may be increased by 70 percent to 0.34 W before the mirror temperature reaches 10.0 K. This

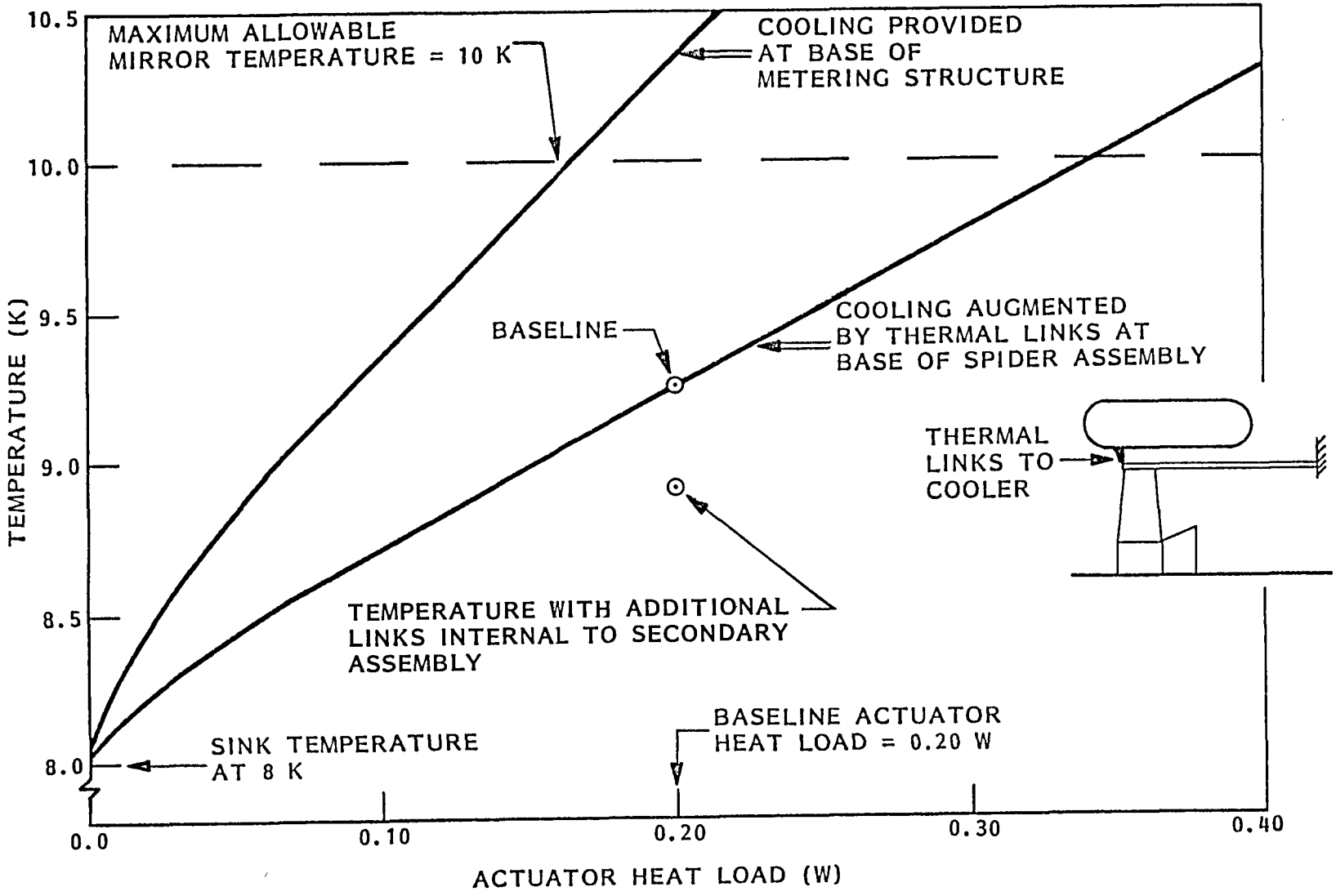

Fig. 7-2 Secondary Mirror Temperature Versus Actuator Heat Load

favorable result achieved by the direct coupling the base of the spider arms to the dewar drove the tank configuration geometry to the toroidal shape described above.

The single data point below the baseline operating point in Fig. 7-2 shows the effect of further reducing gradients within the secondary mirror housing. By adding five each 5.0-in.-long copper thermal links between the secondary mirror and housing, a further drop in mirror temperature to 8.72 K is possible. This latter approch was not adopted at the present time.

7.2 SFHe COOLING OPTIONS

Utilization of the SFHe vapor sensible heat in the baseline configuration is limited to cooling the 6 K temperature station vapor-cooled shield. A schematic of the baseline flow path is shown in Fig. 7-3 as configuration A. Figure 7-3 also shows three other candidate helium flow options that were examined. Configurations B and C direct the flow from the 6 K focal plane to either the secondary or the main optical bench before being directed to the vapor-cooled shield. In configuration D, the flow exits from the 6 K station and is branched into two equal flow paths to provide cooling to both the secondary and optical bench before the flow recombines are sent to the vapor-cooled shield.

Steady-state temperatures and heat rates were determined for each of the alternate flow configurations, with the result presented in Table 7-1. In general, the flow configuration has no significant impact on the instrument temperature and heat rates. Because the primary mirror temperature follows directly from the instrument temperature, the primary mirror also shows no significant temperature change due to a different SFHe flow configuration. The only observed change worth noting was found for the secondary mirror as the average secondary mirror temperature dropped 0.20 to 9.06 K when vapor cooling of the secondary (only) was employed.

Because this option looked promising, an orbital transient analysis was performed. In Fig. 7-4, the primary and secondary mirror temperatures are

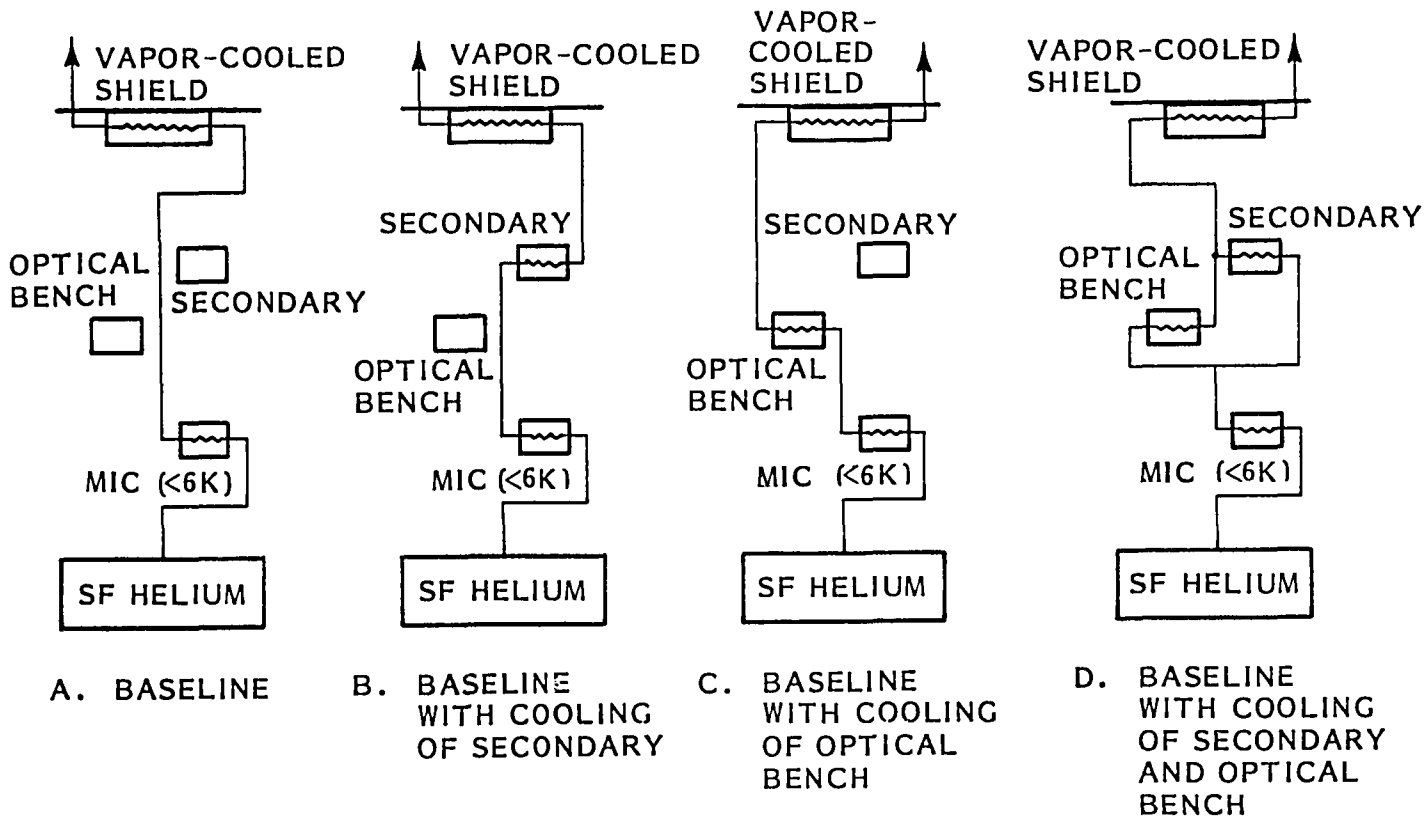

Fig. 7-3 SFHe Flow Network Options Studied

Table 7-1 SFHe FLOW OPTION HEAT RATE AND TEMPERATURE SUMMARY

CONFIGURATION	Q_{MIC} (W)	MIRROR TEMPERATURE PRIMARY (K)	MIRROR TEMPERATURE SECONDARY (K)	INSTRUMENT TEMPERATURE (K)	HEAT RATES SH_2 (W)	HEAT RATES SFHe (W)	COMMENTS
NO SFHe COOLING USED BY SYSTEM	1.00 0.10	9.10 8.50	9.27 9.21	9.69 8.62	3.436 2.793	– –	
A. BASELINE CONFIGURATION	1.00 0.10	9.06 8.45	9.26 9.19	9.65 8.56	3.319 2.647	0.044 0.044	STRAIGHTFORWARD IMPLEMENTATION
B. BASELINE WITH SECONDARY COOLING	1.00 0.10	9.06 8.45	9.06 8.99	9.65 8.56	3.296 2.628	0.044 0.044	LARGEST SECONDARY TEMPERATURE MARGIN, BUT TRANSIENT GRADIENTS TOO HIGH
C. BASELINE WITH OPTICAL BENCH COOLING	1.00 0.10	9.03 8.43	9.26 9.19	9.61 8.53	3.293 2.631	0.044 0.044	SMALL CHANGE IN INSTRUMENT TEMPERATURE. < 1% CHANGES IN SH_2 LIFETIME
D. BASELINE WITH BOTH SECONDARY AND OPTICAL BENCH COOLING	1.00 0.10	9.04 8.44	9.16 9.09	9.63 8.55	3.294 2.629	0.044 0.044	SAME FEATURES AS "B" AND "C"

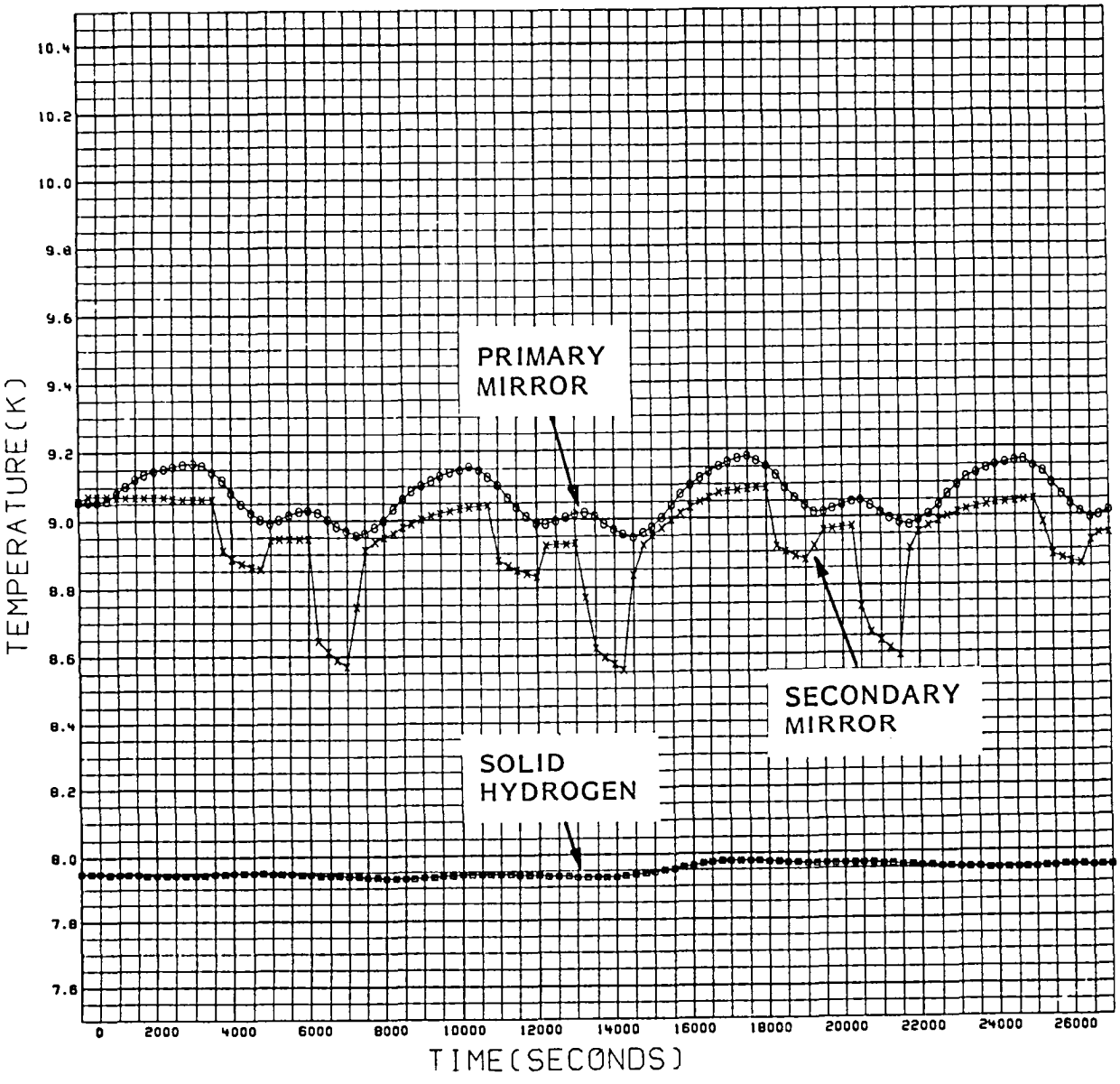

Fig. 7-4 Primary and Secondary Mirror Temperatures: Flow Configuration B

shown as a function of time along with the solid hydrogen temperature. Because of the varying SFHe flow rate, excursions in the secondary temperature to as low as 8.56 K, are observed with temporal gradients exceeding the 3.6 K/h maximum allowed value. Although it is quite possible to use a heater and feedback loop to dampen these excursions to acceptable levels while still maintaining some reduction in the average mirror temperature, the simpler, more direct and conservative approach of not using the helium to cool the secondary mirror was selected.

7.3 ORBITAL VENT LINE

The design of the hydrogen orbital vent line is critical for SIRTF to achieve the temperature required to maintain the primary and secondary mirrors below 10 K. Low temperatures require low pressures over the cryogen, which dictates a vent line with maximum vapor flow conductance. Larger conductances translates to larger diameter and shorter lengths - quite the opposite required for efficient cooling of the vapor-cooled shield. The SIRTF long-life hydrogen orbital vent line geometry shown in Fig. 7-5 represents a good compromise between these opposing requirements.

Between the hydrogen dewar and vapor-cooled shield, 2.25-in.-long by 0.625-in.-diameter line is provided. The first 1.41 in. of the line is a section of metalized convoluted Teflon to maintain a high thermal impedance between temperature zones. Tests have been conducted at LMSC on bare (uncoated) teflon tubes in which solid hydrogen has been vented without affecting pressure or heat rate. There is a finite diffusion rate of H_2 through the teflon tubes and it may be necessary to metallize the tubes to reduce this. Tests are presently underway on the effect of coating teflon to reduce the diffusion rate for a solid cooler program with a similar vent system (CLAES). It should be pointed out, however, that the diffusion rate from a solid hydrogen pressure of 0.14 Torr is approximately 2 x 10 times lower than at atmospheric pressure and the rates for a base tube are probably insignificant. The remaining 0.84 in. of the line is a compact heat exchanger consisting of 30 each, 0.10-in.-diameter parallel holes, drilled through a 0.625-in.-diameter slug of aluminum rod. The heat exchanger shell is bonded with epoxy to the vapor-cooled shield to provide single-point vent-gas cooling to the shield.

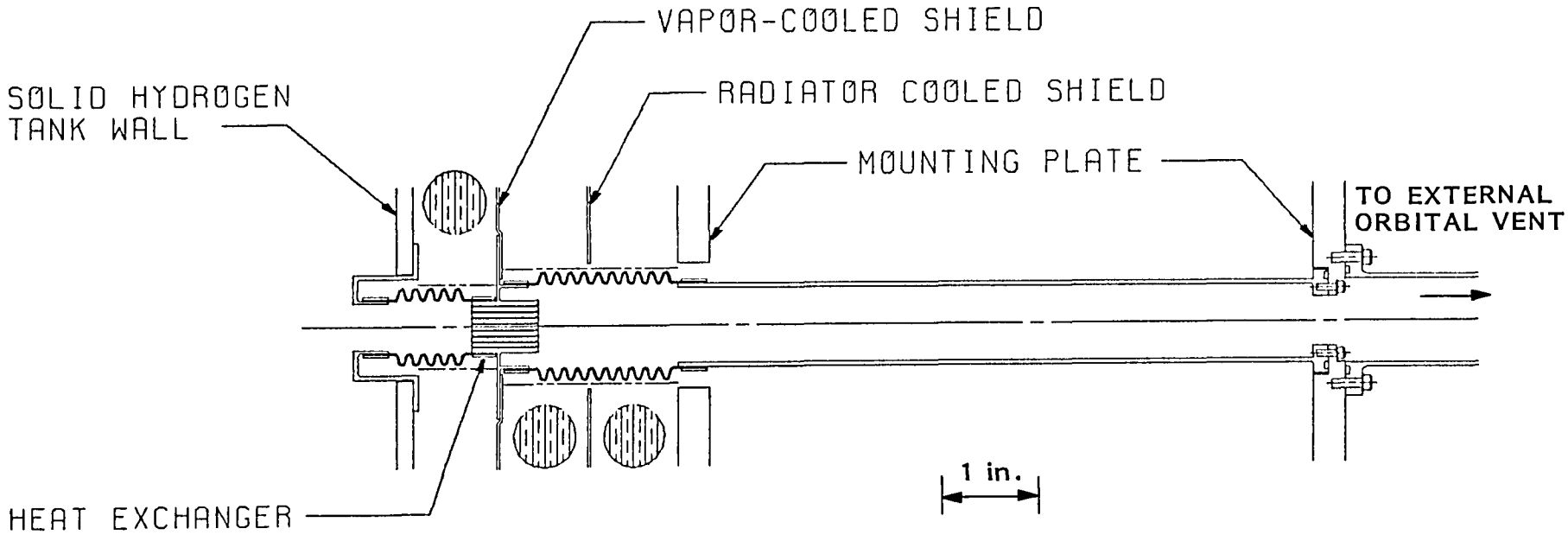

Fig. 7-5 Orbital Vent-Line Configuration

This heat exchanger is basically a standard compact heat exchanger design and operates at continuum flow conditions. The bonding of the teflon to the aluminum heat exchanger is quite similar to construction techniques used at LMSC in which teflon vent lines have been bonded to nipples and radiation baffles in flight programs utilizing solid coolers. Additional studies of the sensitivity of the heat exchanger efficiency on system performance should be done, and depending upon these results a development test of this exchanger may be required. From the vapor-cooled shield, the flow continues through a 2.50-in. section of 1.0-in.-diameter metallized convoluted Teflon. The Teflon tube is bonded to a 7.25-inch-long by 1.0-in.-diameter aluminum tube that terminates at the outer surface of the mounting plate. At the mounting plate, the external plumbing hardware is attached for removal of the hydrogen vapor to some remote vent location (or to the cooler ground servicing equipment).

The critical design feature of the orbital vent line is to ensure that the heat exchanger is effective in removing heat from the vapor-cooled shield. Shown in Fig. 7-6 is a plot of the heat-exchanger efficiency and hydrogen temperature as a function of the number of heat-exchanger through-holes. The heat-exchanger efficiency was determined by solution to the classical Graetz problem in which each hole is assumed to be an isothermal cavity at the vapor-cooled shield temperature. The flow rate through each cavity is given by $\dot{m}_{HOLE} = \dot{m}/N$, where N = the number of holes and m is the baseline hydrogen flowrate of 0.0075 g/s. The inlet temperature was taken to be 8 K. For the baseline orbital vent-line geometry in which 30 holes are used, a 98 percent heat-exchanger efficiency is predicted.

The pressure drop through the line is computed assuming Poisieulle flow to give a cryogen temperature of 7.97 K. This technique has been well established on other solid cryogen cooler systems, including a laboratory solid hydrogen dewar in which the prediction was found to agree to within 0.1 K of the measured temperatures.

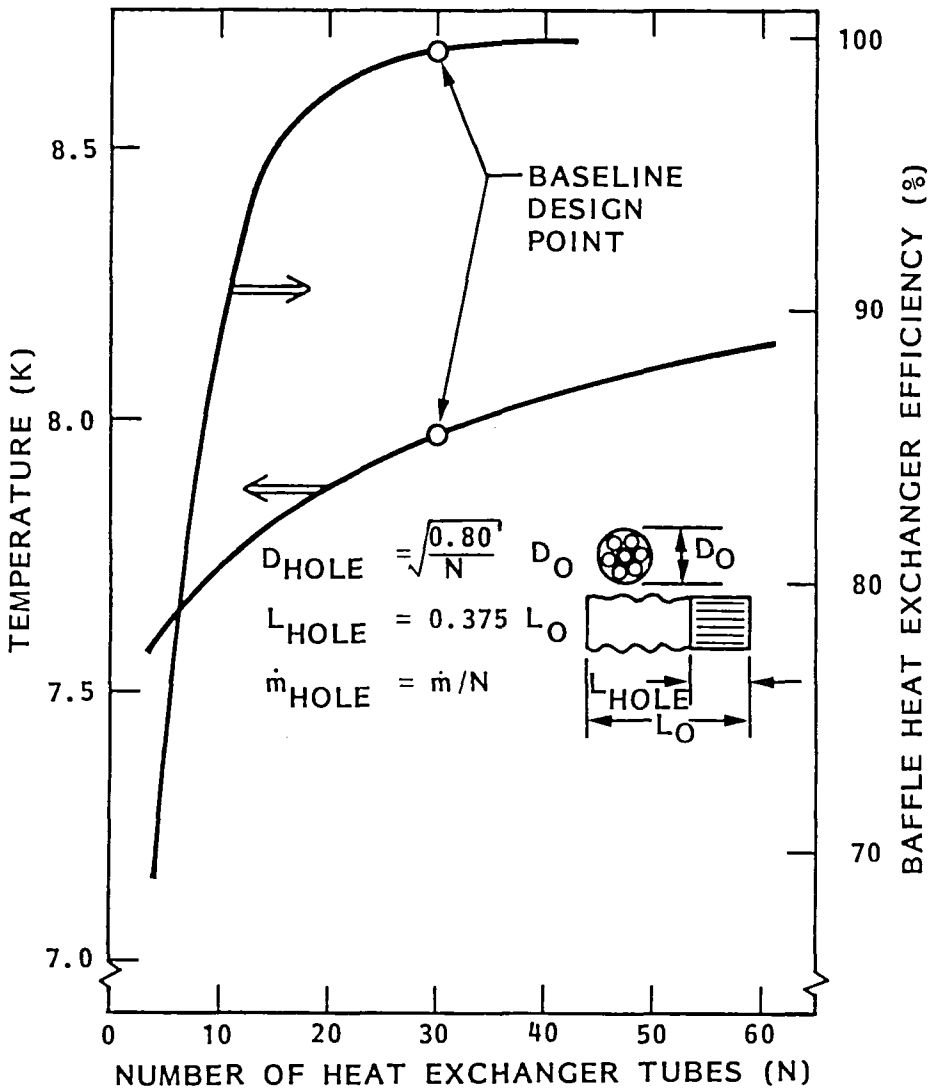

Fig. 7-6 Effect of Heat-Exchanger Hole Number on Cryogen Temperature and Heat-Exchanger Efficiency

The sensitivity of the cryogen temperature to changes in any single line section geometry is shown in Fig. 7-7. The vent line is divided into four sections as described in the Table 7-2. All line sections are maintained at their baseline value except the section for which the sensitivity measurement is being performed. For line sections A, B, and C, the hydrogen temperature is found to be very insensitive to line geometry changes, up to about L/D^4 = 50 $in.^{-3}$. This feature is important because it allows flexibility in the design of the external plumbing where some valves or fittings may impose a slight flow restriction. The pressure drop through the heat exchanger is seen to be the dominant term in establishing the hydrogen operating temperature.

The hydrogen temperature sensitivity to the dewar heat rate (and cryogen mass flowrate) is shown in Fig. 7-8. Worst-case heat rate limits as derived from the minimum and maximum environmental loading would impose a temperature excursion of 0.16 K (7.89 to 8.04 K). In actuality, however, the transient analyses show that the hydrogen mass flowrate will be damped by the hydrogen heat capacity to give temperature excursions of only 0.05 K (7.93 to 7.98 K).

7.4 MLI BLANKET TERMINATION

During the mid-term presentation, NASA/ARC showed some concern as to the heat-load penalty that would be incurred by the termination of the MLI insulation blankets in the area near the sunshade and forebaffle.

The blanket termination geometry is as shown in Fig. 7-9. Both the forebaffle and vapor-cooled shield SN/DAM insulation blankets follow the contour imposed by the shields to the point of termination. At the end, the aluminum shield undergoes a transition to a 0.010-in.-thick fiberglass frustum which forms the boundary to which the edge of the insulation blankets are coupled. Several edge boundary conditions are possible:

- The blanket edge surface is radiatively coupled to the fiberglass frustum.

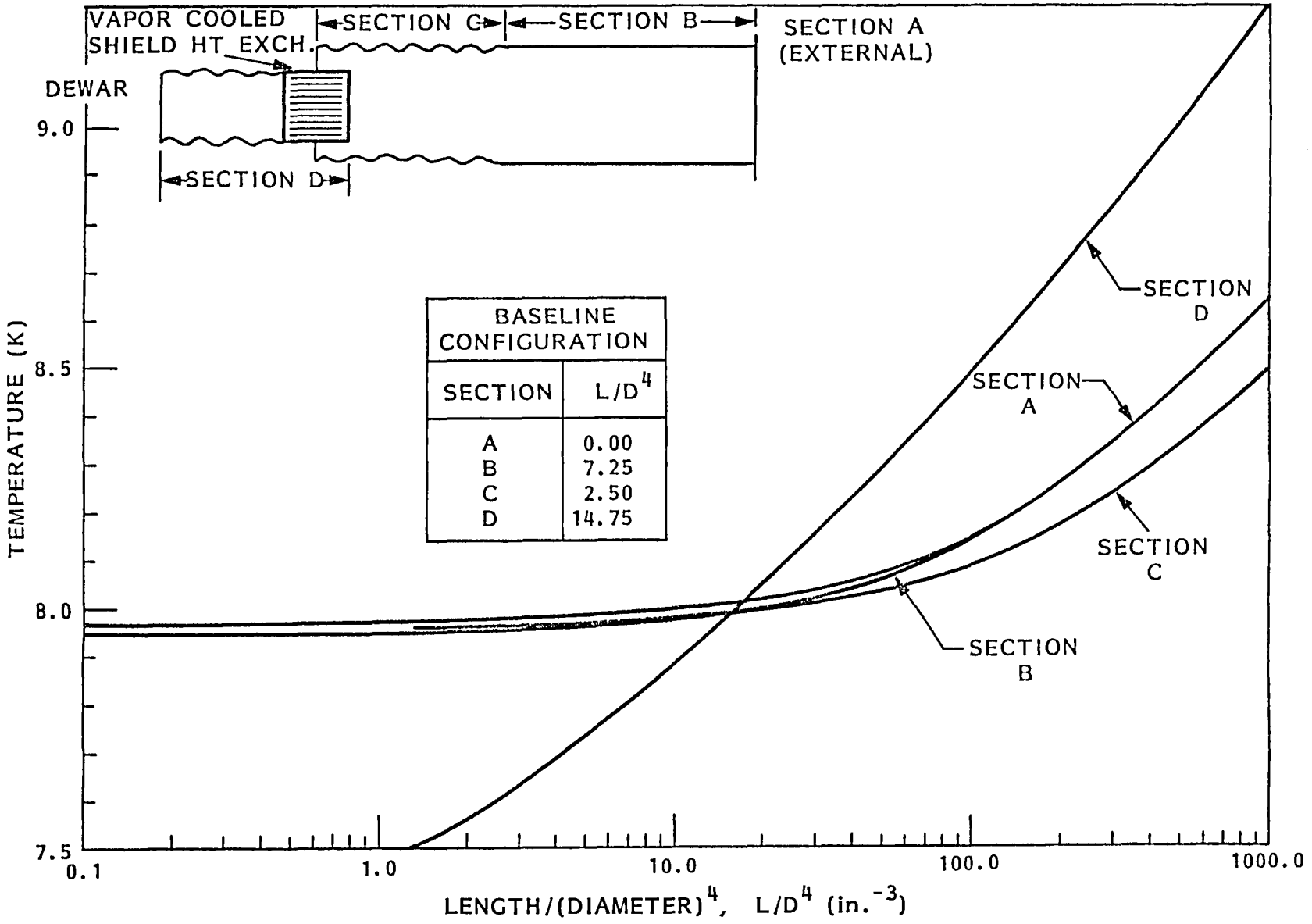

Fig. 7-7 Effect of Changes in L/D^4 for a Single Section of the Orbital Vent Line on Cryogen Temperatures

Table 7-2 VENT LINE CHARACTERISTICS

Section	Description	Baseline $L/D^4(in.^{-3})$
A	External plumbing	0.0
B	1.0-in.-diameter aluminum tube	7.25
C	1.0-in.-diameter convoluted Teflon tube	2.50
D	0.625-in.-diameter convoluted Teflon, plus heat exchanger	14.75

- An interstitial filler of dexiglas, having a thickness of between 0.635 to 1.27 cm, may be used to reduce the radiated heat load at the expense of an additional axial conduction heat load.
- Each of the metallized layers in the MLI blanket are thermally shorted to the fiberglass end piece (significant temperature gradients may exist in the fiberglass sections).

To analyze the impact that these different possible edge effects has on the cooler and vapor-cooled-shield heat balance, a thermal model as shown in Fig. 7-10 was developed. Two annular blankets, each 2.54 cm thick, are built up over a 91.0-cm-diameter cyclinder. The length of the cylinder was taken as 775 cm, which was checked to ensure that all edge effects would be dampened well before the end of the cylinder - regardless of the particular edge boundary configuration. Temperatures of the boundary nodes were taken to be 10, 60, and 185 K.

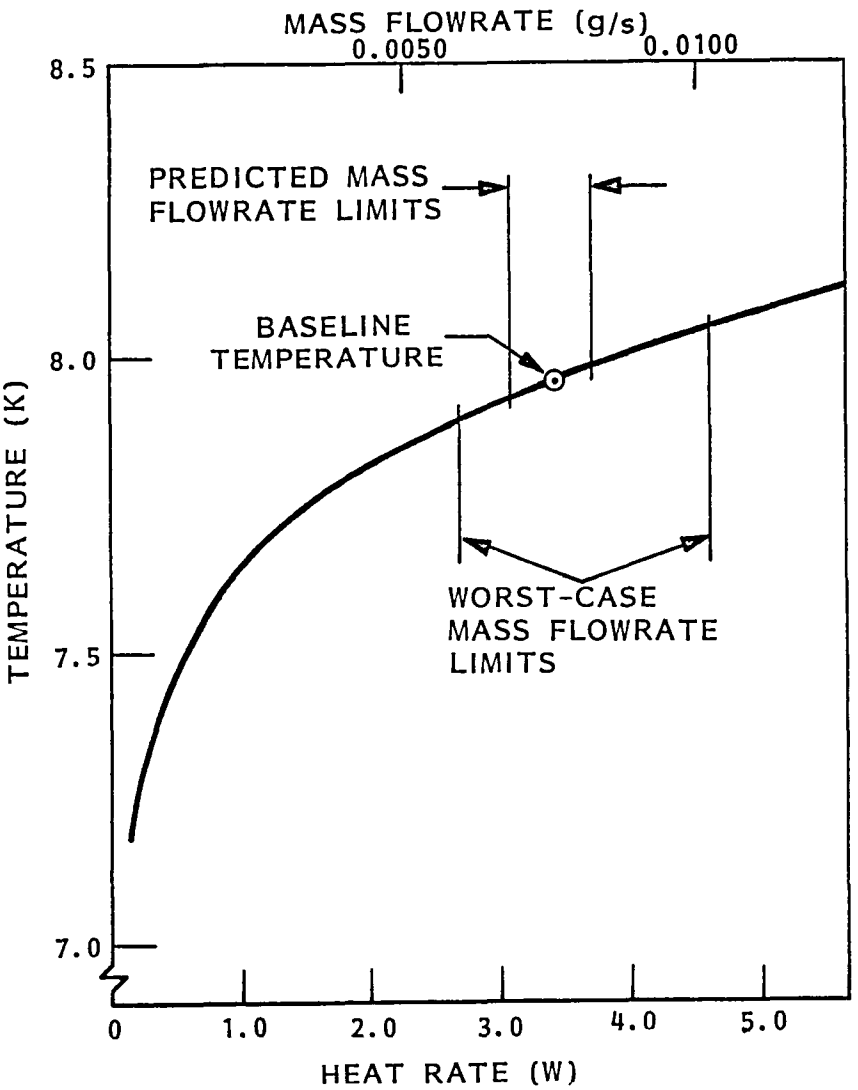

Fig. 7-8 Effect of Solid Hydrogen Temperature Versus Dewar Heat Rate and Mass Flowrate

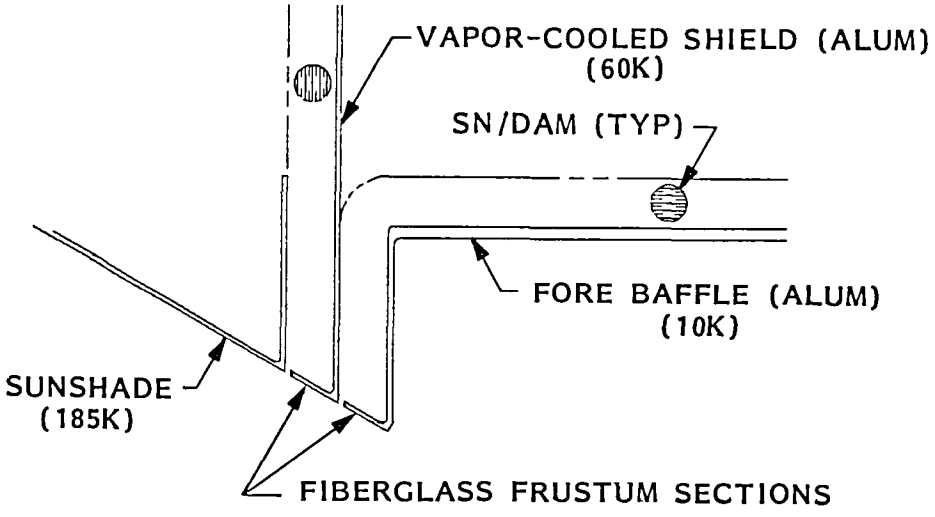

Figure 7-9 MLI Blanket Termination Geometry

For each of the boundary conditions, the steady-state temperature profile within the blanket is determined. Heat rates into the sink temperatures are determined and compared with the derived heat rates for an adiabatic boundary edge. The difference in heat rates, which are also shown in Fig. 7-10, is a direct measure of the edge configuration's impact on heat rate at the two temperature zones. Clearly, radiation coupling at the edges is the preferred termination configuration, with only a small penalty incurred should some degree of thermal shorting occur. The impact that these small changes in heat temperature zones has on the overall system performance is negligible.

7.5 SUPPORT STRUCTURE

A buckling and frequency analysis was performed on the cooler, instrument, and SFHe dewar supports. All supports were sized to survive buckling at a 10 g static load, with a 1.8 factor of safety and a knockdown factor for material imperfections of 0.5 (99 percent probability of survival). The supported mass

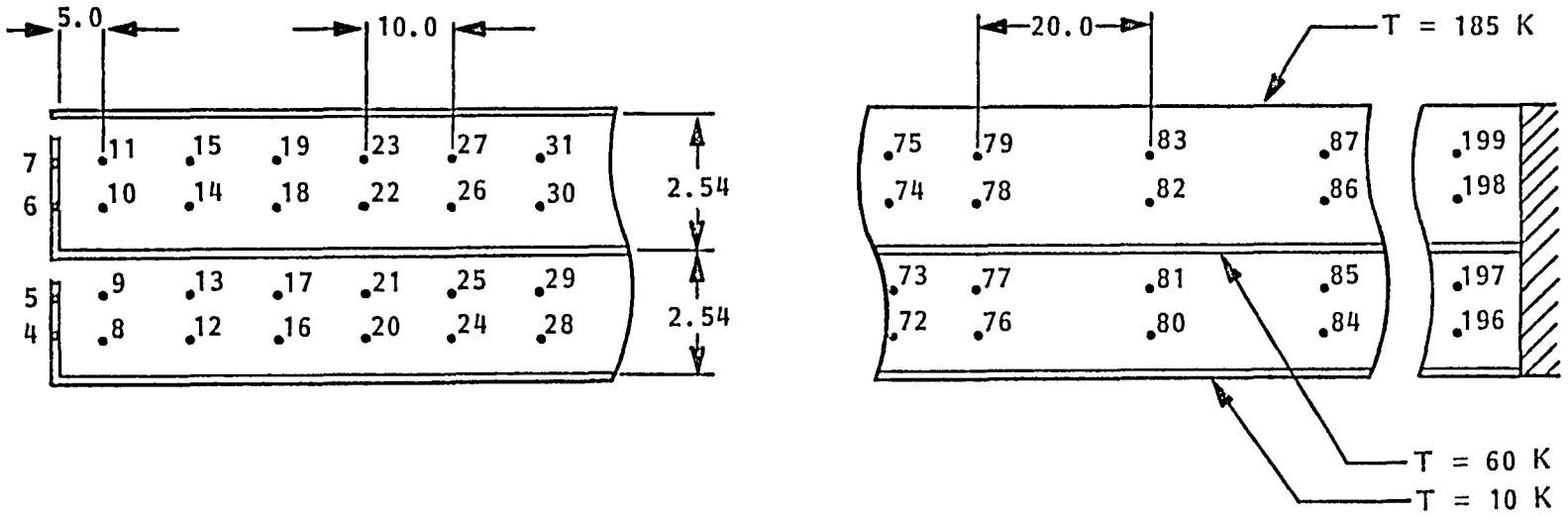

EDGE TERMINATION CONFIGURATION	EFFECT ON HEAT RATE (W)	
	10 K SHIELD	60 K SHIELD
ADIABATIC	0.000	0.000
RADIATION COUPLED	0.004	0.064
0.635-cm DEXIGLAS	0.033	0.165
1.270-cm DEXIGLAS	0.074	0.209
THERMAL SHORT	0.004	0.069

Fig. 7-10 MLI Blanket Termination Thermal Model and Results

and tube radii were given with the required thickness determined as a function of the unsupported tube length. At each thickness and length design point, the characteristic primary resonance was determined and is shown in Fig. 7-11. The fiberglass frustrum configuration of the previous study was used.

The minimum allowable design frequency was specified at 20 Hz. At the design point a considerable margin in frequency is maintained for all three supports, as the lowest resonance for any of the three supports at their baseline design point is 61 Hz (tank support).

The safety factor in stress was found to be greater than 10 for all supports at their baseline design points.

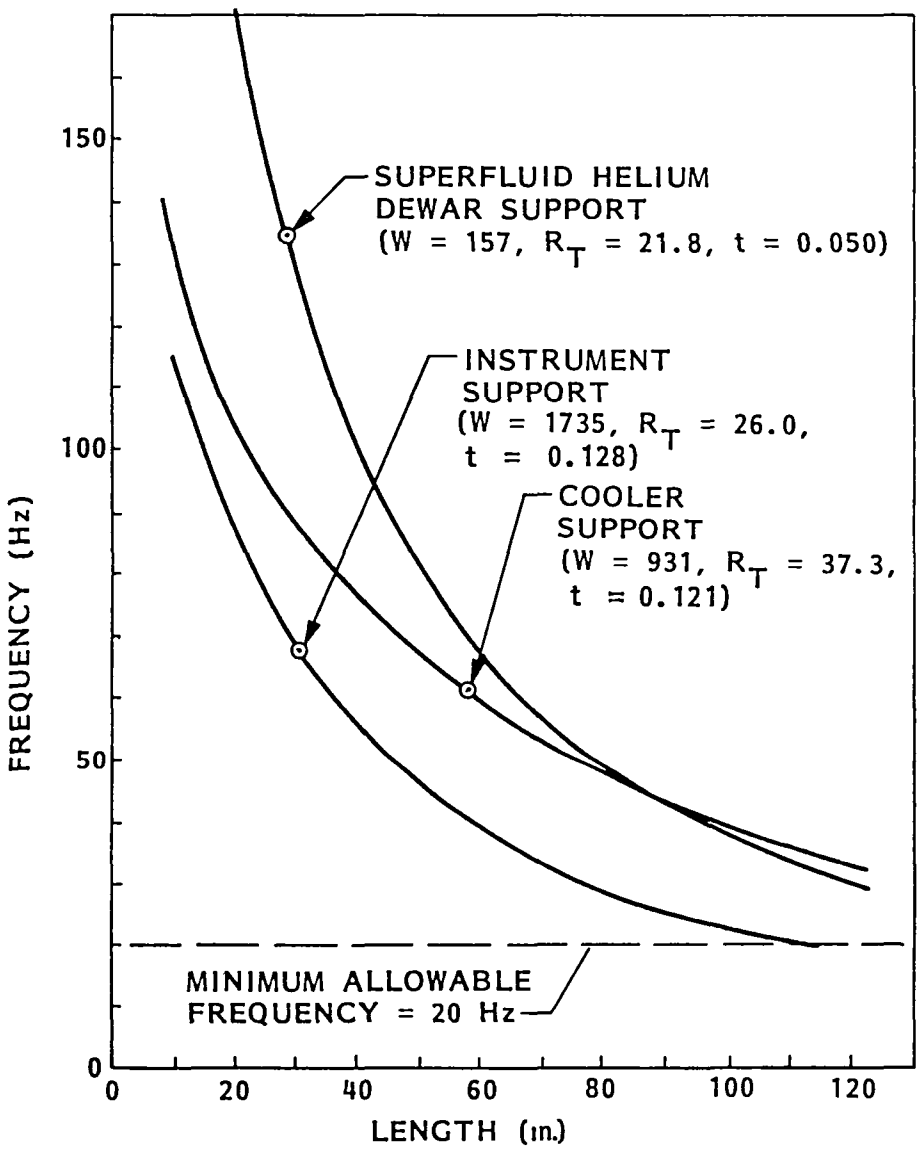

Fig. 7-11 Support Tube Frequency Versus Length

Section 8
BASELINE PERFORMANCE

The performance of the baseline long-life SIRTF is described from 2 days before launch through long-term orbital operation. Longer unaccessed ground hold issues are also discussed. Because the mirror temperatures are required to be less than 10 K for the first 30 days only, the orbital results are shown for that time, when the tank would be 20 percent depleted. Study limitations did not permit the orbital analyses to be extended to include the end-of-life transients. Similarly, SORTIE operation was not investigated.

8.1 LAUNCH AND MISSION ABORT OPERATIONS

Cooler operations for a nominal launch through deployment are shown in Fig. 8-1.

Various scenarios for fulling and subcooling of the hydrogen have been under study for the CLAES program. The baseline approach is to fill the tank with liquid hydrogen and freeze and subcool with liquid helium. The requirements for both fill time and total helium required for the initial charging are summarized in Fig. 8-0. This data is taken from a flow model which includes the heat exchanger elements. The efficiency factor varies with the flow rate as indicated. For subsequent recooling between 13.8 K and 5°K the helium usage is the order of 10 percent of the quantities shown for initial filling.

A typical plumbing schematic showing the required elements for the solid hydrogen system is shown in Fig. 8-a. This schematic is compatible with operation with supercritical helium, however, the orbital vent line would require the incorporation of an absolute pressure relief valve. A heater would be incorporated at the tank wall for either SH_2 or ScHe flow rate and pressure control in orbit and also for ground operations requiring cryogen

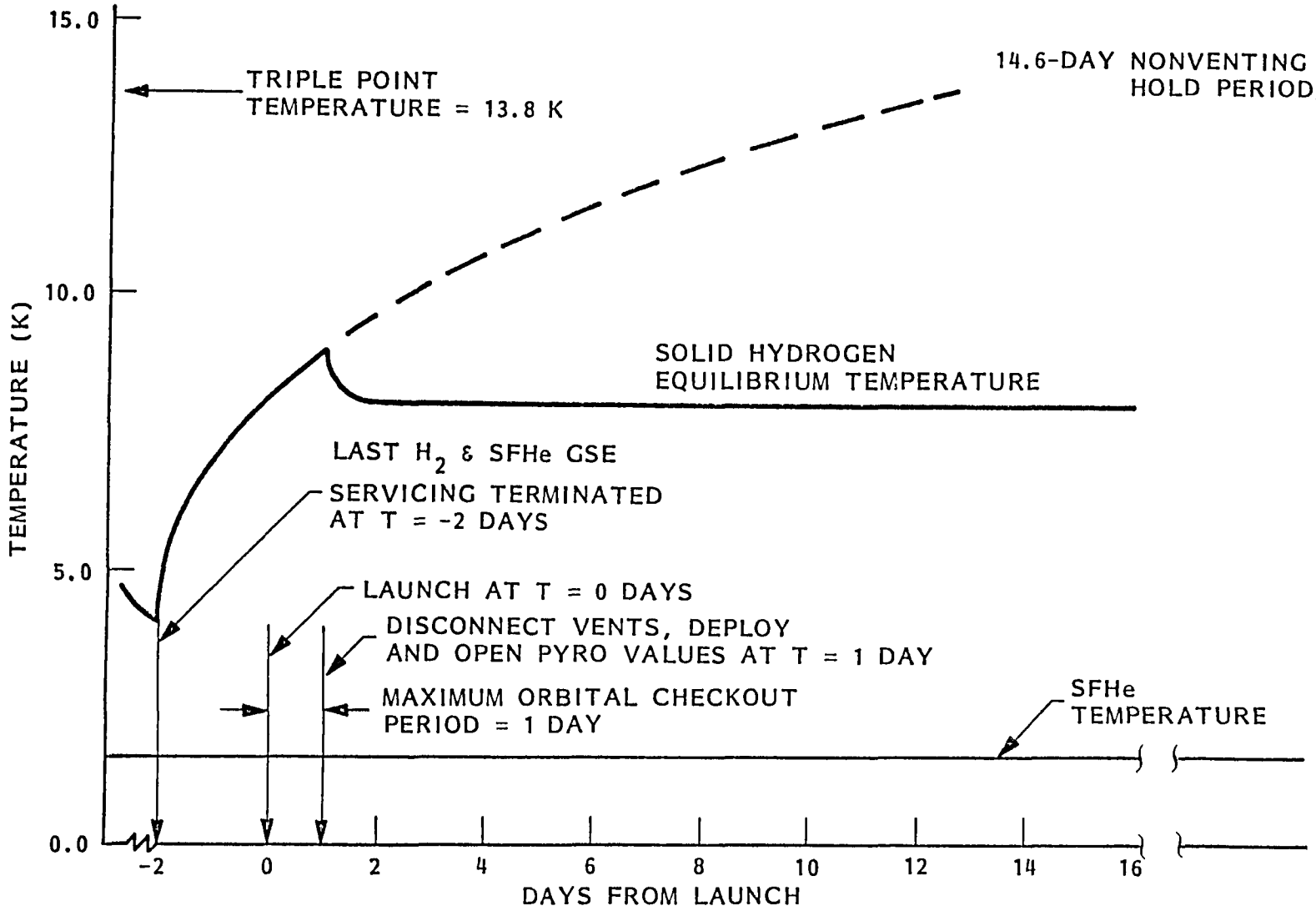

Fig. 8-1 Cooler Operation - Nominal Scenario

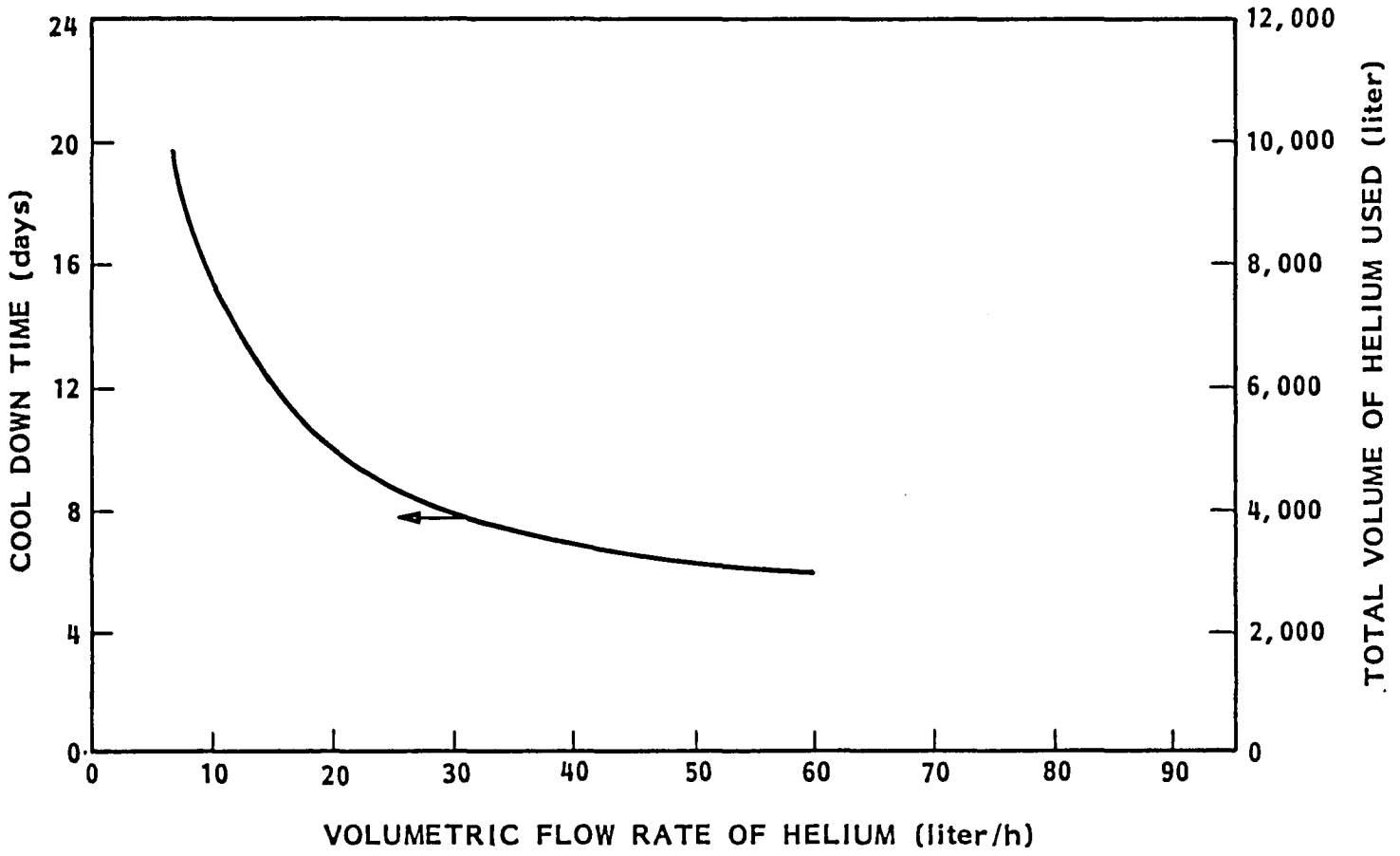

Fig. 8-0 Initial Cool-Down and H_2 Solidification

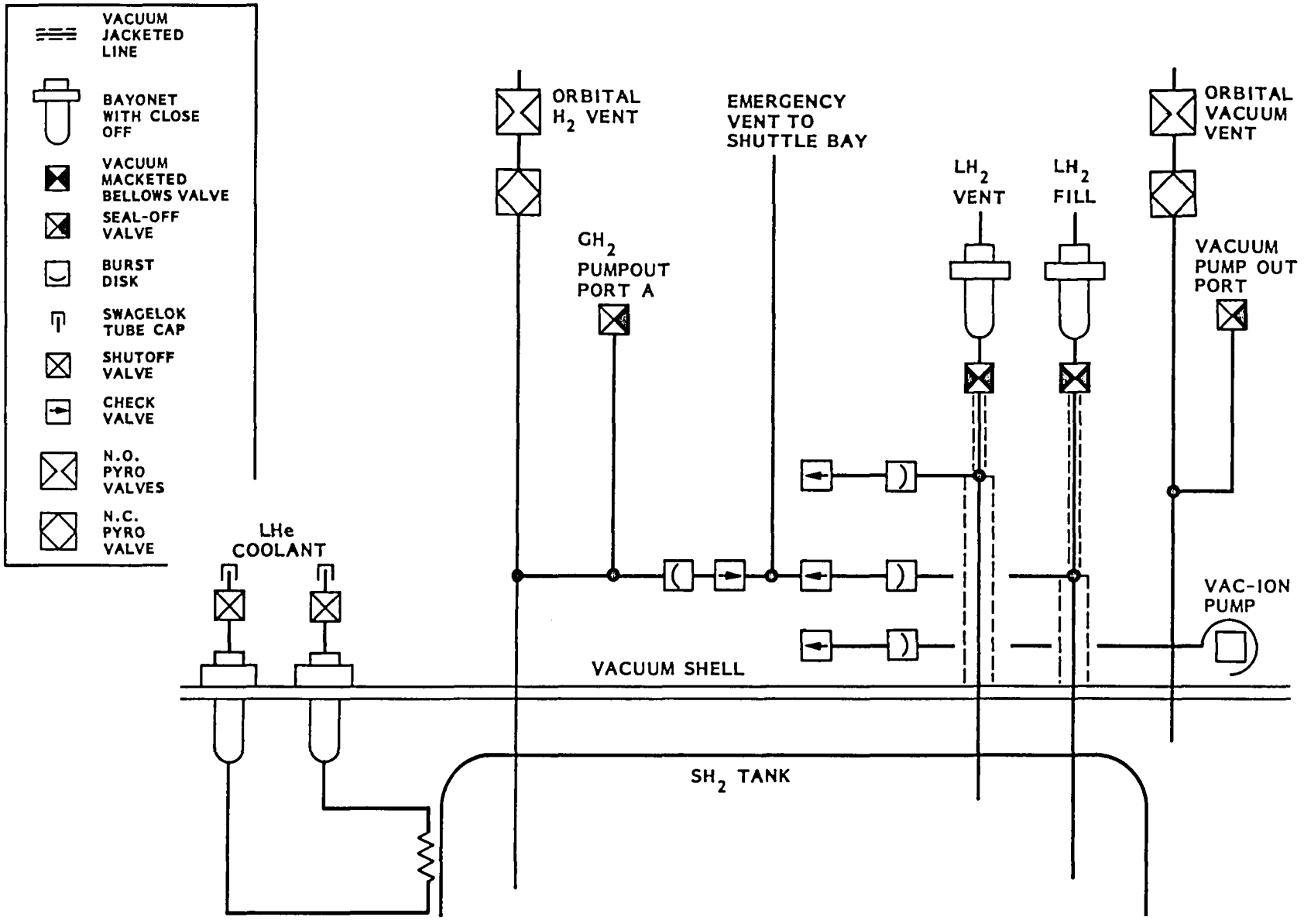

Fig. 8-a Plumbing Schematic

emptying. The vent line includes both normally open and normally closed pyro valves for contingency operations.

Beginning 2 days prior to launch, the last servicing of the solid hydrogen and SFHe will be completed. The hydrogen will be subcooled to less than 5 K with the liquid helium coolant, and the SFHe will be pumped to reduce its temperature to below 1.6 K. After servicing, all valves on the cooler are closed, the ground service lines are disconnected, and the cryogens are left to slowly warm without discharge of their vapors. The solid hydrogen will warm to its triple point temperature of 13.8 K before the solid begins to melt, while the SFHe must remain below its transition temperature of 2.18 K.

At T = 0, SIRTF is launched with the hydrogen warmed to 8.2 K. Once in orbit, a maximum period of 1 day is allowed for checking systems while the payload remains in the cargo bay. By the end of this checkout period, a decision to deploy will have been made, during which time the hydrogen warms another 0.8 to 9.0 K. At this point a comfortable 11.6-day hold time margin exists before the hydrogen reaches its triple point temperature.

During the deployment sequence, the first action is to disconnect the emergency bay vent line. This line provides a direct link from the cooler safety discharge hardware to a cargo bay vent port to ensure that no effluence is spilled into the cargo bay should a failure of the hydrogen system occur during ground handling or launch. Once removed, the SIRTF is free to be deployed from the cargo bay.

By the time SIRTF is deployed into orbit, the hydrogen temperature is higher than its 8 K equilibrium temperature. Therefore, when the pyro valves are fired to initiate orbital pumping on the cryogen, a momentary high vent rate can be expected as the tank "blows down" to its equilibrium pressure. Temperature of the superfluid helium will rise only 0.02 K. Prior programs with solid coolers at LMSC have not incorporated low thrust vents but have directed the thrust through the vehicle roll axis. A study will be required

for SIRTF to determine if low thrust vents are required. As shown in section 8.2, the total mass flow rate is only 9×10^{-3} g/sec.

Cooler operations during a mission abort scenario are summarized in Fig. 8-2. The events through the launch times are identical to the mission scenario. However, during the course of the 1-day checkout a decision is made to either abort the mission or at least delay the deployment decision to some later time. A maximum 7-day period is allocated during which time a decision to abort will be finalized. At this point, the temperature of the hydrogen has risen to 12.1 K and the shuttle expendibles become depleted, requiring a return to earth. Deployment during this internal will again result in cryogen blow down to the 8 K equilibrium temperature.

Once abort occurs and the shuttle has landed, the cargo bay will be accessed within a maximum time of 8 days, assuming the landing occurred at some nonremote area where facilities and equipment exist to open the bay doors. At remote sites, this period may be longer. During this period the solid hydrogen will have reached its triple point temperature and begin an isothermal and isobaric melt. This melt may continue for 35 days before the lower liquid density reduces the ullage in the tank to zero. Anytime during this 35-day period, the ground support equipment (GSE) may be connected to the cryostat to initiate a cryogen off-load or other servicing operation. In the event that the GSE is not accessed before this period, a hydrostatic pressure will begin to build within the tank. This pressure is relieved well below the tank burst pressure by one of two redundant burst disks located in the cooler fill and vent lines. The vented hydrogen is then safely discharged outside the cargo bay through an emergency cargo bay vent line. If the connection to the cargo bay vent was separated prior to abort decision, the cooler will vent into the cargo bay. In this case cargo bay purging or access will be needed before the 35-day limit is reached.

LMSC feels that the present 14.6-day ground hold time (for hydrogen) is an ample contingency to accommodate both a nominal and aborted shuttle mission without compromise in safety. However, because longer ground hold times

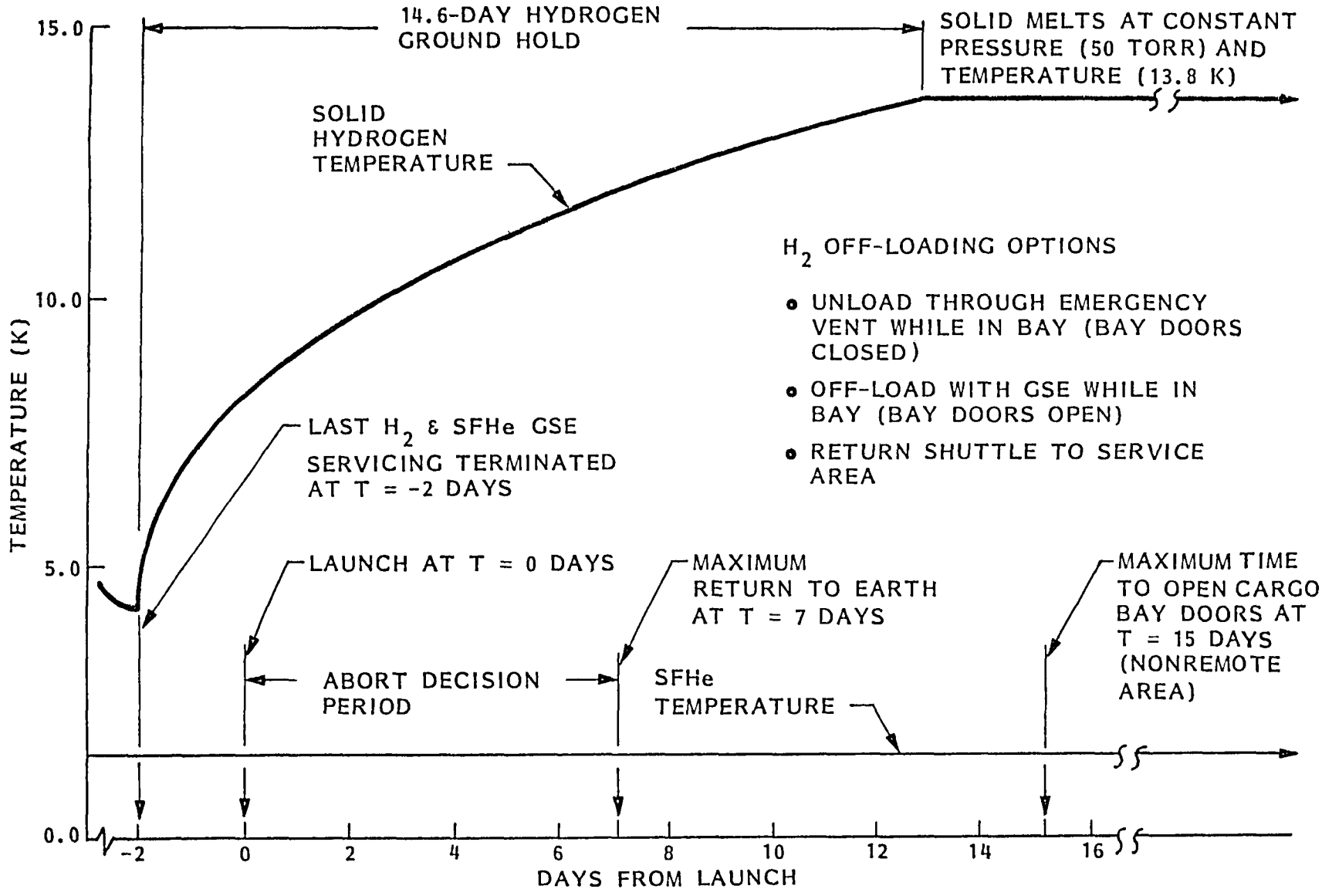

Fig. 8-2 Cooler Operation - Mission Abort Scenario

simplify ground logistics during engineering tests and shuttle operations, some approaches to increasing the ground hold time have been addressed. The results of these studies are summarized in Table 8-1, where configuration 1 represents performance of the current baseline design.

The aperture door has two MLI blankets that are supported by a thin aluminum panel; one faces the aperture forebaffle and the other faces the radiator surface. Configurations 2 and 3 show the effect of reducing the cooler parasitic heat load by cooling either of these blanket support panels with liquid nitrogen.

The effect of cooling the radiator shield panel is shown in configuration 2. The radiator surface temperature drops from 275 to ~150 K, which greatly reduces the parasitic heat loads into the cooler. The effect on ground hold is to more than double the time required for the hydrogen to reach its triple point temperature to 34.3 days. Unfortunately, the heat balance on the liquid nitrogen reservoir shows that at least 300 kg of LN_2 is required, which is felt to be impractical. In configuration 3, the aperture panel is cooled, with the result that the ground hold extends an additional 5 to 19.4 days. Only 3 kg of liquid nitrogen is required to provide this cooling, making this a reasonable option for further study. The LN_2 would be for ground operation only, and vented prior to launch. Venting into the cargo bay would be acceptable for most shuttle missions.

For configurations 4 and 5, the hydrogen tank is only filled to a 10 percent ullage. Liquid helium then fills the remaining void and boils off at a 1-atm pressure, cooling the vapor-cooled shield while maintaining the solid hydrogen at 4.2 K. Since helium has the effect of retarding the start time for warming the hydrogen, ground-hold times can be extended to between 32 and 57 days for an uncooled and cooled aperture MLI panel. This helium would be vented through the payload vent line.

Note that even for the longest hydrogen ground hold of 57 days, the SFHe warms to only 1.89 K.

Table 8-1 EXTENDED GROUND-HOLD OPTIONS

	CONFIGURATION	SH_2 TEMPS		SFHe TEMPS		GROUND HOLD TIME (DAYS)	COMMENTS
		INITIAL	FINAL	INITIAL	FINAL		
1.	SH_2 SUBCOOLED, "WARM" COVER DOOR	4.2	13.8	1.60	1.69	14.6	BASELINE CONFIGURATION; HYDROGEN REULATES SERVICING INTERVALS – NOT SFHe
2.	SH_2 SUBCOOLED, COVER DOOR RAD PANEL BACK COOLED WITH LN_2	4.2	13.8	1.60	1.79	34.3	NOT PRACTICAL; REQUIRES 300 kg OF LIQUID NITROGEN
3.	SH_2 SUBCOOLED, COVER DOOR APER. PANEL BACK COOLED WITH LN_2	4.2	13.8	1.60	1.72	19.4	REQUIRES 3.0 kg OF LIQUID NITROGEN
4.	LHe TOP-OFF, "WARM" COVER DOOR	4.2	4.2	1.60	1.64	17.2	180 LITER OF LIQUID HELIUM (10% OF SH_2 TANK). MASS PENALTY OF 27 TO 43 kg
	(INCL. WARM TO T.P.)	4.2	13.8	1.60	1.74	~32	
5.	LHe TOP-OFF, COOLED COVER DOOR APERTURE PANEL	4.2	4.2	1.60	1.70	37.4	180 LITER OF LIQUID HELIUM (10% OF SH_2 TANK). MASS PENALTY OF 33 TO 48 kg
	(INCL. WARM TO T.P.)	4.2	13.8	1.60	1.89	~57	

8.2 ORBITAL TRANSIENTS RESULTS

The 157-node orbital transient model was exercised through 5 orbits. Time dependent enviornmental heat rates were derived from the two heat rates of the reference mission orbit (80 percent duty cycle) for the first two and last two orbits. Heat rates for the third orbit were assumed to be those of the reference mission orbit 1 (20 percent duty cycle). Start temperatures were determined from a steady-state analysis performed for the time-averaged environmental heat rates. The following paragraph summarizes the results.

8.2.1 Cryostat Heat Loads (Fig. 8-3)

The net cryostat heat load into the hydrogen dewar is shown as a function of time along with the three components of the heat load: cooler parasitic load, instrument heat load (generated and parasitic), and aperture* heat load. The wide excursions in the aperture heat load are due almost exclusively to the varying solar heat load incident to the sunshade, which increases the IR thermal load. Scattered solar load is of second-order importance.

8.2.2 Cryogen Mass Flowrate (Fig. 8-4)

The hydrogen and SFHe mass flow rate that occurs as a result of the above heat-load profile is shown in Fig. 8-4. Although the heat rate to the hydrogen was seen to vary about the average by -15 to +42 percent, the mass flow rate varies by only -8 to +9 percent. This gentler excusion in the mass flow rate occurs because of the damping afforded by the large hydrogen thermal capacity. The SFHe flowrate followed directly from the applied instrument heat load. The heat capacity of the SFHe was not included in the model. Inclusion of this would cause some damping of the helium flowrates.

*The 0.20-W actuator heat load is included in the aperture heat-load term.

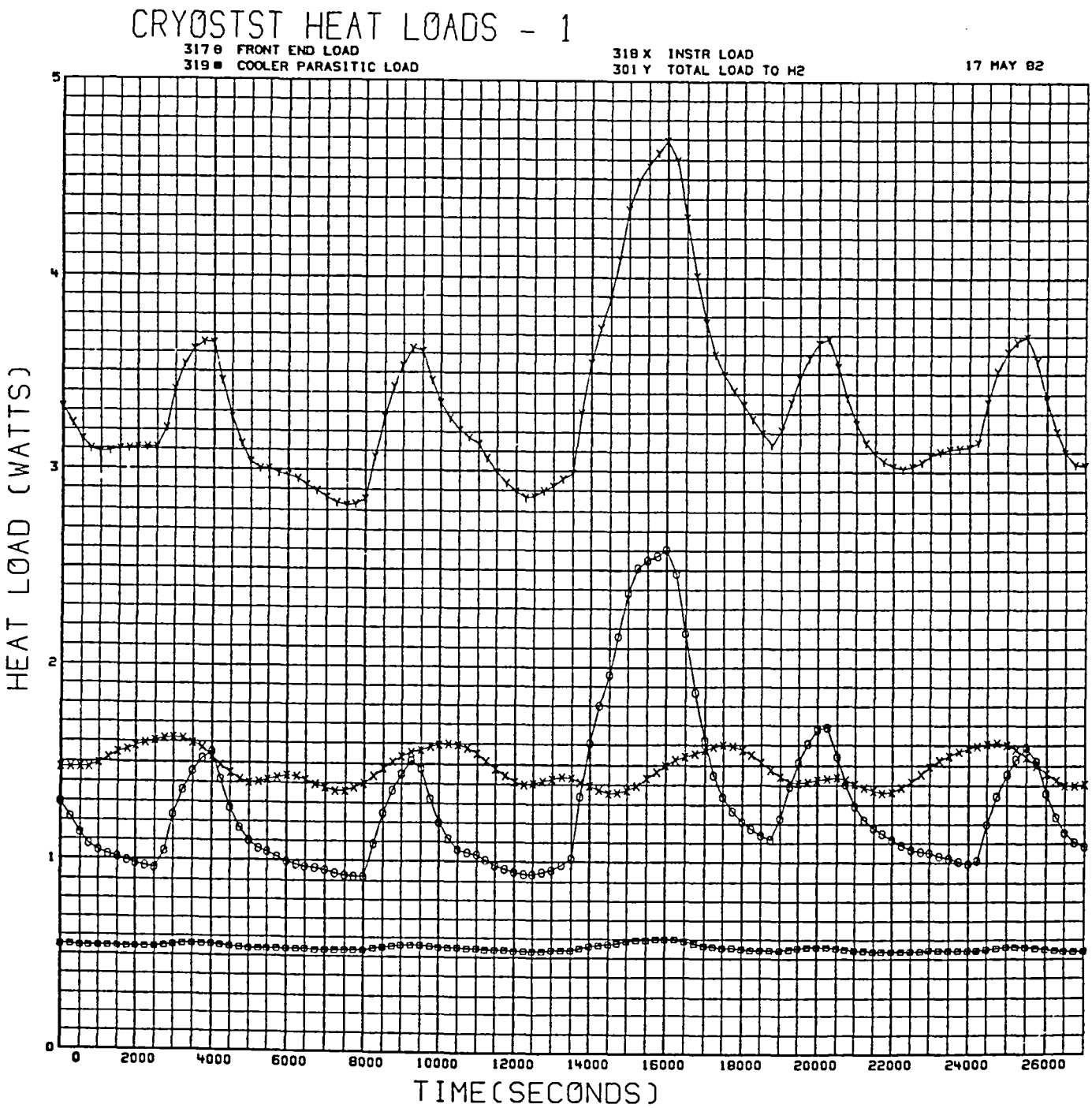

Fig. 8-3 Hydrogen Cryostat Heat Loads

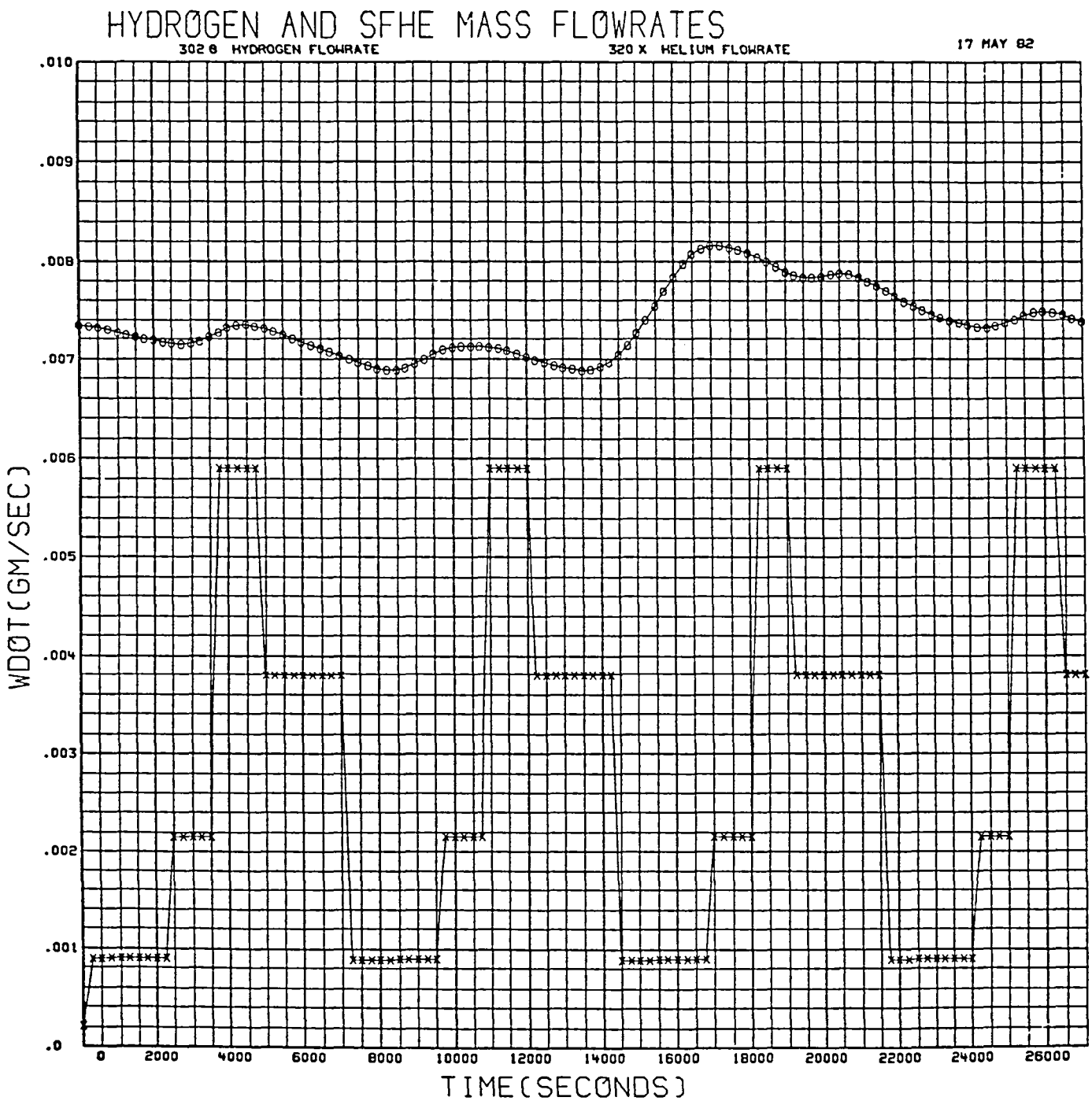

Fig. 8-4 Hydrogen and SFHe Mass Flowrate

8.2.3 MIC Temperatures (Fig. 8-5)

The MIC instrument temperatures are shown with the solid hydrogen temperature profile. When quiescent, all instrument temperatures follow a profile fairly similar to each other, experiencing excursions from 9.45 to 9.75 K. As the instruments are turned on, their temperatures increase to between 9.9 - 10.1 K. Temperature of the solid hydrogen is stable to within 0.03 K at 7.95 K.

8.2.4 Primary and Secondary Mirror Temperatures (Fig. 8-6)

The temperature profile of the primary and secondary mirrors are shown along with the solid hydrogen. The primary mirror exhibits the same general profile as that seen for the MIC instruments. Absolute excusions of between 8.95 to 9.18 K are observed, with maximum temporal temperature gradients of ±0.4 K/h - 10 times less than the maximum allowable value. Temporal stability of the secondary mirror is even better at ± 0.09 K/h. The model also allows visibility into the magnitude of radial mirror gradients, which were found to be less than ±0.001 K at any time in the orbit, from mirror center to edge.

8.2.5 Dewar Temperatures (Fig. 8-7)

There was some concern generated by NASA/ARC as to whether the solid hydrogen can maintain sufficient cooling as the solid sublimes away from the heat generation sources. In this orbital transient analysis, the solid was assumed to be positioned away from the tank walls with heat transferred to the solid hydrogen through a series resistor formed by the internal aluminum foam heat exchanger and its epoxy bond to the tank wall.

The temperature of the tank wall at the three principal locations where heat is being dumped into the dewar is shown . At the point where the cooler support tube ties into the dewar, the tank wall is within 0.01 K of the solid hydrogen temperature. At the point where the instrument ties into the dewar the gradient is on the order of 0.05 K. A larger gradient of between 0.05 and

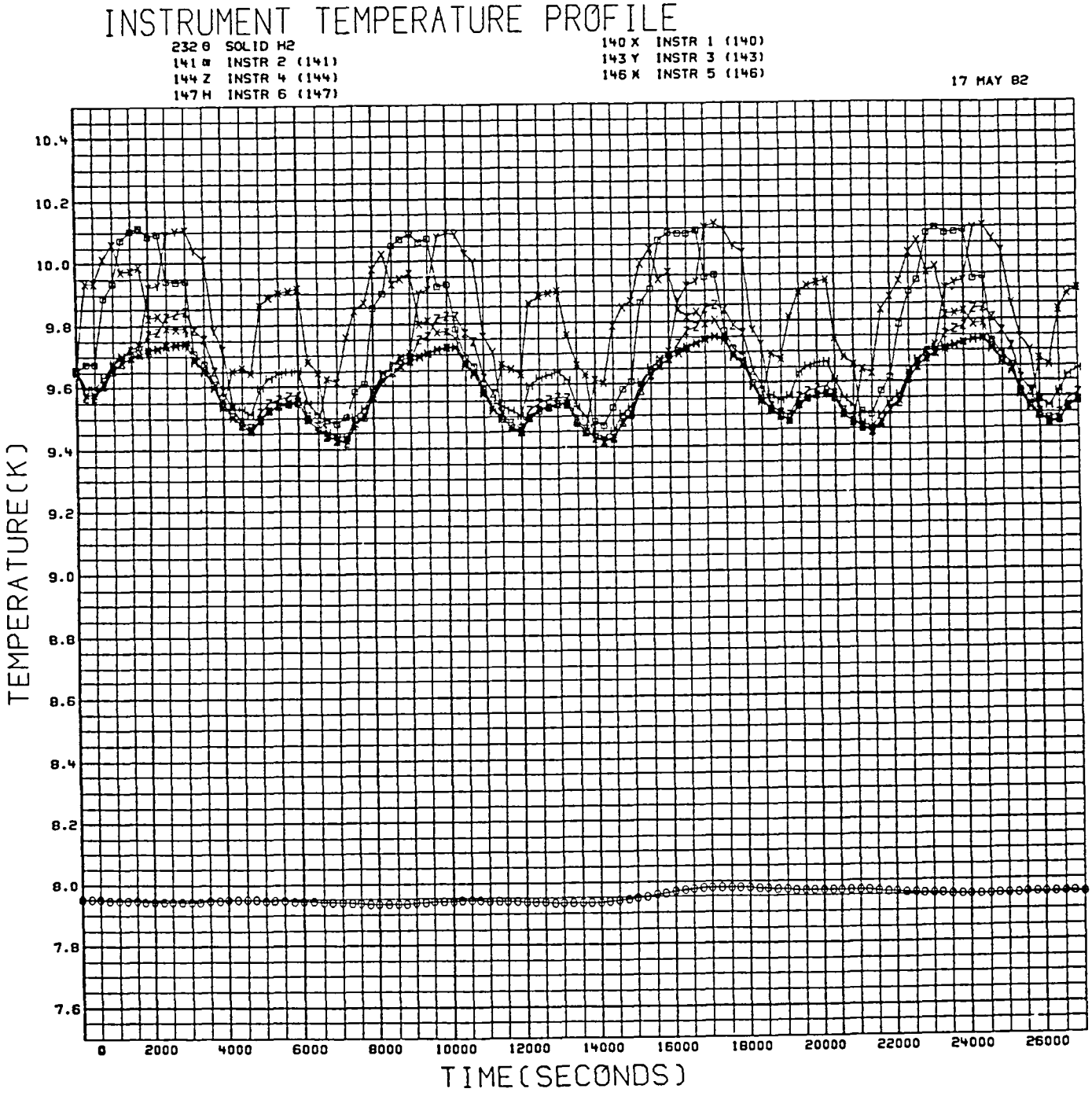

Fig. 8-5 MIC Instrument Temperature Profile

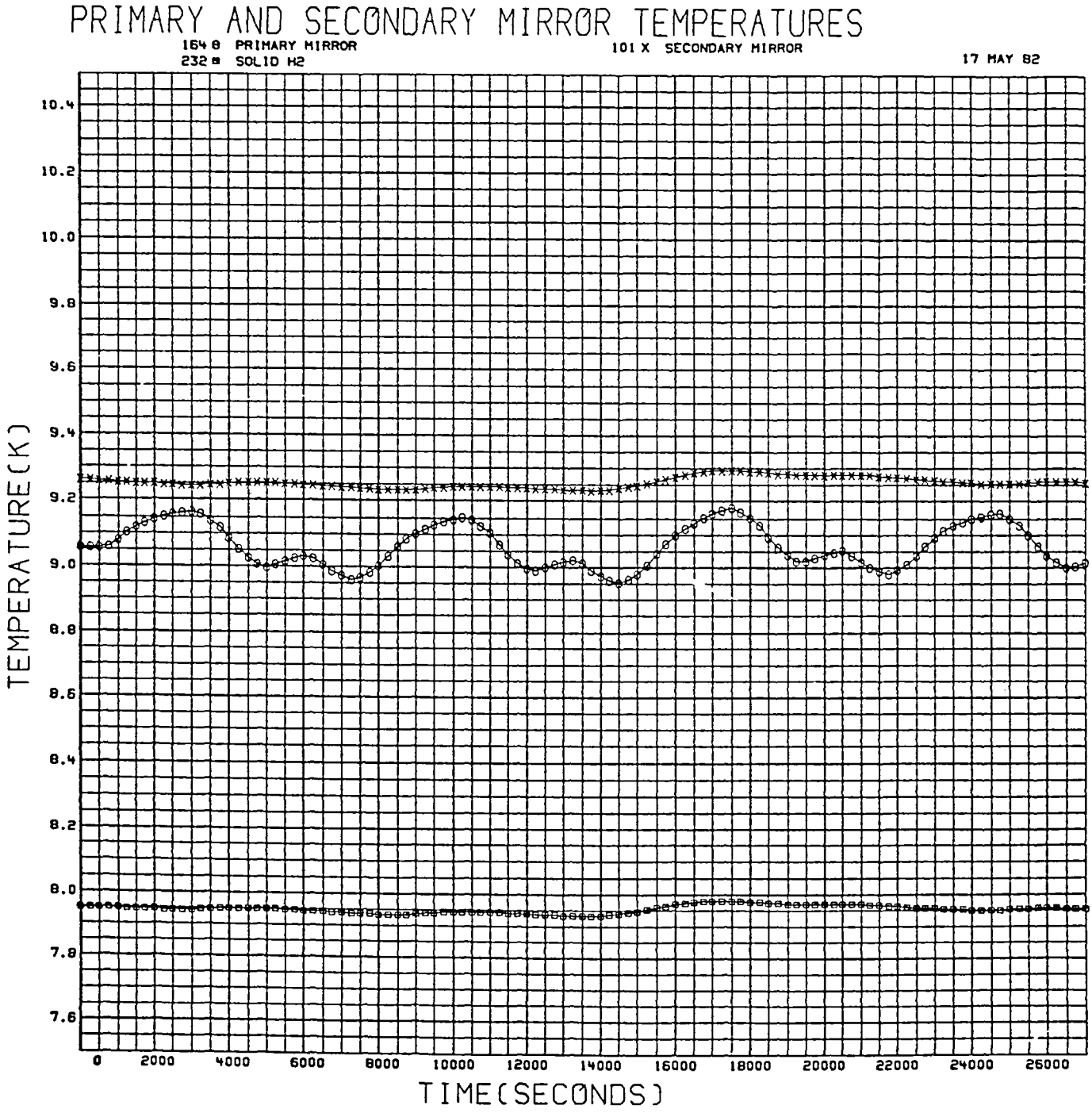

Fig. 8-6 Primary and Secondary Mirror Temperatures

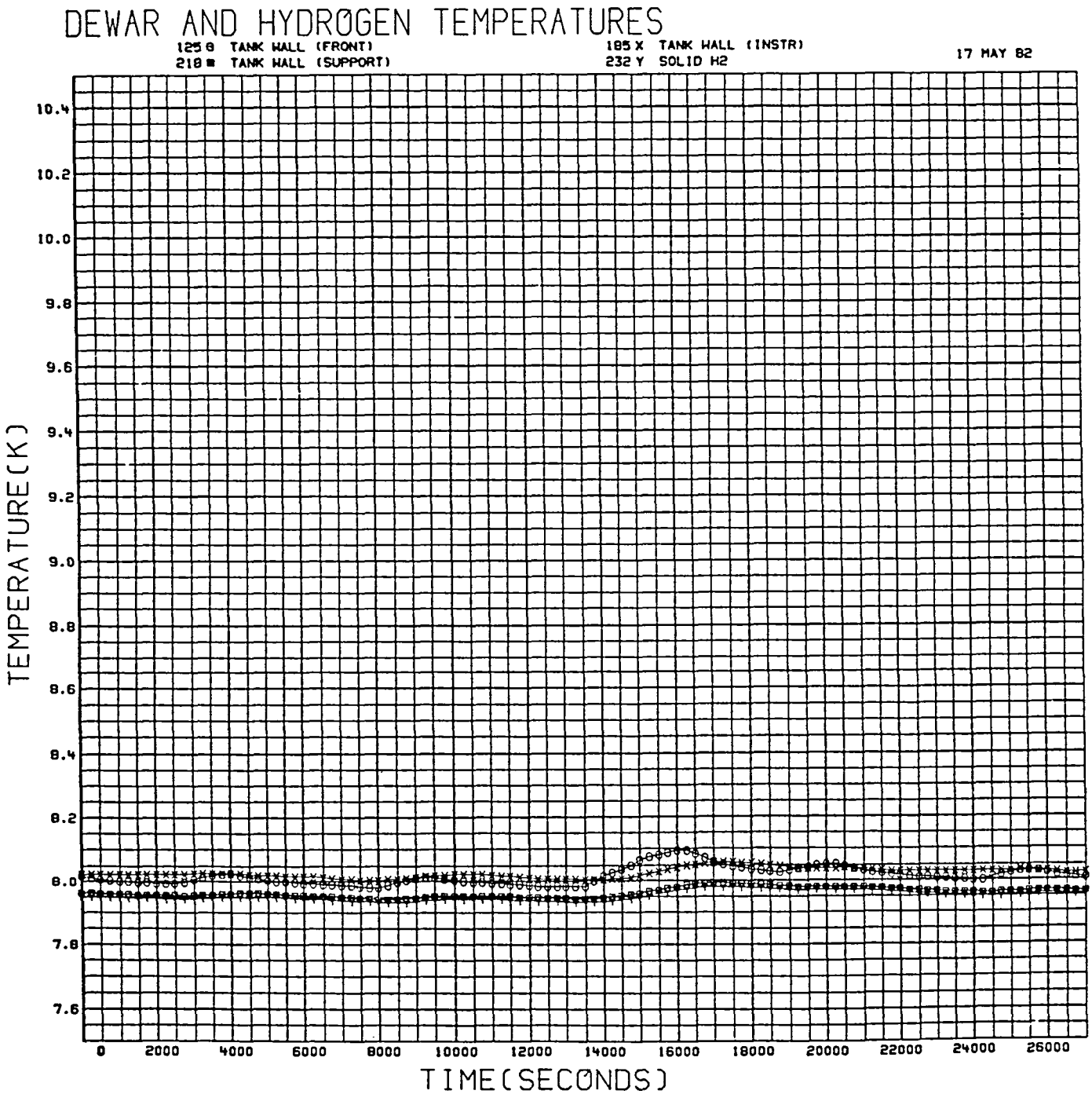

Fig. 8-7 Dewar and Hydrogen Temperature

0.10 K is maintained where the aperture load ties into the dewar wall. It can be concluded that the aluminum foam heat exchanger is very effective in reducing the thermal gradients within the hydrogen dewar.

8.2.6 Vapor-Cooled Focal Plane Temperatures (Fig. 8-8)

The resulting temperature of the SFHe vapor-cooled focal planes is shown. The goal was to maintain these temperatures to less than 6 K when operating and that achieved thus far is between 6.1 to 6.3 K. Because bringing these temperatures within specifications will have such a small impact on the performance of the overall SIRTF long-life configuration, these trades were not re-run at this time.

8.2.7 Radiator Temperatures (Fig. 8-9)

Temperatures of both the radiator inner and outer edge and radiator-cooled shield (over the cooler and instrument) are shown. Equilibrium temperatures during the warm and cold soak periods are never reached on the radiator panel. Away from the radiator surface along the radiator-cooler shield, however, the transients are well dampened to the point where a very stable temperature profile is maintained over both the instrument and cooler.

8.2.8 Sunshade Temperatures (Fig. 8-10)

Sunshade temperatures are shown for each of five equal length sections of the sunshade. During the cooling portion of the curves, the sunshade tracks the radiator temperature to within 5 K. Some divergence is observed, however, during those times when a solar load is imposed on the sunshade and radiator. The largest gradient occurs during the orbit 1 solar heating period (14,000 to 16,000 s) in which a 21 K difference is sustained along the sunshade, with a 10 K increase between the sunshade and radiator.

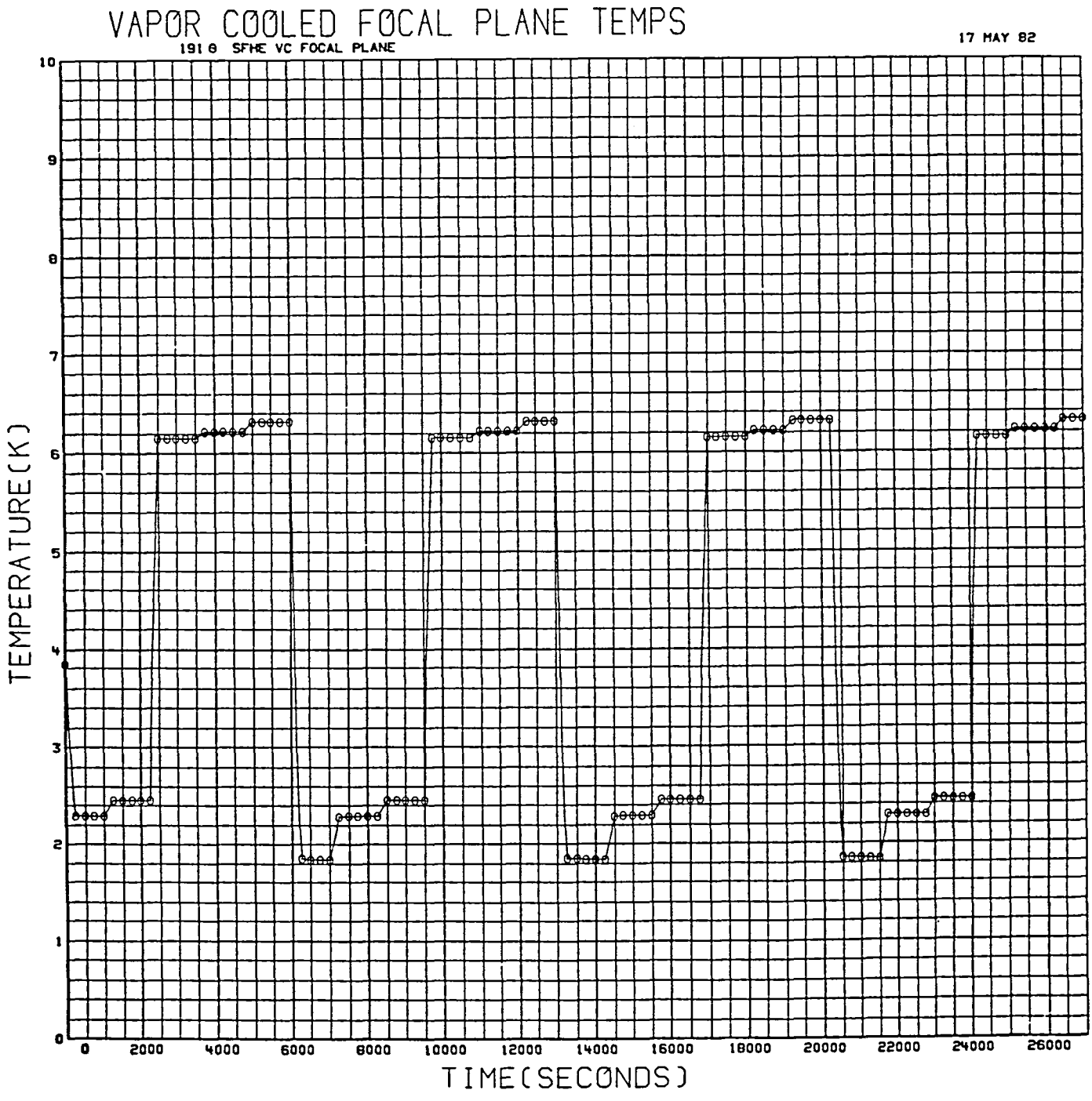

Fig. 8-8 Vapor-Cooled Focal Plane Temperatures

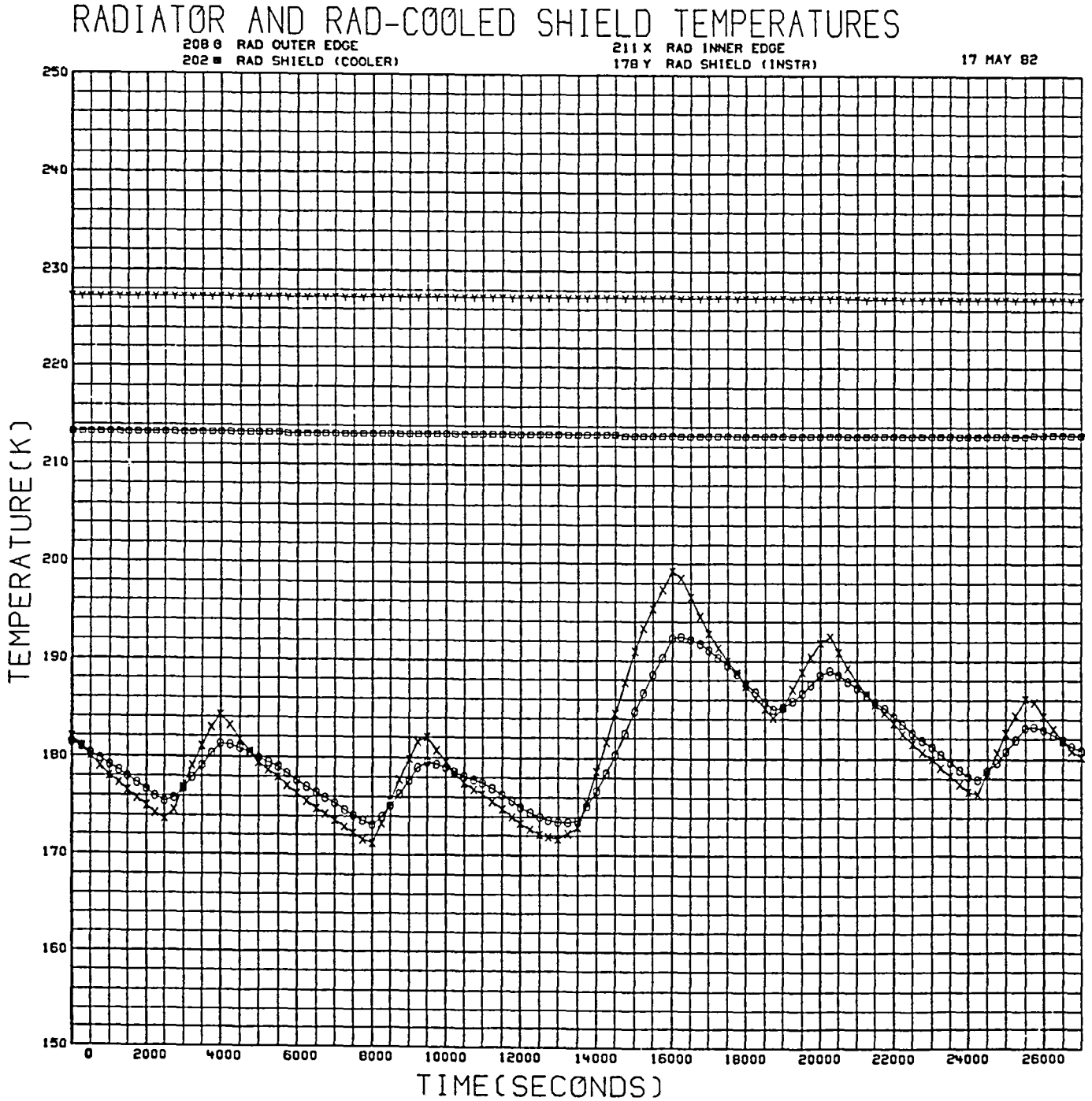

Fig. 8-9 Radiator and Radiator-Cooled Shield Temperature

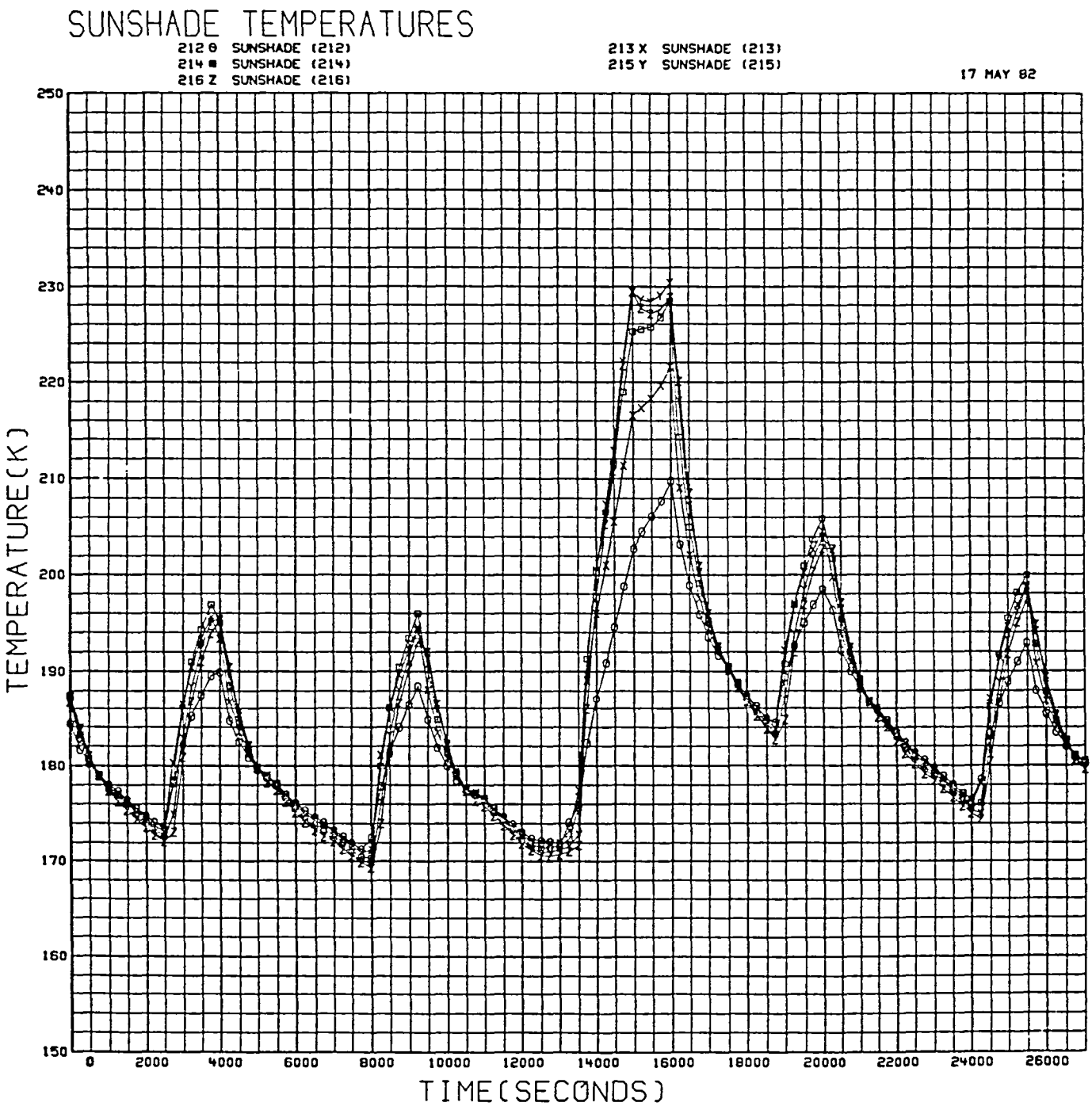

Fig. 8-10 Sunshade Temperatures

The varying IR radiated aperture heat load caused by this sunshade temperature profile leads directly to the structure in the cryostat heat load profile shown in Fig. 8-3.

Section 9
BASELINE SENSITIVITY

A sensitivity study has been performed on the baseline long-life SIRTF configuration to determine the change in either cryogen lifetime or instrument operating temperatures as a function of a change in any single design parameter. The results of this study are described in the following paragraphs. All of these results are focused on a system designed for 6 month lifetime. Longer lifetimes designed into the basic system could substantially affect these conclusions. For example, a 35 percent lifetime increase is achieved with a neon secondary cryogen, at a cost of 1,347 Kg. The same lifetime could be achieved by increasing the basic hydrogen capacity with significantly less mass penalty (a 2-year lifetime would be substantially less than this figure).

9.1 SIRTF STEADY-STATE TEMPERATURE VERSUS MIC POWER DISSIPATION (Fig. 9-1)

The change in temperature of facility components is shown as a function of the MIC power dissipation. For MIC heat loads greater than 0.62 W, the maximum instrument interface temperature (in the central hub of the MIC near the fine guidance sensor) sets the upper temperature limits within the MIC. Average MIC heat loads may be increased to 1.45 W before this maximum MIC temperature reaches 10 K. Because the primary mirror mounts to the primary support ring, it is seen to operate lower than the minimum instrument temperature by about 0.1 K. Even for MIC loads as high as 2.0 W, both the primary and secondary mirror temperature will operate less than 10 K. As expected, changes in the MIC power have a very small effect on the secondary mirror temperature.

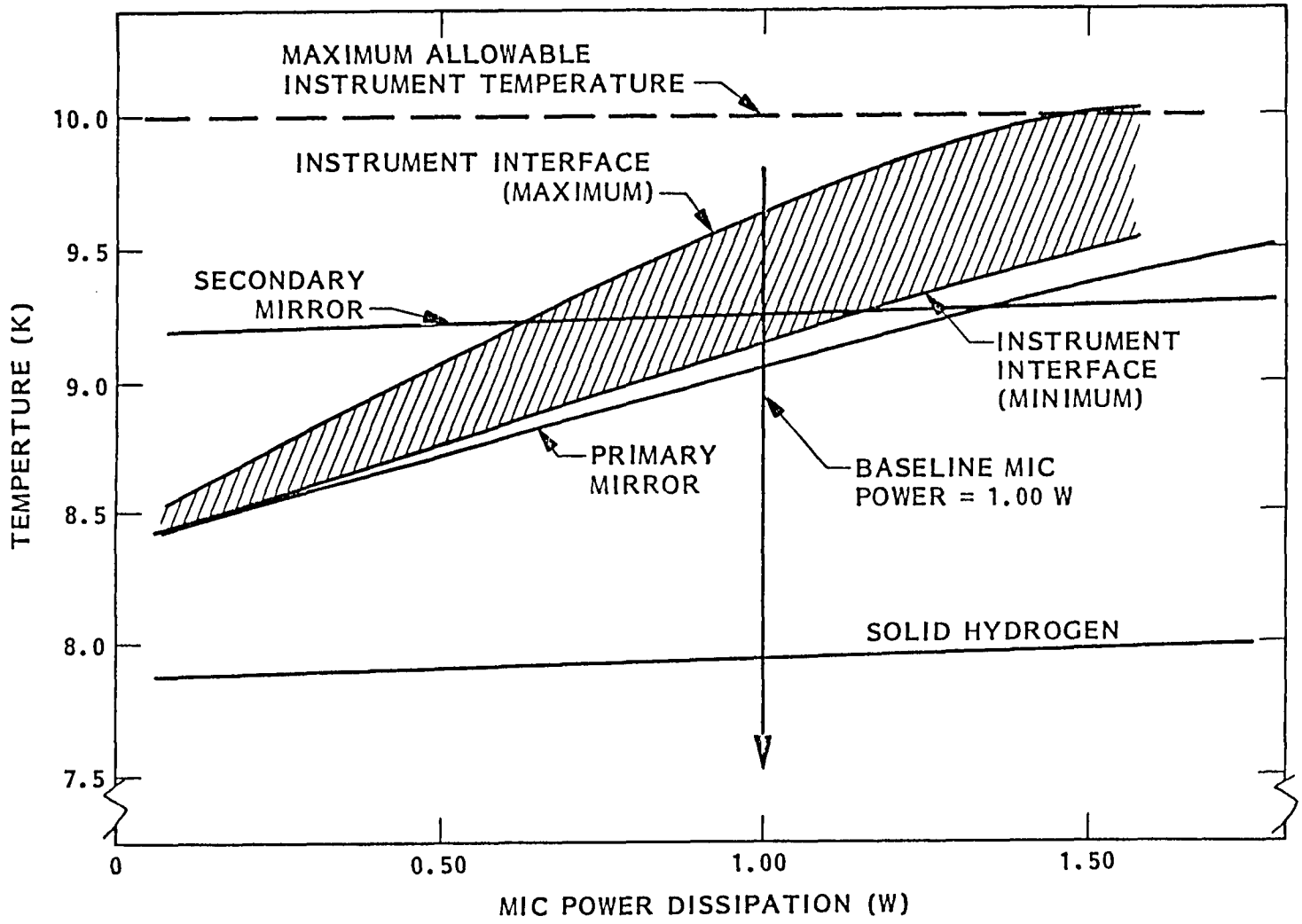

Fig. 9-1 SIRTF Steady-State Temperature Versus MIC Power Dissipation

9.2 COMPONENT POWER DISSIPATION AND ABSORBED ENVIRONMENTAL HEAT RATE (Fig. 9-2)

The change in total heat rate to the solid hydrogen dewar is determined for changes in the MIC instrument load, fine guidance sensor, and combined environmental heat load to the radiator and sunshade from the baseline value. The lifetimes also shown on the plots have been normalized to give 6.0 months at the baseline heat load of 3.319 W.

The item found to have the least sensitivity to relative changes in heat rate is seen to be the fine guidance sensor. Even by doubling the power to 0.20 W at the 10 K zone and 1.80 W to the vapor-cooled shield only decreases the lifetime by 6 percent to 5.6 months.

More dramatic changes in lifetime can be realized through changes in both the MIC and environmental heat loads. Following the MIC heat load curve to zero gives the limiting improvement in lifetime to 7.72 months. This value is almost achieved when the MIC heat load of 0.017 W, as defined for the "First" instruments,* gives a 7.69-month lifetime. From the environmental loading curve, the effect of restricting the sun angles greater than 90 deg (while retaining the same pointing profile to the earth limit) is seen to increase the lifetime to between 7.90 and 8.13 months, depending on whether 100 or 0 earth albedo is assumed.

9.3 MLI BLANKET DEGRADATION FACTOR (Fig. 9-3)

The performance of any MLI system can be characterized by the ratio of the effective measured thermal conductivity as applied on tankage compared to the performance of the same MLI system as measured in flat-plate calorimeter tests. This ratio is called the degradation factor and has been measured for several different insulation systems on large-diameter tanks at LMSC. Results of these tests at cold bondary temperatures as low as 60 K suggest that a

* From Table 1.7 - ER408, Design Optimization Study Final Technical Report, Sept. 1979.

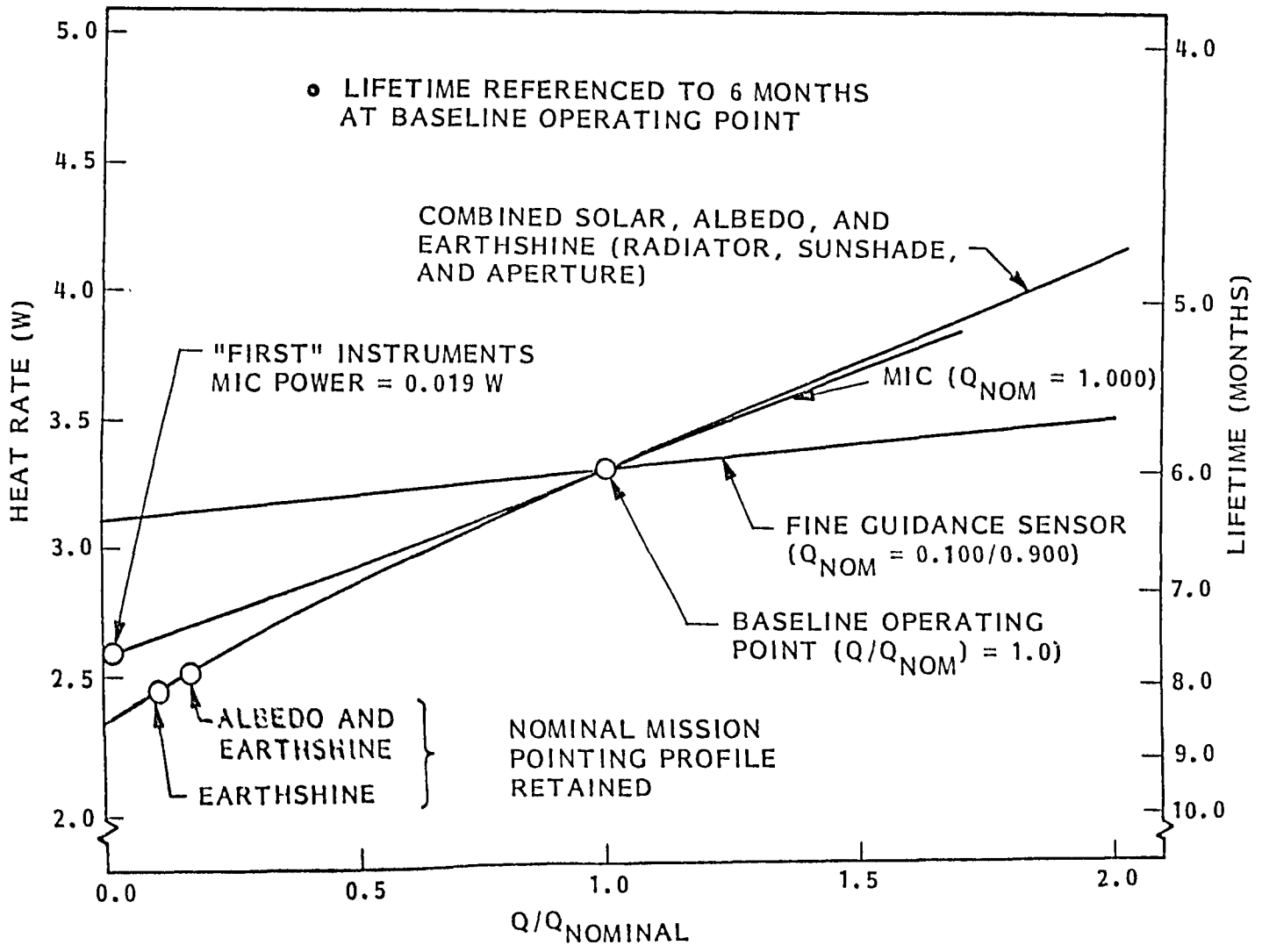

Fig. 9-2 Hydrogen Heat Rate and Lifetime Versus Component Power Dissipation and/or Absorbed Heat Rate

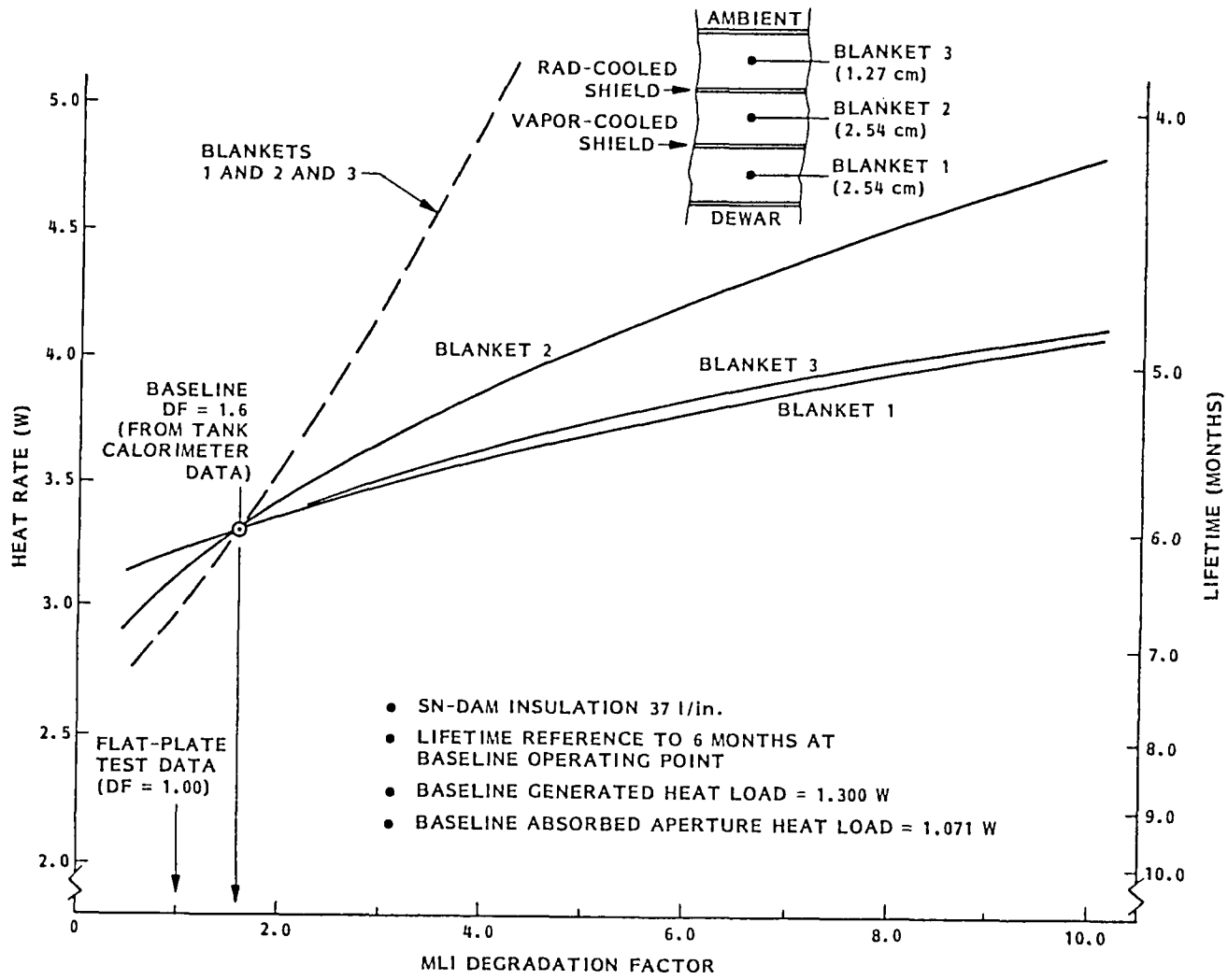

Fig. 9-3 Hydrogen Heat Rate in Lifetime Versus MLI Degradation Factor

degradation factor of 1.6 should be used for silk-net/double-aluminized mylar insulation systems wrapped at a 37-layer/in. density. The sensitivity to change from this baseline degradation factor is explored in Fig. 9-3. The solid curves show the change in performance as the MLI degradation factor for only the blanket indicated is varied from 0.5 (better than flat plate) to 10.0. The effect of varying the degradation factor used in all three blankets simultaneously is also shown in the figure by the dashed line.

Because considerable test data exist within the temperature boundaries of blankets 2 and 3, LMSC has a high confidence in the degradation factor of 1.6 used in the analysis. This same level of confidence is not felt for the lower boundary temperature regime of blanket 1. Fortunately, blanket 1 shows the least sensitivity of all three blankets to change in degradation factor. Indeed, at a factor as high as 5.0, only a modest 11 percent reduction in lifetime to 5.4 months is incurred.

9.4 FIBERGLASS SUPPORT CONDUCTANCE (Fig. 9-4)

The change in the total heat load to the solid hydrogen dewar is determined as a function of the change in conductance of the fiberglass support system. The baseline conductance is that derived for a support tube having 1543/E787 cloth wrapped with the warp in the circumferential direction. Although wrapping in this manner reduces the stress margin on the tube, it enhances the resistance to buckling which sets the tube thickness in this design. For tubes with the warp wrapped in the longitudial direction, the lifetime decreases to 5.3 months.

The figure also shows the potential benefit by incorporating the PODS support concept into the baseline design. The total heat rate is reduced to 2.43 W, only slightly above the 2.37 W generated in the instrument or absorbed through the aperture. This reduction in heat rate translates to an 8.20-month lifetime, a 37 percent increase.

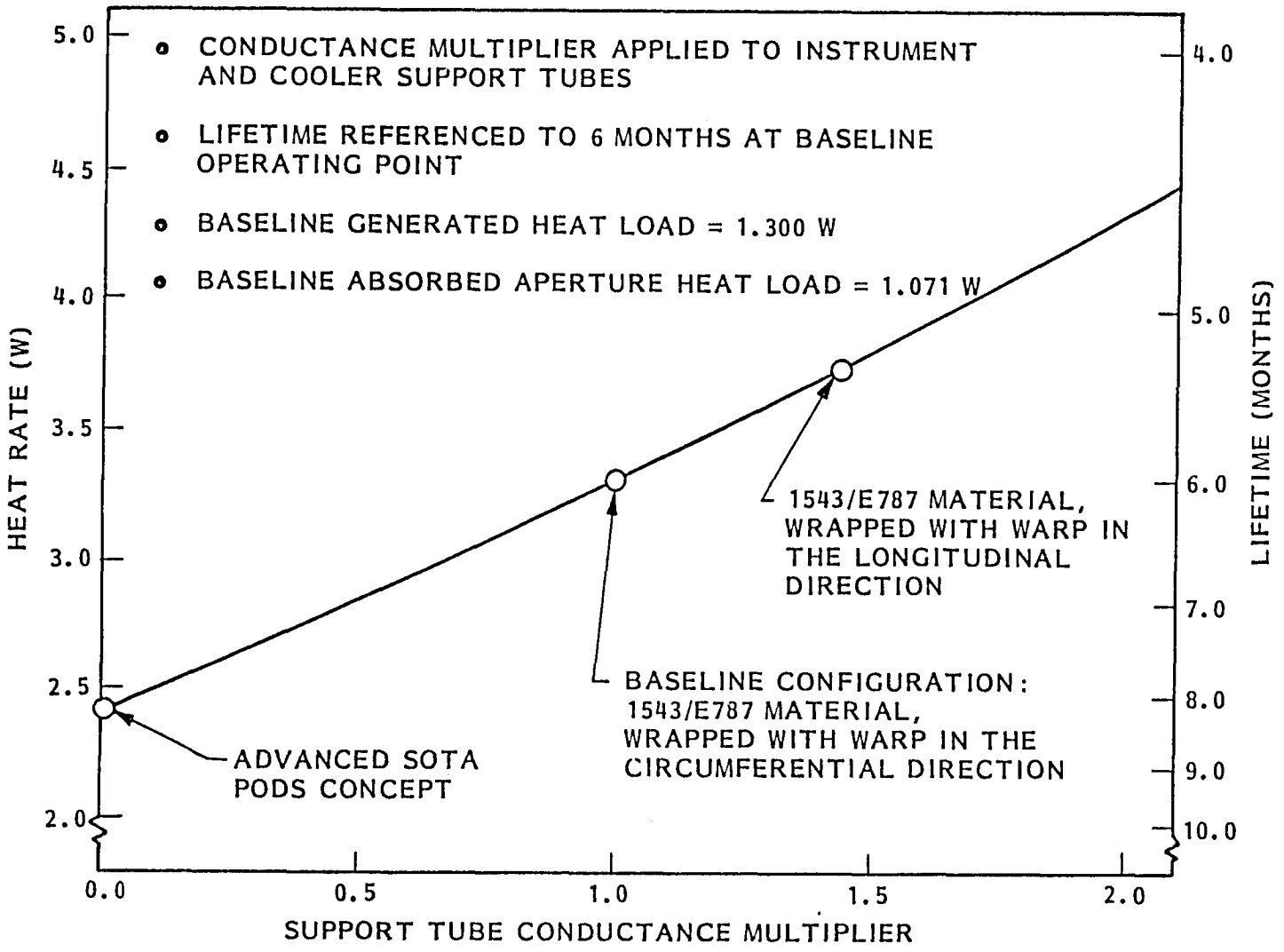

Fig. 9-4 Hydrogen Heat Rate and Lifetime Versus Fiberglass Support Tube Conductance

9.5 RADIATOR SIZE AND OPTICAL PROPERTIES (Fig 9-5)

The baseline radiator has an outer radius of 120 cm and inner radius of 91 cm, and assumes that the surface optical properties are those of a degraded (or end-of-life) optical solar reflector (α_s/ϵ = 0.16/0.86). Figure 9-5 shows how the hydrogen dewar heat rate changes with selection of the outer radius (i.e., radiator area and temperature).

Increasing the radiator radius to much more than 150 cm begins to impact on the maximum available cylindrial envelope that can be accommodated by the shuttle. At 150 cm, the average radiator temperature drops to ~169 K, which provides a marginal 6 percent increase in lifetime to 6.4 months. Indeed, the sensitivity of radiator outer radius (area) has a relatively small impact on the hydrogen lifetime from 110 to 150 cm. At 110 cm, the penalty incurred in lifetime is at 6 percent and begins to increase rapidly with smaller radius.

A difference of 3 percent in lifetime for aluminum OSR and 6 percent for silver OSR is realized between the beginning-of-life and end-of-life optical properties.

9.6 AUGMENTED COOLING OF VAPOR-COOLED SHIELD (Fig. 9-6)

The lifetime benefit realized by augmented cooling of the vapor-cooled shield is shown. The curve shows the equilibrium temperature and hydrogen heat rate as a function of the refrigeration provided to the vapor-cooled shield by either a mechanical refrigerator or a secondary solid cryogen system.

For the dual stage solid cryogen system, the hydrogen heat rate is seen to be reduced to between 2.47 W (neon) and 2.92 W (methane). The lower heat rates allow a smaller hydrogen tank volume and mass, which must be sufficient to offset the increased mass and complexity imposed by the secondary cryogen. The change in mass for the dual stage system is summarized in Table 9-1. For all secondary cryogens, a net mass penalty of from 176 kg (CH_4) to 1347 kg (Ne) is incurred by incorporating a secondary cryogen.

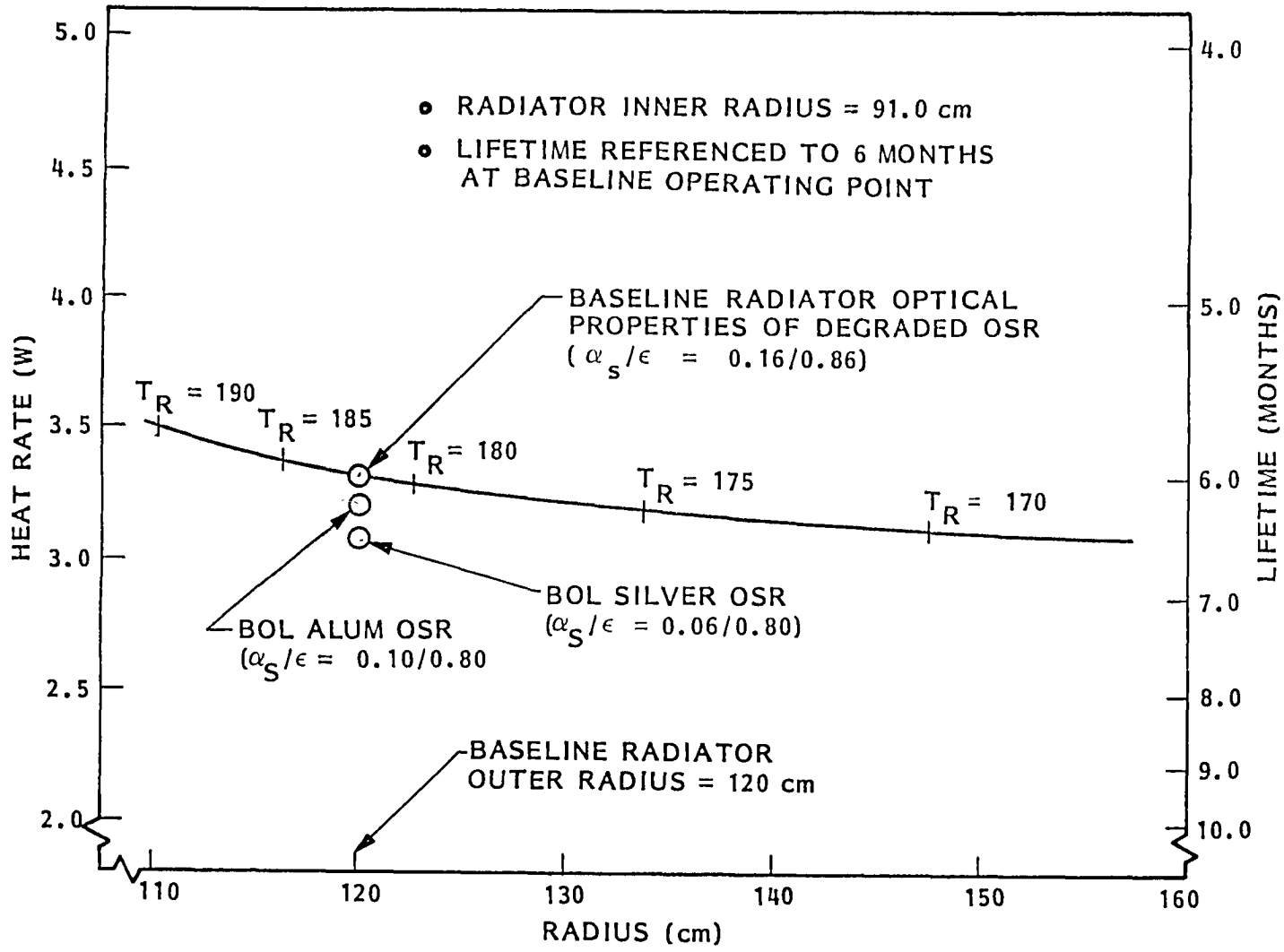

Fig. 9-5 Hydrogen Heat Rate in Lifetime Versus Radiator Outer Radius and Optical Properties

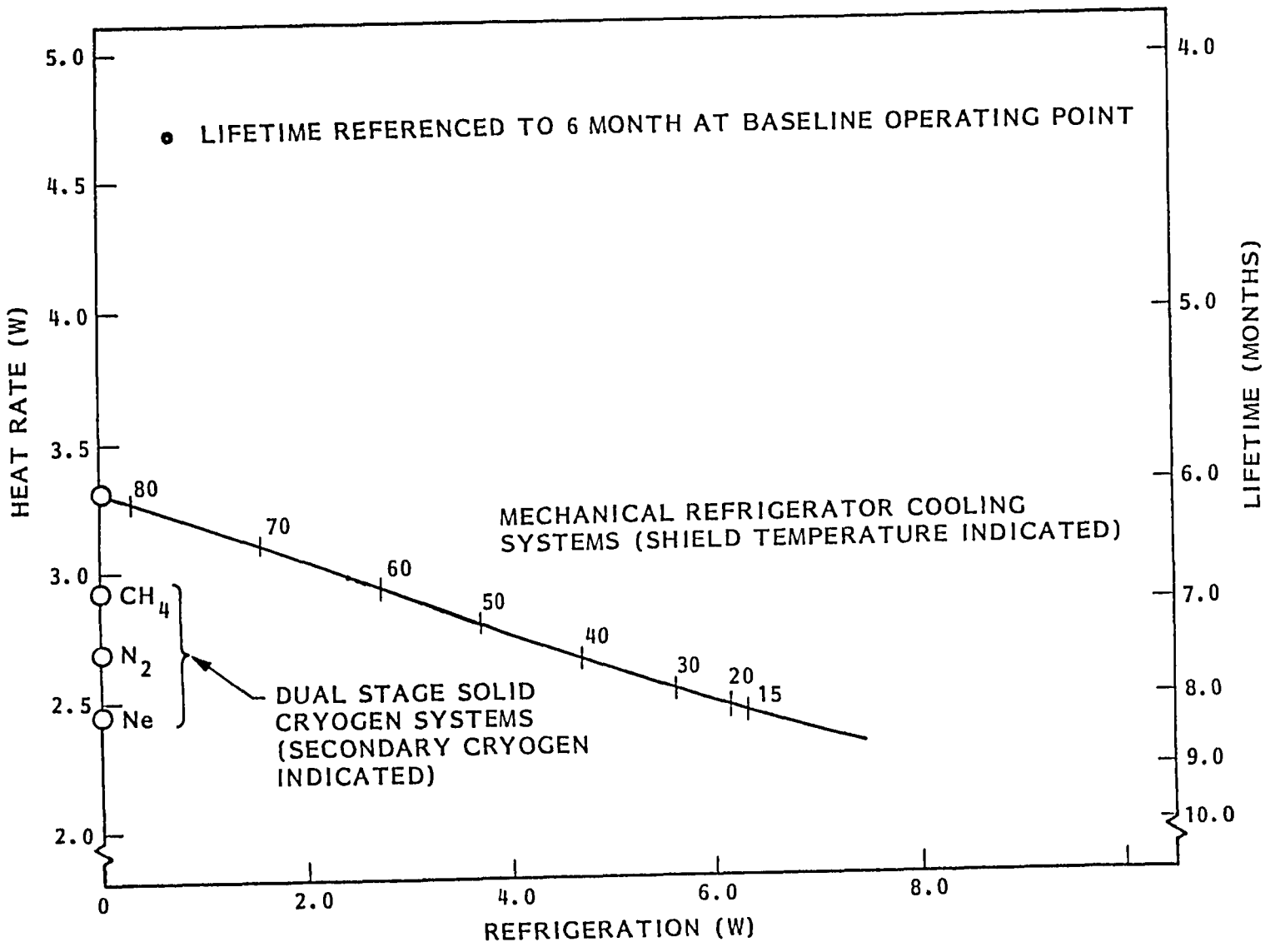

Fig. 9-6 Hydrogen Heat Rate and Lifetime Versus Augmented Refrigeration to Vapor-Cooled Shield

Table 9-1 SIRTF MASS CHANGE FOR DUAL-STAGE SYSTEM

SECONDARY CRYOGEN	TEMP (K)	HYDROGEN HEAT RATE (W)	SECONDARY HEAT RATE (W)	HYDROGEN SYSTEM MASS CHANGE (kg)	SECONDARY SYSTEM MASS CHANGE (kg)	NET SIRTF SYSTEM MASS CHANGE (kg)
NONE	83	3.317	0.0	--	--	--
METHANE	60	2.92	2.73	-48.7	225	176
NITROGEN	43	2.69	4.45	-76.7	445	368
NEON	15	2.47	6.31	-103.4	1450	1347

Section 10
SECONDARY ACTUATOR DESIGN

This study was undertaken to examine the feasibility of utilizing proprietary Lockheed electrodynamic actuator technology for application to the SIRTF secondary mirror. Of particular concern was the requirement for large-excursion/high-frequency actuation coupled with minimized thermal dissipation during chopping. Effort was directed in two areas: analysis of fundamental electrodynamic force generating priciples was undertaken as a part of this long life study contract, and laboratory measurement of actuator performance at both room-ambient and cryogenic temperatures, pursued on LMSC IR D funds. The results of these investigations permitted the development of mathematical models to generate an optimal (minimum power, maximum force) design and predict energy dissipation for a given configuration under SIRTF operating conditions.

10.1 PERFORMANCE CRITERIA AND POTENTIAL ADVANTAGES OF ELECTRODYNAMIC ACTUATORS

The performance criteria for the SIRTF secondary mirror are as follows:

- 20 Hz, 90 percent duty cycle chop
- ± 24 arcmin amplitude (± 7.5 arcmin movement of system LOS)
- 1000 g-cm^2 mirror inertia
- Reactionless design
- Energy dissipation of <200 mW
- Actuator dimensions not to exceed secondary mirror envelope
- Operation at < 10°K

These pose extremely challenging problems for the control system designer. The usual requirements of aerospace systems for small size, light weight, and low power are augmented by the need to generate forces on the order of 50 to 100 N in a time frame of only 200 to 600 μs while maintaining cryogenic temperatures.

Electrodynamic actuators are differentiated from the electromagnetic variety by their lack of a fixed magnetic field (see Figs. 10-1 and 10-2). By using two coils to generate the interactive magnetic fields, electrodynamic actuators are capable of delivering substantially more force than a electromagnetic device of comparable size. This is possible because flux concentration is improved in electrodynamic motors by use of the actively (rather than passively) generated field, high permeability core material to focus the field effects, and gaps between moving parts as small as 25 μm, which minimize losses in field strength.

Two characteristics of electrodynamic actuators; the comparatively large inertia of the moving portion and the additional power consumed by the use of two coils (rather than the single coil in an electromagnetic machine) are potential disadvantages for the SIRTF application.

Given the performance criteria, the questions to be answered are:

- Could any actuator, with physically realizable dimensions, produce the force required
- What is the optimum actuator-linkage geometry, given the size and inertia-cancelling constraints on the mirror-actuator system
- What is the predicted energy dissipation of the proposed design under SIRTF operating conditions

10.2 DEVELOPMENT OF AN ANALYTICAL MODEL FOR ACTUATOR OPTIMIZATION

The relationship between the physical parameters used to describe the geometry of a generic mirror-actuator system are shown in Fig. 10-3. An operating system would consist of a pair of actuators, as seen in Fig. 10-4, so that both forces and moments will be cancelled. The analysis is somewhat simplified, however, by assuming the use of a single actuator.

The control system parameters α and β, which affect the design of the actuator, are illustrated in Figs. 10-5 and 10-6. The ratio of the total transition time t_T to the time during which the actuator is used to apply

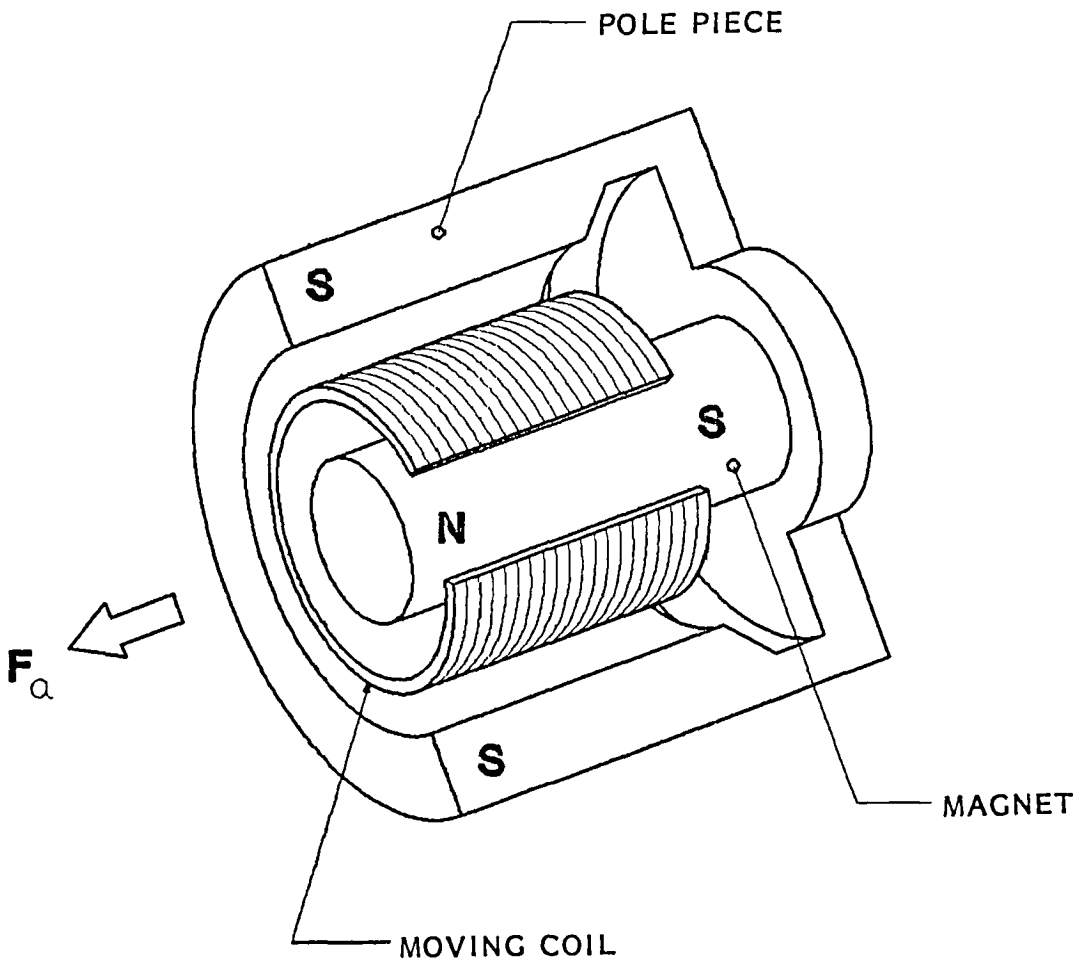

Fig. 10-1 Electromagnetic Actuator Cutaway View

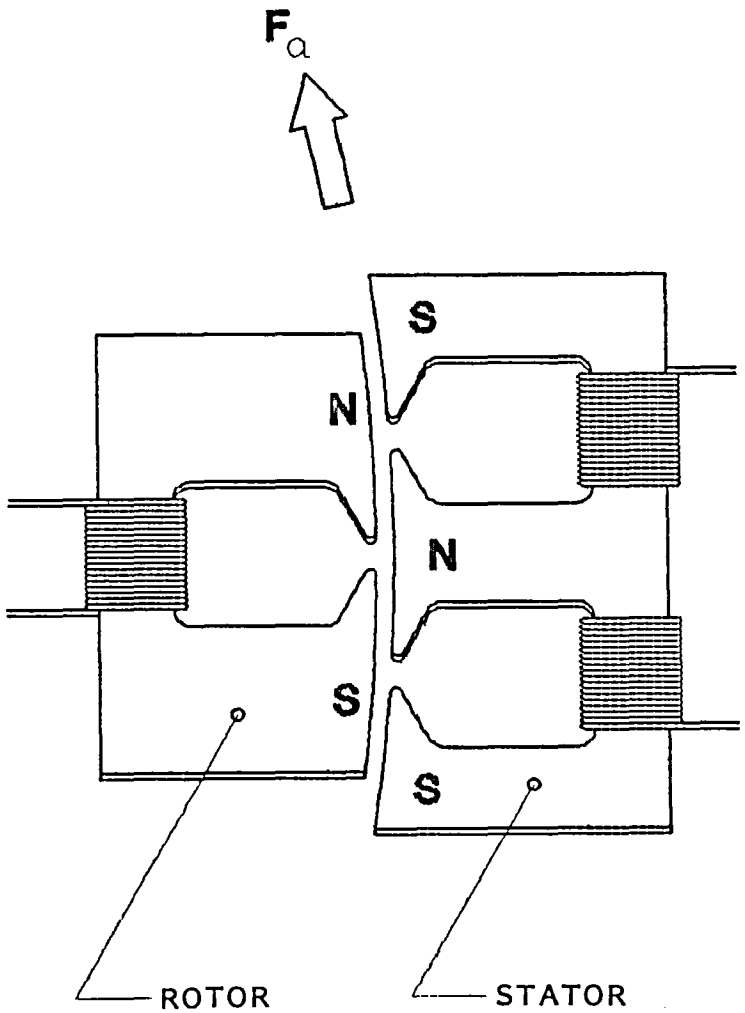

Fig. 10-2 Electrodynamic Actuator Detail

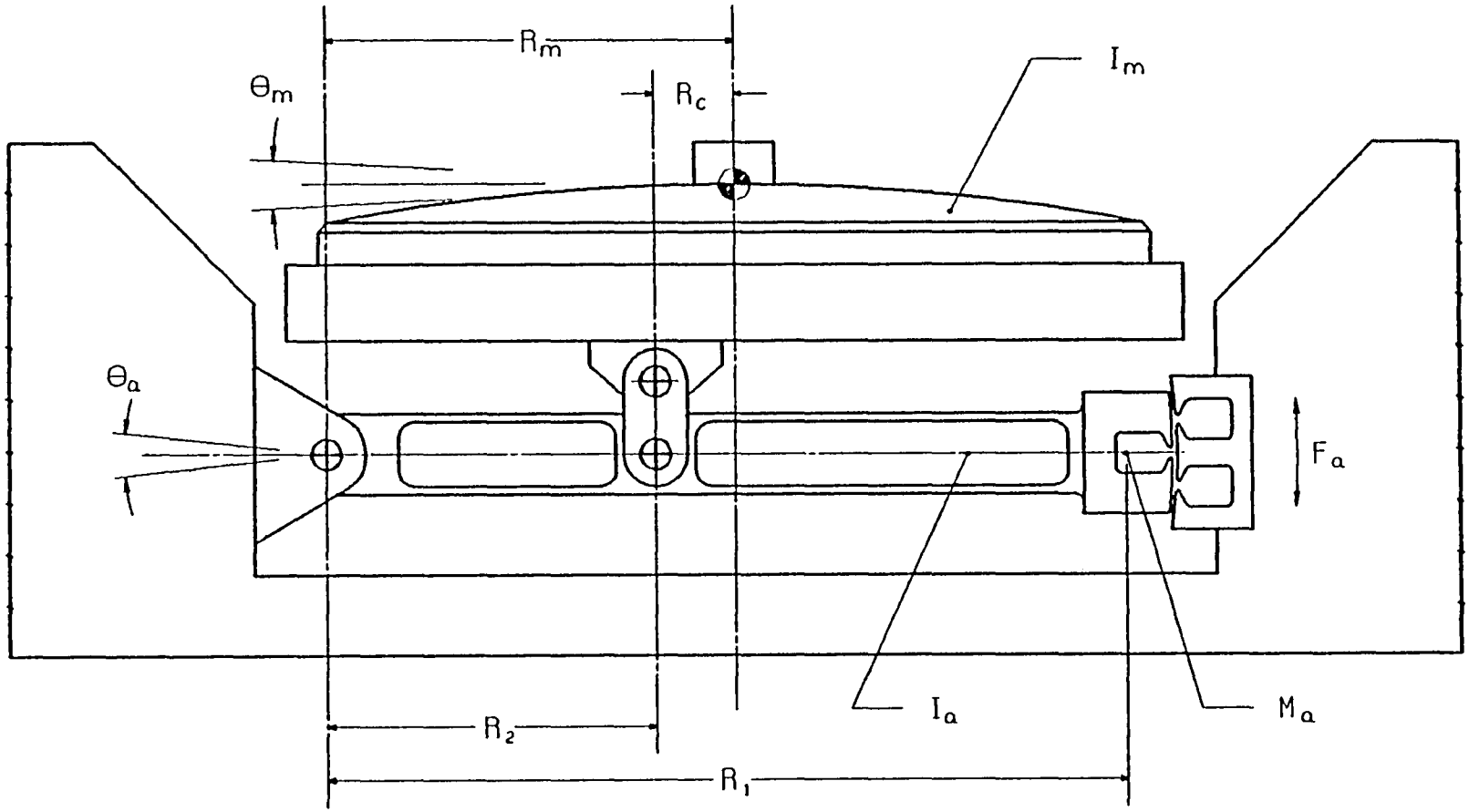

Fig. 10-3 Secondary Mirror Actuator, Cross-Sectional View

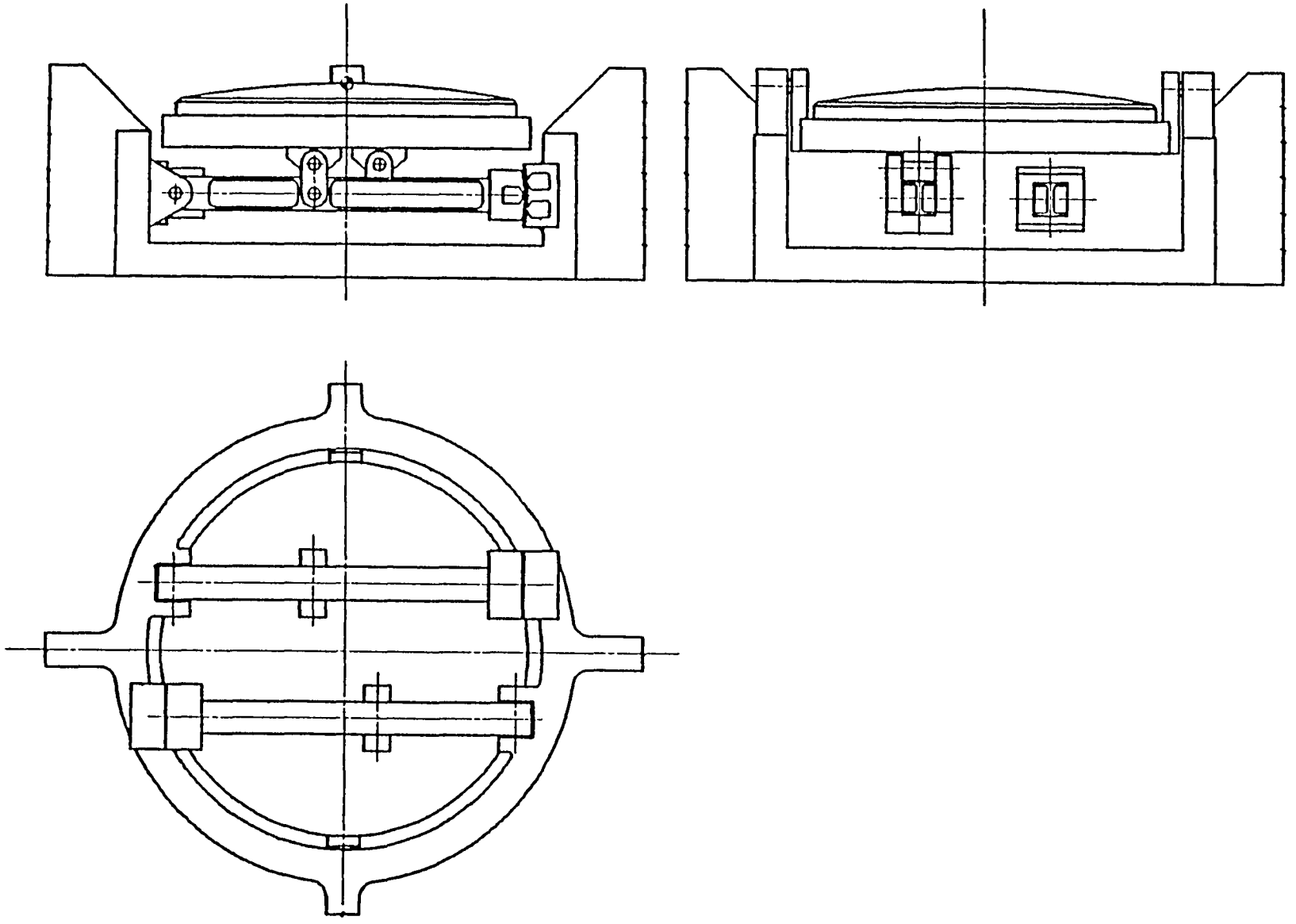

Fig. 10-4 Secondary Mirror Actuator

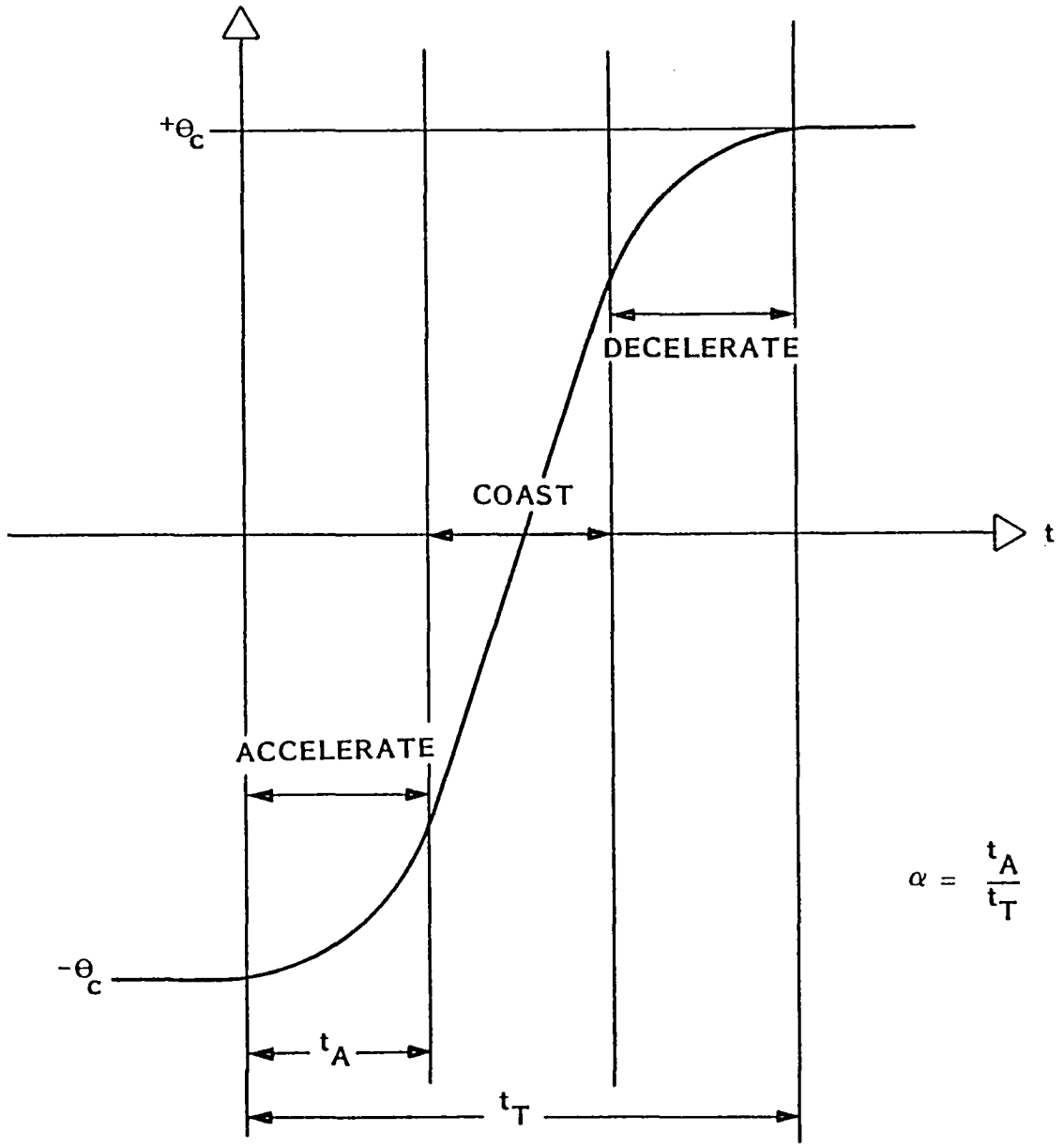

Fig. 10-5 Transition Period Detail

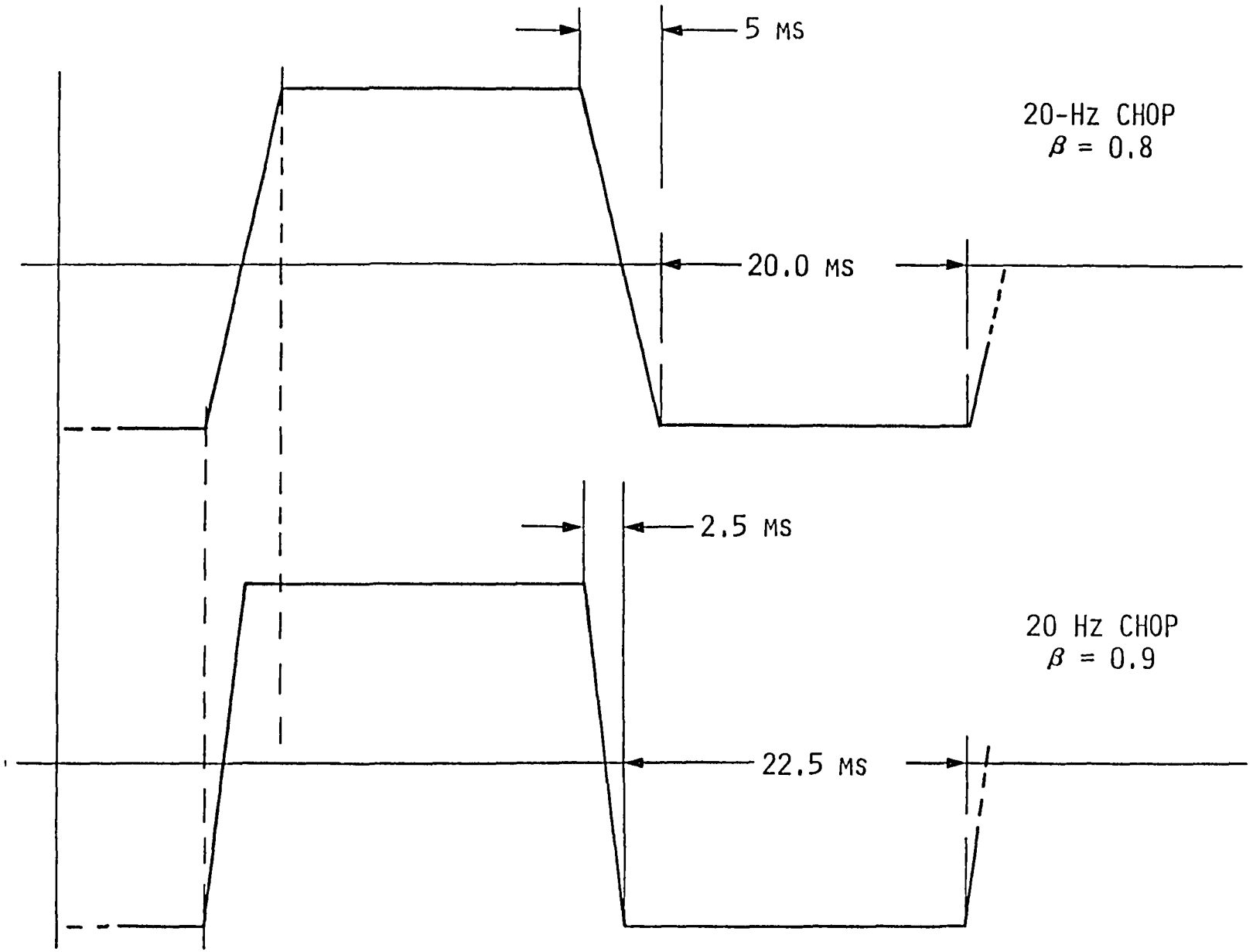

Fig. 10-6 Effect of Duty Cycle Variation

a force t_A (for either acceleration or deceleration) is defined as α. The duty cycle, or percentage of a total chop cycle during which the mirror is actually available to the optical system, is defined as β. Together, α and β represent important tradeoff parameters in both the design of the mirror-actuator system and the overall philosophy of the telescope system. Figure 10-6 demonstrates the impact on the actuator requirements of an 11 percent decrease in data-taking capability during a 20-Hz chop (β changed from 0.9 to 0.8). The force required to accelerate the mirror decreases by a factor of three, thus placing substantially lower demands on actuator performance and power consumption.

Equations (10.1) through (10.8) were derived by analyzing the requirements for mirror acceleration/deceleration, cancellation of moments and forces, and linkage geometry of the mirror and actuator system. The physical quantities in Eqs. (10.1) through (10.8) are shown in Fig. 3. Force required

$$F_a = K_\theta^2 \frac{\delta_a}{K_a (I_m - I_a \gamma)} \frac{(\gamma + 1)^2}{\gamma} \tag{10.1}$$

Actuator gear ratio

$$\gamma \triangleq \frac{R_c}{R_2}$$

$$\gamma = \frac{\frac{K_a I_m}{\delta_a R_1} - K_\theta}{\frac{K_a I_a}{\delta_a R_1} - K_\theta} \tag{10.2}$$

Mass of actuator rotor pole piece

$$m_a = k_\theta^2 \frac{1}{(I_m - I_a\gamma)} \left(\frac{K_a}{\delta_a}\right)^{-2} \frac{(\gamma + 1)^2}{\gamma} \qquad (10.3)$$

where

$$k_\theta \triangleq \frac{8 I_m \theta_c \nu^2}{(1 - \beta)^2 \alpha (1 - \alpha)}$$

$\nu \triangleq$ chop frequency

$\theta_c \triangleq$ commanded angle of mirror

The lengths of actuator linkage connections, assuming a geometry in which $R_2 + R_c = Rm$, are

$$R_2 = \frac{Rm}{(1 + \gamma)} \quad \text{and} \quad R_c = \frac{Rm\gamma}{(1 + \gamma)} \qquad (10.4)$$

The force available from the actuator F_{AV} has been assumed to be

$$F_{AV} = \frac{K_a}{\delta_a} m_a \qquad (10.5)$$

or

$$F_{AV} = \frac{k_F}{d\ell} m_a \qquad (10.6)$$

In Eq. (10.5) the model uses the ratio of force developed per unit cross-sectional area, K_a, to pole piece mass per unit area δ_a. Equation (10.6) models the force as an efficiency factor k_F times the inverse of the product of the core density d, and magnetic path length . The difference between the pure attractive (or repulsive) force of a clapper (solenoid) and the translational force generated during operation of a real actuator is expressed as the efficiency factor k_F, and is approximately 8×10^4 kg/m-s^2.

Both of these estimates [Eq. (10.5) and (10.6)] of available actuator force are highly simplified approximations and are heavily dependendent on core material and geometry.

The basic relationship for energy dissipation in a resistor

$$E_R = \int_0^t R\, i^2 dt$$

leads to the expression for average power dissipated by a pulse actuated system

$$P_{AVE} = \frac{8}{3} \nu R' m_a i_{max}^2 t_A$$

where the term $R'm_a$ represents the total resistance of the coil winding, which increased linearly as a function of the size of the core. In this model, the core has a fixed cross sectional area; thus mass, and hence resistance, is a function of core length only.

Substitution of relationahips for t_A, α, and β yields

$$P_{AVE} = \frac{4}{3} R' m_a i_{max}^2 \alpha(1 - \beta) \qquad (10.7)$$

The average mechanical power used to physically move the mirror/actuator can be calculated from the kinetic energy imparted to the two components during the acceleration and deceleration periods.

$$E_K = 2 \left[\frac{I_m \dot{\theta}_m^2}{2} + \frac{(I_a + R_1^2 m_a)}{2} \dot{\theta}_a^2 \right]$$

Substituting expressions for I_a, R_1, m_a, and θ_a gives

$$P_{AVE} = \frac{8 I_m \nu^3 \theta_C^2 (1 + \gamma)}{(1 - \beta)^2 (1 - \alpha)^2} \qquad (10.8)$$

10.3 PARAMETRIC EVALUATION OF ACTUATOR REQUIREMENTS

Figures 10-7 to 10-9 display the results of calculations to determine actuator performance requirements as a functon of the parameters R_1, α, and β. For all these calculations, the actuator design constant K_a/δ_a has been assumed equal to 250 m/s^2. While versions of the pivoted proof mass actuator (PPM) measured in our laboratory exhibited a $K_a/\delta_a = 100$ for these tests, improved versions of the PPM and other actuators have demonstrated a K_a/δ_a of as much as 250 m/s^2.

In Fig. 10-7, the change in force and linkage geometry is plotted as a function of actuator length. Two important conclusions to draw from Fig. 10-7 are (1) the mirror diameter (2 R_m) is about the right length for the actuator, i.e., making it longer does not reduce the required force appreciably, and (2), the selection of $\alpha = 0.2$ provides a substantial lowering of the necessary force.

The changes in required force and the average mechanical and electrical power for the mirror-actuator system are shown in Fig. 10-8 as a function of α. An important point to note is that while there is some increase in average power

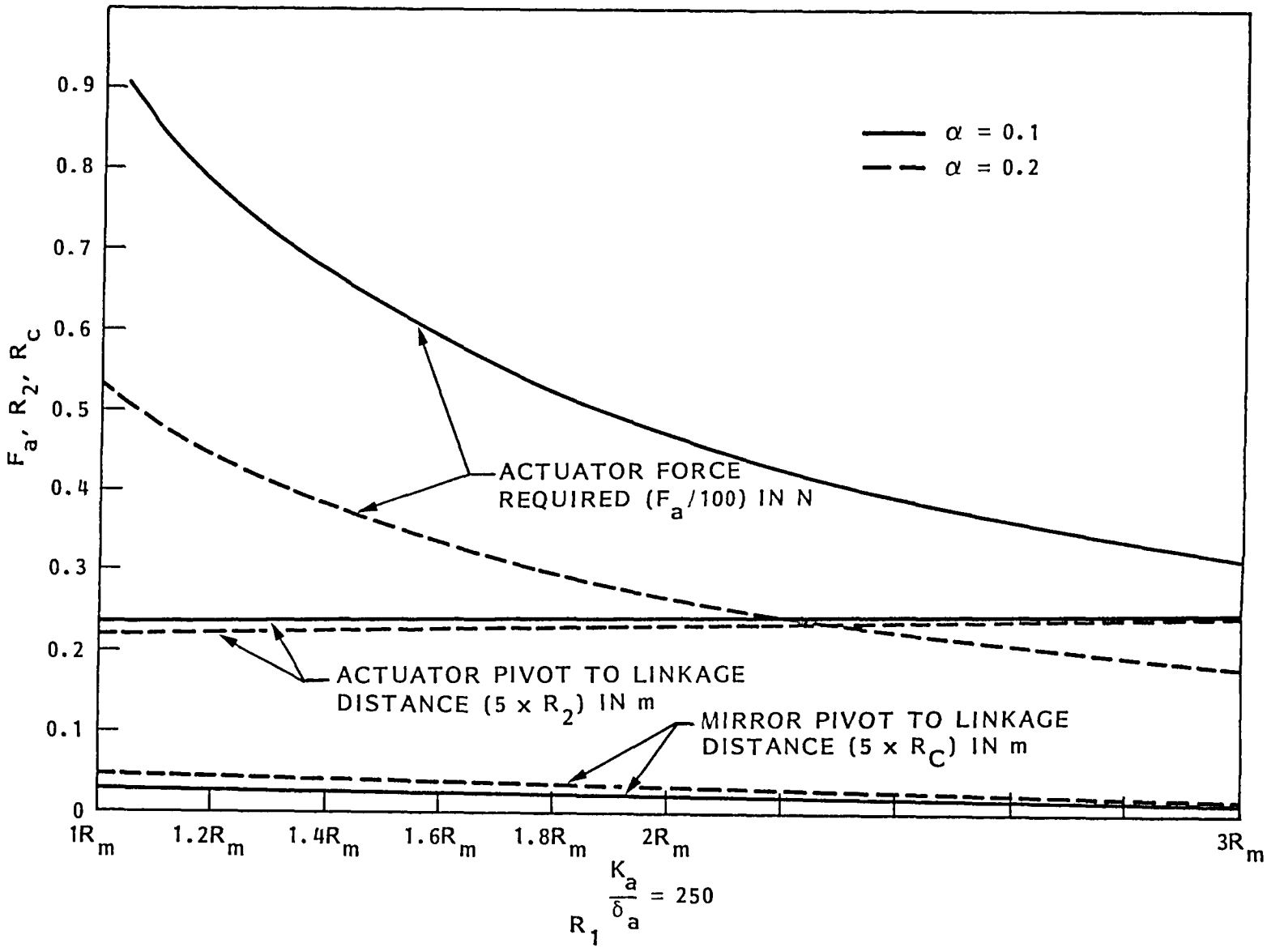

Fig. 10-7 Required Force and Actuator Linkage Radii as a Function of Actuator Arm Length

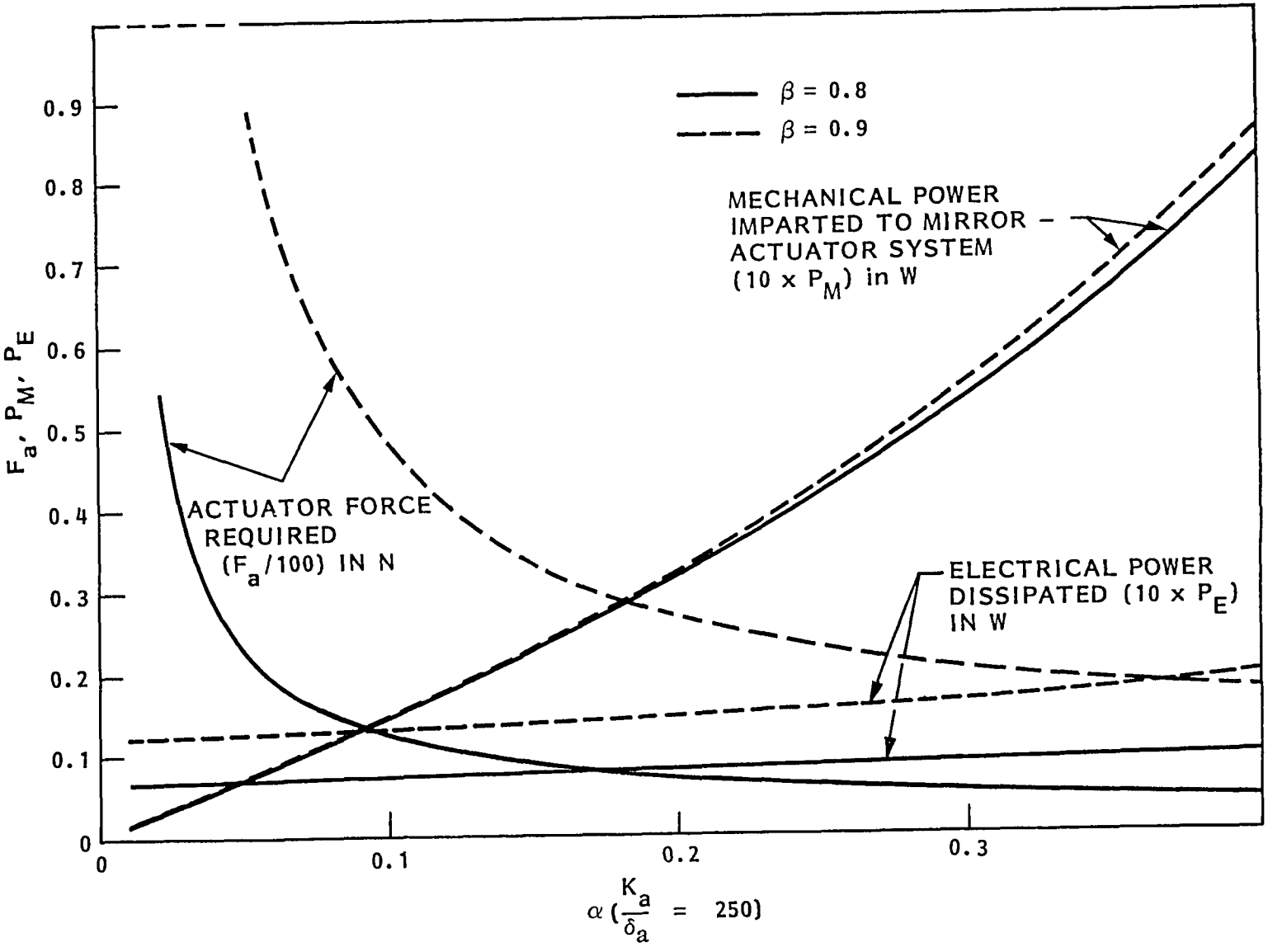

Fig. 10-8 Required Force, Average Mechanical Power, and I^2R Loss as a Function of Acceleration Time Ratio

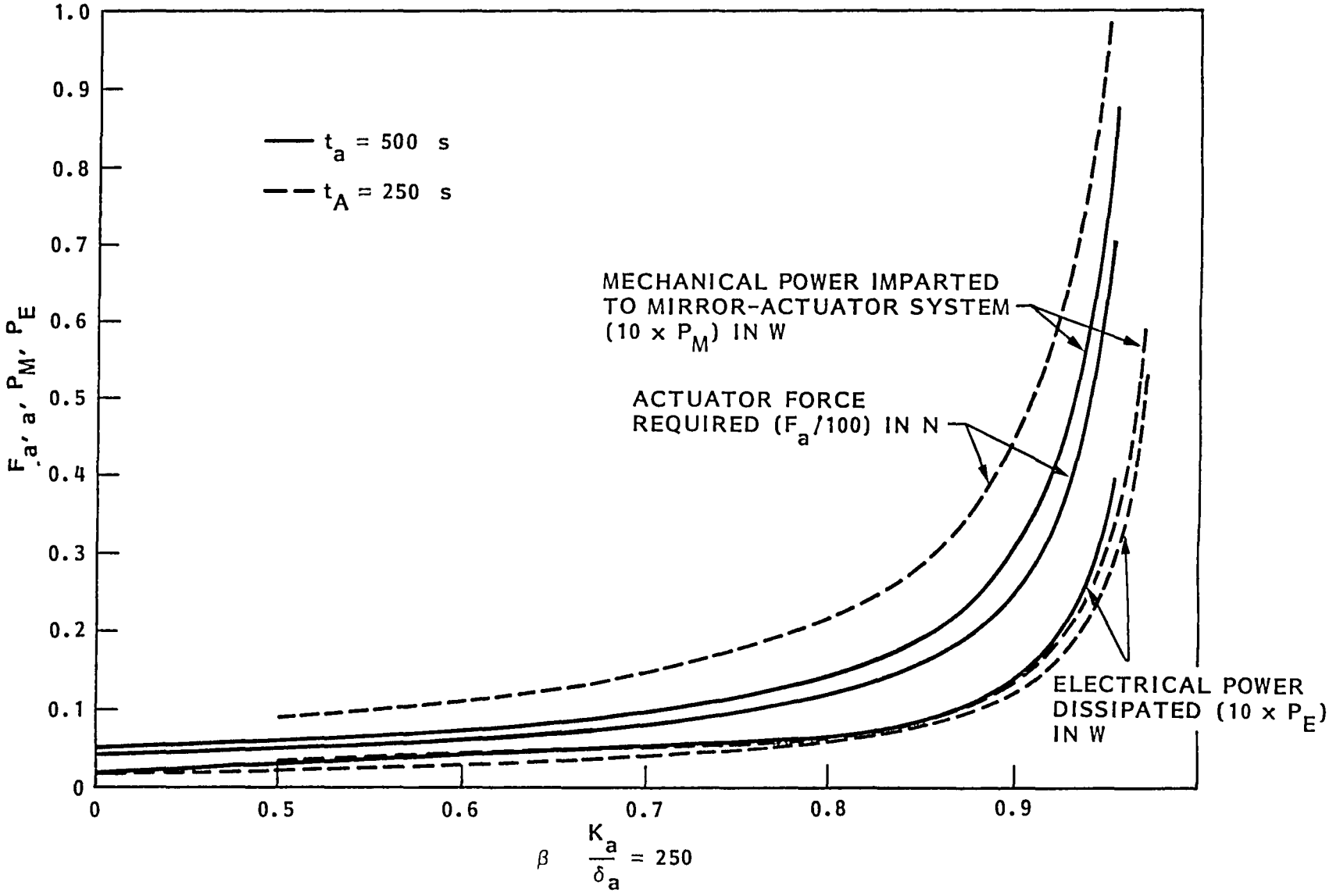

Fig. 10-9 Required Force, Average Mechanical Power, and I^2R Loss as a Function of Duty Cycle

dissipated when α increases from 0.1 to 0.2, the increase is relatively small, while the corresponding decrease in F_a is substantial. In addition, by changing the duty cycle β from 0.9 to 0.8, an additional decrease in required force is obtained. This translates directly into the ease with which the system is designed and the amount of margin available in any given design. As an example, an efficient (low power) design ($\alpha = 0.1$) with maximum duty cycle ($\beta = 0.9$) requires about 48 N from the actuator. For a design which actually uses less power (at $\alpha = 0.2$) but has only an 80 percent duty cycle ($\beta = 0.8$) giving 11 percent less viewing time, the actuator force has been reduced to approximately 7.5 N, a factor of six reduction.

Figure 10-9 shows the change in power and force as a function of duty cycle for two fixed acceleration times. The effect of increasing duty cycle is seen to be quite dramatic for values of $\beta > 0.9$. The conclusion to be drawn from Figs. 10-8 and 10-9 is that a 90 percent duty cycle is probably the upper limit of realistic actuator design for a 20-Hz chop and 45-arcmin actuator amplitude. Consideration of reduced duty cycle, especially as a function of selected chop frequency, will significantly ease the actuator design problem.

Section 11
ACTUATOR EXPERIMENT VALIDATION

Preliminary laboratory experiments were conducted to verify the validity of the concepts and design of the SIRTF secondary mirror and its actuator(s). In this first phase of this IR D effort, tests were conducted on the electrodynamic actuators only to verify force levels and power consumption at ordinary and cryogenic temperatures. The actuator chosen for the test was of the electrodynamic type but had not been specially optimized in view of SIRTF applications, and thus the actual performance is below the requirements. However, the results are readily scalable to an actual SIRTF design and are sufficient to demonstrate feasibility. Moreover, the original techniques developed for these tests and the experience gained, particularly at cryogenic temperatures, constitute a solid basis for designing future tests of the fully actuated SIRTF secondary mirror.

11.1 MEASUREMENT PRINCIPLES

11.1.1 Force Measurements

Force measurements are made using a technique similar to the ballistic pendulum. The reasons for choosing this particular method are two-fold: first, it uses the actuator in a mode which closely resembles the actual operating mode and, second, it is simple to implement and extremely accurate results can be obtained. A current pulse of short duration (200 to 1200 μs) is sent to the actuator coils, communicating a certain amount of kinetic energy to the system, which is gradually transformed into potential energy as the actuator swings and loads up the spring system constituted by the pivot and the gravity field. Thus the magnitude of the amplitude deflection is a measure of initial force imparted to the actuator. To quantify these principles, the dynamic model shown in Fig. 11-1 is used. The actuator is mounted vertically, with its CG below the flex pivot, and the equations of motion are given by

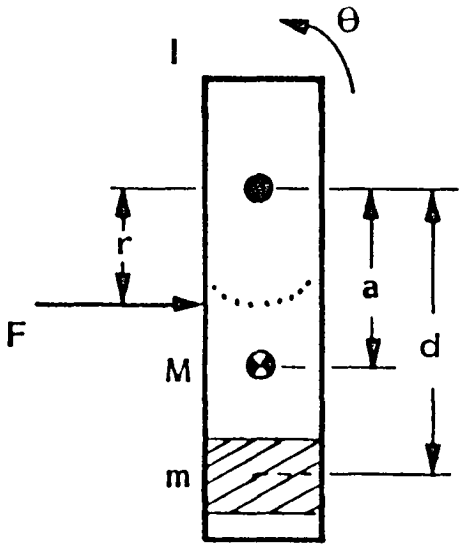

Fig. 11-1 Dynamic Model

$$I\ddot{\theta} + (k + Mga)\,\theta = Fr \tag{11.1}$$

where I is the actuator inertia about the pivot, k is the pivot spring constant, M is the total mass of the moving part, a is the position of the center of mass, g is the acceleration due to gravity, F is the electrodynamic force generated between the pole pieces at a distance r from the pivot, and θ is the deflection angle.

For a pulse of short duration Δt, the angle θ does not change significantly during the time interval Δt, and thus

$$I\dot{\theta}_{\Delta t} \sim \int_0^{\Delta t} Frdt = r\,F\Delta t \tag{11.2}$$

where $\overline{F\Delta t}$ denotes the integral.

The kinetic energy stored is then

$$\frac{1}{2} I\dot{\theta}^2 \Delta t = \frac{1}{2} (k + Mga) \theta_{max}^2 \qquad (11.3)$$

Thus, by measuring θ_{max} and using Eqs. (11.2) and (11.3), the average force F is:

$$F = \frac{\theta_{max}}{r \Delta t} \sqrt{I (k + Mga)} \qquad (11.4)$$

Since Eq. (11.4) requires the knowledge of I and k + Mga, these quantities are first determined by measuring the natural frequency of oscillation of the actuator in the following cases:

(1) Nominal position
(2) Upside down position (center of mass above flex pivot)
(3) Nominal position with added mass m at distance d from the pivot

The corresponding frequencies are given by

$$\omega_1^2 = I/(k + Mga)$$

$$\omega_2^2 = I/(k - Mga)$$

$$\omega_3^2 = (I + md^2)/[k + (Mga + mgd]$$

from which I, k, and Mga can be determined. [Mga + mgd]

11.1.2 Actuator Force Coefficient

In an electrodynamic actuator, the force produced is directly proportional to the product of the currents in the rotor (i_1) and stator (i_2) coils:

$$F = k_F i_1 i_2$$

where the coefficient k_F is expressed in newtons per square ampere.

Because of the coil inductance, saturation of the power amplifiers driving the coils, and other nonlinearities, the pulse shapes are usually not square, expecially for short durations. The measurements give an average value

$$\bar{F}\Delta t = \int_0^{\Delta t} Ft = K_F \int_0^{\Delta t} i_1 i_2 dt$$

Thus, the force coefficient must be determined by the formula:

$$k_F = \frac{F\ \Delta t}{\int_0^{\Delta t} i_1 i_2\ dt} \tag{11.5}$$

This coefficient will be strictly a constant if all the mechanical energy is rotational, but, since some of it may be found in structural deformations of the actuator itself, it can be expected that some variations will appear in this constant and more so for short pulses which tend to excite more of the structural modes. Also, as the currents i_1 and i_2 are increased, the magnetic material will saturate, causing k_F to apparently diminish. In these studies, however, the maximum achievable F is more important for the design than the actual value of k_F, but the linear range must be assessed as well as the saturation range for scalability and extrapolation to different designs.

11.1.3 Power Measurement Principle

The electrical power dissipated in the actuator is of primary concern for the SIRTF design, and accurate measurement is essential. The method chosen here is purely electrical. A general circuit model for one of the actuator coils

is shown in Fig. 11-2. The main constituants of this circuit are the inductance L, the resistance R, and an induction voltage e, which includes the interactions of the coil with the other part of the actuator and other kinds of losses.

Typically, e includes hysteresis, magnetic and eddy current losses, and induction from the other coil. This latter is primarily the transformer effect and the back emf due to relative motion between the two coils.

Measuring the input voltage V and current i in the coils leads to an evaluation of the total energy fed to the system during the interval Δt

$$E_T = \sum_k \int_0^{\Delta t} V_k \, i_k \, dt \qquad k = 1,2 \tag{11.6}$$

The resistive losses are obtained by

$$E_R = \sum_k \int_0^{\Delta t} R_k \, i_k^2 \, dt \qquad k = 1, 2 \tag{11.7}$$

It was shown earlier that the mechanical energy was given by

$$E_M = \overline{F\Delta t} = k_F \int_0^{\Delta t} i_1 \, i_2 \, dt \tag{11.8}$$

The energy balance requires that

$$E_T = E_M + E_R + E_\theta \tag{11.9}$$

where E_θ represents nonresistor losses.

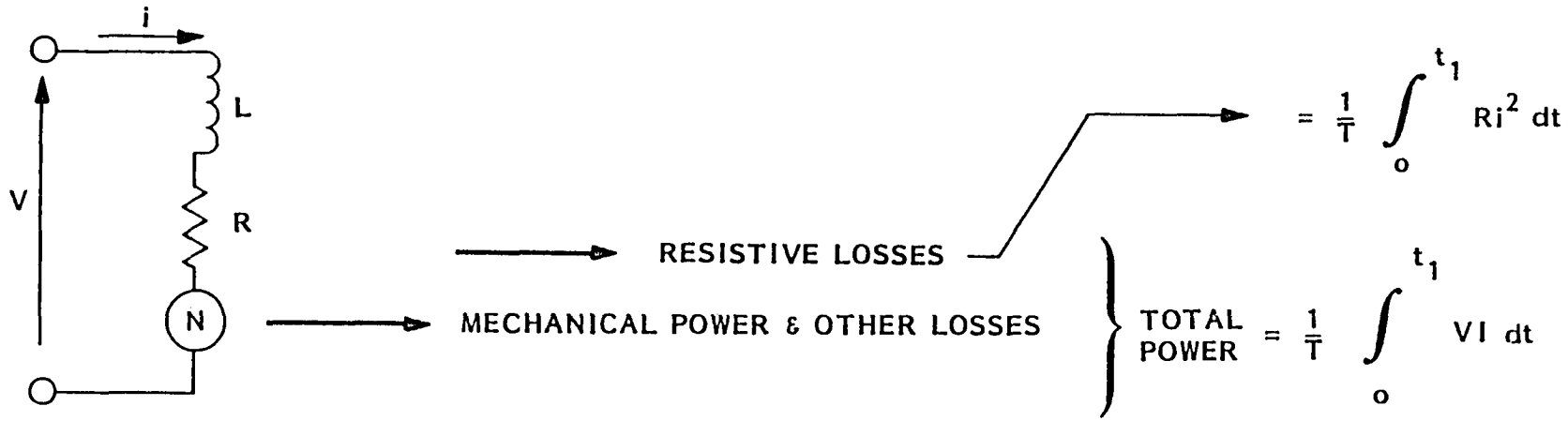

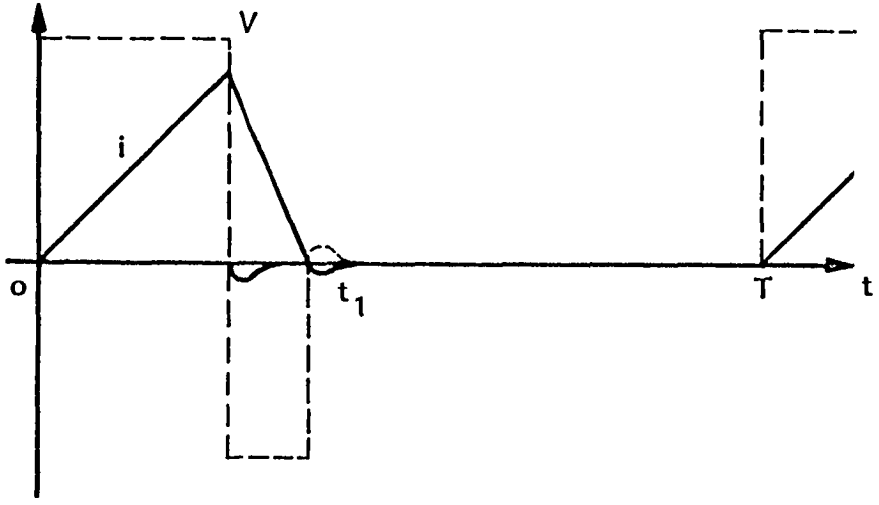

Fig. 11-2 Power Measurements

It is thus seen that measurements of V, i, and R can be used to determine the energy losses in the actuator and thus the heat generated.

Here again, because the pulse shapes are not square, it is necessary to perform an actual integration over some period of time Δt during which there is electrical activity present in the system. (This time may in fact significantly exceed the original pulse width of the input of the power amplifiers.) Thus, each value determined for E_T, E_R, etc., represents the energy per pulse, and the average power is then calculated by multiplying these values by the number of pulses per second.

11.2 DATA ACQUISITION AND PROCESSING

The actuator dynamic characterization and the force and power measurements were performed using a sophisticated digital data acquisition and processing system involving an STI/DEC 11-23 microporocessor, A/D and DAC interfaces, a separate digital frequency generator, a pulse generator and power amplifiers, and a data analysis software package (VAMP).

This system is used in two different modes:

(1) A slow mode (see Fig. 11-3) in which the actuator is pulsed every 5 or 10 s, and the data are taken at a 200-Hz sampling rate. A signal is issued by the 11-23 command generator via its DAC, which triggers the pulse generator. This mode is used for dynamic characterization and force measurement since the main measurement in this case is the oscillation of the actuator that occurs at low frequency (typically from 5 to 15 Hz). Recorded by time history is a decaying sine function as shown in Fig. 11-4. Data can be obtained directly from the CRT display, and the maximum amplitude θ_{Max} is determined in this way. The oscillator frequency is determined from the Fourier transform of this time history (shown in Fig. 11-5). (The software can also perform curve fitting operations to determine the damping as well).

(2) A fast mode (see Fig. 11-6) in which the actuator is pulsed at a 200.1-Hz rate by an independent frequency generator triggering the pulse generator. The 11-23 is still taking data at 200 Hz and, because of the slight difference in frequencies, it is now possible to record the shape of the very short current pulses themselves, as explained in Fig. 11-7. As shown in the figure, the sampling gate shifts its relative position with respect to the waveform to be analyzed at each sampling period, because of the asynchronicity, thus recording the entire waveform shape on a different time scale. The equivalent (or virtual) sampling time of such system is given by

$$T_S = \frac{1}{200} - \frac{1}{200.1} = 2.5\ \mu s$$

Thus, for a pulse length of 100 μs and above, this system gives very accurate results, and its great advantage is the capability of storing in the computer memory all the time histories for the various quantities of interest and of manipulating the data at a later time through the VAMP system (computing products, sums, integrals, averages, etc.).

11.3 CRYOGENIC MEASUREMENTS SETUP

These measurement were made using a helium dewar as shown in Fig. 11-8. A small window allows a laser beam to be reflected on a mirror attached to the actuator. The reflected beam is detected by a linear photo sensor whose output is thus proportional to the actuator rotation angle θ. The current into and voltage across the coils are picked up outside of the dewar, near the connector. Thermistors are glued to various parts of the actuator and internal fixtures to determine the local temperatures. Power data are acquired in a short burst to minimize heat dissipation, which would be otherwise significant for 200-Hz operations. Because of the short time available at low temperature due to the limited helium capacity and insulation of the dewar, all the various measurements are stored in memory to be processed and studied later. Oscilloscopes are used to monitor the data during the tests.

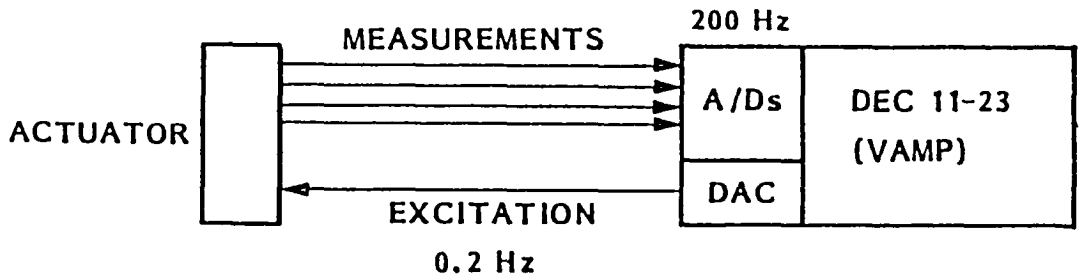

Fig. 11-3 Data Acquisition and Processing System, Force Measurements

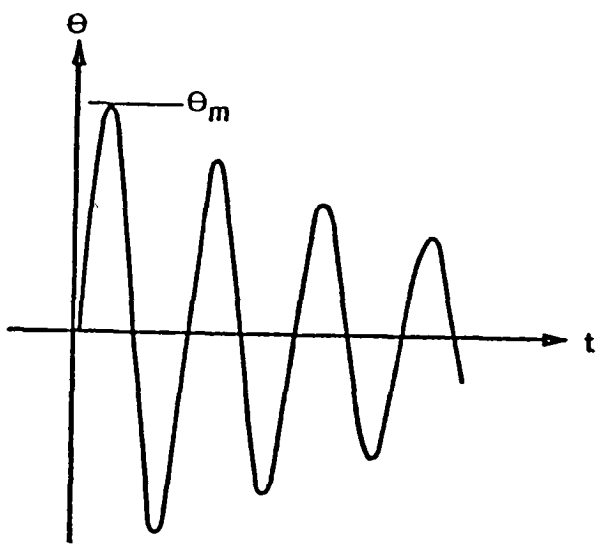

Fig. 11-4 Time History of Actuator Displacement for a Single Pulse

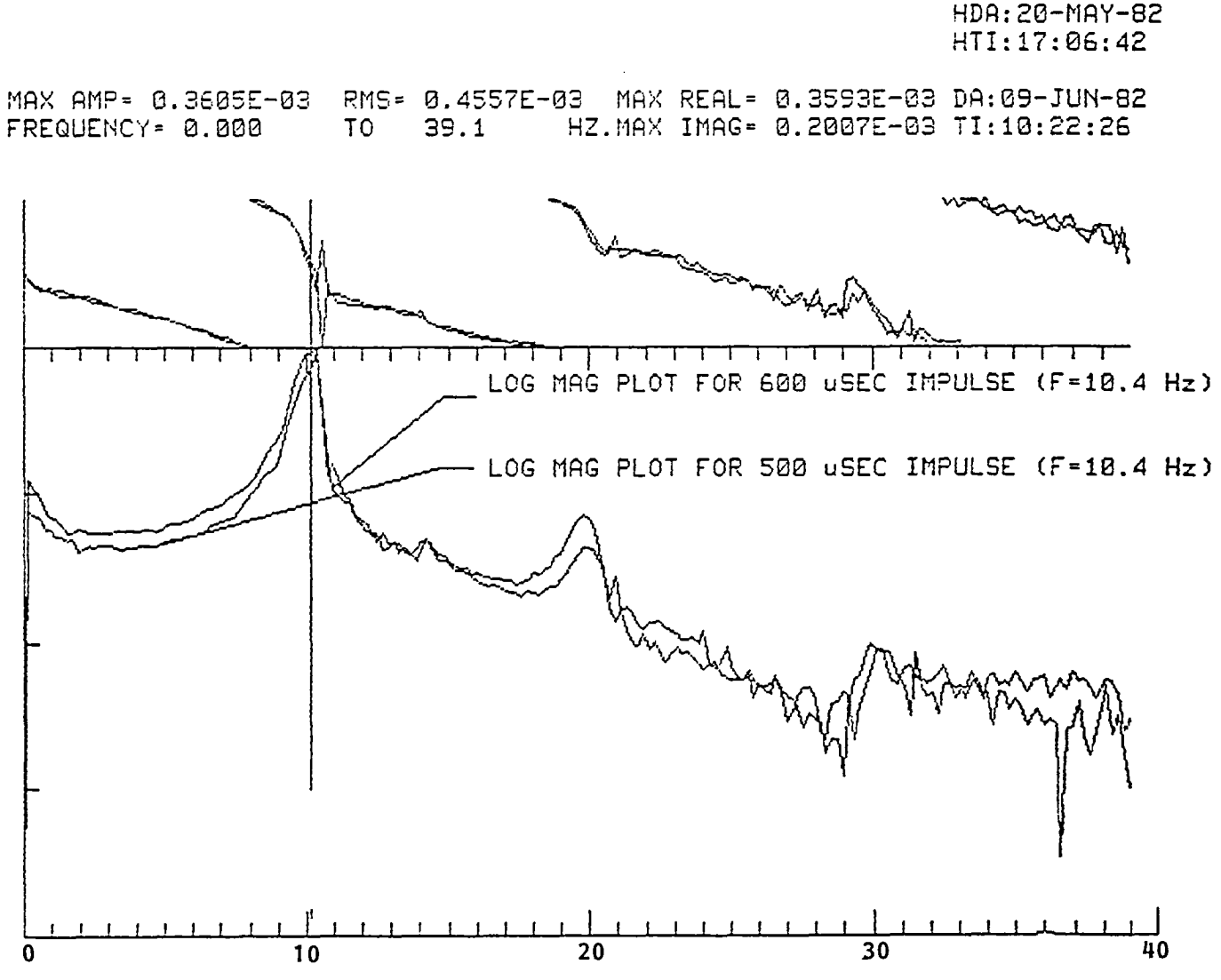

Fig. 11-5 Fourier Transform of Actuator Pulse Response

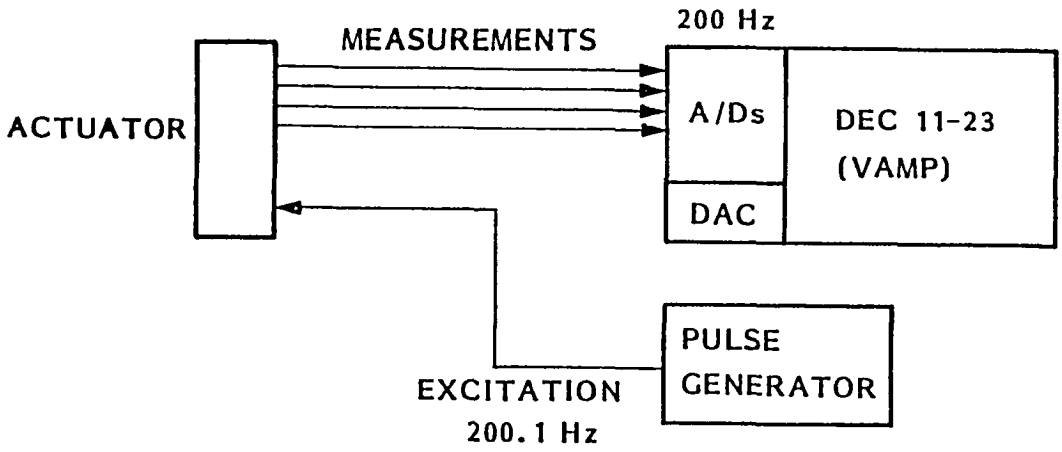

Fig 11-6 Data Acquisition and Processing System, Power Measurements

11.4 EXPERIMENTAL RESULTS

Data were taken at ordinary temperature and at temperatures around 16 K. In both cases the actuator was installed inside the dewar, except for preliminary measurements of mass/inertia properties.

11.4.1 Mass/Inertia Properties

The actuator under test was found to have the following characteristics:

$k = 0.69$ N-m/rad

$Mga = 2.95 \times 10^{-2}$ N-m/rad

$I = 1.60 \times 10^{-4}$ kg-m^2

The value of r (application point of the electrodynamic force) is 0.0212 m.

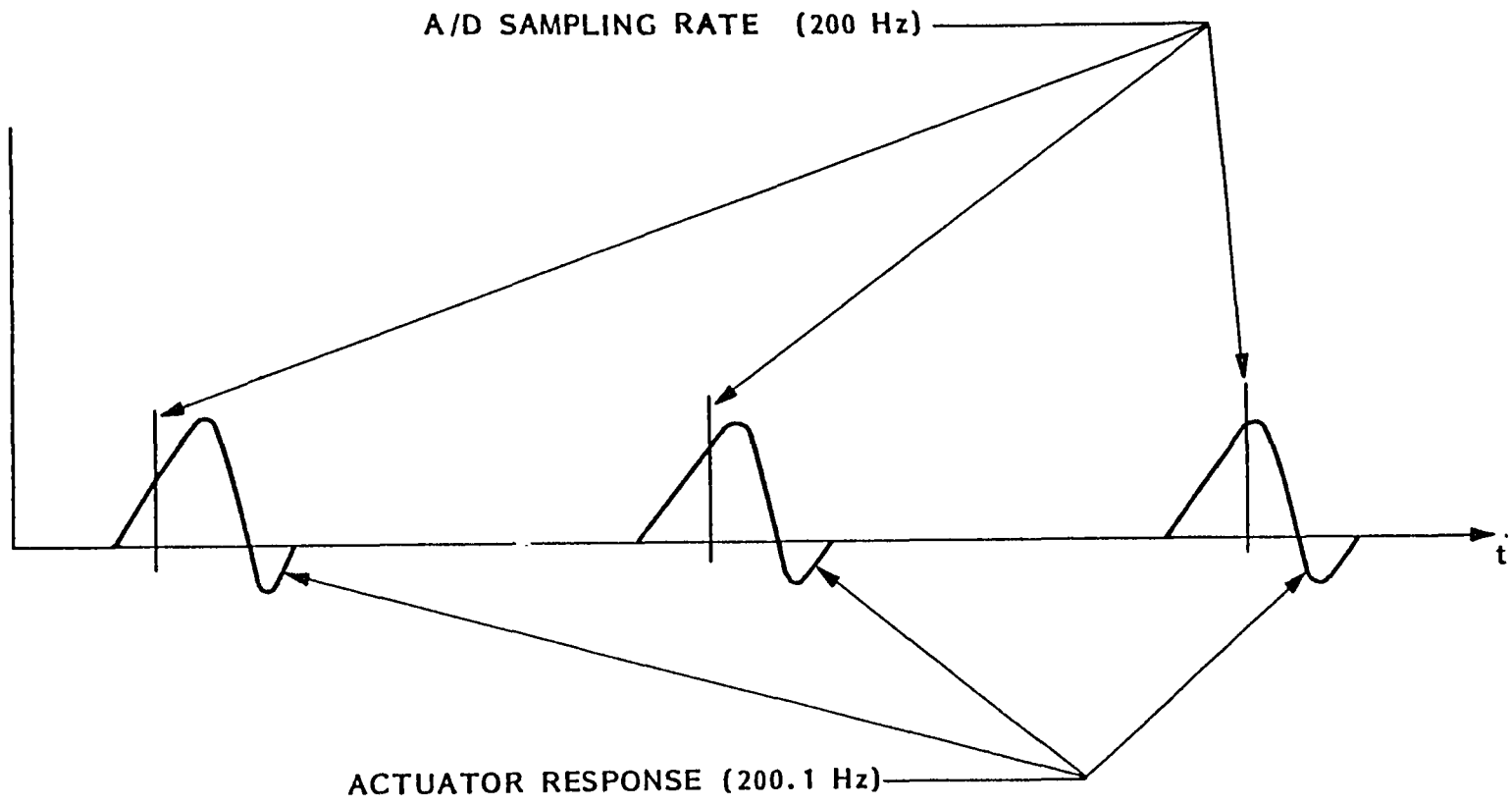

Fig. 11-7 Short Pulses Data Acquisition by Asynchronous Sampling

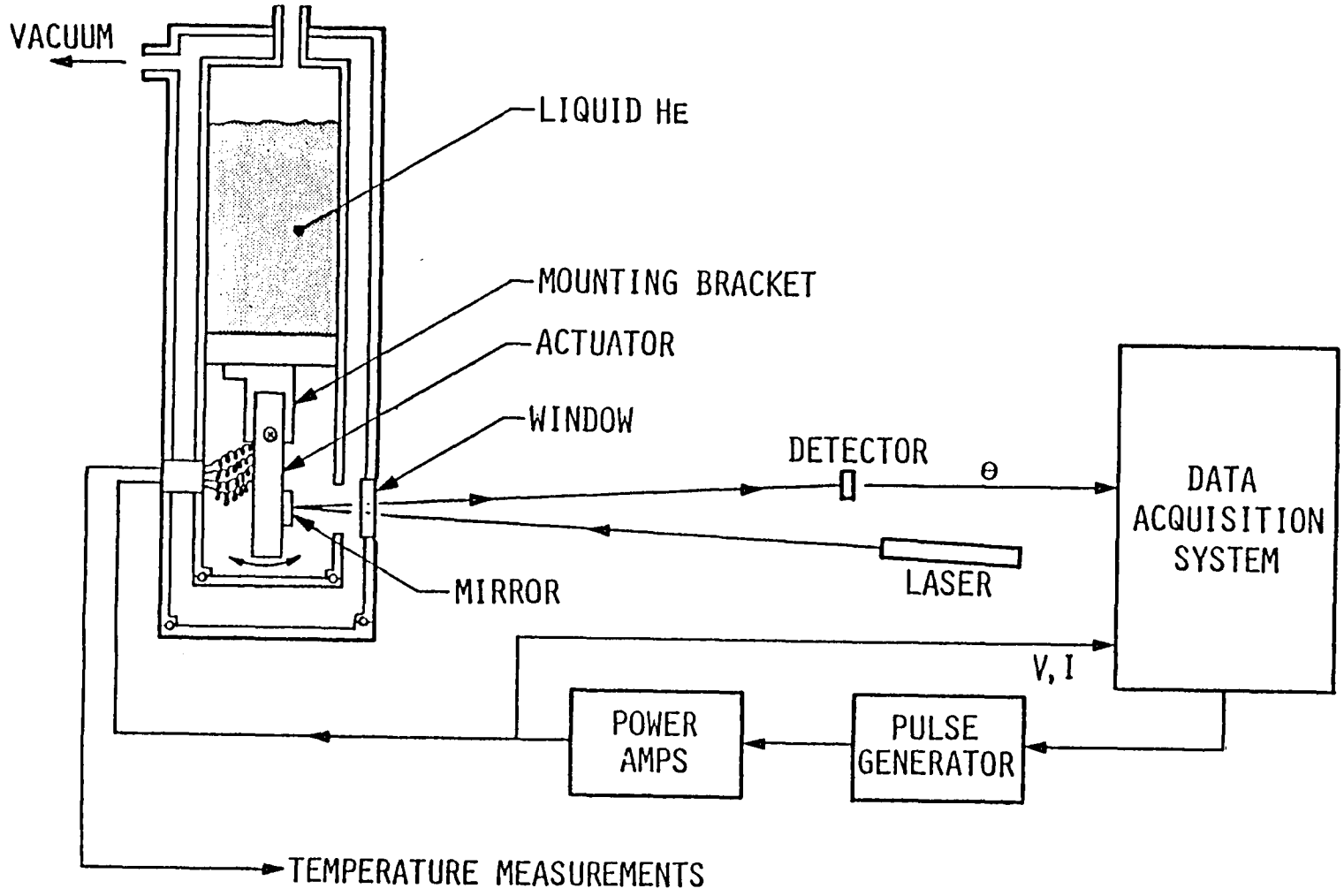

Fig. 11-8 Cryogenic Measurements

11.4.2 Force Measurements

These measurements were taken for commanded pulse lengths of 400, 600, and 1200 μs at room temperature and at 500 and 600 μs at cryogenic temperatures. A typical data set for the cryogenic runs is shown in Fig. 11-9. Values for the actuator force coefficient were found to be in the range of 0.3 to 0.6 N/A^2. A set of calculations indicating the step-by-step procedure for making detailed predictions of actuator force characteristics as a function of pulse length are shown in Fig. 11-10. Figure 11-11 plots the relationship between the calculated values and those measured experimentally. The assumption of $Ka/\delta_a = 100\ m/s^2$ for this actuator appears to be substantially correct based on the fidelity of the computed values in Fig. 11-11.

11.4.3 Power Measurements

Data taken with the PPM actuator cooled to cryogenic temperatures (E-core at 60 K and C-core at 16 K) are displayed in Figs. 11-12 through 11-19. The results of these tests are summarized in Table 11-1:

Table 11-1 COLD TEST RESULTS

Pulse Length (μs)	Average Total Power			
	Per 1200 μs (W)		i^2 Per 1200 μs (A^2)	
	C-Core	E-Core	C-Core	E-Core
500	2.785	4.653	3.541	4.886
600	1.544	5.970	5.083	6.692

Measurements of the C-core and E-core winding resistance indicated a drop of approximately a factor of 10 from room temperature values. The chart in Fig. 11-20 indicates that pure copper should decrease in resistivity by about a factor of 100 to 150 between room temperature and 16 K. To verify the assumption of greatly increased conductivity, a separate test was conducted in which the complete E and C cores of a disassembled PPM actuator were cooled directly in an LHe bath until they stabilized at 4.2 K. These data, summarized in Table 11-2, support the claim that substantially lowered resistivity will occur at SIRTF secondary mirror operating temperatures, even without the use of high-purity, annealed copper wire.

Table 11-2 COPPER RESISTANCE CHANGE WITH TEMPERATURE

Temperature (K)	E-Core Resistance (ohms)	C-Core Resistance (ohms)	Reduction
Room Ambient	1.935	1.660	---
77	0.220	0.203	8.5
4.2	0.017	0.013	12.0

Data from Tables 11-1 and 11-2 and Fig. 11-11 may now be combined to show force generated and the asssociated energy dissipation (Table 11-3).

Table 11-3 SUMMARY OF TEST RESULTS

Commanded Pulse Length (μs)	Force Generated (N)	Total i^2R Energy Loss (E+C Cores) Per Pulse (J)
500	2.91	1.55×10^{-4}
600	3.32	2.16×10^{-4}

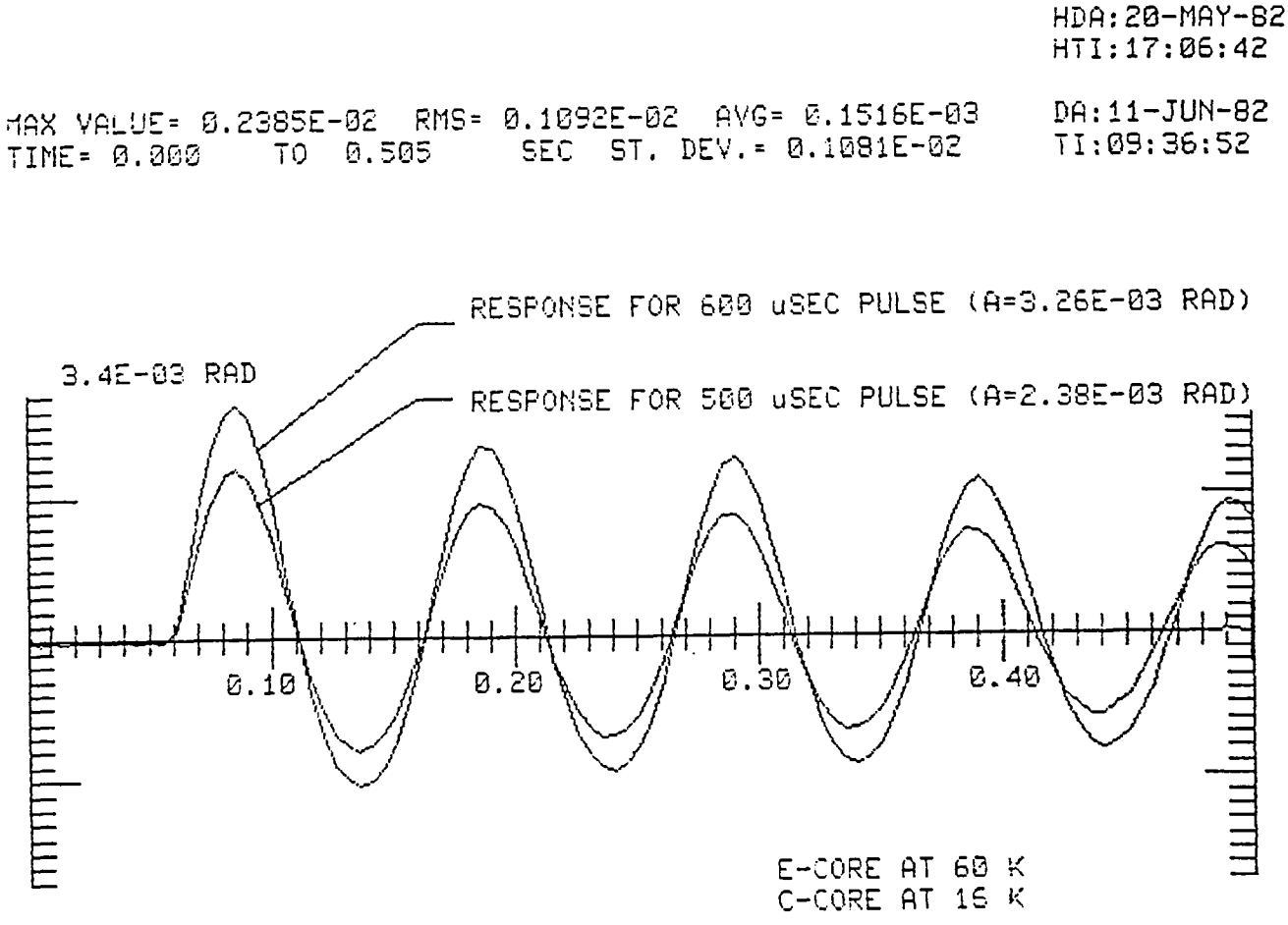

Fig. 11-9 Impulse Response for Inverted PPM Actuator

(1) $$\frac{i_1}{\Delta t_1} = \frac{V_{max}\ell}{\mu_o\mu n^2 S} = \frac{1.6}{4 \times 10^{-4}} = 4 \times 10^3$$

$$\frac{\mu_o\mu n^2 S}{\ell} = \frac{15}{4 \times 10^3} = 3.75 \times 10^{-3}$$

(CALCULATION OF $\mu_o\mu$)

$$\bar{F} = k_f \frac{S\mu_o^2 \mu^2 n^2}{\ell^2} \frac{(2\Delta t_1 + \Delta t_2)(\frac{2}{3}\Delta t_1 + \Delta t_2)(\bar{i})^2}{(\Delta t_1 + \Delta t_2)^2}$$

$@ t_1 = 400\ \mu sec,\ \Delta t_2 = 0$

(2) $$\bar{F} = \frac{4}{3} k_f (3.75 \times 10^{-3})^2 \frac{1}{n^2 S} (\bar{i})^2$$

$$k_f = dl \frac{K_a}{S_a} = (8 \times 10^3)(.02)(100) = 1.6 \times 10^4$$

(FORCE EFFICIENCY CONSTANT FROM MEASUREMENTS)

(3) $$\bar{F} = \frac{4}{3} \frac{(1.6 \times 10^4)(3.75 \times 10^{-3})^2}{(90^2)(5.75 \times 10^{-5})} (\bar{i})^2$$

$$\bar{F} = 0.644\ (\bar{i})^2$$

(4) @ 400 μs $\quad \bar{F} = 0.644\ (0.84)^2 = 0.455$ N

$\bar{F}_{MEAS} = 0.489$ N

@ 600μs

$\Delta t_1 = 200\mu s$

$\Delta t_2 = 400\mu s$ $\Rightarrow$ $\bar{F} = 0.303\ (\bar{i})^2$

$\bar{F} = 0.303\ (0.87)^2 = 0.229$ N

$F_{MEAS} = 0.193$ N

@ 1200μs

$\Delta t_1 = 200\mu s$ $\quad \bar{F} = 0.309\ (\bar{i})^2$

$\bar{F} = 0.309\ (0.97)^2 = 0.290$ N

$\Delta t_2 = 1000\mu s$ $\quad F_{MEAS} = 0.230$ N

Fig. 11-10 Laboratory Verification of Analytical Results

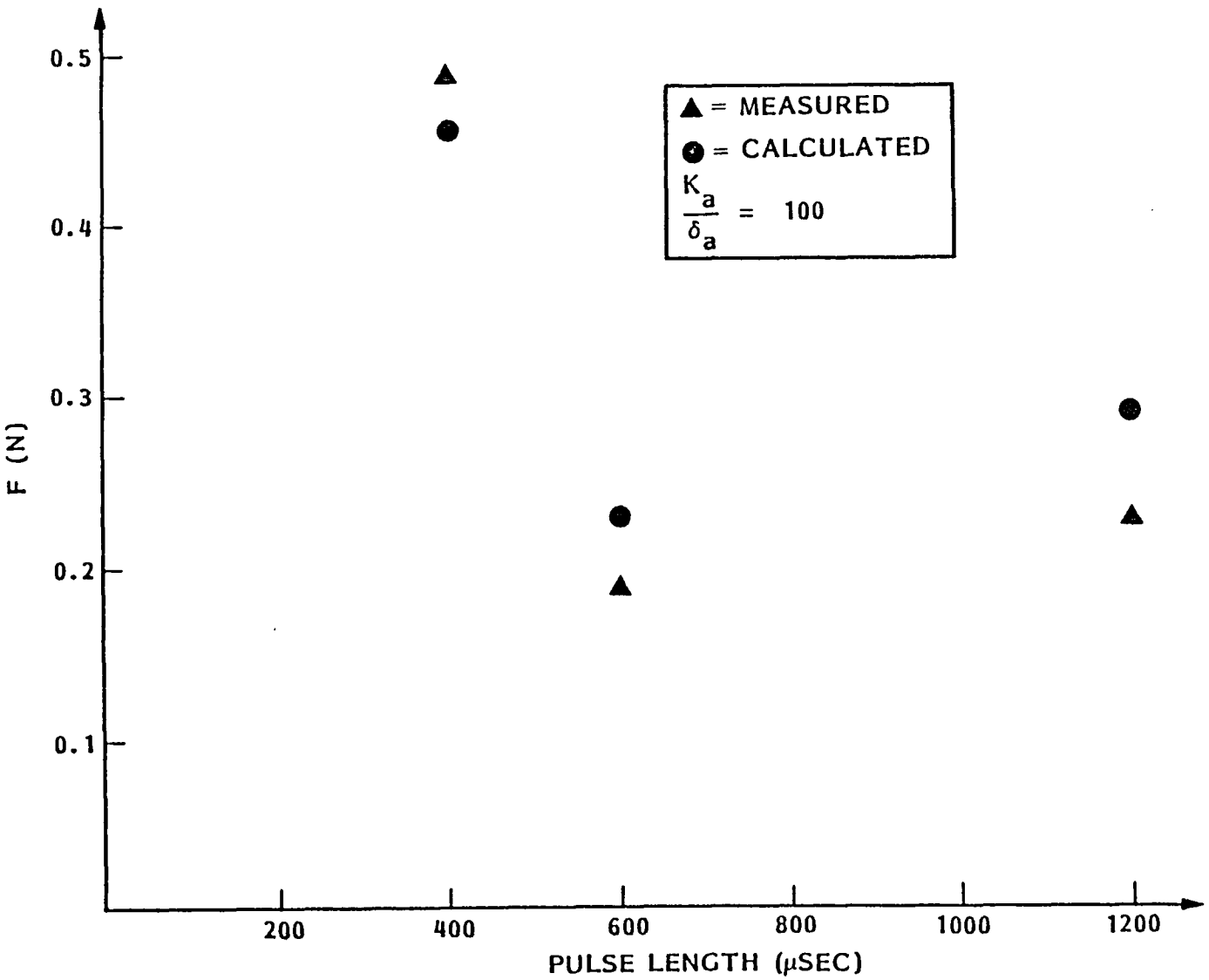

Fig. 11-11 Actuator Force for Various Pulse Lengths

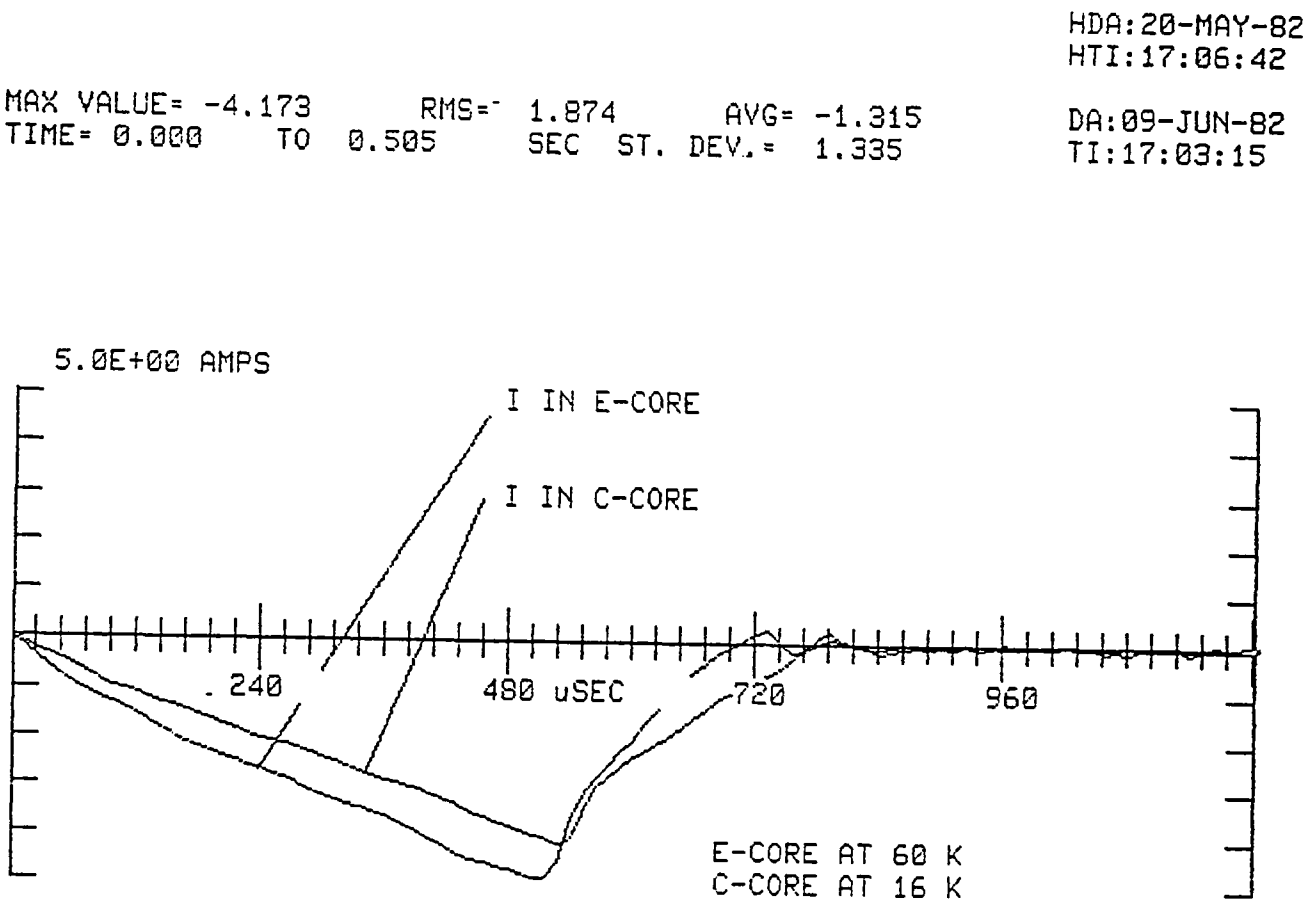

Fig. 11-12 Current in C and E-Cores for 500-μs Pulse

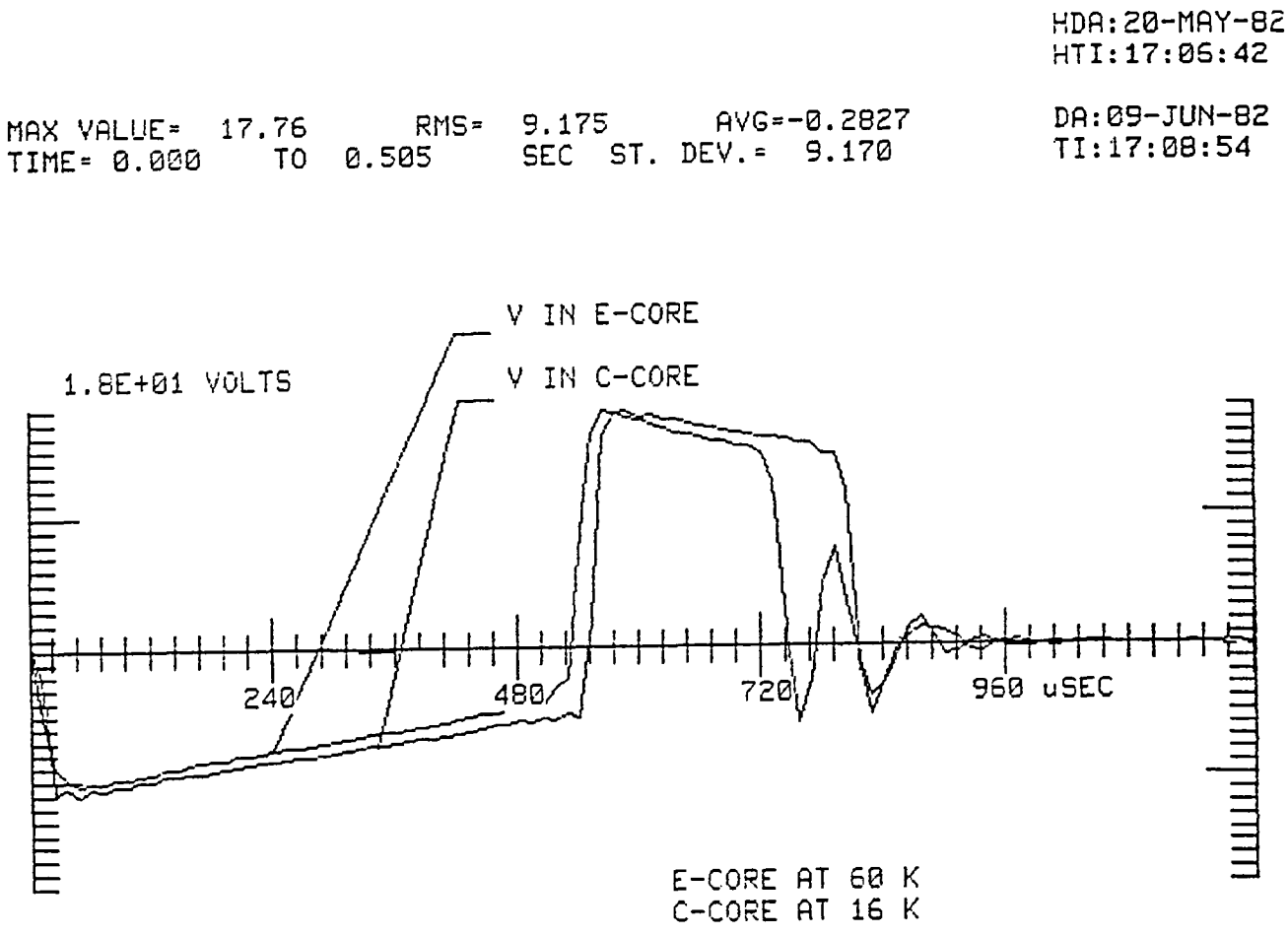

Fig. 11-13 Voltage in C and E-Cores for 500-μs Pulse

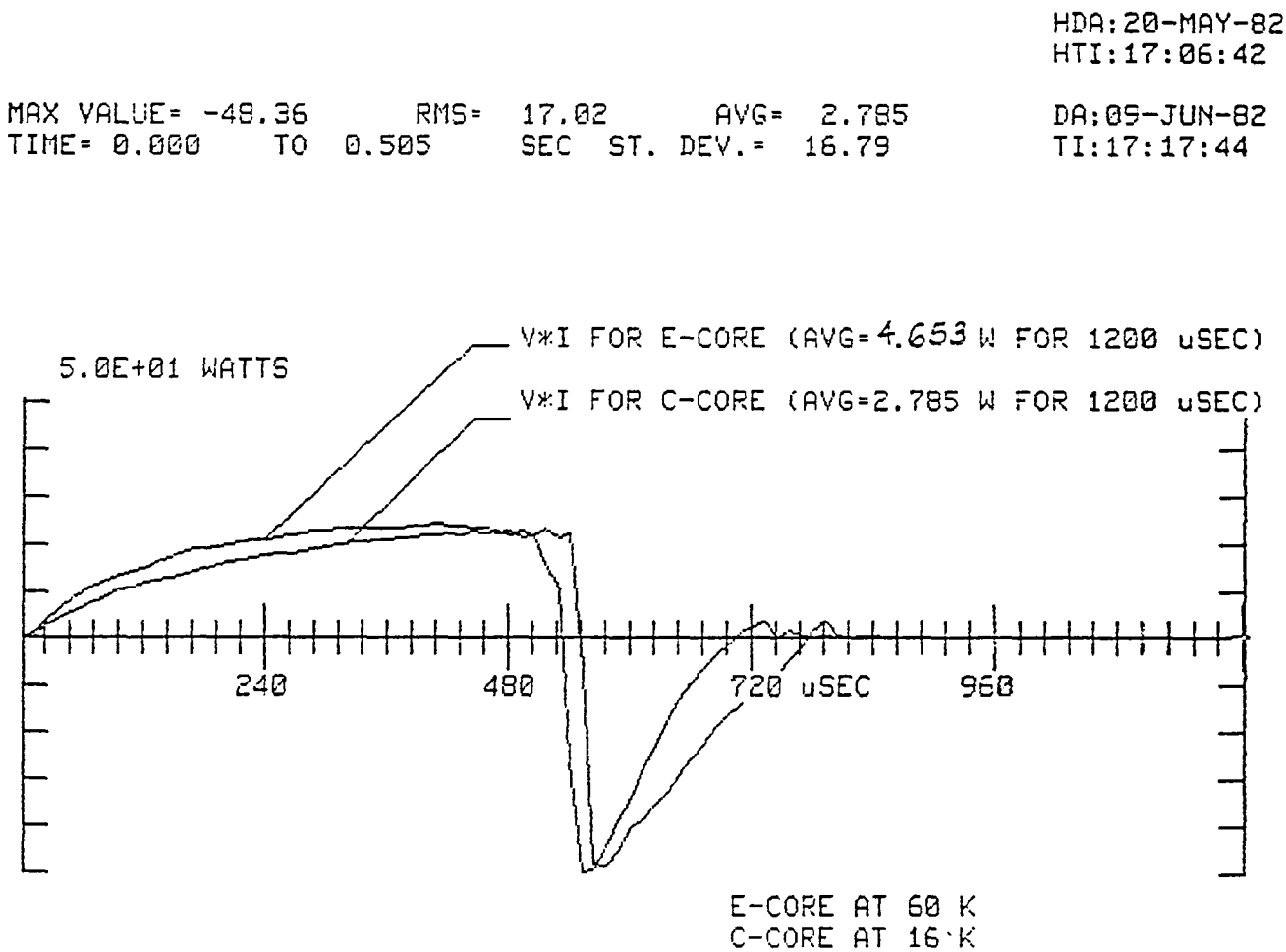

Fig. 11-14 Total Pulse Power in C and E-Cores for 500-μs Pulse

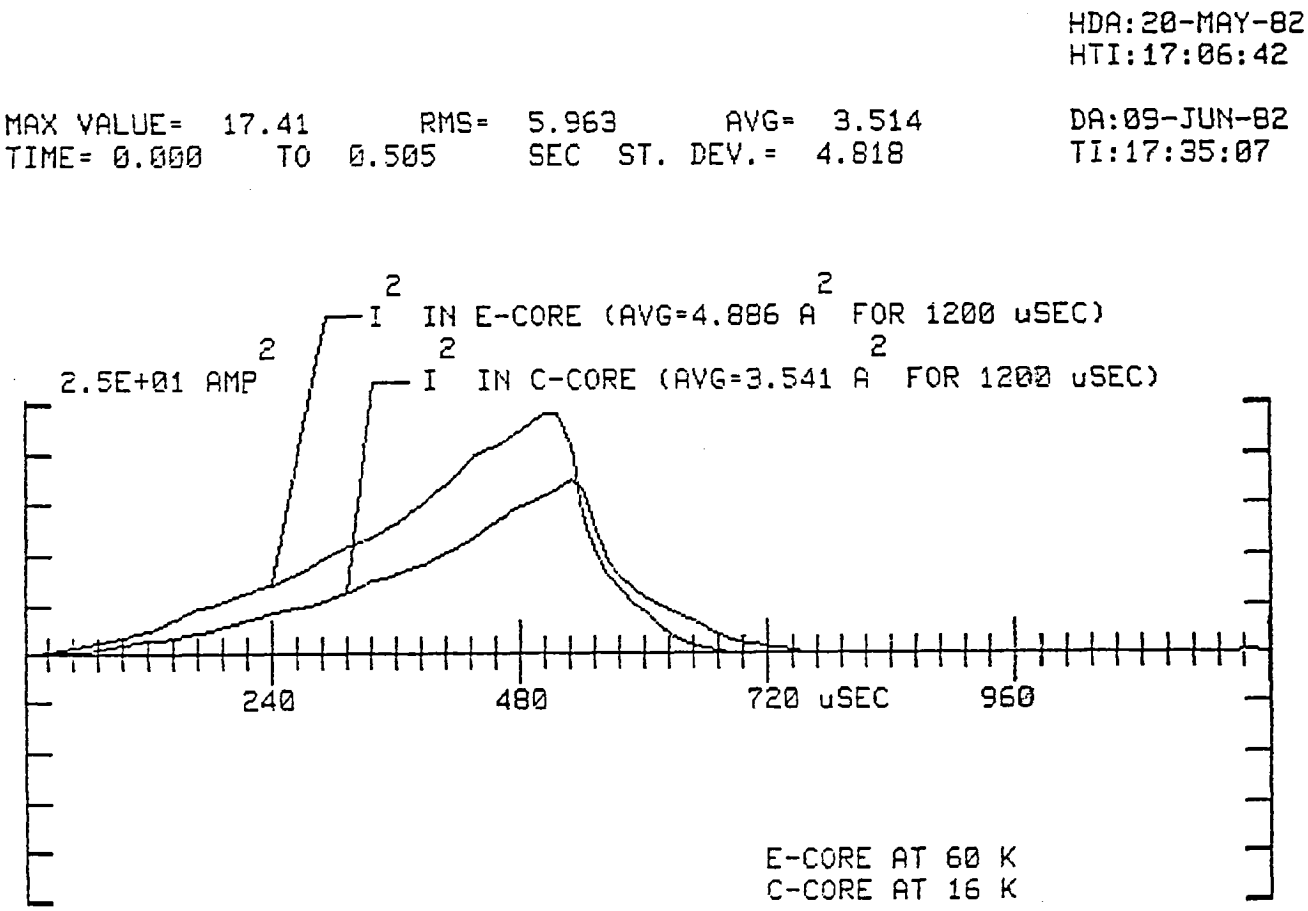

Fig. 11-15 Current Squared per Pulse in C and E-Cores for 500-μs Pulse

HDA:20-MAY-82
HTI:17:06:42

MAX VALUE= -4.498 RMS= 2.254 AVG= -1.665 DA:10-JUN-82
TIME= 0.000 TO 0.505 SEC ST. DEV.= 1.520 TI:11:02:51

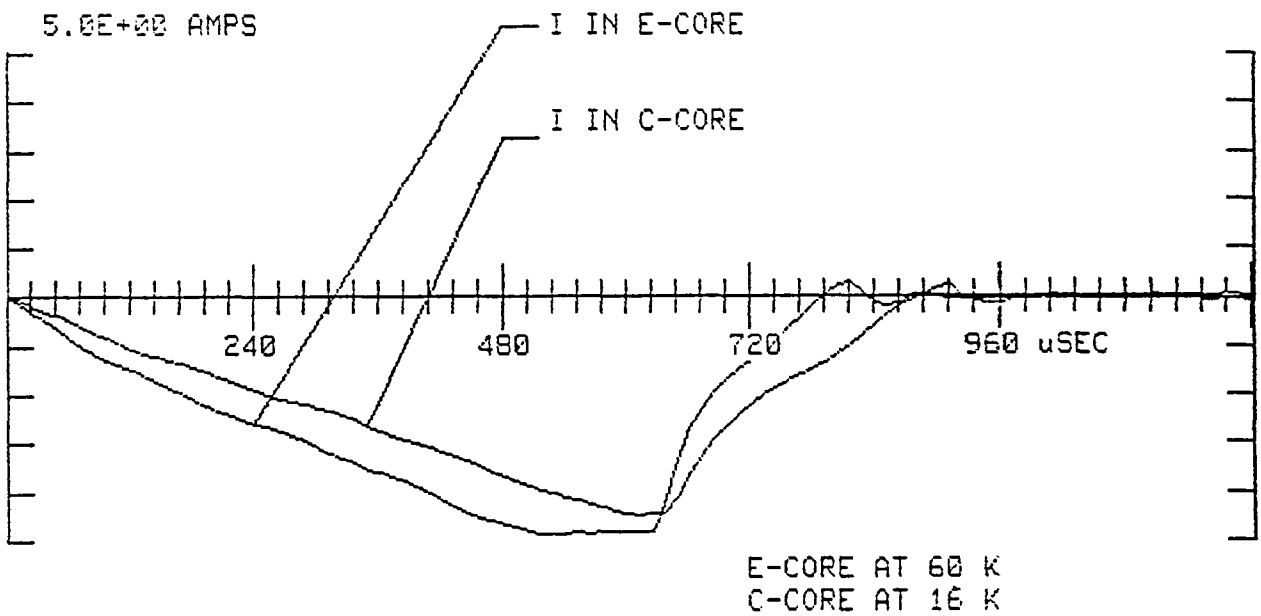

Fig. 11-16 Current in C and E-Cores for 600-μs Pulse

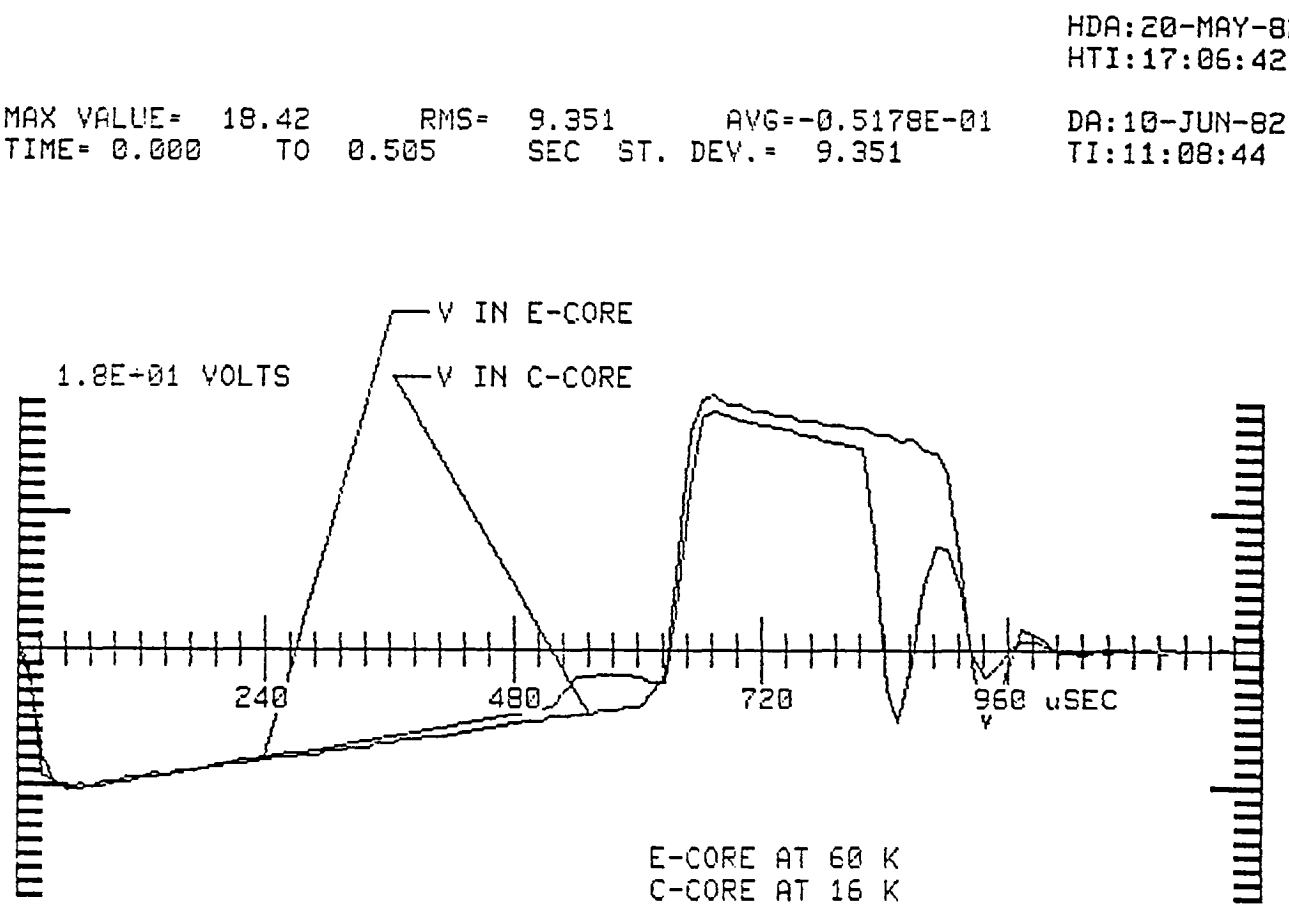

Fig. 11-17 Voltage in C and E-Cores for 600-μs pulse

HDA:20-MAY-82
HTI:17:06:42

MAX VALUE= -45.76 RMS= 16.15 AVG= 5.970 DA:10-JUN-82
TIME= 0.000 TO 0.505 SEC ST. DEV.= 15.01 TI:11:22:42

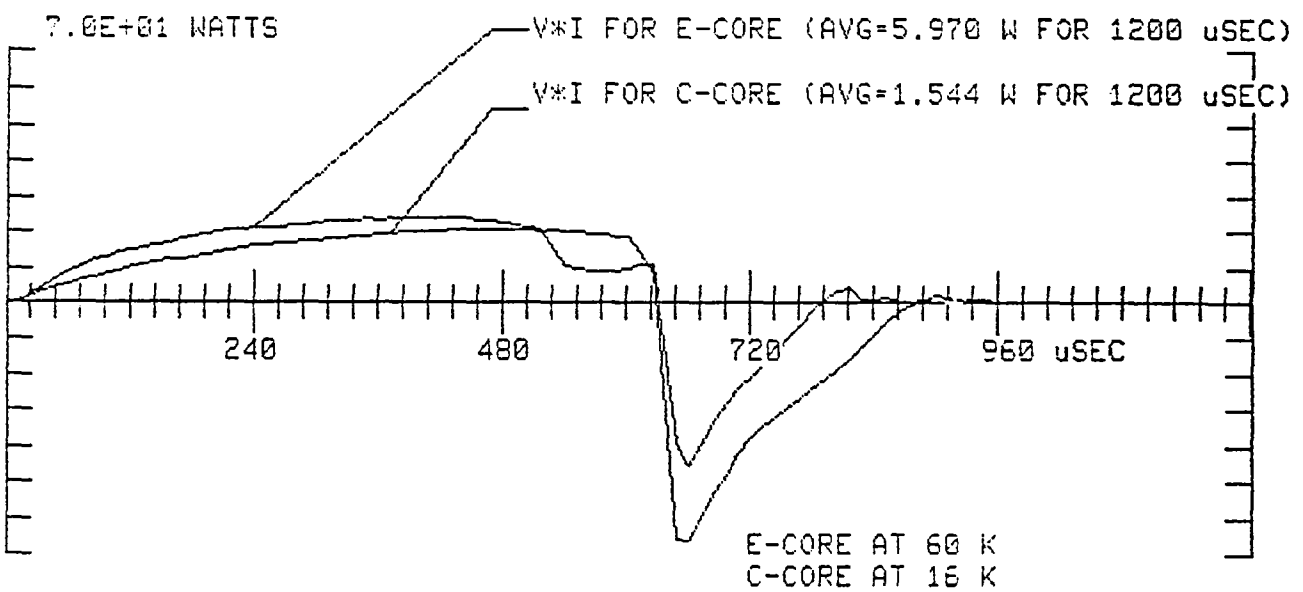

Fig. 11-18 Total Pulse Power in C and E-Cores for 600-μs Pulse

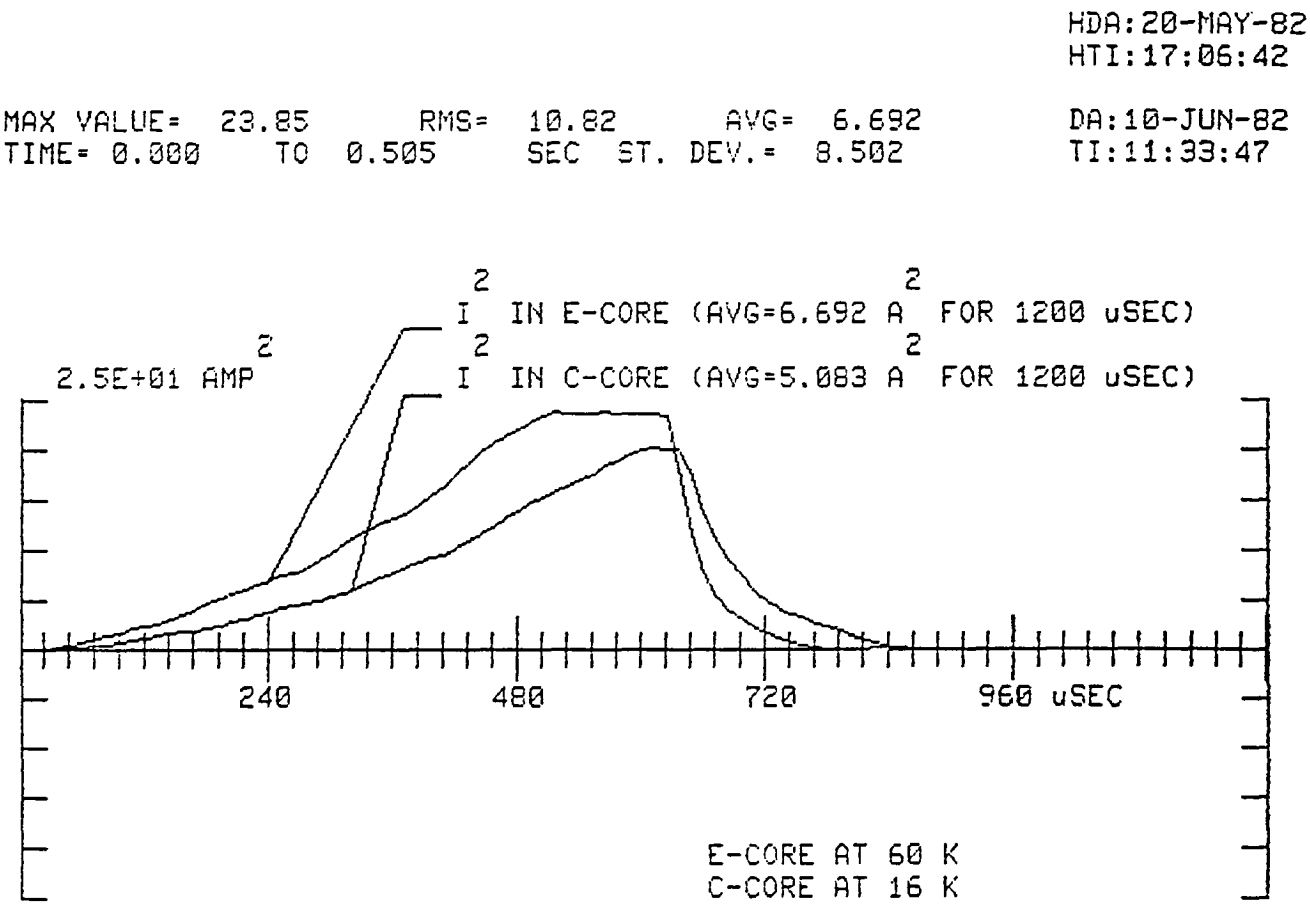

Fig. 11-19 Current Squared Per Pulse in C and E-Cores for 600-μs Pulse

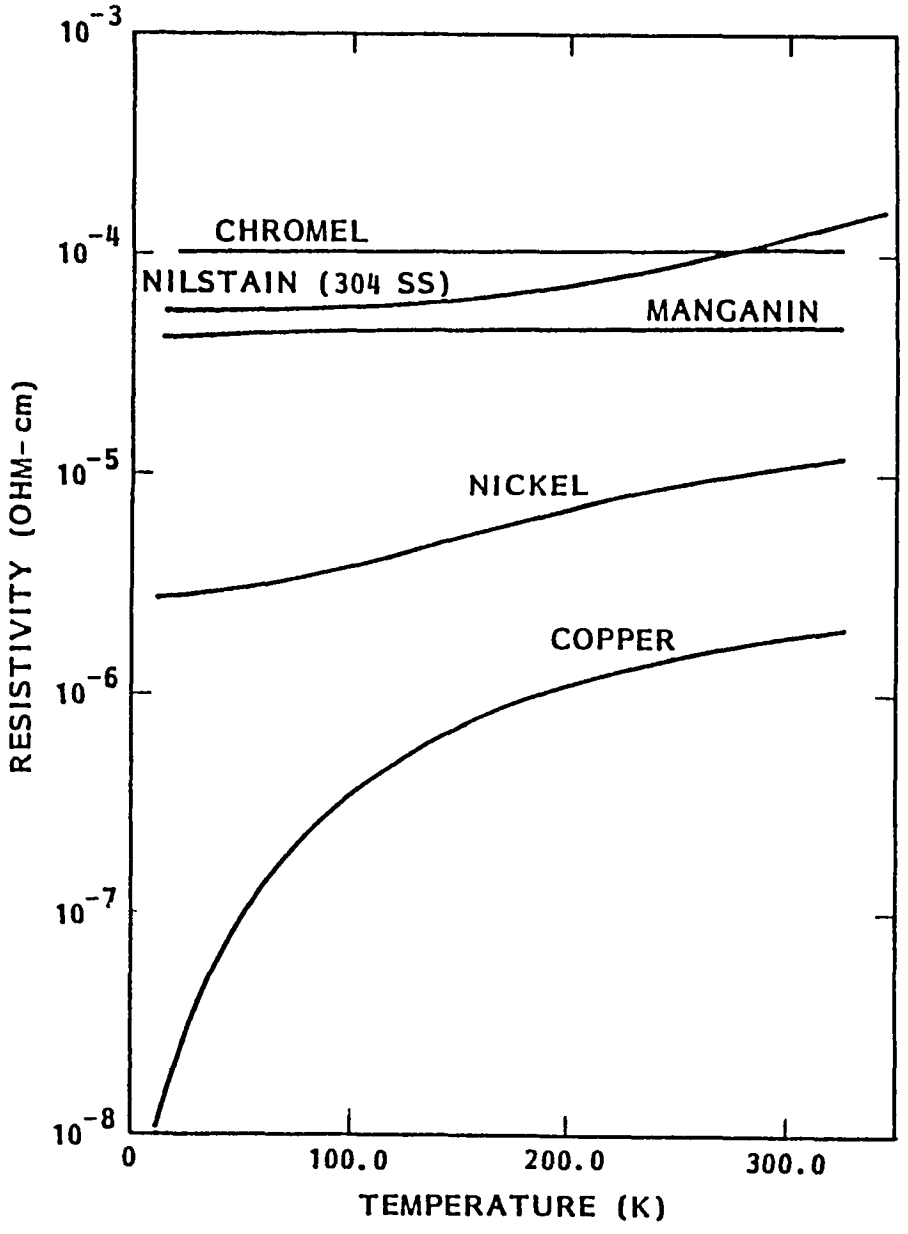

Fig. 11-20 Electrical Resistivity of Candidate Materials

11.4.4 Predicted Performance for SIRTF Actuators

Using the fact that both the force generated by this type of actuator and the resistive losses are a function of i^2, we can write

$$F_1 = k_F i_1^2$$

$$P_{AVE1} = k_F i_1^2$$

so that

$$\frac{F_1}{F_2} = \frac{i_1^2}{i_2^2}$$

$$\frac{P_{AVE1}}{P_{AVE2}} = \frac{i_1^2}{i_2^2}$$

thus

$$P_{AVE2} = P_{AVE1} \frac{F_2}{F_1} \qquad (11.10)$$

The average power P_{AVE} can therefore be computed by knowing the resistive energy dissipated per pulse, desired force level, and chop frequency. Combining these numbers with data from Table 11-3 in Eq. (11.10) gives the results in Table 11-4. Note that even at a 90 percent duty cycle, total power dissipation is less than 60 mW. The predictions in Table 11-4 are dependent on a number of assumptions made in the actuator model described in Section 10. While LMSC is confident in the values presented, changes in those assumptions, especially to more pessimistic values, could affect the predicted heat dissipation. Further work on this IR D effort will seek to demonstrate an optimized SIRTF actuator and validate the design assumptions.

Table 11-4 POWER ESTIMATES FOR MODELED SIRTF ACTUATOR

Duty Cycle (500 μ/s pulse)	Force Level Required (20 Hz at 45 arcmin amplitude) (N)	Average Power Dissipated By Resistive Losses, K_a/δ_a = 2.00 (W)
β = 0.8 (80 percent) α = 0.1	12.5	0.0266
β = 0.90 (90 percent) α = 0.2	27.5	0.0586

1. Report No.	2. Government Accession No.	3. Recipient's Catalog No.
NASA CR-3722		

4. Title and Subtitle	5. Report Date
Long Life Feasibility Study for the Shuttle Infrared Telescope Facility	June 1985
	6. Performing Organization Code

7. Author(s)	8. Performing Organization Report No.
	LMSC D877125

9. Performing Organization Name and Address	10. Work Unit No.
Lockheed Missiles and Space Company, Inc. Palo Alto Research Laboratory 3251 Hanover Street Palo Alto, CA 94304	J.O. T-5493
	11. Contract or Grant No. NAS2-11155

12. Sponsoring Agency Name and Address	13. Type of Report and Period Covered
National Aeronautics and Space Administration Washington, DC 20546	Contractor Report
	14. Sponsoring Agency Code 422-50-06

15. Supplementary Notes POINT OF CONTACT: PHONE: 415/ 694-6530
TECHNICAL MONITOR, DR. WALTER BROOKS, M.S. 244-15
AMES RESEARCH CENTER, MOFFETT FIELD, CA 94035

16. Abstract

A study was conducted to assess the feasibility of designing an Infrared Telescope of the 1 meter class which would operate effectively as a Shuttle-borne, 14-day Spacelab payload and then be adapted with little modification to work as a 6 month Space station or free flyer payload. The optics configuration and requirements from a previous study were used without modification. In addition, an enhancement to 2-year mission lengths was studied. The cryogenic system selected was a hybrid design with an internal solid Hydrogen tank at 8 Kelvin and an internal superfluid tank at 2 K. In addition to the cryogenic design, a detailed look at secondary mirror actuators for chopping, focus and decenter was conducted and analysis and cryo test reported.

17. Key Words (Suggested by Author(s))	18. Distribution Statement
Infrared Telescope Cryogenic Solid Hydrogen	Unclassified - Unlimited Star Category 89

19. Security Classif. (of this report)	20. Security Classif. (of this page)	21. No. of Pages	22. Price
Unclassified	Unclassified	174	A08

For sale by the National Technical Information Service, Springfield, Virginia 22161

NASA-Langley, 1985

National Aeronautics and Space Administration

Washington, D.C.
20546

Official Business
Penalty for Private Use, $300

SPECIAL FOURTH CLASS MAIL
BOOK

Postage and Fees Paid
National Aeronautics and
Space Administration
NASA-451

NASA

POSTMASTER: If Undeliverable (Section 158 Postal Manual) Do Not Return